UNIVERSIDAD COMPLUTENSE DE MADRID

FACULTAD DE CIENCIAS FÍSICAS

TESIS DOCTORAL

Estructuras hadrónicas y física de jets en teorías efectivas de QCD

———

Hadronic Structures and jet physics in QCD Effective Theories

MEMORIA PARA OPTAR AL GRADO DE DOCTOR

PRESENTADA POR

Rafael Fernández del Castillo

DIRIGIDA POR

Ignazio Scimemi
Miguel García Echevarría

Hadronic Structures and Jet Physics in QCD Effective Theories

Estructuras hadrónicas y física de jets en teorías efectivas de QCD

Autor

Rafael Fernández del Castillo

Directores

Ignazio Scimemi

Miguel García Echevarría

UNIVERSIDAD
COMPLUTENSE
MADRID

Facultad de Ciencias Físicas - Programa de doctorado en Física

Instituto de Física de Partículas y del Cosmos

A mis padres y a mi abuela

R.F.C. is supported by the Spanish Ministry grant PID2019-106080GB-C21 and PID2022-136510NB-C31. This project has received funding from the European Union Horizon 2020 research and innovation program under grant agreement Num. 824093 (STRONG-2020).

List of publications and conferences

The original results of this Ph.D. thesis appear in the following publications

- **Transverse Momentum Measurements with Jets at Next-to-Leading Power**

  Rafael F. del Castillo, Max Jaarsma, Ignazio Scimemi, Wouter Waalewijn

  Published in JHEP 02 (2024) 074. arXiv: 2307.13025

- **Transverse momentum dependent distributions in dijet and heavy hadron pair production at EIC**

  Rafael F. del Castillo, Miguel G. Echevarria, Ignazio Scimemi, Yiannis Makris

  Published in JHEP 03 (2022) 047. arXiv: 2111.03703

- **TMD factorization for dijet and heavy-meson pair in DIS**

  Rafael F. del Castillo, Miguel G. Echevarria, Ignazio Scimemi, Yiannis Makris

  Published in JHEP 01 (2021) 088. arXiv: 2008.07531

The following publications have been published during the Ph.D. thesis, although their content is not included in this text

- **One-loop evolution of twist-2 generalized parton distributions**

  Valerio Bertone, Rafael F. del Castillo, Miguel G. Echevarria, Óscar del Río, Simone Rodini

  Published in Phys.Rev.D 109 (2024) 3, 034023. arXiv: 2311.13941

The content of these publications has been presented at the following international conferences and workshops

- **16th International Conference on the Structure of Baryons (Baryons 2022)**

  TMDs in dijet production in SIDIS

  Universidad Pablo de Olavide, Sevilla

  May 2022

- **DIS2022: XXIX International Workshop on Deep-Inelastic Scattering and Related Subjects**

  TMDs in dijet and heavy hadron pair production in SIDIS

  Instituto Galego de Física de Altas Enerxías (IGFAE)

  May 2022

- **24th International Spin Symposium (SPIN2021)**

  TMD cross-section factorization for dijet production at the EIC

  RIKEN, Japan

  October 2021

- **Particles and Nuclei International Conference 2021**

  TMD cross-section factorization for dijet production at the EIC

  University of Lisbon

  September 2021

- **World SCET 2021**

  TMD factorization for dijet and heavy meson pair production in DIS

  Online conference

  April 2021

- **Resummation, Evolution, Factorization 2020**

  Transverse momentum dependent cross-section factorization for dijet and heavy-meson pair processes in DIS

  Higgs Centre for Theoretical Physics, University of Edinburgh

  December 2020

The content of these publications has contributed to the following conference proceedings

- **TMD cross-section factorization for dijet production at the EIC**

  Rafael Fernández del Castillo

  Published in PoS PANIC2021 (2022) 373. Contribution to: PANIC 2021, 373

- **TMD Cross-Section Factorization for Dijet Production at the EIC**

  Rafael F. del Castillo

  Published in JPS Conf.Proc. 37 (2022) 020201. Contribution to: SPIN 2021

Contents

Prelude

The exploration of hadron structure and quark distribution lies at the heart of modern particle physics, offering a window into the intricate dynamics governed by Quantum Chromodynamics (QCD). Within this rich variety of subatomic phenomena, Parton Distribution Functions (PDFs) emerge as indispensable tools, encapsulating the probabilistic distribution of quarks and gluons within hadrons.

Transverse Momentum Dependent Distributions (TMDs) represent a sophisticated framework within the realm of quantum chromodynamics that captures the intricate dynamics of partons within hadrons with respect to their transverse momentum. Unlike conventional PDFs, which describe the probability of finding a parton with a certain momentum fraction along the longitudinal direction of the parent hadron, TMDs provide additional momentum information by considering the transverse momentum of the parton relative to the direction of motion of the hadron. This distinction is crucial as it unveils the three-dimensional structure of hadrons and offers insights into the correlations between the momentum distribution of the parton and its spin within the hadron. TMDs are indispensable in various high-energy scattering processes, offering a deeper understanding of phenomena such as the spin structure of the nucleon, the transverse spin effects in hadron collisions, and the dynamics of hadronization in particle interactions.

In this thesis, we explore TMDs in detail, recognizing their pivotal role in illuminating the underlying mechanisms governing hadron structure and parton distributions. We delve into the multifaceted nature of TMDs, examining their significance across various theoretical frameworks. In particular, we study their manifestation in factorization theorems, which underpin crucial processes such as Drell-Yan (DY), semi-inclusive deep inelastic scattering (SIDIS), and semi-inclusive annihilation (SIA).

In our study of TMDs and TMD factorization, we adopt a multifaceted approach by employing two distinct theoretical frameworks: Soft-Collinear Effective Theory (SCET) and the background field method. SCET provides a powerful formalism for systematically analyzing the dynamics of particles with vastly different energy scales, making it particularly well-suited for studying the intricate interplay between soft and collinear modes inherent in TMD processes. On the other hand, the background field method offers a complementary perspective and facilitates the extension of factorization theorems beyond the leading power. By following these complementary approaches, we aim to gain a deeper insight into the underlying principles governing TMDs and their factorization, thereby advancing our understanding of hadron structure and parton distributions.

This thesis contributes novel insights through the study of two new processes. The first process involves dijet production in SIDIS, which we factorize within the framework

of SCET. This process, anticipated to be probed at future Electron-Ion Collider (EIC) experiments, offers a unique opportunity to access gluon TMDs, typically challenging to constrain. We present a comprehensive phenomenological analysis, providing factorization theorems and plots showing the expected cross-section values for this process. This process is also factorized in terms of a new TMD soft function, which describes the soft physics of the process and appears in this work for the first time.

The second novel process under scrutiny is dijet production in SIA, where we extend factorization up to next-to-leading power (NLP) in the small transverse momentum expansion with the help of the background field method. This approach yields a factorization theorem expressed in terms of jet TMDs, greatly simplifying the physics at NLP. Moreover, our analysis unveils insights into NLP TMD distributions, a novel feature of this research endeavor. Through the investigation of these two new processes, we aim to expand the frontiers of knowledge in the realm of TMD physics, offering fresh perspectives on hadron structure and parton dynamics.

In this way, this thesis is structured into two distinct parts, with chapters 1, 2 and 4 being a review of the aspects needed to tackle both novel processes that we explore in our work for the first time. These processes are presented in chapters 3 and 5.

Thus, the first part begins with a detailed review of the construction of the SCET Lagrangian and the scaling of the different momentum modes, presented in chapter 1. Chapter 2 is a review of TMD distributions, TMD factorization theorems, as well as the evolution equations and divergences associated with TMD physics. Subsequently, chapter 3 offers a thorough examination of the dijet production process in SIDIS, where SCET is used as the basis for factorization.

In the second part of this thesis, attention shifts toward the background field method and its application to TMD physics, along with the extension of factorization theorems up to next-to-leading power (NLP), as reviewed in chapter 4. Chapter 5 then applies the background field method in order to provide a comprehensive analysis of the process of dijet production in SIA, detailing its theoretical intricacies and experimental implications. Through this structured approach, this thesis endeavors to offer insight into TMD physics, bridging theoretical foundations with practical applications in experimental high-energy physics.

Chapter 1

Soft-Collinear Effective Theory

Effective Field Theories (EFTs) serve as valuable tools in addressing challenges within quantum field theory involving multiple energy scales. These theories enable the expansion of physical quantities by considering the small ratio of scales, effectively distinguishing between the low-energy and high-energy contributions to a given problem.

In Quantum Chromodynamics (QCD), the study involves a dual nature: a nonperturbative low-energy regime and a perturbative high-energy domain. EFTs play a pivotal role in disentangling these facets, allowing for separate calculations using appropriate techniques. This is particularly pertinent in the context of a thesis focused on hadron-collider observables, where nonperturbative contributions find expression through parton distribution functions.

Traditionally, EFTs have been applied to low-energy QCD, with a significant emphasis on flavor physics. However, recent years have witnessed a shift, with EFTs finding applications in high-energy physics. This shift is logical given that high-energy collider processes inherently involve diverse energy scales. Processes in hadron colliders, for instance, incorporate physics at both large scales, such as the center-of-mass energy, and very low scales, such as the proton mass. Effectively addressing theoretical predictions for these processes requires disentangling the physics associated with these varied scales.

The traditional approach to achieve this disentanglement involves diagrammatic methods, establishing properties based on Feynman diagrams in the high-energy limit. An alternative formalism, Soft-Collinear Effective Theory (SCET), allows to obtain factorization theorems and provides an effective Lagrangian that simplifies computational procedures. There exists a close connection between EFTs and the traditional diagrammatic methods. Specifically, the diagrams of SCET correspond one-to-one with the expanded QCD diagrams, underscoring the complementary nature of these approaches.

In this chapter, we describe the strategy of regions as a more comprehensive example of the aim of constructing SCET. Then, we move to the derivation of the SCET lagrangian, describing in detail the different modes contributing, their interaction terms, scaling and evolution. This theoretical introduction is based on refs. [1, 2, 3].

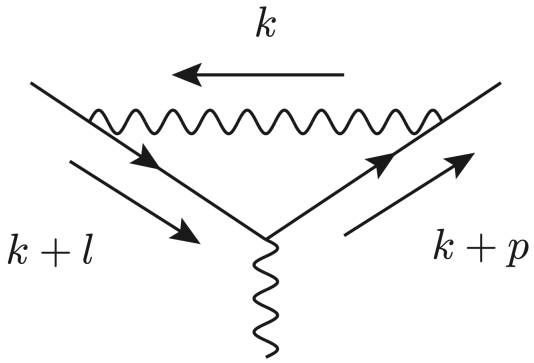

Figure 1.1: One-loop vertex corrections. Spin structure is ignored. Figure credit to T. Becher, A. Broggio, A. Ferroglia, ref. [1].

1.1 The strategy of regions

In this section, we motivate the construction of SCET through the strategy of regions. The approach known as the strategy of regions, see ref. [4], enables the asymptotic expansion of loop integrals in dimensional regularization around various limits [5]. This expansion involves dividing the integration into different regions and appropriately expanding the integrand. In the context of effective theories, distinct regions are represented by corresponding effective fields. The expanded integrals, achieved through the strategy of regions technique, exhibit a one-to-one correspondence with Feynman diagrams of effective field theories regularized in dimensional regularization.

For those solely interested in expanding a perturbative result with a small parameter, employing the strategy of regions method directly is a viable option without the necessity of constructing an effective Lagrangian. However, establishing an effective field theory provides significant advantages, particularly when aiming to derive all-order statements. In particular, the use of an effective Lagrangian allows us to derive factorization theorems as well as to resum large logarithmic contributions using Renormalization Group (RG) equations. Moreover, gauge invariance is evident in the Lagrangian, which can not be said for individual diagrams. The effective Lagrangian also offers a systematic approach to arrange higher power corrections by incorporating subleading terms.

The general approach for expanding a given Feynman integral in a specified kinematic limit involves the following steps [5]:

1. Identify all regions of the integrand that lead to singularities in the considered limit.

2. Expand the integrand in each identified region and integrate each expansion over the entire phase space.

3. Sum the results of the integrations over different regions to obtain the expansion of the original integral.

To ensure the effectiveness of this procedure, it is crucial to properly regularize all expanded integrals. Dimensional regularization alone may not always suffice, and additional analytic regulators or subtraction techniques might be necessary. Additionally, it is essential to consider each integration region only once to prevent double counting. While identifying regions leading to singularities is typically straightforward, it is important to note that certain cases may necessitate adding new regions to the list when increasing the number of loops in the diagram [6].

Now, we examine the most straightforward example relevant to the context of SCET, specifically a one-loop vertex diagram, as shown in fig. 1.1. This example is presented in ref. [1] and we revisit it here. For simplicity, we disregard complications associated with particle spin, as the momentum regions encountered in the computation of tensor integrals align with those in the scalar integral discussed below. Referring to fig. 1.1, the vertex correction involves assessing the following Feynman integral, where all internal propagators are assumed to be massless

$$I = i\pi^{-d/2}\mu^{4-d}\int d^dk \frac{1}{(k^2+i0)\left[(k+l)^2+i0\right]\left[(k+p)^2+i0\right]}\,, \tag{1.1}$$

where $d = 4-2\varepsilon$ is the dimensional regulator. We introduce the following Lorentz invariants

$$L^2 \equiv -l^2 - i0\,, \qquad P^2 \equiv -p^2 - i0\,, \qquad Q^2 \equiv -(l-p)^2 - i0\,. \tag{1.2}$$

we want to compute the integral in the limit in which the external legs carry large energies but small invariant masses, this is $L^2 \sim P^2 \ll Q^2$. We now introduce some basic notation used in SCET, light-cone coordinates. It is useful to define the four-vector

$$n^\mu = \frac{1}{\sqrt{2}}(1,0,0,1)\,. \tag{1.3}$$

We also define a conjugate vector $\bar{n}^\mu$ by reversing the sign of the spatial coordinates. Thus, n^μ and $\bar{n}^\mu$ satisfy,

$$n^2 = \bar{n}^2 = 0, \qquad \bar{n}\cdot n = 1. \tag{1.4}$$

Using the vectors n^μ and $\bar{n}^\mu$ we can decompose any other four-vector, p^μ, into its light-cone components,

$$p^\mu = p_+\bar{n}^\mu + p_- n^\mu + p_\perp^\mu = (p_+, p_-, p_\perp)_n, \tag{1.5}$$

with

$$p_+ = n\cdot p, \qquad p_- = \bar{n}\cdot p, \qquad p^2 = 2p_+p_- + p_\perp^2 = 2p_+p_- - \boldsymbol{p}^2. \tag{1.6}$$

where we use the notation $\boldsymbol{p} \equiv \vec{p}_\perp$. Light cone coordinates are commonly used in SCET literature (with slight changes in normalization) and we use them throughout this thesis. For completeness, we comment on them again in future sections.

We now introduce an expansion parameter λ which vanishes in the limit in which we are interested

$$\lambda^2 \sim \frac{P^2}{Q^2} \sim \frac{L^2}{Q^2}\,, \qquad \text{and} \qquad p^2 \sim l^2 \sim \lambda^2 Q^2\,. \tag{1.7}$$

Once again, this is the typical SCET expansion parameter. We choose the reference vectors in the directions of large momentum flow $p^\mu \approx Qn^\mu$ and $l^\mu \approx Q\bar{n}^\mu$. The components of p and l will then typically scale as follows

$$p^\mu \sim \left(\lambda^2, 1, \lambda\right) Q\,, \qquad \text{and} \qquad l^\mu \sim \left(1, \lambda^2, \lambda\right) Q\,. \tag{1.8}$$

However, the scaling is not unique. For instance, we could select the reference vector n^μ in a way that the perpendicular components of p^μ are zero, aligning with eq. 1.8, but also compatible with $\left(1, \lambda^2, \lambda^n\right), Q$ for any $n > 1$. Nevertheless, when employing the strategy of regions to compute the loop diagram, one finds that only scalings $k^\mu \sim (\lambda^a, \lambda^b, \lambda^c)Q$, where $a + b = 2c$, are significant. This scaling describes particles approaching the on-shell condition as $\lambda \to 0$. In this way, upon expanding the integrals, only the following four regions yield non-vanishing contributions

- **Hard** (denoted by h in the following) where the components of the integration momentum scale as $k^\mu \sim (1, 1, 1)\, Q$,
- **Collinear to $\boldsymbol{p}$** (denoted by c) where k scales as $k^\mu \sim (\lambda^2, 1, \lambda)\, Q$,
- **Collinear to $\boldsymbol{l}$** (denoted by $\bar{c}$) where k scales as $k^\mu \sim (1, \lambda^2, \lambda)\, Q$,
- **Soft** (denoted by s) where k scales as $k^\mu \sim (\lambda^2, \lambda^2, \lambda^2)\, Q$.

All other potential scalings of the integration momentum that do not match one of the four cases mentioned above result in scaleless integrals upon expansion. Consequently, they do not contribute to the final result. In SCET, each of the low-energy regions outlined above corresponds to a different field.

We can now compute the contribution of each non-vanishing region. However, it is insightful to start by considering an example of a scaling that does not contribute to the form factor case. In particular, we examine a soft scaling $k^\mu \sim (\lambda, \lambda, \lambda)Q$. The expansion of the propagator denominators in this scenario takes the form

$$(k+l)^2 = \overbrace{k^2}^{\mathcal{O}(\lambda^2)} + 2(\overbrace{k_+ \cdot l_-}^{\mathcal{O}(\lambda^3)} + \overbrace{k_- \cdot l_+}^{\mathcal{O}(\lambda)} + \overbrace{k_\perp \cdot l_\perp}^{\mathcal{O}(\lambda^2)}) + \overbrace{l^2}^{\mathcal{O}(\lambda^2)} = 2k_- \cdot l_+ + \mathcal{O}(\lambda^2)\,, \tag{1.9}$$

and analogously

$$(k+p)^2 = 2k_+ \cdot p_- + \mathcal{O}(\lambda^2)\,, \tag{1.10}$$

after which the hypothetical contribution becomes

$$i\pi^{-d/2}\mu^{4-d} \int d^d k \frac{1}{(k^2 + i0)\,(2k_- \cdot l_+ + i0)\,(2k_+ \cdot p_- + i0)}\,. \tag{1.11}$$

This integrals vanishes. It is interesting to observe that in the soft region the square of a four-momentum is proportional to λ^4:

$$p_s^2 \sim \lambda^4 Q^2 \sim \frac{L^2 P^2}{Q^2}\,. \tag{1.12}$$

The momenta scaling as λ^4 are often called *ultra soft* in the literature to distinguish them from the soft modes scaling as $p^2 \sim \lambda^2$, as the one we have just considered. Such modes

contribute for example to observables that are sensitive to small transverse momenta. The relevant theory in the presence of soft modes with $p^2 \sim \lambda^2$ is usually called $\mathrm{SCET_{II}}$. We discuss the difference between $\mathrm{SCET_I}$ and $\mathrm{SCET_{II}}$ in the following sections. It is crucial to check which momentum modes contribute to a given process and include all relevant regions in the effective Lagrangian.

To identify the integral that requires evaluation when the integration momentum is treated as hard, we examine the scaling behavior of the terms in the propagators as given in eq. 1.1. It is evident that $k^2 \sim \lambda^0 Q^2$; for the remaining two propagators, we observe

$$(k+l)^2 = \overbrace{k^2}^{\mathcal{O}(1)} + 2(\overbrace{k_+\cdot l_-}^{\mathcal{O}(\lambda^2)} + \overbrace{k_-\cdot l_+}^{\mathcal{O}(1)} + \overbrace{k_\perp\cdot l_\perp}^{\mathcal{O}(\lambda)}) + \overbrace{l^2}^{\mathcal{O}(\lambda^2)} = k^2 + 2k_-\cdot l_+ + \mathcal{O}(\lambda)\,, \tag{1.13}$$

and, similarly

$$(k+p)^2 = k^2 + 2k_+\cdot p_- + \mathcal{O}(\lambda)\,. \tag{1.14}$$

Therefore, in the hard region we have

$$I_h = i\pi^{-d/2}\mu^{4-d}\int d^dk \frac{1}{(k^2+i0)\,(k^2+2k_-\cdot l_+ + i0)\,(k^2+2k_+\cdot p_- + i0)}\,; \tag{1.15}$$

it coincides with the form factor integral with on shell external legs (i.e. calculated by setting $p^2 = l^2 = 0$ from the start). The integral evaluates to

$$\begin{aligned} I_h &= \frac{\Gamma(1+\varepsilon)}{2l_+\cdot p_-}\frac{\Gamma^2(-\varepsilon)}{\Gamma(1-2\varepsilon)}\left(\frac{\mu^2}{2l_+\cdot p_-}\right)^{\varepsilon} \\ &= \frac{\Gamma(1+\varepsilon)}{Q^2}\left(\frac{1}{\varepsilon^2}+\frac{1}{\varepsilon}\ln\frac{\mu^2}{Q^2}+\frac{1}{2}\ln^2\frac{\mu^2}{Q^2}-\frac{\pi^2}{6}\right)+\mathcal{O}(\varepsilon)\,. \end{aligned} \tag{1.16}$$

Whe collinear to p the integration momentum scales as $k^\mu \sim (\lambda^2, 1, \lambda)Q$. In this region $k^2 \sim \lambda^2 Q^2$, while

$$(k+l)^2 = 2k_-\cdot l_+ + \mathcal{O}(\lambda^2)\,, \qquad (k+p)^2 = \mathcal{O}(\lambda^2)\,. \tag{1.17}$$

By keeping only the leading term we find

$$\begin{aligned} I_c &= i\pi^{-d/2}\mu^{4-d}\int d^dk \frac{1}{(k^2+i0)\,(2k_-\cdot l_+ + i0)\,[(k+p)^2+i0]} \\ &= -\frac{\Gamma(1+\varepsilon)}{2l_+\cdot p_-}\frac{\Gamma^2(-\varepsilon)}{\Gamma(1-2\varepsilon)}\left(\frac{\mu^2}{P^2}\right)^{\varepsilon} \\ &= \frac{\Gamma(1+\varepsilon)}{Q^2}\left(-\frac{1}{\varepsilon^2}-\frac{1}{\varepsilon}\ln\frac{\mu^2}{P^2}-\frac{1}{2}\ln^2\frac{\mu^2}{P^2}+\frac{\pi^2}{6}\right)+\mathcal{O}(\varepsilon)\,. \end{aligned} \tag{1.18}$$

We observe that the integral scales as $P^{-2\varepsilon}$. Clearly, the calculation of the integral in the region collinear to l is identical to the calculation of the integral in the region collinear to p, eq. 1.18, except that one needs to replace P^2 with L^2 in the final result.

Finally, in the soft region all of the components of the integration momentum are proportional to λ^2, therefore

$$k^2 = \mathcal{O}(\lambda^4)\,, \quad (k+l)^2 = 2k_-\cdot l_+ + l^2 + \mathcal{O}(\lambda^3)\,, \text{ and } \quad (k+p)^2 = 2k_+\cdot p_- + p^2 + \mathcal{O}(\lambda^3)\,, \tag{1.19}$$

and the integral in the soft region is

$$\begin{aligned} I_s &= i\pi^{-d/2}\mu^{4-d}\int d^dk \frac{1}{(k^2+i0)\,(2k_-\cdot l_+ + l^2 + i0)\,(2k_+\cdot p_- + p^2 + i0)} \\ &= -\frac{\Gamma\,(1+\varepsilon)}{2l_+\cdot p_-}\Gamma(\varepsilon)\Gamma\,(-\varepsilon)\left(\frac{2l_+\cdot p_-\mu^2}{L^2P^2}\right)^{\varepsilon} \\ &= \frac{\Gamma(1+\varepsilon)}{Q^2}\left(\frac{1}{\varepsilon^2}+\frac{1}{\varepsilon}\ln\frac{\mu^2Q^2}{L^2P^2}+\frac{1}{2}\ln^2\frac{\mu^2Q^2}{L^2P^2}+\frac{\pi^2}{6}\right)+\mathcal{O}\,(\varepsilon)\,. \end{aligned} \tag{1.20}$$

The poles in the last line of eq. 1.20 are of ultraviolet origin. As expected, the result depends on the new soft scale $\Lambda^2_{\text{soft}} \sim P^2L^2/Q^2$.

To prevent any potential double counting between different regions, it is required that we subtract the overlap (known as zero-bin contribution) from the collinear region, see ref. [7]. This zero-bin contribution is derived by expanding the collinear integrand around the soft limit. The resulting overlap contribution is characterized by scaleless integrals, which conveniently vanish when using dimensional regularization. As both the soft and collinear integrals are dependent on a single scale (namely, P^2 for collinear integrals and Λ^2_{soft} for soft integrals), any further expansions of the integrands lead to scaleless integrals. Consequently, systematic expansions across different regions eliminate the need for zero-bin subtractions in dimensional regularization.

However, if higher-order terms are not consistently expanded, the possibility of non-zero overlap contributions arises, necessitating subtraction to avoid double counting. Examples where non-vanishing zero-bin contributions have been encountered in SCET include processes such as Drell-Yan production and dijet production, discuss further in subsequent chapters. These cases involve soft and collinear phase-space integrals with multiple scales, adding complexity to the resummation process. The coexistence of non-vanishing zero-bin contributions points to an incomplete scale separation, arising consideration of whether an effective theory can be formulated to achieve complete scale separation.

In this way, the final analytical expression for the integral in eq. 1.1 under the condition where $L^2 \sim P^2 \ll Q^2$ is as follows

$$I_h = \frac{\Gamma\,(1+\varepsilon)}{Q^2}\left(\frac{1}{\varepsilon^2}+\frac{1}{\varepsilon}\ln\frac{\mu^2}{Q^2}+\frac{1}{2}\ln^2\frac{\mu^2}{Q^2}-\frac{\pi^2}{6}+\mathcal{O}(\lambda)\right), \tag{1.21}$$

$$I = \frac{\Gamma\,(1+\varepsilon)}{Q^2}\left(-\frac{1}{\varepsilon^2}-\frac{1}{\varepsilon}\ln\frac{\mu^2}{P^2}-\frac{1}{2}\ln^2\frac{\mu^2}{P^2}+\frac{\pi^2}{6}+\mathcal{O}(\lambda)\right), \tag{1.22}$$

$$I = \frac{\Gamma\,(1+\varepsilon)}{Q^2}\left(-\frac{1}{\varepsilon^2}-\frac{1}{\varepsilon}\ln\frac{\mu^2}{L^2}-\frac{1}{2}\ln^2\frac{\mu^2}{L^2}+\frac{\pi^2}{6}+\mathcal{O}(\lambda)\right), \tag{1.23}$$

$$I_s = \frac{\Gamma\,(1+\varepsilon)}{Q^2}\left(\frac{1}{\varepsilon^2}+\frac{1}{\varepsilon}\ln\frac{\mu^2Q^2}{L^2P^2}+\frac{1}{2}\ln^2\frac{\mu^2Q^2}{L^2P^2}+\frac{\pi^2}{6}+\mathcal{O}(\lambda)\right), \tag{1.24}$$

thus

$$I \equiv I_h + I + I + I_s = \frac{1}{Q^2}\left(\ln\frac{Q^2}{L^2}\ln\frac{Q^2}{P^2}+\frac{\pi^2}{3}+\mathcal{O}(\lambda)\right) \tag{1.25}$$

The result remains independent of the dimensional regulator ε and it coincides with the result achieved by directly computing the integral in eq. 1.1 and subsequently expanding the result in the limit as λ approaches 0.

We emphasize that the infrared divergences identified in the hard region cancel against the ultraviolet divergences arising from the combined soft and collinear contributions. This characteristic holds universally and demands an interplay of the logarithmic terms present in the different integrals, canceling the intermediate scales:

$$-\frac{1}{\varepsilon}\ln\frac{\mu^2}{P^2}-\frac{1}{\varepsilon}\ln\frac{\mu^2}{L^2}+\frac{1}{\varepsilon}\ln\frac{\mu^2Q^2}{L^2P^2}=-\frac{1}{\varepsilon}\ln\frac{\mu^2}{Q^2}\,. \tag{1.26}$$

The necessity for the infrared divergences originating from the hard region to cancel the ultraviolet divergences emerging from the soft and collinear regions imposes a constraint on the infrared pole structure in a generic amplitude.

1.2 SCET$_{\rm I}$

The exercise presented in the last section serves as an example of what we achieve by constructing an effective theory. Nonetheless, the construction of an effective lagrangian is advantageous with respect to the strategy of regions as it allows us to derive all-order statements, obtain factorization theorems and resum large logarithms. Once all momentum regions are identified we need to obtain a Lagrangian whose Feynman rules reproduce the same diagrams obtained by the strategy of regions. Some complications arise when considering QCD, in particular

1. Different components of the quark and gluon fields scale differently with the expansion parameter λ.
2. The theory should be gauge invariant, and it is also necessary for gauge transformations to preserve the scaling of the fields.
3. Wilson lines are needed in order to preserve gauge invariance of non-local operators.

1.2.1 Scaling of the fields

Following the example presented when studying the strategy of regions, we consider four different regions with their momentum scaling as follows

- **Hard** (h) with momentum $k^\mu\sim(1,1,1)\,Q$,
- **Collinear** (c) with momentum $k^\mu\sim(\lambda^2,1,\lambda)\,Q$,
- **Anticollinear** $(\bar c)$ with momentum $k^\mu\sim(1,\lambda^2,\lambda)\,Q$,
- **Soft** (s) with momentum $k^\mu\sim(\lambda^2,\lambda^2,\lambda^2)\,Q$.

In the effective field theory, we need an effective field corresponding to each of the different momentum scalings. Thus, we introduce the following effective fields for quark and gluon fields respectively

$$\begin{aligned}\psi&\to\psi_c+\psi_{\bar c}+\psi_s,\\ A^\mu&\to A^\mu_c+A^\mu_{\bar c}+A^\mu_s,\end{aligned} \tag{1.27}$$

In order to derive the effective lagrangian, we substitute the effective fields in the QCD Lagrangian and eliminate the suppressed terms, the resulting expression holds at tree level. At higher orders, certain matching corrections emerge, but they can be addressed by adjusting the coefficients of tree-level operators.

In order to properly identify the suppressed terms, we need to know how each field scales with the expansion parameter λ. We can obtain the proper scaling of each component by computing the propagator of the field.For the gluon field we have the following

$$\langle 0|T\{A_\mu^a(x)A_v^b(0)\}|0\rangle = \int \frac{d^4p}{(2\pi)^4}\frac{i}{p^2+i0}e^{-ip\cdot x}\left[-g_{\mu v}+\xi\frac{p_\mu p_v}{p^2}\right]\delta^{ab}, \tag{1.28}$$

where a, b are color indices ($A_\mu = A_\mu^a t^a$, where t^a are the generators of SU(N)). In the following, we consider $A_\mu = A_\mu^a t^a$. The position x^μ is the Fourier conjugate of the momentum p^μ so that $p\cdot x \sim \mathcal{O}\left(\lambda^0\right)$. The part of the propagator that involves the gauge parameter ξ scales like $d^4p/(p^2)^2 p_\mu p_v \sim p_\mu p_v$. As gauge symmetry transforms as their associated momentum we expect that in a general gauge $A_\mu \sim p_\mu$. For soft and collinear gluons the field components scale as

$$\begin{aligned}\left(n\cdot A_s, \bar{n}\cdot A_s, A_{s\perp}^\mu\right) &\sim \left(\lambda^2,\lambda^2,\lambda^2\right)\\ \left(n\cdot A_c, \bar{n}\cdot A_c, A_{c\perp}^\mu\right) &\sim \left(\lambda^2,1,\lambda\right).\end{aligned} \tag{1.29}$$

Soft gluons appear suppressed with respect to the collinear component, except for the n-component. The soft quark propagator is given by

$$\left\langle 0\left|T\left\{\psi_s(x)\bar{\psi}_s(0)\right\}\right|0\right\rangle = \int \frac{d^4p}{(2\pi)^4}\frac{i\not{p}}{p^2+i0}e^{-ip\cdot x} \sim \left(\lambda^2\right)^4\frac{\lambda^2}{\lambda^4} = \lambda^6, \tag{1.30}$$

yielding $\psi_s(x) \sim \lambda^3$. The collinear case needs some special treatment as it should be further factorized into two distinct fields, which scale differently with the parameter λ, this is

$$\psi_c = \xi_c + \eta_c = P_+\psi + P_-\psi, \tag{1.31}$$

where we have define the projectors

$$P_+ = \frac{\not{n}\bar{\not{n}}}{2}, \quad P_- = \frac{\bar{\not{n}}\not{n}}{2}. \tag{1.32}$$

One can immediately check that they are indeed projection operators and that they verify $P_+ + P_- = 1$ and $P_\pm^2 = P_\pm$. In this way, the quark propagator

$$\begin{aligned}\left\langle 0\left|T\left\{\xi_c(x)\bar{\xi}_c(0)\right\}\right|0\right\rangle &= \int \frac{d^4p}{(2\pi)^4}e^{-ip\cdot x}\frac{\not{n}\bar{\not{n}}}{2}\frac{i\not{p}}{p^2+i0}\frac{\bar{\not{n}}\not{n}}{2}\\ &= \int \frac{d^4p}{(2\pi)^4}e^{-ip\cdot x}\frac{i\bar{n}\cdot p\,\not{n}}{p^2+i0} \sim \frac{\lambda^4}{\lambda^2} = \lambda^2.\end{aligned} \tag{1.33}$$

Thus, $\xi_c \sim \lambda$. The exact same derivation can be done for η_c which yields $\eta_c \sim \lambda^2$. The fields ξ and η are usually known as good and bad components, as η (bad) is suppressed with respect to ξ (good). Soft quark fields are suppressed with respect to collinear ones.

Anticollinear fields scale the same way as collinear ones. To sum up, we find that quark and gluon fields scale as

$$\xi_{c/\bar{c}} \sim \lambda \tag{1.34}$$

$$\eta_{c/\bar{c}} \sim \lambda^2 \tag{1.35}$$

$$(n \cdot A_s, \bar{n} \cdot A_s, A^\mu_{s\perp}) \sim (\lambda^2, \lambda^2, \lambda^2) \tag{1.36}$$

$$(n \cdot A_{c/\bar{c}}, \bar{n} \cdot A_{c/\bar{c}}, A^\mu_{c/\bar{c}\perp}) \sim (\lambda^2, 1, \lambda). \tag{1.37}$$

1.2.2 Effective Lagrangian at leading power

Once the scaling of the effective fields has been established, the next step to build the effective lagrangian is to substitute the effective fields in the full QCD action. This can be schematically written as

$$S = S_s + S_c + S_{\bar{c}} + S_{c+s} + S_{\bar{c}+s}, \tag{1.38}$$

where the different terms are collected in terms of their content. S_s contains purely soft interaction, S_c the collinear terms and S_{c+s} describes the collinear and soft mixed interactions. The anticollinear terms are the same as the collinear ones and can be obtained just by changing collinear fields to anticollinear fields. In this way, the collinear action is given by

$$\begin{aligned} S_c &= \int d^4x \left(\bar{\xi}_c + \bar{\eta}_c\right) \left[\not{n}\, i\bar{n}\cdot D_c + \not{\bar{n}}\, in\cdot D_c + i\not{D}_{c\perp}\right] (\xi_c + \eta_c) - \frac{1}{4}\left(F^{c,a}_{\mu\nu}\right)^2 \\ &= \int d^4x \bar{\xi}_c \not{\bar{n}}\, in\cdot D_c \bar{\xi}_c + \bar{\xi}_c i\not{D}_{c\perp}\eta_c + \bar{\eta}_c i\not{D}_{c\perp}\bar{\xi}_c + \bar{\eta}_c \not{n}\, i\bar{n}\cdot D_c\eta_c - \frac{1}{4}\left(F^{c,a}_{\mu\nu}\right)^2. \end{aligned} \tag{1.39}$$

where the covariant derivative is defined as

$$iD^s_\mu = i\partial_\mu + gA^s_\mu(x), \quad iD^c_\mu = i\partial_\mu + gA^c_\mu(x) \tag{1.40}$$

This form of the action is not ideal since $\xi_c \sim \lambda$ and $\eta_c \sim \lambda^2$ fields are mixed. Due to the action being quadratic in η_c, we can integrate over the suppressed fields exactly. This is done by performing the shift

$$\eta_c \to \eta_c - \frac{\not{\bar{n}}}{2}\frac{1}{i\bar{n}\cdot D_c} i\not{D}_{c\perp}\xi_c. \tag{1.41}$$

Therefore, the collinear action can be rewritten as

$$S_c = \int d^4x \bar{\xi}_c \left[in\cdot D_c + i\not{D}_{c\perp}\frac{1}{i\bar{n}\cdot D_c} i\not{D}_{c\perp}\right]\xi_c - \frac{1}{4}\left(F^{c,a}_{\mu\nu}\right)^2 + \bar{\eta}_c \not{\bar{n}}\, i\bar{n}\cdot D_c\eta_c, \tag{1.42}$$

which can be integrated over. There are some details to the integration that we do not discuss here and can be found in ref. [1]. The collinear part is finally written as

$$S_c = \int d^4x \bar{\xi}_c \left[in\cdot D_c + i\not{D}_{c\perp}\frac{1}{i\bar{n}\cdot D_c} i\not{D}_{c\perp}\right]\xi_c - \frac{1}{4}\left(F^{c,a}_{\mu\nu}\right)^2. \tag{1.43}$$

The soft action is obtained in the same way and is given by

$$S_s = \int d^4x \bar{\psi}_s i \not{D}_s \psi_s - \frac{1}{4} \left(F^{s,a}_{\mu\nu}\right)^2 , \tag{1.44}$$

where the soft field strength is given

$$igF^{s,a}_{\mu\nu} t^a = \left[iD^s_\mu, iD^s_v\right] . \tag{1.45}$$

Next, we examine the soft and collinear mixed effective action, S_{s+c}. While the general construction of such terms is intricate and typically carried out in position space formalism, we focus specifically on investigating the leading power terms. A more detailed discussion on how to treat subleading terms is given in chapter 4 of this thesis. Consequently, we need to consider certain aspects: ψ_s exhibits power suppression in comparison to collinear fermion fields, resulting in the absence of soft fermion fields in leading power interactions with collinear fields. Additionally, since $\bar{n} \cdot A_s$ and $A^\mu_{s\perp}$ are power suppressed relative to their collinear counterparts, only terms involving $n \cdot A_s$ emerge. Consequently, these conditions dictate that the leading power term of S_{s+c} is derived by substituting

$$A^\mu_c \to A^\mu_c + n \cdot A_s \bar{n}^\mu \tag{1.46}$$

in S_c. To obtain the final result, it is necessary to perform a derivative expansion in the resultant action, corresponding to an expansion in small momentum components. Consequently, we delve into the interaction between a soft gluon and a collinear fermion

$$S_{s+c} = \int d^4x \bar{\xi}_c(x) \not{\bar{n}}\, n \cdot A_s(x) \xi_c(x). \tag{1.47}$$

This expression emerges from substituting the condition in eq. 1.46 into the S_c action. The momentum is composed of both a soft and a collinear component, with a scaling akin to that of a collinear momentum. Specifically, this implies the scaling of the form

$$\begin{aligned} p^\mu_c + p^\mu_s \sim p^\mu_c &\sim \left(\lambda^2, 1, \lambda\right) , \\ x^\mu &\sim \left(1, \lambda^{-2}, \lambda^{-1}\right) , \end{aligned} \tag{1.48}$$

where only the term involving x_- is leading power. Thus, we expand the action S_{s+c} into a Taylor series

$$\begin{aligned} S_{s+c} &= \int d^4x \bar{\xi}_c(x) \frac{\not{\bar{n}}}{2} \xi_c(x) \left[1 + x_\perp \cdot \partial_\perp + x_+ \cdot \partial_+ + \ldots\right] n \cdot A_s(x) \Big|_{x=x^-} \\ &= \int d^4x \bar{\xi}_c(x) \frac{\not{\bar{n}}}{2} \xi_c(x) n \cdot A_s\left(x_-\right) + \mathcal{O}(\lambda), \end{aligned} \tag{1.49}$$

since all terms containing derivatives in eq. 1.49 contribute to subleading terms. This expansion is referred to as the multipole expansion, as outlined in ref. [8]. By examining the various terms within the SCET effective action, we reach the conclusive expression for the SCET Lagrangian at leading power

$$\mathcal{L}_{\text{SCET}} = \bar{\psi}_s i \not{D}_s \psi_s + \bar{\xi}_c \not{\bar{n}} \left[in \cdot D + \frac{i}{2} \not{D}_{c\perp} \frac{1}{i\bar{n} \cdot D_c} i \not{D}_{c\perp}\right] \xi_c - \frac{1}{4} \left(F^{s,a}_{\mu\nu}\right)^2 - \frac{1}{4} \left(F^{c,a}_{\mu\nu}\right)^2 + \{c \to \bar{c}\}, \tag{1.50}$$

where the anticollinear part is obtained by changing $c \to \bar{c}$, $n \leftrightarrow \bar{n}$ and $x_- \to x_+$. The mixed covariant derivative is

$$in \cdot D = in \cdot \partial + gn \cdot A_c(x) + gn \cdot A_s\left(x_-\right), \tag{1.51}$$

and the collinear field strength is given by

$$igF^{c,a}_{\mu\nu} t^a = \left[iD_\mu, iD_v\right]. \tag{1.52}$$

The covariant derivative that appears in the second commutator is as follows

$$D^\mu = n \cdot D \bar{n}^\mu + \bar{n} \cdot D_c n^\mu + D^\mu_{c\perp}. \tag{1.53}$$

1.2.3 Gauge transformations

In this section, we briefly explore gauge transformations of the recently examined effective Lagrangian. Given the splitting of the gauge field into distinct soft and collinear components and the necessity for gauge transformations to preserve the scaling of the fields, we perform different gauge transformations for each field:

$$V_s(x) = \exp\left[i\alpha^a_s(x) t^a\right], \tag{1.54}$$
$$V_c(x) = \exp\left[i\alpha^a_c(x) t^a\right], \tag{1.55}$$

for soft and collinear gauge transformations respectively. The gauge transformations exhibit scaling behavior as their corresponding fields: $\partial\alpha^a_s(x) \sim \lambda^2 \alpha^a_s(x)$ and $\partial_\mu \alpha^a_c(x) \sim \left(\lambda^2, 1, \lambda\right) \alpha^a_c(x)$. The soft gauge transformation operates on the soft fields in the usual manner

$$\psi_s(x) \to V_s(x) \psi_s(x) \tag{1.56}$$
$$A^\mu_s(x) \to V_s(x) A^\mu_s(x) V^\dagger_s(x) + \frac{i}{g} V_s(x) \partial_\mu V^\dagger_s(x) \tag{1.57}$$
$$D^\mu_s(x) \to V_s(x) D^\mu_s V^\dagger_s(x) \tag{1.58}$$

The soft gauge transformations act over collinear fields as

$$\psi_c(x) \to V_s\left(x_-\right) \psi_c(x), \tag{1.59}$$
$$A^\mu_c(x) \to V_s\left(x_-\right) A^\mu_c(x) V^\dagger_s\left(x_-\right) \tag{1.60}$$
$$D^\mu(x) \to V_s\left(x_-\right) D^\mu(x) V^\dagger_s\left(x_-\right). \tag{1.61}$$

It is important to highlight the use of the multipole expansion and the substitution of $x \to x_-$ in the soft fields. This expansion is crucial in preventing the emergence of a series of troublesome power corrections. Additionally, the collinear gauge field transforms similar to a matter field, devoid of an inhomogeneous term. This ensures the appropriate transformation of the mixed covariant derivative. When examining the collinear gauge transformation on collinear and soft fields, it becomes evident that soft fields remain unaffected, while collinear fields transform the usual way

$$\xi_c(x) \to V_c(x) \xi_c(x), \qquad D^\mu \to V_c(x) D^\mu V^\dagger_c(x), \tag{1.62}$$

$$\psi_s(x) \to \psi_s(x), \qquad D_s^\mu \to D_s^\mu, \tag{1.63}$$

$$A_c^\mu(x) \to V_c(x) A_c^\mu V_c^\dagger(x) + \frac{1}{g} V_c(x) \left[i\partial^\mu + g\bar{n}^\mu n \cdot A_s\left(x_-\right), V_c^\dagger(x) \right]. \tag{1.64}$$

Having established the transformation of covariant derivatives, it is straightforward to confirm that the effective Lagrangian remains invariant under both soft and collinear gauge transformations.

1.2.4 SCET vector current and matching coefficient

The effective Lagrangian dictates the interaction between soft and collinear fields, as well as mixed interactions between them. However, what is currently absent are operators detailing the interaction between the two collinear sectors. The tree-level diagram in QCD can be substituted with the SCET operator

$$J^\mu = \bar{\psi}\gamma^\mu\psi \to \bar{\xi}_c \gamma^\mu \xi_{\bar{c}} \tag{1.65}$$

We can decompose γ^μ in terms of its light cone components and using the projection properties we find that only the transverse term survives, this is

$$\bar{\xi}_c \gamma^\mu \tilde{\xi}_{\bar{c}} = \bar{\xi}_c \left[n^\mu \bar{\not{n}} + \bar{n}^\mu \not{n} + \gamma_\perp^\mu \right] \xi_{\bar{c}} = \bar{\xi}_c \gamma_\perp^\mu \xi_{\bar{c}} \tag{1.66}$$

Nevertheless, this operator proves inadequate for loop calculations or when incorporating collinear gluons. Typically, operators involving derivatives are power-suppressed, but in SCET, the derivatives related to the large momentum component of collinear fields, generally denoted as $\bar{n} \cdot \partial \phi_c$, exhibit a scaling of $\sim \lambda^0 Q \phi_c$. Therefore, to formulate a more comprehensive gauge-invariant operator at leading power, we explore the series:

$$\phi_c(x + t\bar{n}) = \sum_{n=0}^{\infty} \frac{t^n}{n!} (\bar{n} \cdot \partial)^n \phi_c(x) \tag{1.67}$$

When including this expansion into a convolution we get

$$\int dt C(t) \phi_c(x + t\bar{n}) = \sum_{n=0}^{\infty} \frac{C_n}{n!} (\bar{n} \cdot \partial)^n \phi_c(x) \tag{1.68}$$

where C_n is the n-th moment of the coefficient function

$$C_n = \int dt C(t) t^n \tag{1.69}$$

Rather than incorporating an arbitrary number of derivatives, we opt to smear the field ϕ_c along the light cone, as depicted in equation 1.68. The function $C(t)$ encapsulates information regarding the Wilson coefficients of the higher derivative operators. The introduction of this field smearing renders the operator non-local, necessitating careful attention to maintain gauge invariance. We consider now the operator defining the quark parton distribution function

$$\bar{\xi}_c(x + t\bar{n}) \frac{\bar{\not{n}}}{2} \xi_c(x). \tag{1.70}$$

This operator is not gauge invariant. To solve this problem we need to transport the gauge transformation at the point x to the point $x+t\bar{n}$. This can be achieved using the collinear version of the Wilson line, defined as

$$[x+t\bar{n},x]=\mathbf{P}\exp\left[ig\int_0^t dt'\bar{n}\cdot A_c(x+t\bar{n})\right] \tag{1.71}$$

It is important to observe that the exponent is a color matrix, signifying that the symbol $\mathbf{P}$ denotes an ordering prescription. The path ordering establishes that the color matrix at a later time is positioned to the left of the earlier ones. The Wilson line gauge transforms as follows

$$[x+t\bar{n},x]\to V_c(x+t\bar{n})[x+t\bar{n},x]V_c^\dagger(x) \tag{1.72}$$

which renders the operator in eq. 1.70 gauge invariant. In SCET is useful to define a Wilson line running from infinity along $\bar{n}^\mu$ to x^μ as

$$W_c(x)=[x,x-\infty\bar{n}] \tag{1.73}$$

so a Wilson line defined over a finite segment can be written as

$$[x+t\bar{n},x]=W_c(x+t\bar{n})W_c^\dagger(x) \tag{1.74}$$

This implies that to transition from x to $x+t\bar{n}$, we initially travel from x to infinity and then return to $x+t\bar{n}$. The segment traveled in both directions cancels out due to the unitarity of the matrix, resulting in the finite matrix element. Utilizing the Wilson line, $W_c(x)$, we can establish the basic SCET building blocks

$$\chi_c(x)\equiv W_c^\dagger(x)\xi_c(x), \tag{1.75}$$

$$\mathcal{A}_c^\mu(x)\equiv W_c^\dagger(x)D_c^\mu W_c(x), \tag{1.76}$$

These blocks remain invariant by collinear gauge transformations that approach zero at infinity. These building blocks facilitate the construction of gauge-invariant SCET operators. The introduction of soft Wilson lines will be addressed subsequently to disentangle soft interactions. With these considerations, we can now formulate the more comprehensive SCET current operator at leading power.

$$J^\mu(0)=\int ds\int dt\tilde{C}_V(s,t)\bar{\chi}_c(t\bar{n})\gamma_\perp^\mu\chi_{\bar{c}}(sn). \tag{1.77}$$

Notice that at the leading order, the matching coefficient $\tilde{C}_V(s,t)=\delta(s)\delta(t)$. It is pertinent to consider that the Fourier transform of this coefficient depends solely on the large component of the transferred momentum, denoted as $Q^2=(n\cdot l)(\bar{n}\cdot p)$. To demonstrate this, we shift the field to the origin $x=0$ using the momentum operator and subsequently take the matrix element between a state featuring an incoming quark with momentum l^μ and an outgoing quark with momentum p^μ, this is

$$\langle q(p)\left|J^\mu(0)\right|q(l)\rangle=\int ds\int dt\tilde{C}_V(s,t)e^{-isn\cdot l}e^{it\bar{n}\cdot p}\bar{u}(p)\gamma_\perp^\mu u(l)$$

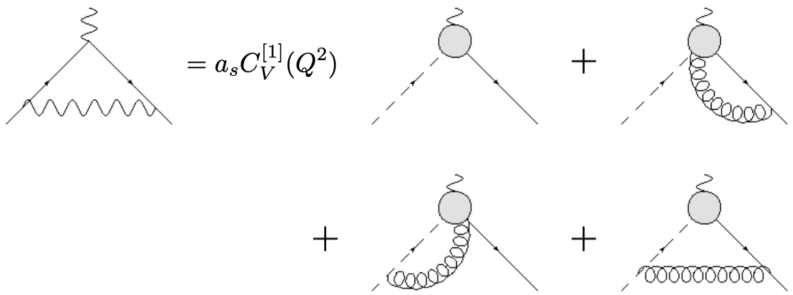

Figure 1.2: Diagrams that contribute to the one-loop contribution of C_V. Figure credit to D. Gutierrez-Reyes, ref. [3].

$$= C_V\big((n\cdot l)(\bar{n}\cdot p)\big)\bar{u}(p)\gamma_\perp^\mu u(l). \tag{1.78}$$

This fact arises from the fact that SCET exhibits invariance under a rescaling transformation, where $n^\mu \to \alpha n^\mu$ and $\bar{n}^\mu \to 1/\alpha \bar{n}^\mu$. This rescaling, known as reparametrization invariance ref. [9], ensures that the physics remains independent of the precise choice of reference vectors employed in establishing the effective theory.

1.2.5 Matching coefficient at NLO

In this section, we briefly explore the computation of the explicit one-loop contribution of C_V. The relevant Feynman diagrams are illustrated in fig. 1.2. Alongside the loop diagrams involving collinear fields and soft exchanges, there exists a contribution coming from the one-loop correction to the Wilson coefficient. The vertices, where a collinear gluon is emitted from the current, are derived by expanding the Wilson line in terms of the coupling using the building blocks.

Setting the low-energy scales P^2 and L^2 to zero renders the soft and collinear integrals scaleless. Consequently, the full theory equates to the hard region, and on the effective theory side, only the one-loop contribution of the Wilson coefficient persists. Thus, we determine the Wilson coefficient by computing the on-shell form factor with $P^2 = L^2 = 0$

$$C_V^{\text{bare}}\left(\epsilon, Q^2\right) = 1 + a_s(\mu) C_F \left(-\frac{2}{\epsilon^2} - \frac{3}{\epsilon} + \frac{\pi^2}{6} - 8 + \mathcal{O}(\epsilon)\right)\left(\frac{Q^2}{\mu^2}\right)^{-\epsilon} + \mathcal{O}\left(a_s^2\right), \tag{1.79}$$

where $a_s(\mu) = \alpha_s(\mu)/(4\pi)$ and the color structure is given by $t^a t^a = C_F \mathbf{1} = \left(N_c^2 - 1\right) / \left(2N_c\right)\mathbf{1}$. This coefficient needs to be renormalized by absorbing the divergencies into a multiplicative Z-factor

$$C_V\left(Q^2, \mu^2\right) = Z^{-1}\left(\epsilon, Q^2, \mu\right) C_V^{\text{bare}}\left(\epsilon, Q^2\right). \tag{1.80}$$

The final result is given by

$$C_V\left(Q^2, \mu^2\right) = 1 + a_s(\mu) C_F \left(-\ln^2\frac{Q^2}{\mu^2} + 3\ln\frac{Q^2}{\mu^2} + \frac{\pi^2}{6} - 8\right) + \mathcal{O}\left(a_s^2\right) \tag{1.81}$$

A distinctive aspect of this computation, compared to other analogous calculations in quantum field theory, is the appearance of a $1/\epsilon^2$ divergence. This divergence emerges due to the presence of both soft and collinear divergences. Consequently, the Wilson coefficient encompasses double logarithms, and the anomalous dimension regulating the RG equation of the Wilson coefficient incorporates a logarithmic term

$$\frac{d}{d\ln\mu}C_V\left(Q^2,\mu\right)=\left[\Gamma_{\rm cusp}\ \left(a_s\right)\ln\frac{Q^2}{\mu^2}+\gamma_V\left(a_s\right)\right]C_V\left(Q^2,\mu\right) \tag{1.82}$$

The cusp, $\Gamma_{\rm cusp}$, and non-cusp, γ_V, anomalous dimensions are known up to $\mathcal{O}\left(a_s^4\right)$. While their explicit expressions are not provided here, they can be found in ref. [10]. The matching coefficient C_V is similarly known up to the same accuracy, refs. [11, 12]. The additional logarithm in the anomalous dimension, as present in the RG equation in eq. 1.82, serves as a distinctive feature. It is essential to recognize that the dependence on this logarithm is solely linear, thereby preserving the integrity of the expansion of the anomalous dimensions despite the presence of large logarithms.

1.2.6 Decoupling soft and collinear modes

Our final consideration involves the disentanglement of soft radiation from the collinear fields. This can be achieved by introducing the soft Wilson line

$$S_n(x)=\mathbf{P}\exp\left[ig\int_{-\infty}^{0}dsn\cdot A_s(x+sn)\right] \tag{1.83}$$

which fulfills the equality $n\cdot D_s S_n(x)=0$. We can then redefine the collinear fields as

$$\xi_c=S_n\left(x_-\right)\xi_c^{(0)} \tag{1.84}$$

$$A_c^{\mu}=S_n\left(x_-\right)A_c^{(0)\mu}S_n^{+}\left(x_-\right). \tag{1.85}$$

The soft and collinear mixed interaction Lagrangian can be rewritten as follows

$$\begin{aligned}\mathcal{L}_{c+s}&=\bar{\xi}_c\frac{\bar{\not{n}}}{}in\cdot D\xi_c=\bar{\xi}_c\frac{\bar{\not{n}}}{}\left(in\cdot D_s+n\cdot A_c\right)\xi_c\\&=\bar{\xi}_c^{(0)}\frac{\bar{\not{n}}}{}\left(in\cdot\partial_s+n\cdot A_c^{(0)}\right)\xi_c^{(0)}=\bar{\xi}_c^{(0)}\frac{\bar{\not{n}}}{}in\cdot D_c^{(0)}\xi_c^{(0)},\end{aligned} \tag{1.86}$$

where the decoupling has removed the soft and collinear mixed interactions from the leading power Lagrangian. In this way, the full SCET Lagrangian takes the form

$$\mathcal{L}_{\rm SCET}=\mathcal{L}_c^{(0)}+\mathcal{L}_{\bar{c}}^{(0)}+\mathcal{L}_s. \tag{1.87}$$

This expression signifies that we are dealing with independent theories governing soft and collinear particles. Additionally, the states can be separated as

$$|X\rangle=|X_c\rangle\otimes|X_{\bar{c}}\rangle\otimes|X_s\rangle \tag{1.88}$$

The decoupling of soft radiation does not imply its complete elimination; instead, it appears as soft Wilson lines aligned with the direction of energetic particles. For instance, the vector current can be rewritten as

$$\bar{\chi}_c(t\bar{n})\gamma_{\perp}^{\mu}\chi_{\bar{c}}(sn)=\bar{\chi}_c^{(0)}(t\bar{n})\bar{S}_n^{\dagger}(0)\gamma_{\perp}^{\mu}S_{\bar{n}}(0)\chi_{\bar{c}}^{(0)}(sn) \tag{1.89}$$

In chapter 2, we show how the soft Wilson lines lead to the appearance of a soft function that encapsulates the contribution of soft gluon radiation.

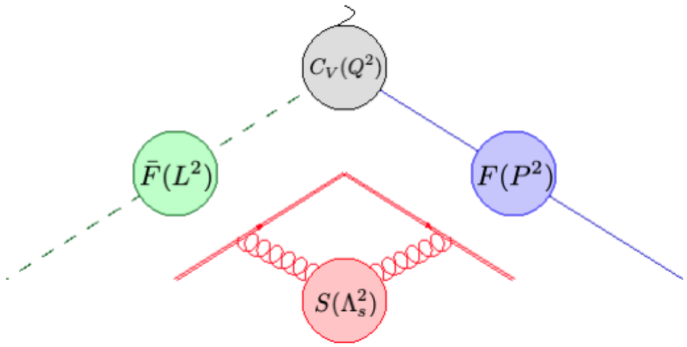

Figure 1.3: Factorized Sudakov form factor. Figure credit to D. Gutierrez-Reyes, ref. [3].

1.2.7 Resummation and evolution

As a result of the derived Lagrangian and the decoupling of soft and collinear interaction, the Sudakov form factor can be rewritten as

$$\mathcal{F}\left(Q^2, L^2, P^2\right) = C_V\left(Q^2, \mu\right) F\left(P^2, \mu\right) \bar{F}\left(L^2, \mu\right) S\left(\Lambda_s^2, \mu\right). \tag{1.90}$$

where both collinear F and anticollinear $\bar{F}$ functions are identical. The soft function is dependent on a soft scale given by $\Lambda_s^2 = L^2P^2/Q^2$. This decomposition is shown graphically in fig. 1.3. Each of the items satisfies distinct RG equations, and solving them allows for the resummation of significant perturbative logarithms inherent in fixed-order calculations. This process involves assessing each function in eq.1.90 at its intrinsic scale and subsequently evolving them to a common reference scale. Consequently, logarithmic terms like $\alpha^n \ln^m\left(Q^2/p^2\right)$ with $m \leq 2n$ and $p^2 = P^2, L^2, Q^2$ are effectively resummed. This resummation safeguards the conventional perturbative expansion of these functions. Notably, processes such as the one depicted in fig.1.3 exhibit Sudakov logarithms, characterized by $m = 2n$, arising from the intricate interplay of soft and collinear physics.

All the matrix elements in the effective theory depend on the renormalization scale, μ. Since any given cross section can not depend on this scale, the dependence must cancel in the product in eq. 1.90. Therefore, the sum of the anomalous dimensions of every function should cancel. In eq. 1.82 we gave an RG equation for the Wilson coefficient and here we show the same equation for collinear and soft factors,

$$\frac{d}{d\ln\mu} F\left(P^2, \mu\right) = -\left[\Gamma_{\text{cusp}}\left(a_s\right) \ln\frac{P^2}{\mu^2} + \gamma_F\left(a_s\right)\right] F\left(P^2, \mu\right), \tag{1.91}$$

$$\frac{d}{d\ln\mu} S\left(\Lambda_s^2, \mu\right) = \left[\Gamma_{\text{cusp}}\left(a_S\right) \ln\frac{\Lambda_s^2}{\mu^2} + \gamma_S\left(a_S\right)\right] S\left(\Lambda_s^2, \mu\right). \tag{1.92}$$

The cancellation of the anomalous dimensions is given by

$$\Gamma_{\text{cusp}}\left(a_S\right) \ln\frac{Q^2}{\mu^2} + \gamma_V\left(a_s\right) - \Gamma_{\text{cusp}}\ \left(a_S\right)\left(\ln\frac{P^2}{\mu^2} + \ln\frac{L^2}{\mu^2}\right) - 2\gamma_F\left(a_S\right)$$

$$+\Gamma_{\rm cusp}\left(a_s\right)\ln\frac{\Lambda_s^2}{\mu^2}+\gamma_S\left(a_s\right)=0 \tag{1.93}$$

To achieve a complete cancelation of the logarithms, it is imperative that all anomalous dimensions exhibit linearity in the logarithmic terms, and their coefficients remain uniform across various instances. To effectively resum the extensive logarithms within the form factor, each component is evaluated at its characteristic scale and subsequently evolved to a shared common scale by solving the corresponding RG equation. The characteristic scale for each function is precisely the value of μ which cancels the logarithms in the perturbative result. As an example, the hard factor, with a characteristic scale denoted as $\mu_h \sim Q$, is evolved by the following equation

$$\begin{aligned} C_V\left(Q^2,\mu\right) &= \exp\left\{\int_{\mu_h}^{\mu} d\ln\bar{\mu}\left[\Gamma_{\rm cusp}\ \left(a_s\right)\ln\frac{Q^2}{\bar{\mu}^2}+\gamma_V\left(a_s\right)\right]\right\} C_V\left(Q^2,\mu_h\right) \\ &= U\left(\mu_h,\mu\right) C_V\left(Q^2,\mu_h\right). \end{aligned} \tag{1.94}$$

The RG equation is solved perturbatively and is an essential part of the computation of any cross section. In chapters 2 and 3 we show how to evolve functions depending on two different scales (i.e. the rapidity scale) and show how evolution plays a role in the phenomenology of a given process.

1.3 SCET$_{\rm II}$

After comprehensively examining the formulation of the effective Lagrangian within SCET$_{\rm I}$, a systematic exploration of what is known as SCET$_{\rm II}$ can be performed. The principal distinction between these two effective theories lies in the scaling of modes relative to the expansion parameter. In SCET$_{\rm II}$, the scaling behaviors of collinear and soft modes are

$$p_n \sim \left(1,\lambda^2,\lambda\right)Q \tag{1.95}$$

$$p_s \sim (\lambda,\lambda,\lambda)Q \tag{1.96}$$

where the expansion parameter is $\lambda = \Lambda_{\rm QCD}/Q$. It is noteworthy that altering the expansion parameter to $\lambda = \sqrt{\Lambda_{\rm QCD}/Q}$ results in the soft modes scaling the same as those in SCET$_{\rm I}$ (ultrasoft modes). However, the scaling behavior of collinear modes deviates from that in SCET$_{\rm I}$. Furthermore, observe that, in SCET$_{\rm II}$, collinear modes do not interact with soft modes due to their off-shell nature, i.e., $pn + p_s = (1,\lambda,\lambda)$. This crucial distinction from SCET$_{\rm I}$ simplifies the construction of the effective Lagrangian for SCET$_{\rm II}$. Consequently, the effective Lagrangian for SCET$_{\rm II}$ is expressed as

$$\mathcal{L}_{\rm SCET_{II}} = \mathcal{L}_c + \mathcal{L}_{\bar{c}} + \mathcal{L}_s. \tag{1.97}$$

The collinear and anticollinear Lagrangians remain identical to those derived for SCET$_{\rm I}$, while the soft Lagrangian mirrors that of SCET$_{\rm I}$ with a modification: the substitution of ultrasoft modes with the newly defined soft modes.

In SCET$_{\rm II}$, a noteworthy characteristic is that the invariant masses of both soft and collinear particles scale proportionally as $Q^2\lambda^2$. Consequently, in a physical process, these

particles are solely distinguished by their rapidities. This leads to a significant feature where a boost can interchange the roles of soft and collinear particles, resulting in the invariance of the physical process. This contrasts with SCET_I, where the mass scaling differs, with collinear particles scaling as $Q^2\lambda^2$ and soft particles scaling as $Q^2\lambda^4$.

Given the similarity between the soft modes in SCET_II and their counterparts in SCET_I, the matching between these theories involves replacing ultrasoft Wilson lines in eq. 1.83 with the corresponding Wilson lines for soft fields. The functional form of these Wilson lines remains the same as those for ultrasoft modes.

In contrast, soft modes now overlap with collinear modes. In this way, a zero-bin subtraction to deal with the overlap is always necessary to properly define collinear matrix elements, like TMD distributions, as we explore in the next chapter. The soft modes result from a rapidity cut in phase space and must include regulators that are non-standard in dimensional regularization. Obtaining universal collinear distributions that are universal and can be extracted from experiments is one of our main goals so these complications are noteworthy.

Due to these issues, the derivation of a Lagrangian for SCET_II is not very useful in these particular cases. Instead, the existence of these modes is considered in the factorization for specific processes like TMD-dependent differential cross-sections, as presented in chapter 2.

In recent years, factorization for these same cross-sections has been provided following the background-field method. In this formulation, the soft modes are purely zero-bin modes and are not included in the effective Lagrangian. We expand on this method in chapters 4 and 5.

Chapter 2

TMD factorization theorems and evolution

Processes involving hadrons present challenges, primarily because their contributions to cross sections cannot be calculated using the perturbative approach employed in QCD. Hadrons consist of partons (quarks and gluons) distributed within them, and the probability distribution of these partons is described by parton distribution functions (PDFs).

PDFs play a pivotal role in unraveling hadron structure and provide insights into the longitudinal momentum distribution of quarks and gluons inside hadrons, offering essential information for probing the dynamics of strong interactions governed by QCD. These distributions are vital ingredients in theoretical calculations aiming to describe a wide range of phenomena, from high-energy scattering processes to the properties of hadrons observed in experiments. These distributions are indispensable for predicting the outcomes of high-energy collisions at particle accelerators like the LHC, where probing the internal structure of particles is a primary objective.

Due to their nonperturbative nature, these objects cannot be computed within perturbation theory in QCD and are typically extracted from experimental data. However, PDFs alone do not provide a complete picture of hadron structure. While they offer valuable information about the longitudinal momentum distributions of partons, they lack crucial insights into their transverse momentum distribution. This limitation led to the development of TMDs, which can be understood as a generalization of PDFs and constitute a more comprehensive framework for characterizing the three-dimensional structure of hadrons. TMDs are indispensable for understanding phenomena involving the intrinsic transverse motion of partons inside hadrons, such as the spin structure of the nucleon and the orbital angular momentum. TMDs are far from being the only type of distribution describing the three-dimensional structure of the hadron. We also have, for example, Generalized Parton Distributions (GPDs), which offer insight into the transverse position of the partons in the nucleon.

TMDPDFs are defined in an energy regime where $q_T \ll Q$, with Q representing the hard scale of the process. Notably, for $q_T \gg \Lambda_{\mathrm{QCD}}$ (where Λ_{QCD} denotes the position of the Landau pole), perturbative information can be derived, complemented by nonperturbative information extracted from experiments or Lattice QCD. In this regime, the perturbative part of the distributions can be separated from non-perturbative physics (PDFs

in collinear factorization). Thus, having perturbative information on TMDPDFs is crucial for minimizing theoretical errors and obtaining clearer insights into nonperturbative physics.

The precise definition of TMDPDFs is established through transverse momentum-dependent factorization theorems. This concept was originally explored in refs. [13, 14]. In this chapter, we use the principles of SCET to derive factorization theorems for the q_T-differential cross section. We present the derivation of a factorization theorem for the Drell-Yan (DY) process, an instructive example illustrating the development of more intricate factorizations discussed in this thesis. Additionally, we delve into TMD evolution and the application of the ζ-prescription.

The DY process is characterized by a proton-proton collision leading to a pair of leptons in the final state,

$$pp \to l^+ l^- + X \tag{2.1}$$

where X represents all the unidentified particles that are emitted in the process. Consider a hard partonic process involving two incoming partons with momenta p_1 and p_2 along the directions n and $\bar{n}$ as defined in the previous chapter, this is the collinear and anticollinear modes. These partons give rise to a virtual photon with virtuality $Q^2 = q^2 > 0$, where q^μ represents its four-momentum. While a neutral gauge boson like the Z boson could also be generated, we exclude this possibility for simplicity. The virtual photon exhibits a non-negligible transverse momentum, denoted as q_T. Consequently, the momentum of the outgoing photon scales as $Q(1, 1, \lambda)$, where $\lambda \sim q_T/Q$ serves as the expansion parameter for SCET. The DY factorized cross-section is given by

$$d\sigma = H\left(Q^2, \mu_H^2\right) F_n\left(\mu_F, \zeta_1\right) \otimes F_{\bar{n}}\left(\mu_F, \zeta_2\right) \otimes S\left(\mu_F, \zeta_{1,2}\right) \tag{2.2}$$

where the physics at the hard scale is defined by the hard factor denoted as H, the collinear modes are represented by the TMDPDF, labeled as $F_{n(\bar{n})}$, and the soft modes are characterized by the soft function, denoted as S. Detailed definitions for these components are provided in this chapter. The symbol $\otimes$ denotes either multiplication or convolution, depending on the specific space we are considering, and μ_H and μ_F serve as the high-energy and factorization scales, respectively. Additionally, the scale ζ emerges as an extra parameter linked to transverse momentum, associated with the characteristic rapidity divergences inherent in such processes. It is important to note that, in principle, different ζ scales may apply to distinct collinear sectors. It is worth mentioning that the factorized formula neglects power corrections of order $\left(q_T^2/Q^2\right)^n$, which will be explored further in chapter 4 and 5.

As introduced in the previous chapter, in the effective theory framework employed for deriving factorization theorems soft particles scale as $Q(\lambda, \lambda, \lambda)$, and collinear particles scale as $Q\left(1, \lambda^2, \lambda\right)$ ($Q\left(\lambda^2, 1, \lambda\right)$ for anticollinear ones), where $\lambda \sim q_T/Q$. In the framework that specifically describes interactions between soft gluons and collinear particles, the virtuality of the particles is of the order of q_T^2, in contrast to $\mathrm{SCET_{II}}$, where it is of the order of Λ_{QCD}. However, $\mathrm{SCET_{II}}$ becomes essential for performing an operator product expansion (OPE) at the scale q_T to separate the perturbative component of the TMDPDF from the integrated PDF (in q_T). The decoupling of soft gluons from collinear ones is accomplished by introducing soft Wilson lines, as introduced in chapter 1.

It becomes imperative to address the issue of double counting that emerges from the overlap between soft and collinear modes, which can be described by the soft function. This consideration holds crucial importance and can impact the accurate definition of TMDPDFs. To deal with the zero-bin contributions we reformulate the factorization theorem as follows:

$$d\sigma = H\left(Q^2, \mu^2\right) \left[\hat{F}_n \otimes S^{-1}\right] \otimes \left[\hat{F}_{\bar{n}} \otimes S^{-1}\right] \otimes S, \tag{2.3}$$

In this expression, the quantities with hats denote the unsubtracted result of the collinear functions which overlaps with the soft radiation region. The combination $\hat{F}_n \otimes S^{-1}$ yields a non-overlapping function. However, this rendition of the factorization theorem is not ideal since both the collinear and soft functions, taken individually, suffer from unregulated and unresolved divergences, rendering them undefined. These divergences manifest perturbatively as integrals of the form:

$$\int_0^1 \frac{dt}{t} \tag{2.4}$$

which are manifestations of light-cone singularities. These divergences also arise with certain infrared regulators in fully integrated PDFs. However, these divergences are canceled when combining real and virtual contributions, a result that does not extend to TMDPDFs. The emergence of light-cone divergences results from defining soft and collinear Wilson lines along light-like trajectories, enabling gluons with infinite rapidities to interact. To circumvent these singularities we can tilt the Wilson lines off the light cone, a technique employed in refs. [15, 16]. In our methodology, all Wilson lines remain on the light cone, and the TMDPDF is defined accordingly. A more comprehensive explanation is presented in this chapter, outlining how we address light-cone singularities within our framework.

This chapter is based on the work presented in refs. [17, 18] and it is a review of the work described in those references. This review allows us to illustrate factorization theorems in a simple example, such as Drell-Yan, and properly introduce precise definitions for TMDPDFs, the soft function and rapidity divergencies. A more intricate interplay with rapidity divergencies and a new soft function will appear in chapter 3, which is described in our work for the first time, being one of the novel features of this thesis.

2.1 TMD definition and Drell-Yan factorization

In this section, we factorize the Drell-Yan cross-section as an example of the factorization process for TMD distributions. The factorization process will naturally lead us to the proper TMD definition and subtraction of the zero-bin contribution. We start from the complete DY cross-section expression which can be found in ref. [17]. Then, we apply the SCET formalism to factorize this expression into different functions that describe the physics of each correspondent momentum region present in the process. We show how the TMD distributions arise from this formula and the role of the soft function. The DY cross-section is given by

$$d\sigma = \frac{4\pi\alpha_{em}^2}{3Q^2 s} \frac{d^4q}{(2\pi)^4} \frac{1}{4} \sum_{\sigma_1\sigma_2} \int d^4y e^{-i(q\cdot y)}$$

$$\times (-g_{\mu\nu}) \langle N_1(P_1,\sigma_1) N_2(P_2,\sigma_2) |J^{\mu\dagger}(y) J^{v}(0)| N_1(P_1,\sigma_1) N_2(P_2,\sigma_2)\rangle, \tag{2.5}$$

where $N_{1,2}$ represent the two hadrons in the process with momenta $P_{1,2}$ and $s = (P_1 + P_2)^2$. Note that the scaling of the position variable y is $1/Q(1,1,1/\lambda)$ as it is the conjugate variable of the photon momentum. J^μ is the electromagnetic current, defined as

$$J^\mu = \sum_q e_q \bar{\psi} \gamma^\mu \psi, \tag{2.6}$$

with e_q the quark electric charge in units of the electron charge. The full QCD current is matched onto the SCET one

$$J^\mu = C_V\left(Q^2/\mu^2\right) \sum_q e_q \bar{\chi}_{\bar{n}} S^{T\dagger}_{\bar{n}} \gamma^\mu S^T_n \chi_n \tag{2.7}$$

where C_V denotes the quark form factor introduced in chapter 1, and the description of collinear fields involves the building blocks $\chi_{n(\bar{n})} = W^{T\dagger}_{n(\bar{n})} \xi_{n(\bar{n})}$. The collinear fields $\xi_{n(\bar{n})}$ were introduced in the preceding chapter. The definitions of collinear and soft Wilson lines, namely $W^T_{n(\bar{n})}$ and $S^T_{n(\bar{n})}$, are consistent with chapter 1, but with the addition of the superscript T indicating an extra transverse Wilson line. The inclusion of transverse Wilson lines is crucial for maintaining gauge invariance of $\chi_{n(\bar{n})}$ across regular and singular gauges, refs. [19, 20, 21, 22]. However, we use Feynman gauge, rendering transverse Wilson lines irrelevant in subsequent calculations. In the case of DY kinematics, collinear Wilson lines are defined as follows:

$$W^T_{n(\bar{n})}(x) = T_{n(\bar{n})} W_{n(\bar{n})} \tag{2.8}$$

$$W_n(x) = \bar{P} \exp\left[ig \int_{-\infty}^0 ds \bar{n}\cdot A_n(x + s\bar{n})\right] \tag{2.9}$$

$$T_n(x) = \bar{P} \exp\left[ig \int_{-\infty}^0 d\tau l_\perp \cdot A_{n\perp}\left(x^+, \infty^-, x_\perp + l_\perp \tau\right)\right] \tag{2.10}$$

$$T_{\bar{n}}(x) = \bar{P} \exp\left[ig \int_{-\infty}^0 d\tau l_\perp \cdot A_{\bar{n}\perp}\left(\infty^+, x^-, x_\perp + l_\perp \tau\right)\right] \tag{2.11}$$

$$S^T_{n(\bar{n})}(x) = T_{sn(\bar{n})} S_{n(\bar{n})}, \tag{2.12}$$

$$S_n(x) = P \exp\left[ig \int_{-\infty}^0 ds n \cdot A_s(x + sn)\right], \tag{2.13}$$

$$T_{sn}(x) = P \exp\left[ig \int_{-\infty}^0 d\tau l_\perp \cdot A_{s\perp}\left(x^+, \infty^-, x_\perp + l_\perp \tau\right)\right], \tag{2.14}$$

$$T_{s\bar{n}}(x) = P \exp\left[ig \int_{-\infty}^0 d\tau l_\perp \cdot A_{s\perp}\left(\infty^+, x^-, x_\perp + l_\perp \tau\right)\right], \tag{2.15}$$

Notice that $\bar{n}$ Wilson lines can be derived from n Wilson lines by substituting $n \leftrightarrow \bar{n}$ and $P \leftrightarrow \bar{P}$ for both collinear and soft Wilson lines. Averaging over nucleon spins and with the help of Fierz transformations we can rewrite the hadronic element in eq. 2.3 as

$$(-g_{\mu v}) \langle N_1(P_1,\sigma_1) N_2(P_2,\sigma_2) |J^{\mu\dagger}(y) J^{v}(0)| N_1(P_1,\sigma_1) N_2(P_2,\sigma_2)\rangle \rightarrow$$

$$\left|C_V\left(Q^2/\mu^2\right)\right|^2 \sum_q e_q^2 \frac{1}{N_c} \left\langle N_1\left(P_1,\sigma_1\right) N_2\left(P_2,\sigma_2\right)\right| \left(\bar{\chi}_{\bar{n}}(y)\frac{\not{\bar{n}}}{2}\chi_{\bar{n}}(0)\right)$$
$$\times \left(\bar{\chi}_n(y)\frac{\not{n}}{2}\chi_n(0)\right) \mathrm{Tr}\left[\bar{T}\left(S_n^\dagger(y)S_{\bar{n}}(y)\right) T\left(S_{\bar{n}}^\dagger(0)S_n(0)\right)\right] \left|N_1\left(P_1,\sigma_1\right) N_2\left(P_2,\sigma_2\right)\right\rangle . \tag{2.16}$$

Collinear and soft fields operate on distinct Hilbert spaces, allowing for the disentanglement of the overall Hilbert space into a direct product of three distinct Hilbert spaces, each corresponding to different modes refs. [23, 24]. The cross-section in equation 2.3 is rewritten as:

$$d\sigma = \frac{4\pi\alpha_{em}^2}{3Q^2S}\frac{d^4q}{(2\pi)^4}\sum_{\sigma_1\sigma_2}\int d^4y e^{-i(q\cdot y)} H\left(Q^2/\mu^2\right)\sum_q e_q^2 F_n(y)F_{\bar{n}}(y)S(y) \tag{2.17}$$

where $H\left(Q^2/\mu^2\right) = \left|C_V\left(Q^2/\mu^2\right)\right|^2$ encodes the physics in the hard region and

$$F_n(y) = \frac{1}{2}\sum_{\sigma_1}\langle N_1\left(P_1,\sigma_1\right)|\bar{\chi}_n(y)\frac{\not{n}}{2}\chi_n(0)|N_1\left(P_1,\sigma_1\right)\rangle, \tag{2.18}$$

$$F_{\bar{n}}(y) = \frac{1}{2}\sum_{\sigma_2}\langle N_2\left(P_2,\sigma_2\right)|\bar{\chi}_{\bar{n}}(y)\frac{\not{\bar{n}}}{2}\chi_{\bar{n}}(0)|N_1\left(P_2,\sigma_2\right)\rangle, \tag{2.19}$$

$$S(y) = \langle 0|\,\mathrm{Tr}\left[\bar{T}\left(S_n^\dagger(y)S_{\bar{n}}(y)\right) T\left(S_{\bar{n}}^\dagger(0)S_n(0)\right)\right]|0\rangle, \tag{2.20}$$

which are collinear, anticollinear and soft distributions respectively, although this is not their final form. Taylor expanding eq. 2.17 in the physical limit that we are interested in and taking into account that the derivatives of the fields scale in the same way as their correspondent momentum scaling

$$\left(y^-\frac{\partial}{\partial y^-}F_n, y^+\frac{\partial}{\partial y^+}F_n, y_\perp\frac{\partial}{\partial y_\perp}F_n\right) \sim \left(1,\lambda^2,1\right) \tag{2.21}$$

$$\left(y^-\frac{\partial}{\partial y^-}F_{\bar{n}}, y^+\frac{\partial}{\partial y^+}F_{\bar{n}}, y_\perp\frac{\partial}{\partial y_\perp}F_{\bar{n}}\right) \sim \left(\lambda^2,1,1\right) \tag{2.22}$$

$$\left(y^-\frac{\partial}{\partial y^-}S, y^+\frac{\partial}{\partial y^+}S, y_\perp\frac{\partial}{\partial y_\perp}S\right) \sim (1,1,\lambda), \tag{2.23}$$

similarly to how we kept only y^- dependence in chapter 1. The leading power cross-section is then given by

$$d\sigma = \frac{4\pi\alpha_{em}^2}{3N_cQ^2S}\frac{d^4q}{(2\pi)^4}\sum_{\sigma_1\sigma_2}\int d^4y e^{-i(q\cdot y)} H\left(Q^2/\mu^2\right)$$
$$\times\sum_q e_q^2 F_n\left(0^+,y^-,y_\perp\right) F_{\bar{n}}\left(y^+,0^-,y_\perp\right) S\left(0^+,0^-,y_\perp\right) + \mathcal{O}(\lambda). \tag{2.24}$$

It is worth noting that while both collinear distributions depend on collinear and transverse components, the soft distribution depends only on transverse ones. The fact that the soft

function depends solely on transverse components is crucial for establishing a well-defined TMDPDF. From now on, we focus on the leading power contribution to the partonic cross-section, but for simplicity, we denote the partonic versions using the notation of their corresponding hadronic counterparts. In momentum space,

$$d\sigma = \frac{4\pi\alpha_{em}^2}{3N_c Q^2}\frac{dx_1 dx_2 d^2q_T}{2(2\pi)^4} H\left(Q^2/\mu^2\right)\sum_q e_q^2 \times \int d^2k_{n\perp}d^2k_{\bar{n}\perp}d^2k_{s\perp}\delta\left(q_T - k_{n\perp} - k_{\bar{n}\perp} - k_{s\perp}\right) F_n\left(x_1, k_{n\perp}\right) F_{\bar{n}}\left(x_2, k_{\bar{n}\perp}\right) S\left(k_{s\perp}\right). \tag{2.25}$$

In this expression, $x_{1,2}$ are the Bjorken variables, defined as follows

$$x_{1,2} = \frac{\sqrt{Q^2+q_T^2}}{\sqrt{s}}e^{\pm y}, \quad y = \frac{1}{2}\ln\left(\frac{q^0+q^z}{q^0-q^z}\right), \tag{2.26}$$

where y is the rapidity of the photon. Thus, the collinear and soft functions are

$$F_n\left(x_1, k_{n\perp}\right) = \frac{1}{2}\int\frac{dr^- d^2r_\perp}{(2\pi)^3}e^{-i\left(r^- x_1 p_1^+/2 - r_\perp\cdot k_{n\perp}\right)}F_n\left(0^+, r^-, r_\perp\right), \tag{2.27}$$

$$F_{\bar{n}}\left(x_2, k_{\bar{n}\perp}\right) = \frac{1}{2}\int\frac{dr^+ d^2r_\perp}{(2\pi)^3}e^{-i\left(r^+ x_2 p_2^-/2 - r_\perp\cdot k_{\bar{n}\perp}\right)}F_n\left(r^+, 0^-, r_\perp\right), \tag{2.28}$$

$$S\left(k_{s\perp}\right) = \int\frac{d^2r_\perp}{(2\pi)^2}e^{ir_\perp\cdot k_{s\perp}}S\left(0^+, 0^-, r_\perp\right). \tag{2.29}$$

The cross-section in eq. 2.25 encounters an issue associated with the presence of a novel form of unregulated and uncancelled divergences in collinear and soft functions, known as rapidity divergencies. These divergencies are a manifestation of light-cone singularities since we are letting gluon with infinite rapidities to be interacted with through light-cone Wilson lines. Each of the three elements in eqs. 2.27-2.29 lacks a well-defined nature and lacks individual physical meaning. This can be sorted by taking specific combinations of these elements, in particular

$$F_n^R\left(x_1, k_{n\perp}\right) = \frac{1}{2}\int\frac{dr^- d^2r_\perp}{(2\pi)^3}e^{-i\left(r^- x_1 p_1^+/2 - r_\perp\cdot k_{n\perp}\right)}F_n\left(0^+, r^-, r_\perp\right)\sqrt{S\left(0^+, 0^-, r_\perp\right)}, \tag{2.30}$$

$$F_{\bar{n}}^R\left(x_2, k_{\bar{n}\perp}\right) = \frac{1}{2}\int\frac{dr^+ d^2r_\perp}{(2\pi)^3}e^{-i\left(r^+ x_2 p_2^-/2 - r_\perp\cdot k_{\bar{n}\perp}\right)}F_n\left(r^+, 0^-, r_\perp\right)\sqrt{S\left(0^+, 0^-, r_\perp\right)}. \tag{2.31}$$

It can be shown that these quantities, which we denote with the superscript R, are devoid of rapidity divergences. The divergences cancel when subtracting the soft function perturbative result from the collinear function perturbative result. This redefinition of the collinear elements remains valid for any polarization under consideration.

In order to deal with the regularization of such divergences we use the so-called δ-regulator. The δ-regulator allows us to precisely define the overlap between collinear and soft regions, commonly referred to as the zero-bin contribution. This zero-bin contribution

is exactly equal to the soft function. Subtracting the zero-bin contribution leads to the proper definition of the TMDPDF, which is $F_n \to F_n/S$ or $F_n^R \to F_n^R/S$:

$$F_n^R\left(x_1, k_{n\perp}\right) = \frac{1}{2}\int \frac{dr^- d^2 r_\perp}{(2\pi)^3} e^{-i\left(r^- x_1 p_1^+/2 - r_\perp \cdot k_{n\perp}\right)} \frac{F_n\left(0^+, r^-, r_\perp\right)}{\sqrt{S\left(0^+, 0^-, r_\perp\right)}}, \tag{2.32}$$

$$F_{\bar{n}}^R\left(x_2, k_{\bar{n}\perp}\right) = \frac{1}{2}\int \frac{dr^+ d^2 r_\perp}{(2\pi)^3} e^{-i\left(r^+ x_2 p_2^-/2 - r_\perp \cdot k_{\bar{n}\perp}\right)} \frac{F_n\left(r^+, 0^-, r_\perp\right)}{\sqrt{S\left(0^+, 0^-, r_\perp\right)}}. \tag{2.33}$$

In this way, the square root of the soft function is subtracted from each collinear distribution, leading to the proper definition of the TMDPDF free of rapidity divergences and overlap between regions. The cross-section can then be rewritten in terms of the TMDPDFs.

$$\begin{aligned} d\sigma =& \frac{4\pi\alpha_{em}^2}{3N_c Q^2}\frac{dx_1 dx_2 d^2 q_T}{2(2\pi)^4} H\left(Q^2/\mu^2\right)\sum_q e_q^2 \\ &\times \int d^2 k_{n\perp} d^2 k_{\bar{n}\perp} d^2 k_{s\perp}\, \delta\left(q_T - k_{n\perp} - k_{\bar{n}\perp} - k_{s\perp}\right) F_n^R\left(x_1, k_{n\perp}\right) F_{\bar{n}}^R\left(x_2, k_{\bar{n}\perp}\right). \end{aligned} \tag{2.34}$$

Notice that there is no soft function in this expression since it is absorbed by the TMD distributions. However, this is not the final form of the cross-section since we need to take a closer look at it in the regime $q_T \gg \Lambda_{\rm QCD}$, which gives us very useful insight into the separation of perturbative and non-perturbative behavior of the TMD distribution.

Particularly, in this regime, our TMDPDF can be further refactorized into a perturbative matching coefficient and a purely non-perturbative PDF. This involves a secondary matching process of SCET_{qT}, which characterizes the physics at the intermediate scale q_T, onto $\mathrm{SCET}_{\rm II}$, describing on the nonperturbative physics at the scale ΛQCD, proper of the PDF.

As the scale of this region, q_T, is sufficiently large to be treated perturbatively, its corresponding conjugate coordinate, denoted as b (commonly referred to as impact parameter), is small enough to facilitate an operator product expansion (OPE) in impact parameter space. Consequently, we restructure the TMDPDF as defined in impact parameter space.

$$F_n(x, b, \mu) = \int d^2 k_{n\perp} e^{i k_{n\perp}\cdot b} F_n\left(x_1, k_{n\perp}, \mu\right) \tag{2.35}$$

as

$$F_n(x, b, \mu) = \int_x^1 \frac{dx'}{x'} C\left(\frac{x}{x'}, b, \mu\right) f_n\left(x', \mu\right) + \mathcal{O}\left(b^2 \Lambda_{\rm QCD}\right), \tag{2.36}$$

where μ is known as the factorization scale and f_n is the integrated PDF, defined as

$$f_n(x, \mu) = \frac{1}{2}\int \frac{dy^-}{2\pi} e^{i y^- x p^+} \langle p|\bar{\chi}_n\left(0^+, y^-, 0_\perp\right)\frac{\not{n}}{2}\chi_n(0)|p\rangle, \tag{2.37}$$

where p denotes the momentum of the specific parton under consideration. In this way, the TMDPDF is separated into a perturbative calculable part, the matching coefficient C, and a purely collinear and non-perturbative part which can be extracted from experiments, the integrated PDF. The TMDPDF also requires a non-perturbative transverse momentum dependent model to define its behavior when we are far from the large-q_T (small-b) region, we comment on this in more detail in chapter 3.

2.2 Rapidity divergences

Rapidity divergences arise from unregulated and uncancelled logarithmic divergences in perturbative computations of the collinear and soft elements within the factorization theorem. These divergences manifest due to the use of eikonal propagators following the Feynman rules of soft and collinear Wilson lines. To address and regularize these divergences, a specific regularization scheme must be adopted. Various options in the literature exist for regulating rapidity divergences (see, for instance, refs. [17, 25, 26, 27, 28, 29, 30]). Here, we use the δ-regularization scheme, as outlined in refs. [29, 30].

2.2.1 δ-regularization scheme

δ-regularization, as introduced in ref. [17], relies on an infinitesimal shift of the $i0$-prescriptions found in eikonal propagators. Consequently, at the diagrammatic level, this regularization approach involves substituting these prescriptions, as exemplified by the absorption of a gluon by a Wilson line $[\infty^+, 0]$

$$\frac{1}{k^+ - i0} \to \frac{1}{k^+ - i\delta^+}, \tag{2.38}$$

replacing $i0$ with $i\delta^+$. However, this regularization approach lacks the precision required for computations at higher orders. In particular, this simple substitution fails to ensure equality between the soft function and the zero-bin contribution beyond NLO. Consequently, equation 2.30 does not hold true for all orders in perturbation theory. To address these shortcomings, modifications to the original δ-regularization scheme were proposed in refs. [29, 30]. The adjusted regularization scheme is implemented at the operator level, designed to address issues such as non-abelian exponentiation and the preservation of equality between the soft function and the zero-bin at higher orders.

The redefinition at the operator level involves a modification of collinear and soft Wilson lines operator definitions. Specifically, the alteration is applied to the soft Wilson lines, leading to the following adjustment:

The δ-regularization is incorporated at the operator level, modifying the definition of soft Wilson lines in the following way

$$\tilde{S}_{\bar{n}}(0) = P\exp\left[-ig\int_0^\infty dsA_{s+}(s\bar{n})\right] \to P\exp\left[-ig\int_0^\infty dsA_{s+}(s\bar{n})e^{-i\delta^+ s}\right], \tag{2.39}$$

$$S_n(0) = P\exp\left[ig\int_{-\infty}^0 dsA_{s-}(sn)\right] \to P\exp\left[ig\int_{-\infty}^0 dsA_{s-}(sn)e^{+i\delta^- s}\right]. \tag{2.40}$$

The Feynman diagram rule for the modified eikonal propagator in the case of the absorption of an arbitrary number n of gluons by a Wilson lines $[\infty^+, 0]$ is given by

$$\frac{1}{\left(k_1^+ - i0\right)\left(k_2^+ - i0\right)\ldots\left(k_n^+ - i0\right)} \to \frac{1}{\left(k_1^+ - i\delta^+\right)\left(k_2^+ - 2i\delta^+\right)\ldots\left(k_n^+ - ni\delta^+\right)}, \tag{2.41}$$

where the momentum of the gluons are ordered so they fulfill the condition $|k_n^+| \leq \left|k_i^+\right| \forall i$. Due to the violation of rescaling invariance by the regulators $\delta^\pm$, the diagram expressions

are now contingent on a singular combination of regulators, namely $\delta^+\delta^-$. The arrangement of poles in the eikonal propagators holds significance in maintaining the non-abelian exponentiation theorem for color factors, ref. [31]. In the context of δ-regularization, only diagrams featuring non-abelian color prefactors emerge in the exponent, allowing the soft function to be expressed conventionally.

$$\tilde{S}(b) = \exp\left[a_S C_F \left(S^{[1]} + a_S S^{[2]} + \dots\right)\right] \tag{2.42}$$

In the same way, collinear Wilson lines need to be modified for TMD distributions:

$$W_n(x) = P\exp\left[ig\int_{-\infty}^{0} dsA_-(x+sn)\right] \to P\exp\left[ig\int_{-\infty}^{0} dsA_-(x+sn)e^{+i\delta^- xs}\right], \tag{2.43}$$

$$W_n(z) = P\exp\left[ig\int_{-\infty}^{0} dsA_-(z+sn)\right] \to P\exp\left[ig\int_{-\infty}^{0} dsA_-(z+sn)e^{+i\left(\delta^-/z\right)s}\right], \tag{2.44}$$

for the TMDPDF and TMDFF respectively. It is essential to acknowledge that the δ-regularized Wilson line breaks the rules of gauge transformations, although this violation is power-suppressed in terms of δ. Consequently, during calculations, δ is treated as an infinitesimal parameter to prevent contributions that would compromise gauge invariance and it should be sent to 0 at the end of any computation.

To facilitate the combination of the soft function with the bare definition of the TMDPDF and eliminate rapidity divergences, a splitting of the soft function is undertaken, giving rise to the introduction of a new rapidity scale. In the computation of the soft function, the entire dependence on rapidity regulators is encapsulated within a singular function, denoted as $\ln\left(\mu^2/\left(\delta^+\delta^-\right)\right)$. Recognizing that each δ regulator corresponds to the rapidity divergences originating from each TMDPDF in the factorization theorem, the soft function can be reformulated by introducing new scales, denoted as $\zeta_{1,2}$:

$$S\left(b, \ln\left(\frac{\mu^2}{\delta^+\delta^-}\right)\right) = S^{1/2}\left(b, \ln\left(\frac{\mu^2}{\left(\delta^+/p^+\right)\zeta_1}\right)\right) S^{1/2}\left(b, \ln\left(\frac{\mu^2}{\left(\delta^-/p^-\right)\zeta_2}\right)\right) \tag{2.45}$$

where $\zeta_1\zeta_2 = \left(p^+p^-\right)^2 = Q^4$, with Q^2 the hard scale of the considered process. The ζ scale can be included in the computation of a TMD distribution by the following substitution

$$\delta^- = \delta^+ \frac{\zeta}{\left(p^+\right)^2}. \tag{2.46}$$

This expression should be modified once we tackle dijet production in chapter 3. In the next section we describe the ζ-scale in more detail.

2.3 ζ-prescription and TMD evolution

A novel feature of TMD distributions is the presence of the ζ-scale introduced in the previous section, associated with the δ-regulator. One can think about the appearance of this new scale in analogy to the μ scale associated with the ϵ-regulator in dimensional

regularization. In the same way as for the μ scale, perturbative results depend on logarithms of the ζ scale that can potentially spoil the perturbative expansion. We have the freedom to set the value of ζ to try to cancel the logarithms and then apply differential evolution equations to evolve our TMD distribution to a common scale. Essentially, TMD distributions are double-scale distributions that evolve in a certain path in a (μ, ζ)-plane. In this section, we describe how to perform this evolution and discuss the path dependence of the process. The discussion here presented is based on the more in-depth analysis of TMD evolution in the (μ, ζ)-plane in reference [32].

The differential evolution equations governing TMD distributions are determined by the factorization theorem, however, the choice of boundary conditions for their solutions remains arbitrary. These conditions play a crucial role in the convergence of perturbative series and influence the theoretical description of processes where TMDs are implicated. The ζ-prescription, as described in [33, 34] is introduced as a guide to treating the double-scale nature of the TMD. The essence of this prescription lies in defining the TMD distribution along a null-evolution line. This line has the unique property of maintaining an evolution factor equal to one for all values of b. The resulting TMD distribution is free from any mixing with perturbative evolution factors evaluated at different b values, making it completely non-perturbative. This independence from perturbative parameters allows for a flexible parameterization of the distribution without being tied to specific perturbative orders. Evolution equations for TMD distributions are given by

$$\frac{d}{d\ln\mu}F(x,b;\mu,\zeta) = \gamma_F(\mu,\zeta)F(x,b;\mu,\zeta), \tag{2.47}$$

$$\frac{d}{d\ln\zeta}F(x,b;\mu,\zeta) = -\mathcal{D}(\mu,b)F(x,b;\mu,\zeta), \tag{2.48}$$

where F is any renormalized and zero-bin substracted TMD distribution (collinear and anticollinear subindex is removed for simplicity). The eq. 2.47 is a standard renormalization group equation, which comes from the renormalization of the ultraviolet divergences, with the function $\gamma_F(\mu,\zeta)$ being the anomalous dimension. The eq. 2.48 results from the factorization of rapidity divergences. The function $\mathcal{D}(\mu,b)$ is known as the rapidity anomalous dimension (RAD). The RAD is a non-perturbative function that can be computed at small values of b in perturbation theory. Both scales μ and ζ are independent since they have different origins, which implies the double-scale evolution of the TMD distribution in the (μ,ζ)-plane. The differential equation system governing this evolution can be solved. In particular, for a TMD evolving from (μ_i,ζ_i) to a point (μ_f,ζ_f) we have

$$F(x,b;\mu_f,\zeta_f) = \exp\left[\int_P\left(\gamma_F(\mu,\zeta)\frac{d\mu}{\mu} - \mathcal{D}(\mu,b)\frac{d\zeta}{\zeta}\right)\right]F(x,b;\mu_i,\zeta_i). \tag{2.49}$$

Here, P represents any path in the (μ,ζ)-plane connecting the initial point (μ_i,ζ_i) to the final point (μ_f,ζ_f). The evolution value is, in principle, path-independent due to the integrability condition, also known as the Collins-Soper (CS) equation [35]):

$$-\frac{d\gamma_F(\mu,\zeta)}{d\ln\zeta} = \frac{d\mathcal{D}(\mu,b)}{d\ln\mu} = \Gamma_{\text{cusp}}(\mu), \tag{2.50}$$

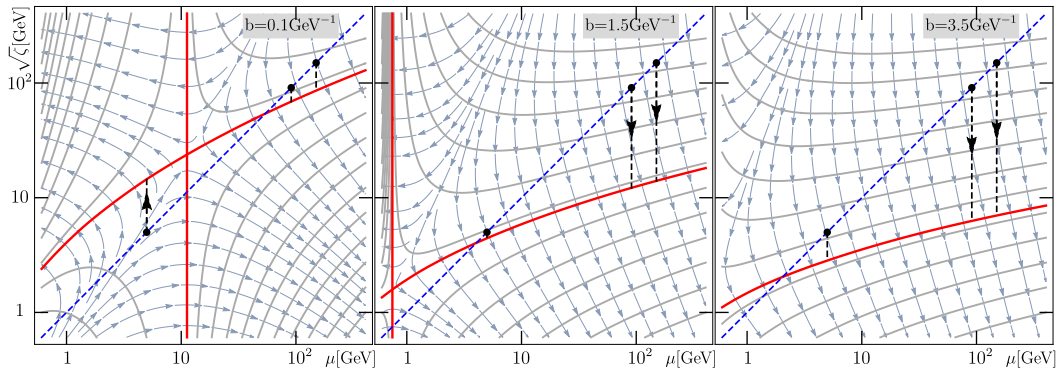

Figure 2.1: (μ, ζ)-plane for TMD evolution. Force lines of the TMD evolution field $\mathbf{E}$ at varying values of b (depicted in grey with arrows) are shown. The thick continuous grey lines represent null-evolution (equipotential) lines. Red lines signify equipotential lines crucial for defining the saddle point. The red line traversing each panel from left to right corresponds to the special evolution curve where the TMD is defined. The blue dashed lines in each plot correspond to the final scale choice (μ_f, ζ_f) typically employed in experimental measurements. The black points denote the initial evolution scales for cases with $Q = 5$, 91, and 150 GeV. Black dashed lines with arrows denote the paths of evolution implemented in eq. 2.55. Figure credit to A. Vladimirov and I. Scimemi, ref. [32].

where $\Gamma_{\rm cusp}(\mu)$ is the cusp anomalous dimension. This equation governs the logarithmic structure of anomalous dimensions. The formal path-independence of equation (2.49) is broken at any given perturbative order and the penalty term is proportional to the area enclosed by paths. This penalty can be substantial, especially when dealing with widely separated scales. As expected, with higher perturbative orders the deviance is numerically smaller [33].

In the following, we describe how the evolution procedure takes shape with an example. In particular, we focus on the case described in this chapter for DY, where the final scales of the evolution are bound to the hard scale of factorization such that $\mu_f^2 \sim Q^2$ and $\zeta_{1f}\zeta_{2f} = Q^4$. We choose the symmetric point for the final scales, given by

$$\mu_f^2 = Q^2, \qquad \zeta_{1f} = \zeta_{2f} = Q^2. \tag{2.51}$$

The choice of the TMD initial scale is determined using the ζ-prescription as follows. In the ζ-prescription, the scales μ and ζ are constrained to a null-evolution line, parametrized as $(\mu, \zeta_\mu(b))$. To identify this null-evolution line, we can recall that the system of equations (2.47, 2.48) forms a two-dimensional gradient equation ($\boldsymbol{\nabla} F = \mathbf{E} F$) with the field $\mathbf{E} = (\gamma_F(\mu, \zeta)/2, -\mathcal{D}(\mu, b))$. Consequently, the null-evolution line corresponds to an equipotential line of the field $\mathbf{E}$. This line defines $\zeta_\mu(b)$ such that it fulfills

$$\Gamma_{\rm cusp}(\mu) \ln\left(\frac{\mu^2}{\zeta_\mu(b)}\right) - \gamma_V(\mu) = 2\mathcal{D}(\mu, b)\frac{d\ln\zeta_\mu(b)}{d\ln\mu^2}, \tag{2.52}$$

where we have used the form of the TMD anomalous dimension

$$\gamma_F(\mu,\zeta) = \Gamma_{\rm cusp}(\mu)\ln\left(\frac{\mu^2}{\zeta}\right) - \gamma_V(\mu). \tag{2.53}$$

Among the equipotential lines, there is a special line that passes through the saddle point (μ_0,ζ_0) of the field **E**. The saddle point is defined by the pair of values that cancel both anomalous dimensions.

$$\mathcal{D}(\mu_0,b) = 0, \qquad \gamma_F(\mu_0,\zeta_0) = 0. \tag{2.54}$$

The choice of the special equipotential line containing the saddle point for defining TMD scales is preferable since the evolution field possesses only one saddle point, ensuring the uniqueness of the special null-evolution line. Additionally, the special null-evolution line is the sole line with finite ζ at all μ values (greater than $\Lambda_{\rm QCD}$). These properties are inherent to its definition and prove to be highly beneficial. In fig. 2.1, the force-lines of the evolution field **E** are depicted in grey with arrows, null-evolution lines are represented by thick grey lines orthogonal to the force-lines, and the lines intersecting at the saddle point are shown in red at various b values. In each panel of the figure, the special line is the one progressing from left to right. Results for the null-evolution line can be found in ref. [32].

A TMD distribution $F(x,b;\mu,\zeta_\mu)$ with ζ_μ belonging to the special line is called optimal TMD distribution. Once this distribution is established, we can freely move along the null-evolution line. In particular, this lets us choose the simplest path to the final scale, that is, the path at a fixed value of $\mu = Q$ along ζ from the value $\zeta_f = Q^2$ down to any point of $\zeta_i = \zeta_Q(b)$. In fig. 2.1 this path is visualized by black-dashed lines. The resulting expression for the evolved TMD distributions is

$$F(x,b;Q,Q^2) = \left(\frac{Q^2}{\zeta_Q(b)}\right)^{-\mathcal{D}(b,Q)} F(x,b). \tag{2.55}$$

In the next chapter, we show how this differs for dijet production process and explain how to deal with the ζ-scale in such cases, which is one of the novelties of this thesis.

Chapter 3

Dijet production in SIDIS

One of the main goals of this thesis is the detailed description of two-jet (or dijet) production in semi-inclusive deep inelastic scattering. As stated before, dijet production in SIDIS is a more complex and natural continuation of processes like Drell-Yan, dijet production in electron-positron annihilation and single-jet SIDIS. In this chapter, we present the factorization theorem as well as numerical results for the cross-section.

Gluons play a crucial role in the composition of nuclei, with gluon parton distribution functions (PDFs) often exhibiting numerical magnitudes significantly greater than their corresponding quark distributions, particularly at lower parton energy fractions.

Similarly, gluon transverse momentum dependent distributions (TMDs) are anticipated to display enhancements. However, accessing these distributions proves challenging due to the absence of well-defined processes where cross-section factorization holds and incoming gluons are a predominant effect.

An instance of such a phenomenon is the production of the Higgs boson in hadronic colliders, as discussed in various studies [36, 25, 37, 38, 39]. Nevertheless, deriving gluon transverse momentum dependent distributions (TMDs) from the transverse-momentum spectrum of the Higgs is intricate due to the scalar boson's inherent characteristics, including its large mass. Notably, some works, such as [40] with jet veto considerations and [41] excluding certain TMD effects, address these challenges.

Even in the case of the relatively clean Higgs spectrum process, both unpolarized and linearly polarized gluon distributions play crucial roles in the leading power factorization of the cross-section in the q_T/M_H expansion, where q_T and M_H denote the transverse momentum and mass of the boson, respectively.

The absence of a color-neutral scalar at low energies has shifted attention towards quarkonium production, to be observed in semi-inclusive deep inelastic scattering (SIDIS) at the Electron Ion Collider (EIC) and the Large Hadron Collider (LHC) [37, 42, 43, 44, 45, 46, 47, 48, 49, 50, 51, 52, 53, 54, 55, 56, 57, 58, 59, 60, 61].

However, the factorization of these processes poses challenges, as discussed in works such as [56, 57]. Additionally, a series of QCD effects are present due to the color structure of quarkonia and the complexity of the non-relativistic expansion commonly used in quarkonium production studies.

In this thesis, we consider two alternative processes that are currently gaining increased attention: dijet [62] and heavy-hadron pair [63, 64, 65] production in an electron-hadron

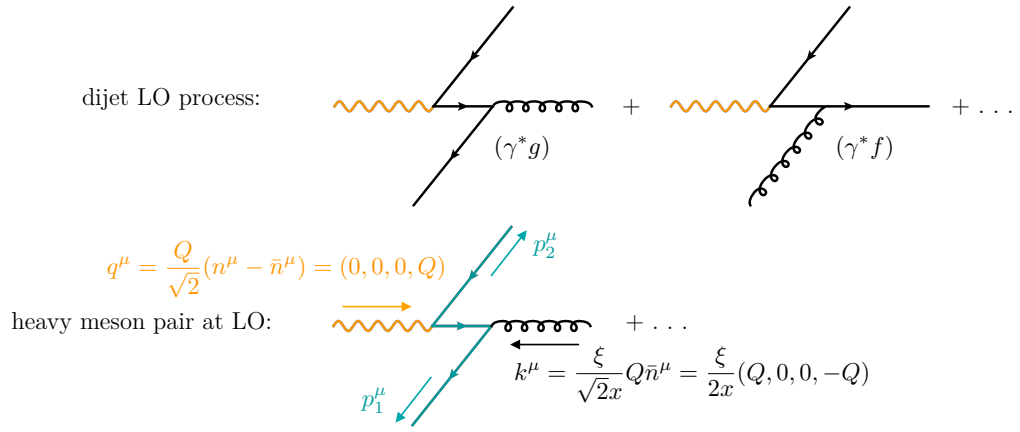

Figure 3.1: Example LO diagrams for the two processes. The momenta q^μ and k^μ (corresponding to the photon and incoming parton momenta respectively) are expressed in the Breit frame.

collider, generated by the $(\gamma^* g)$ and/or $(\gamma^* f)$ hard interactions. The processes under consideration are expressed as:

$$\ell + h \to \ell' + J_1 + J_2 + X, \qquad \text{and} \quad \ell + h \to \ell' + H + \bar{H} + X, \tag{3.1}$$

where ℓ and ℓ' represent the initial and final state leptons, h is the colliding hadron, and J_i and $H/\bar{H}$ denote jets and heavy hadron, respectively. The undetected particles in 3.1 are collectively denoted by X.

Dijet production has been extensively studied at the kinematic regime expected for the future electron-ion collider (EIC), offering sensitivity to polarized and unpolarized gluon transverse momentum dependent distributions [66, 67, 68, 69]. The produced jets, analyzed in the Breit frame, typically have transverse momenta in the range of $p_T \in [5, 40]$ GeV and are located in the central rapidity region. Recent studies, such as [69], suggest the experimental observability of dijet imbalances at the future EIC. Kinematic constraints for the dijet process are chosen to avoid hierarchies among partonic Mandelstam variables, demanding that $\hat{s} \sim |\hat{t}| \sim |\hat{u}|$ to prevent large logarithms in the cross-section's hard factor, which could adversely affect the perturbative expansion.

On the other hand, heavy-hadron pair production is experimentally more challenging due to the need for reconstructing the heavy hadron momenta from its decay products. Additionally, the substantial energy required to produce a boosted heavy-hadron pair makes this process less likely to be observed compared to dijet production. However, Monte Carlo simulations suggest the possibility of observing this phenomenon, especially for charmed mesons. Experimental efforts in charm reconstruction have been explored in refs.[70, 71]. In ref.[72], charm production rates have been investigated at LO and NLO QCD for $ep \to c/\bar{c} + X$. The factorization we introduce below requires the transverse momenta of the heavy hadrons, $p_T^{H/\bar{H}}$, to be parametrically larger than their mass, m_H, i.e., $p_T^{H/\bar{H}} \gg m_H$. Although an alternative factorization can be constructed when this

condition is violated, we do not pursue it here. The details of such factorization involve a hard function incorporating all heavy-quark mass dependence and necessitate a different soft function for which the directions of the quark-antiquark pair are not light-like, given that the heavy hadrons are not boosted to the massless limit. A relevant study on this alternative factorization is available in ref. [63].

At the leading order (LO) and neglecting the intrinsic momentum of partons inside the target hadron, the two hard-scattering processes are schematically illustrated in fig. 3.1. In the case of jets, the initial parton can be either a gluon or a quark, while in the heavy-meson case, only the gluon initial state is relevant. [1]

We consider the differential cross-section

$$\frac{d\sigma}{dx d\eta_1 d\eta_2 dp_T d\boldsymbol{r}_T}\,, \tag{3.2}$$

where x is the Bjorken variable, and η_i, $\boldsymbol{r}_T$ and p_T are respectively the rapidities, the sum of the transverse momenta (with respect to the beam axis) and the average scalar transverse momenta of the two final jets. In the Breit frame, where the virtual photon and target-hadron directions are back-to-back, the factorization holds when $|\boldsymbol{r}_T| \ll p_T$.

The cross-section factorization involves the conventional TMDPDF (we have unpolarized and linearly polarized gluon TMDs as well as quark TMDs) in addition to jet or heavy hadron distributions. It introduces a novel TMD soft function constructed with Wilson lines along the directions of the incoming hadron and the two outgoing jets. This three-directional soft function shares some resemblance with those identified in vector boson + jet processes in hadronic colliders [75, 76]. However, the structure of rapidity divergences significantly differs from the soft function discussed in those studies. The one-loop perturbative calculation of this innovative TMD soft function is carried out herein using the modified δ-regulator introduced in [77, 30]. The consistency of the factorization at the same order is explicitly verified. For the photon-gluon fusion channel, higher orders of the anomalous dimension of the new soft function can be inferred from the consistency of the anomalous dimensions of the factorized cross-section. This is facilitated by the fact that, in the case of heavy-hadron pair production, all other components of the cross-section are also known at higher orders.

The inclusion of the new TMD soft function prompts questions about the universality of TMDs beyond the customary processes of Drell-Yan, SIDIS and di-hadron production in electron-positron annihilation [2]. While the non-perturbative evolution remains universal across the processes under consideration here and in others, the non-perturbative corrections to the soft matrix element have not yet been linked to other processes. Consequently, independently extracting gluon TMDPDF is non-trivial. For a quantitative analysis of these effects, further theoretical and experimental advancements are needed [64, 89, 90, 99].

[1] In principle one may consider the case of incoming quark and outgoing gluon which then fragments into a heavy meson. However, in order to access the TMD region (small $\boldsymbol{r}_T$) this fragmentation needs to occur near threshold, as we discuss later in the main sections, and gluon fragmentation in the kinematic end-point is power suppressed as is discussed both theoretically and phenomenologically in refs. [73, 74].

[2] In the case of quark TMDs the conventional universality class has been recently expanded to include also semi-inclusive jet production in the Breit frame and jet-jet or hadron-jet decorrelation in lepton colliders [78, 79, 80].

This thesis also conducts a phenomenological study of the described processes, including a consideration of theoretical errors. To achieve this, we utilized the arTeMiDe code [81], expanding it with new modules essential for describing the scenarios under investigation. The code already incorporates quark TMDPDFs and the TMD evolution kernel derived from Drell-Yan and semi-inclusive deep inelastic scattering experiments [32].

The cross-section's factorization is presented in position space, characterized by the variable $\boldsymbol{b}$, which is the conjugate of the transverse momentum variable $\boldsymbol{r}_T$. To Fourier transform the factorized cross-section from $\boldsymbol{b}$ space to momentum space, angular integration over ϕ_b is required (i.e., $d^2\boldsymbol{b} = b\,db\,d\phi_b$ and $\boldsymbol{v}_J \cdot \boldsymbol{b} = v_J\, b \cos\phi_b$). This integration, however, becomes non-trivial because the anomalous dimensions of several functions depend on this angle and are complex-valued. We demonstrate that this integration can be carried out in resummed perturbation theory, addressing the challenge of complex values in all anomalous dimensions. Consequently, the ϕ_b-angle integrated cross-section is factorized into distributions that are rotationally invariant with respect to $\boldsymbol{b}$.

The dijet evolution kernel, integrated over the ϕ_b angle, is derived by solving a system of coupled differential equations, akin to the TMD case. We present and discuss a specific scale choice prescription, analogous to the ζ-prescription discussed in [33], which has been implemented in arTeMiDe.

3.1 Dijet production factorization

This section focuses on the cross-section factorization for dijet processes in Deep Inelastic Scattering (DIS) within the framework of the Soft-Collinear Effective Theory (SCET). While we do not provide an exhaustive derivation of the factorization theorem, we present a concise summary of the final outcome. Additionally, we showcase the Next-to-Leading Order (NLO) calculation for the novel three-directional soft function and perform a consistency check by evaluating the invariance of the cross-section under renormalization group evolution. The notation and kinematics introduced here will also prove beneficial for understanding the subsequent section on heavy-hadron pair production.

3.1.1 Notation and kinematics

Assuming that the direction of the beam is along the $\hat{z}$ axis it is useful to define the four-vector

$$n^\mu = \frac{1}{\sqrt{2}}(1,0,0,1)\ . \tag{3.3}$$

We also define a conjugate vector $\bar{n}^\mu$ by reversing the sign of the spacial coordinates. Thus, n^μ and $\bar{n}^\mu$ satisfy,

$$n^2 = \bar{n}^2 = 0, \quad \bar{n}\cdot n = 1. \tag{3.4}$$

Using the vectors n^μ and $\bar{n}^\mu$ we can decompose any other four-vector, p^μ, into its light-cone components,

$$p^\mu = p_+\bar{n}^\mu + p_- n^\mu + p_\perp^\mu = (p_+, p_-, p_\perp)_n, \tag{3.5}$$

with

$$p_+ = n \cdot p, \quad p_- = \bar{n} \cdot p, \quad p^2 = 2p_+p_- + p_\perp^2 = 2p_+p_- - \boldsymbol{p}^2. \tag{3.6}$$

where we use the notation $\boldsymbol{p} \equiv \vec{p}_\perp$. For the direction of the two jets, we use v_1 and v_2, normalized as

$$v_J^2 = \bar{v}_J^2 = 0, \quad v_J \cdot \bar{v}_J = 1, \text{ with } J = 1, 2\,, \tag{3.7}$$

where the conjugate vectors $\bar{v}_J$, as above, are defined by reversing the sign of the spacial components. We define the standard Lorentz invariants,

$$Q^2 = -q^2, \quad x = \frac{Q^2}{2P \cdot q}, \tag{3.8}$$

where q^μ is the momentum of the virtual photon and P^μ is the momentum of the target hadron. In the Breit frame, we have $q^\mu = (0, 0, 0, Q)$ and neglecting mass corrections we can solve for target hadron momentum,

$$P^\mu = \frac{1}{2x}(Q, 0, 0, -Q)\,. \tag{3.9}$$

The ratio of the longitudinal momenta of the incoming parton and the target hadron we denote with ξ,

$$\xi = \frac{k^+}{P^+}\,. \tag{3.10}$$

where k^μ is the momenta of the parton incoming to the hard process. We can then express the variables Q and ξ in terms of the Born level kinematics using the pseudo-rapidities, η_1 and η_2, and the transverse momentum, p_T, of the two outgoing partons,

$$Q = 2p_T \cosh(\eta_-) \exp(\eta_+), \qquad \xi = 2x \cosh(\eta_+) \exp(-\eta_+)\,, \tag{3.11}$$

where

$$\eta_\pm = \frac{\eta_1 \pm \eta_2}{2}\,, \tag{3.12}$$

The partonic Mandelstam variables in terms of the same quantities are,

$$\begin{aligned}
\hat{s} &= (q + k)^2 = +4p_T^2 \cosh^2(\eta_-)\,, \\
\hat{t} &= (q - p_2)^2 = -4p_T^2 \cosh(\eta_-) \cosh(\eta_+) \exp(\eta_1)\,, \\
\hat{u} &= (q - p_1)^2 = -4p_T^2 \cosh(\eta_-) \cosh(\eta_+) \exp(\eta_2)\,,
\end{aligned} \tag{3.13}$$

where p_1^μ and p_2^μ are the momenta of the outgoing partons. It is easy to check that the partonic Mandelstam variables satisfy,

$$\hat{s} + \hat{t} + \hat{u} = -Q^2\,. \tag{3.14}$$

We denote the transverse momentum imbalance of the two jets with $\boldsymbol{r}_T$, where the hard transverse momentum p_T corresponds, up to power corrections, to the average transverse momenta of the two jets,

$$\boldsymbol{r}_T = \boldsymbol{p}_{1T} + \boldsymbol{p}_{2T}, \qquad p_T = \frac{|\boldsymbol{p}_{1T}| + |\boldsymbol{p}_{2T}|}{2} \tag{3.15}$$

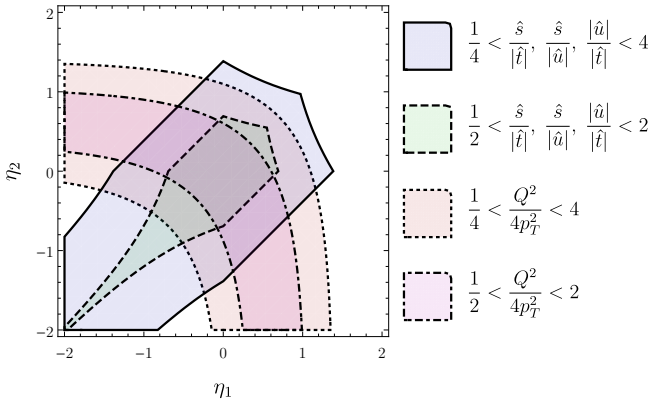

Figure 3.2: The jet-rapidity regions for which $\hat{s} \sim |\hat{t}| \sim |\hat{u}|$: blue-solid ($j = 4$) and green-dashed ($j = 2$) and $Q \sim p_T$: red-dotted $k = 4$ and magenta-dotdashed ($k = 2$). The overlapping region which is found at central rapidities is where we anticipated small contributions to the cross section beyond factorization.

where the sub-index 1 and 2 refer to the final jets. At Born level $\boldsymbol{p}_{1T} = -\boldsymbol{p}_{2T}$ and thus $\boldsymbol{r}_T = 0$. However, hadronization of the outgoing partons will form jet-like configurations along similar directions and wide-angle radiation could escape the jet clustering algorithm, which will then contribute to the imbalance.

We now consider the kinematic region in which the factorization theorem holds in comparison to the coverage of EIC. We first evaluate the constraints on the rapidities of the two jets, η_1 and η_2. To do so we require that $\hat{s} \sim |\hat{t}| \sim |\hat{u}|$ and quantitatively we implement that by imposing,

$$\frac{1}{j} < \frac{\hat{s}}{|\hat{t}|}, \frac{\hat{s}}{|\hat{u}|}, \frac{|\hat{u}|}{|\hat{t}|} < j \tag{3.16}$$

This constrains the values of rapidities within the blue region as illustrated in figure 3.2 for the cases $j = 2$ (green-dashed) and $j = 4$ (blue-solid). In addition, to avoid contributions from the resolved photon processes, we require $Q \sim p_T$ which quantitatively we implement by imposing,

$$\frac{1}{k} < \frac{Q^2}{4p_T^2} < k \tag{3.17}$$

In Figure 3.2, we illustrate the relevant region for the two jet rapidities, delineated by red-dotted and magenta-dot-dashed shaded areas corresponding to $k = 4$ and $k = 2$, respectively. This region is defined by the constraints imposed by 3.17 and 3.16. The overlap of these regions defines the allowable rapidity values where the factorization theorem holds, and the contamination from resolved photo-production processes remains minimal. This implies that the two processes we are investigating can be well-described by two distinct jets (or heavy hadrons) within the central rapidity region. As anticipated, as we tighten the constraint by reducing the values of j and/or k, the relevant region contracts around the central point, $\eta_1 = \eta_2 = 0$.

Restricted to the overlapping rapidity region depicted in Figure 3.2, and for transverse momenta within the range $p_T \in [4, 20]$ GeV and parton momentum fractions in the range $\xi \in [10^{-2}, 1]$, we determine the relevant (x, Q^2) values for the processes under consideration. Figure 3.3 illustrates the corresponding region in (x, Q^2) for two cases: $j = k = 2$ (indicated by the green-dashed area) and $j = k = 4$ (represented by the blue-solid area). Additionally, we have included a brown-shaded region denoting the expected (x, Q^2) coverage at the Electron Ion Collider (EIC) for three different center-of-mass energies: $\sqrt{s} = 140$, 63, and 28 GeV. It's evident that, across all three energy levels, there is a substantial overlap between the processes we are examining and the EIC coverage, with the overlapping region expanding at higher beam energies. Simultaneously, the cases with $j = k = 2$ and $j = k = 4$ do not appear to significantly alter the overlapping region with the EIC coverage in the low Q^2 region. While the shift in the overlapping region is not substantial, the region that is lost is statistically significant. Further investigations using Monte Carlo event generators will be imperative to establish the kinematic constraints on the jets, striking a reasonable balance between statistical precision and accounting for factorization corrections.[3]

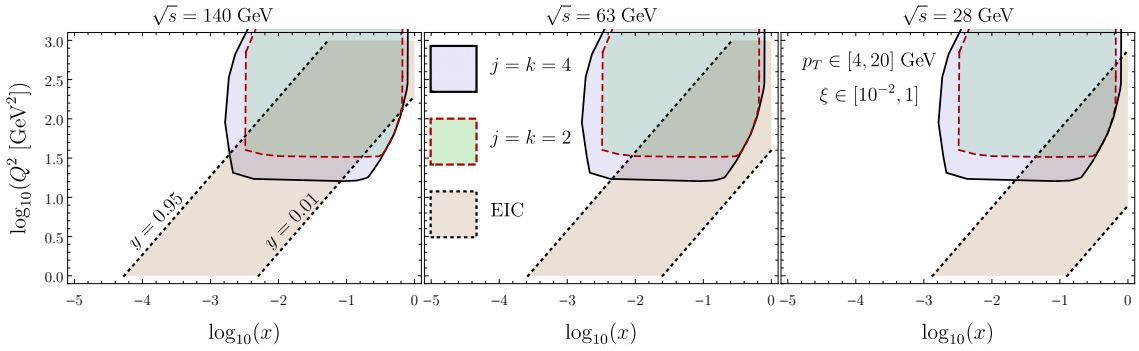

Figure 3.3: The (x, Q^2) coverage of EIC (brown/dashed) compared to the dijet events with $j = k = 4$ factorization regime (blue-solid) and with $j = k = 2$ (green-dashed). The factorization regime has been constructed assuming $p_T \in [4, 20]$ GeV, $\xi \in [10^{-2}, 1]$, and jet rapidities in the overlapping region in figure 3.2.

3.1.2 Factorization theorem for dijet production

There are two channels for the dijet process that we need to consider: a) the gluon-photon fusion channel which corresponds to the partonic process, $\gamma^* g \to f\bar{f}$, and b) the incoming quark or antiquark channel from the partonic process, $\gamma^* f \to gf$. The factorization that we propose holds when $|\boldsymbol{r}_T| \ll p_T$ and we treat the cross-sections only at leading power

[3] It is important to note that in both scenarios, we assume j and k to be equal, even though these variables are independent and could be chosen differently. However, it's crucial that both j and k remain of order $\mathcal{O}(1)$. For instance, in the case where $j = 2$ and $k = 4$ (not depicted here), the impact on the overlapping region with the EIC coverage appears minimal when compared to the scenario where $j = 4$ and $k = 4$.

in an $|\boldsymbol{r}_T|/p_T$ or $|\boldsymbol{r}_T|/Q$ expansion. Within this constraint, the gluon-photon channel factorized cross-section is

$$\frac{d\sigma(\gamma^* g)}{dx d\eta_1 d\eta_2 dp_T d\boldsymbol{r}_T} = \sum_f H^{\mu\nu}_{\gamma^* g\to f\bar{f}}(\hat{s},\hat{t},\hat{u},\mu) \int \frac{d^2\boldsymbol{b}}{(2\pi)^2}\, \exp(i\boldsymbol{b}\cdot\boldsymbol{r}_T)\, F_{g,\mu\nu}(\xi,\boldsymbol{b},\mu,\zeta_1) \times S_{\gamma g}(\boldsymbol{b},\eta_1,\eta_2,\mu,\zeta_2) \Big(\mathcal{C}_f(\boldsymbol{b},R,\mu) J_f(p_T,R,\mu)\Big)\Big(\mathcal{C}_{\bar{f}}(\boldsymbol{b},R,\mu) J_{\bar{f}}(p_T,R,\mu)\Big)\,, \quad (3.18)$$

where the sum runs over all light quark and antiquark flavors f. Here we consider jets with their momentum reconstructed with the so-called E-scheme, that is, the momentum of the jets is given by the sum of all jet constituents. For these jets and for small jet radius ($R \ll 1$) the cross-section can be factorized in terms of the collinear-soft function $\mathcal{C}_i(\boldsymbol{b},R)$, which describes the soft radiation close to the jet boundary and the exclusive jet functions J_i, that describe the collinear and energetic radiation confined within the jet.[4] These functions are calculated up to NLO for generic k_T-type and cone jet algorithms in [83, 75]. The corresponding operator definitions are given in the appendix A.1. In addition, the factorization theorem contains the dijet soft function $S_{\gamma g}$, which is discussed and calculated at one-loop in the next section. Finally, we have the gluon TMDPDF function F_g.

We notice at this point that the latter two functions, $S_{\gamma g}$ and F_g in 3.18, have an intricate interplay due to the rapidity divergences, which introduces the rapidity scale dependence, $\zeta_{1,2}$, in the corresponding functions. In sec. 3.1.4 we explain this issue and the role played by the zero-bin subtractions, which lead to the proper definition of the dijet soft function and the TMDs.

The gluon TMD for an unpolarized proton can be further separated into two pieces, the unpolarized gluon distribution $f_1(\xi,\boldsymbol{b})$ and the linearly polarized gluon contribution $h_1^\perp(\xi,\boldsymbol{b})$:

$$F_g^{\mu\nu}(\xi,\boldsymbol{b}) = f_1(\xi,\boldsymbol{b})\frac{g_T^{\mu\nu}}{d-2} + h_1^\perp(\xi,\boldsymbol{b})\left(\frac{g_T^{\mu\nu}}{d-2} + \frac{b^\mu b^\nu}{\boldsymbol{b}^2}\right), \quad (3.19)$$

with $g_T^{\mu\nu} = g^{\mu\nu} - n^\mu\bar{n}^\nu - \bar{n}^\mu n^\nu$. Both of these functions are known perturbatively up to next-to-next-to leading order (NNLO) [30, 39, 84]. The evolution of the TMDs, which is universal (see e.g. [85, 86]), is also known up to N^{3}LO [77, 87, 88]. In 3.19 we have included only twist-2 TMDs, neglecting higher twists in the TMD expansion. This is sufficient since we consider higher-twist functions suppressed, which is consistent with SIDIS studies as in [32]. The inclusion of the higher-twist contributions is beyond the scope of this work and we leave such considerations for future studies.

The hard function is then decomposed into two tensor structures:

$$H^{\mu\nu}_{\gamma^* g\to f\bar{f}} = \sigma_0^{gU}\, H^U_{\gamma^* g\to f\bar{f}} \frac{g_T^{\mu\nu}}{d-2} + \sigma_0^{gL}\, H^L_{\gamma^* g\to f\bar{f}}\Big(-\frac{g_T^{\mu\nu}}{d-2} + \frac{v_{1T}^\mu\, v_{2T}^\nu + v_{2T}^\mu\, v_{1T}^\nu}{2\, v_{1T}\cdot v_{2T}}\Big), \quad (3.20)$$

where we have ignored all terms proportional to the four-vector n^μ (since they vanish after Lorentz-contraction with the gluon beam function) and any anti-symmetric combinations (since the cross-section is integrated over angles). The coefficients $\sigma_0^{gU(L)}$ are introduced

[4] For recent developments on jet algorithms for DIS see ref. [82]. We also plan in the near future to complete the NLO calculation of jet functions in central rapidity regions for the Centauro algorithm.

such that the leading order hard functions are normalized to the unity, i.e. $H_{\rm LO}^{U(L)} = 1+\mathcal{O}(\alpha_s)$. We can now separate the cross-section into a contribution from the unpolarized gluons and one from the linearly polarized gluons. We write the cross-section as

$$d\sigma(\gamma^* g) = d\sigma^U(\gamma^* g) + d\sigma^L(\gamma^* g)\,, \tag{3.21}$$

where

$$\frac{d\sigma^U(\gamma^* g)}{dx d\eta_1 d\eta_2 dp_T d\boldsymbol{r}_T} = \sum_f \sigma_0^{gU}\, H^U_{\gamma^* g\to f\bar f}(\hat s,\hat t,\hat u,\mu) \int \frac{d^2\boldsymbol{b}}{(2\pi)^2}\, \exp(i\boldsymbol{b}\cdot\boldsymbol{r}_T)\, f_1(\xi,\boldsymbol{b},\mu,\zeta_1) \\ \times S_{\gamma g}(\boldsymbol{b},\zeta_2,\mu)\Big(\mathcal{C}_f(\boldsymbol{b},R,\mu)J_f(p_T,R,\mu)\Big)\Big(\mathcal{C}_{\bar f}(\boldsymbol{b},R,\mu)J_{\bar f}(p_T,R,\mu)\Big), \tag{3.22}$$

and

$$\frac{d\sigma^L(\gamma^* g)}{dx d\eta_1 d\eta_2 dp_T d\boldsymbol{r}_T} = \sum_f \sigma_0^{gL}\, H^L_{\gamma^* g\to f\bar f}(\hat s,\hat t,\hat u,\mu) \int \frac{d^2\boldsymbol{b}}{(2\pi)^2}\, \exp(i\boldsymbol{b}\cdot\boldsymbol{r}_T)\, h_1^\perp(\xi,\boldsymbol{b},\mu,\zeta_1) \\ \times \frac{s_{\boldsymbol{b}}^2 - c_{\boldsymbol{b}}^2}{2}\, S_{\gamma g}(\boldsymbol{b},\zeta_2,\mu)\Big(\mathcal{C}_f(\boldsymbol{b},R,\mu)J_f(p_T,R,\mu)\Big)\Big(\mathcal{C}_{\bar f}(\boldsymbol{b},R,\mu)J_{\bar f}(p_T,R,\mu)\Big). \tag{3.23}$$

We use the shorthand notation $s_{\boldsymbol{b}}$ and $c_{\boldsymbol{b}}$ for the sine and cosine of the angle between the vectors $\boldsymbol{b}$ and $\boldsymbol{v}_{1T}$, respectively. The hard factors are calculated up to NNLO in the unpolarized case in [89, 90], while for the linearly polarized gluons they are calculated at LO in [91]. Hard coefficients can be found in ref. [92] and we list them in the appendix.

Finally, the incoming quark channel has contributions only from the unpolarized gluon jets and the cross-section is given by the following factorized formula:

$$\frac{d\sigma^U(\gamma^* f)}{dx d\eta_1 d\eta_2 dp_T d\boldsymbol{r}_T} = \sigma_0^{fU} \sum_f H^U_{\gamma^* f\to gf}(\hat s,\hat t,\hat u,\mu) \int \frac{d^2\boldsymbol{b}}{(2\pi)^2}\, \exp(i\boldsymbol{b}\cdot\boldsymbol{r}_T)\, F_f(\xi,\boldsymbol{b},\mu,\zeta_1) \\ \times S_{\gamma f}(\boldsymbol{b},\zeta_2,\mu)\Big(\mathcal{C}_g(\boldsymbol{b},R,\mu)J_g(p_T,R,\mu)\Big)\Big(\mathcal{C}_f(\boldsymbol{b},R,\mu)J_f(p_T,R,\mu)\Big), \tag{3.24}$$

where the sum runs over quarks and anti-quarks and F_f is the f-flavor quark/antiquark unpolarized TMDPDF.

3.1.3 Dijet soft function at NLO

The sole new matrix element introduced in the prior section is the soft function. In this section, we present the operator matrix element definition of the soft function and proceed with the NLO calculation. Further elaboration on the calculation specifics is provided in the appendix. We define the soft function for the photon-gluon fusion process:

$$\hat S_{\gamma g}(\boldsymbol{b}) = \frac{1}{C_F C_A}\langle 0|\mathcal{S}_n^\dagger(\boldsymbol{b},-\infty)_{ca'}\mathrm{Tr}\Big[S_{v_2}(+\infty,\boldsymbol{b})T^{a'}S_{v_1}^\dagger(+\infty,\boldsymbol{b}) \\ \times S_{v_1}(+\infty,0)T^a S_{v_2}^\dagger(+\infty,0)\Big]\mathcal{S}_n(0,-\infty)_{ac}|0\rangle. \tag{3.25}$$

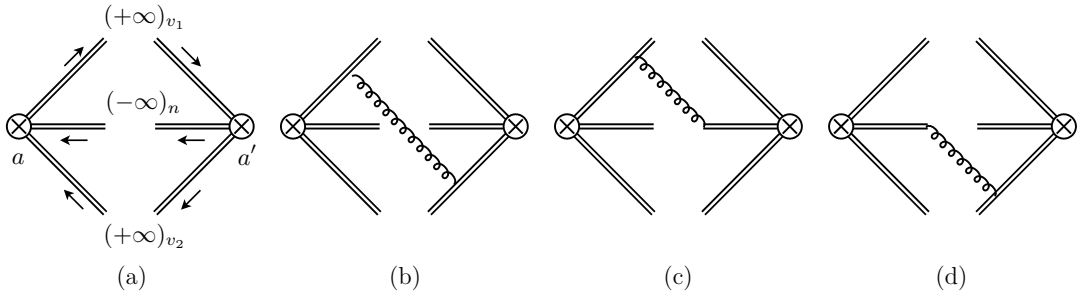

Figure 3.4: Tree level soft function is shown in diagram (a). Each double line represents a Wilson line whose pointing direction is also reported as $(\pm\infty)_u$, $u = n,\ v,\ \bar{v}$; a and a' are color indices. Diagrams (b), (c) and (d) also contribute to the NLO soft function. Virtual contributions vanish and therefore they are not shown here. Mirror diagrams are also not shown.

The soft function corresponding to the case of incoming quark or antiquark is obtained with the exchange

$$\hat{S}_{\gamma f} = \hat{S}_{\gamma g}(n \leftrightarrow v_2)\,. \tag{3.26}$$

since the gluon Wilson line now goes in the v_2 direction. The Wilson lines are defined as

$$\begin{aligned}
S_v(+\infty,\xi) &= P\text{exp}\Big[-ig\int_0^{+\infty} d\lambda\; v\cdot A(\lambda v+\xi)\Big]\,,\\
S_{\bar{v}}^{\dagger}(+\infty,\xi) &= P\text{exp}\Big[ig\int_0^{+\infty} d\lambda\; \bar{v}\cdot A(\lambda \bar{v}+\xi)\Big]\,,\\
S_n(+\infty,\xi) &= \lim_{\delta^+\to 0} P\text{exp}\Big[-ig\int_0^{+\infty} d\lambda\; n\cdot A(\lambda n+\xi)e^{-\delta^+\lambda}\Big]\,.
\end{aligned} \tag{3.27}$$

We omit here T-Wilson lines which are needed in singular gauges. We also distinguish Wilson lines in the adjoint and fundamental $\text{SU}(N_c)$ representations using $\mathcal{S}$ and S respectively. Note that the δ-regulator is introduced only in $S_n(\mathcal{S}_n)$. We write the soft function as a series in $a_s = \alpha_s/(4\pi)$

$$\hat{S} = \sum_{m=0}^{\infty} a_s^m \hat{S}^{[m]}\,. \tag{3.28}$$

At tree level $\hat{S}^{[0]} = 1$, and at one loop only the diagrams with a real gluon give a non-zero result. We can therefore write the one-loop soft function as a sum of diagrams with one real gluon exchange between the three soft Wilson lines,

$$\hat{S}^{[1]} = \frac{1}{2}\sum_{\substack{i\neq j\\ j\in\{1,2,B\}}} C^{ij}\,\hat{S}_{ij}^{[1]}\,, \tag{3.29}$$

where the suffix indicates the Wilson lines connected by the exchanged gluon (1 and 2 for the two jets and B for the beam), including the mirror diagrams as well (note that

$C^{ij} = C^{ji}$ and $\hat{S}^{[1]}_{ij} = \hat{S}^{[1]}_{ji}$). Notice that the mirror diagrams for $\hat{S}_{JB}$ will introduce an additional $i\pi$ component. The coefficients C^{ij} are the color factors and they are different for the two channels $\gamma^* g$ and $\gamma^* f$,

$$C^{1B}_{\gamma g} = C^{2B}_{\gamma g} = C_A\,, \qquad C^{12}_{\gamma g} = 2C_F - C_A,$$
$$C^{2B}_{\gamma f} = C^{12}_{\gamma f} = C_A\,, \qquad C^{1B}_{\gamma f} = 2C_F - C_A. \tag{3.30}$$

The relevant diagrams are shown in fig. 3.4 and the corresponding contributions are

$$\hat{S}^{[1]}_{JB} = \pi(4\pi)^2\mu^{2\epsilon}(n\cdot v_J)I_{JB} + \text{ mir. diag.}\,, \quad \hat{S}^{[1]}_{12} = \pi(4\pi)^2\mu^{2\epsilon}(v_1\cdot v_2)I_{12} + \text{ mir. diag.}, \tag{3.31}$$

where $J = 1, 2$ and the corresponding integrals are

$$I_{JB} = \int \frac{d^dk}{(2\pi)^d}\frac{e^{i\boldsymbol{k}\cdot\boldsymbol{b}}\delta(k^2)\theta(k_+)}{(n\cdot k + i\delta^+)(v_J\cdot k)}\,, \qquad I_{12} = \int \frac{d^dk}{(2\pi)^d}\frac{e^{i\boldsymbol{k}\cdot\boldsymbol{b}}\delta(k^2)\theta(k_+)}{(v_1\cdot k)(v_2\cdot k)}\,, \tag{3.32}$$

with $d = 4 - 2\epsilon$. The results at all orders in ϵ are

$$\hat{S}^{[1]}_{JB} = -2\frac{\mu^{2\epsilon}B^\epsilon}{(4\pi)^{-\epsilon}}\,\Gamma(-\epsilon)\Big[\ln\Big(-\frac{i(\boldsymbol{v}_J\cdot\boldsymbol{b})\,\delta^+}{n\cdot v_J}\Big) + \gamma_E\Big], \tag{3.33}$$

and

$$\hat{S}^{[1]}_{12} = 2\frac{\mu^{2\epsilon}B^\epsilon}{(4\pi)^{-\epsilon}}\,\Gamma(-\epsilon)\Big[\Gamma(-\epsilon)\Gamma(1+\epsilon)\Big(\frac{1+A_{\boldsymbol{b}}}{-A_{\boldsymbol{b}}}\Big)^\epsilon - \frac{\Gamma(-1-\epsilon)}{\Gamma(-\epsilon)}A_{\boldsymbol{b}}\,{}_2F_1(1,1,2+\epsilon,-A_{\boldsymbol{b}})\Big], \tag{3.34}$$

with the shorthand notation,

$$A_{\boldsymbol{b}} = \frac{(v_1\cdot v_2)}{2\,(v_1\cdot\hat{b})\,(v_2\cdot\hat{b})} = -\frac{\hat{s}}{4\,p_T^2\,c_b^2}, \qquad B = \frac{|\boldsymbol{b}|^2}{4}, \tag{3.35}$$

and $\hat{b} = (0,0,\boldsymbol{b})/|\boldsymbol{b}|$. Note that $A_{\boldsymbol{b}}$ is only a function of the angle ϕ_b, which is the angle in between the transverse plane and the jet direction, and it does not depend on $|\boldsymbol{b}|$. $A_{\boldsymbol{b}}$ is also dimensionless, longitudinal boost invariant, and it is bounded to negative values less than -1, i.e., $A_{\boldsymbol{b}} \le -1$. The function ${}_2F_1$ is the standard hypergeometric function and the ϵ expansion for this function can be written as follows

$${}_2F_1(1,1,2+\epsilon,-z) = \frac{1}{z}\ln(1+z) + \frac{\epsilon}{z}\Big[-\frac{\pi^2}{6} + \Big(1+\ln\Big(\frac{1+z}{z}\Big)\Big)\ln(1+z) + \mathrm{Li}_2\Big(\frac{1}{1+z}\Big)\Big] + \mathcal{O}(\epsilon^2). \tag{3.36}$$

Adding all contributions and expanding in ϵ we obtain the bare soft function. For the $\gamma^* g$-channel we have:

$$\hat{S}^{\text{bare}}_{\gamma g}(\boldsymbol{b}) = \hat{S}^{\text{finite}}_{\gamma g}(\boldsymbol{b}) + a_s\Big\{C_A\Big[-\frac{2}{\epsilon^2} + \frac{2}{\epsilon}\Big(2\ln\Big(\frac{\sqrt{2}\,\delta^+}{\mu}\Big) + \ln(2A_n)\Big)\Big] + 2C_F\Big[\frac{2}{\epsilon^2} + \frac{2}{\epsilon}\ln\Big(\frac{B\,\mu^2\,e^{2\gamma_E}}{-A_{\boldsymbol{b}}}\Big)\Big]\Big\}, \tag{3.37}$$

for the $\gamma^* f$-channel:

$$\hat{S}^{\text{bare}}_{\gamma f}(\boldsymbol{b}) = \hat{S}^{\text{finite}}_{\gamma f}(\boldsymbol{b}) + a_s\Big\{C_A\Big[\frac{2}{\epsilon^2} + \frac{2}{\epsilon}\Big(\ln\frac{(n\cdot v_1)(\boldsymbol{v}_2\cdot\boldsymbol{b})}{(n\cdot v_2)(\boldsymbol{v}_1\cdot\boldsymbol{b})} + \ln\Big(\frac{B\mu^2 e^{2\gamma_E}}{-A_{\boldsymbol{b}}}\Big)\Big)\Big] + \frac{4}{\epsilon}C_F\ln\Big(-\frac{i\,\boldsymbol{v_1}\cdot\boldsymbol{b}\,\delta^+ e^{\gamma_E}}{n\cdot v_1}\Big)\Big\}, \quad (3.38)$$

where the finite part of the soft function is

$$\hat{S}^{\text{finite}}_{\gamma g}(\boldsymbol{b}) = 1+a_s\Big\{C_A\Big[\ln\big(B\,\mu^2 e^{2\gamma_E}\big)\Big(\ln\big(B\mu^2 e^{2\gamma_E}\big)+4\ln\Big(\frac{\sqrt{2}\,\delta^+}{\mu}\Big)+2\ln(2A_n)\Big)-\ln^2(-A_{\boldsymbol{b}}) - \frac{\pi^2}{6} - 2\mathrm{Li}_2(1+A_{\boldsymbol{b}})\Big] + C_F\Big[\frac{\pi^2}{3}+2\ln^2\Big(\frac{B\mu^2 e^{2\gamma_E}}{-A_{\boldsymbol{b}}}\Big)+4\mathrm{Li}_2(1+A_{\boldsymbol{b}})\Big]\Big\}, \quad (3.39)$$

and

$$\hat{S}^{\text{finite}}_{\gamma f}(\boldsymbol{b}) = 1+a_s\Big\{C_A\Big[\frac{\pi^2}{6}+\ln^2\Big(\frac{B\mu^2 e^{2\gamma_E}}{-A_{\boldsymbol{b}}}\Big)+2\mathrm{Li}_2(1+A_{\boldsymbol{b}})+2\ln\big(B\mu^2 e^{2\gamma_E}\big)\ln\frac{(n\cdot v_1)(\boldsymbol{v}_2\cdot\boldsymbol{b})}{(n\cdot v_2)(\boldsymbol{v}_1\cdot\boldsymbol{b})}\Big] + 4C_F\ln\big(B\mu^2 e^{2\gamma_E}\big)\ln\Big(-\frac{i\,\boldsymbol{v_1}\cdot\boldsymbol{b}\,\delta^+ e^{\gamma_E}}{n\cdot v_1}\Big)\Big\}. \quad (3.40)$$

To simplify the results we have used the notation

$$A_n = \frac{(v_1\cdot v_2)}{2\,(v_1\cdot n)(v_2\cdot n)}. \quad (3.41)$$

3.1.4 The zero-bin subtraction and the universal TMDs

In this section, we restructure the factorization theorem to represent the cross-section using rapidity divergence-free TMD functions, as delineated in the factorization theorems presented in 3.22, 3.23, and 3.24. This rearrangement helps elucidate the reliance on the universal TMD parton distribution functions (PDFs) and the new dijet TMD soft function. To achieve this, we express the TMD beam function as the ratio of the unsubtracted term in the zero-bin divided by the back-to-back soft function.

$$\hat{B}_i(\xi,\boldsymbol{b},\mu,k^-\delta_+) = \frac{B_i^{\text{un.}}(\xi,\boldsymbol{b},\mu,k^-/\delta^-)}{S(\boldsymbol{b},\mu,\sqrt{\delta^+\delta^-})} \quad (3.42)$$

The back-to-back two-direction soft function operator definition can be found in appendix A.1 and is the same soft function found in a typical Drell-Yan, single jet DIS and electron-positron annihilation. Then, following [93, 77], we can factorize the soft function as

$$S(\boldsymbol{b},\mu,\sqrt{\delta^+\delta^-}) = S^{\frac{1}{2}}(\boldsymbol{b},\mu,\delta^+\nu)S^{\frac{1}{2}}(\boldsymbol{b},\mu,\delta^-/\nu)\,, \quad (3.43)$$

where ν is an arbitrary positive number that plays a bookkeeping role and will be removed from the final result, introducing this way a constraint on the product of rapidity scales. The bare function $\big(S^{\text{bare}}\big)^{\frac{1}{2}}$ is

$$\Big(S_i^{\text{bare}}(\boldsymbol{b},\delta)\Big)^{\frac{1}{2}} = 1 + a_s C_i\Big\{-\frac{2}{\epsilon^2}+\frac{4}{\epsilon}\ln\Big(\frac{\sqrt{2}\,\delta}{\mu}\Big)+\ln\big(B\mu^2 e^{2\gamma_E}\big)\Big[4\ln\Big(\frac{\sqrt{2}\,\delta}{\mu}\Big)+\ln\big(B\mu^2 e^{2\gamma_E}\big)\Big]$$

$$+\frac{\pi^2}{6}\Big\}+\mathcal{O}(a_s^2), \tag{3.44}$$

where here and in the rest of this manuscript we used the shorthand notation

$$\gamma_g=\frac{\beta_0}{2C_A},\qquad \gamma_q=\frac{3}{2},\qquad C_f=C_F=\frac{N_c^2-1}{2N_c},\qquad C_g=C_A=N_c\,. \tag{3.45}$$

In this way, we can now reorganize the beam and soft function matrix elements (denoted by the "hat" notation) into a product of TMDs as they appear in the factorization theorem,

$$\hat{B}_i(\xi,\boldsymbol{b},\mu,k^-\delta_+)\hat{S}_{\gamma i}(\boldsymbol{b},\mu,\sqrt{A_n}\,\delta_+)=F_i(\xi,\boldsymbol{b},\mu,\zeta_1)\;S_{\gamma i}(\boldsymbol{b},\mu,\zeta_2) \tag{3.46}$$

where the functions in the r.h.s. of 3.46 are respectively

$$F_i(\xi,\boldsymbol{b},\mu,\zeta_1)=\left.\frac{B_i^{\text{un.}}(\xi,\boldsymbol{b},\mu,k^-/\delta^-)}{S^{\frac{1}{2}}(\boldsymbol{b},\mu,\delta^-/\nu)}\right|_{\sqrt{2}\,k^-/\nu\to\sqrt{\zeta_1}}, \tag{3.47}$$

that is, the universal TMDPDF as defined in other observables such as Drell-Yan and semi-inclusive DIS and

$$S_{\gamma i}(\boldsymbol{b},\mu,\zeta_2)=\left.\frac{\hat{S}_{\gamma i}(\boldsymbol{b},\mu,\sqrt{A_n}\,\delta^+)}{S^{\frac{1}{2}}(\boldsymbol{b},\mu,\delta^+\nu)}\right|_{\nu/\sqrt{2A_n}\to\sqrt{\zeta_2}}, \tag{3.48}$$

that is the new dijet soft function now incorporated in a rapidity divergent-free ratio. We can thus eliminate the dependence on the arbitrary parameter ν by introducing the following constraint

$$\zeta_1\,\zeta_2=\frac{(k^-)^2}{A_n}=\frac{\hat{u}\,\hat{t}}{\hat{s}} \tag{3.49}$$

where $\hat{s}$, $\hat{t}$, and $\hat{u}$ are the partonic Mandelstam variables and thus the combination $\zeta_1\,\zeta_2$ is Lorentz invariant and in the Breit frame, or any other frame boosted along the proton direction, we have: $\zeta_1\,\zeta_2=p_T^2$. Notice that the procedure to obtain 3.49 is totally analogous to the one used in Drell-Yan or SIDIS [94, 18], TMD factorization theorem. In that case, we have that $\zeta_{1,2}$ have both a square mass dimension and $\zeta_1\zeta_2=Q^4$, while in the present case, ζ_2 is dimensionless quantity but ζ_1, as usual, has dimensions of mass squared. The natural way to choose the values of ζ_1 and ζ_2 is

$$\zeta_1=p_T^2,\qquad \zeta_2=1 \tag{3.50}$$

since they cancel the logarithms in the perturbative result. In this way, we have the standard evolution for the TMDPDF up to the hard scale and the ratio of soft functions in 3.48 has a very similar TMD double-scale evolution.

The renormalized soft function can then be written in terms of the renormalization kernel Z^S and the bare soft function which is simply the ratio of the bare functions that appear in 3.48,

$$S_{\gamma i}^{\text{bare}}(\boldsymbol{b},\zeta_2)=Z_{\gamma i}^S(\boldsymbol{b},\mu,\zeta_2)S_{\gamma i}(\boldsymbol{b},\mu,\zeta_2) \tag{3.51}$$

In the $\overline{\text{MS}}$-scheme for the $(\gamma^* g)$ channel we have

$$S_{\gamma g}(\boldsymbol{b},\mu,\zeta_2) = 1 + a_s\Big\{C_F\Big[\frac{\pi^2}{3} + 2\ln^2\Big(\frac{B\mu^2 e^{2\gamma_E}}{-A_{\boldsymbol{b}}}\Big) + 4\text{Li}_2(1+A_{\boldsymbol{b}})\Big] + C_A\Big[-2\ln\big(B\mu^2 e^{2\gamma_E}\big)\ln\zeta_2 - \ln^2(-A_{\boldsymbol{b}}) - \frac{\pi^2}{3} - 2\text{Li}_2(1+A_{\boldsymbol{b}})\Big]\Big\} + \mathcal{O}(a_s^2), \quad (3.52)$$

and for the $(\gamma^* f)$ channel we have

$$S_{\gamma f}(\boldsymbol{b},\mu,\zeta_2) = 1+a_s\Big\{C_A\Big[\frac{\pi^2}{6}+\ln^2\Big(\frac{B\mu^2 e^{2\gamma_E}}{-A_{\boldsymbol{b}}}\Big)+2\text{Li}_2(1+A_{\boldsymbol{b}})+2\ln\big(B\mu^2 e^{2\gamma_E}\big)\ln\frac{(n\cdot v_1)(\boldsymbol{v}_2\cdot\boldsymbol{b})}{(n\cdot v_2)(\boldsymbol{v}_1\cdot\boldsymbol{b})}\Big] + C_F\ln\big(B\mu^2 e^{2\gamma_E}\big)\Big[\ln\big(B\mu^2 e^{2\gamma_E}\big)-2\ln\zeta_2+2\ln\Big(\frac{2(n\cdot v_2)}{(v_1\cdot v_2)(n\cdot v_2)}\Big)-\frac{\pi^2}{6}+4\ln(-i\,\boldsymbol{v}_1\cdot\hat{\boldsymbol{b}})\Big]\Big\}+\mathcal{O}(a_s^2), \quad (3.53)$$

It is worth noting that the imaginary components nullify when summed, and upon Fourier transforming into momentum space, this leads to a real cross-section, which is verified up to NLO contributions. The associated renormalization functions are as follows:

$$Z^S_{\gamma g}(\boldsymbol{b},\mu,\zeta_2) = 1 + a_s\Big\{C_F\Big[\frac{4}{\epsilon^2} + \frac{4}{\epsilon}\ln\Big(\frac{B\mu^2\, e^{2\gamma_E}}{-A_{\boldsymbol{b}}}\Big)\Big] - C_A\frac{2}{\epsilon}\ln\zeta_2\Big\} + \mathcal{O}(a_s^2), \quad (3.54)$$

and

$$Z^S_{\gamma f}(\boldsymbol{b},\mu,\zeta_2) = 1 + a_s\Big\{C_A\Big[\frac{2}{\epsilon^2} - \frac{2}{\epsilon}\Big(\ln\frac{(n\cdot v_1)(\boldsymbol{v}_2\cdot\boldsymbol{b})}{(n\cdot v_2)(\boldsymbol{v}_1\cdot\boldsymbol{b})}\Big) + \ln\Big(\frac{B\mu^2 e^{2\gamma_E}}{-A_{\boldsymbol{b}}}\Big)\Big] + \frac{2}{\epsilon}C_F\Big[\ln\big(B\mu^2 e^{2\gamma_E}\big) - \ln\zeta_2 + \ln\Big(\frac{2(n\cdot v_2)}{(v_1\cdot v_2)(n\cdot v_2)}\Big) + 2\ln(-i\,\boldsymbol{v}_1\cdot\hat{\boldsymbol{b}})\Big]\Big\} + \mathcal{O}(a_s^2), \quad (3.55)$$

The soft anomalous dimension can be obtained from the renormalization functions as follows,

$$\gamma_{S_{\gamma i}} = -\Big(Z^S_{\gamma i}\Big)^{-1}\frac{d}{d\ln\mu}Z^S_{\gamma_i} \quad (3.56)$$

The one-loop results for the soft function anomalous dimensions are collected in the next section.

3.1.5 Consistency check

Each element of the factorized cross-section has a factorization scale dependence and it satisfies a renormalization group equation,

$$\frac{d}{d\ln\mu}G(\mu) = \gamma_G(\mu)\,G(\mu) \quad (3.57)$$

where G runs over all the functions in the factorization theorem and γ_G is the corresponding anomalous dimension. On the other hand, the cross-section is renormalization group

invariant. Therefore, as required by consistency, the sum of all anomalous dimensions of the terms appearing in the factorized cross-section must vanish. In the impact parameter space, where the cross-section is written as a product of these functions, we have,

$$(\gamma^* g)\text{-channel} \qquad \gamma_{H_{\gamma g}} + \gamma_{S_{\gamma g}} + \gamma_{F_g} + 2\gamma_{J_f} + \gamma_{\mathcal{C}_1} + \gamma_{\mathcal{C}_2} + \gamma_\alpha = 0, \tag{3.58}$$

$$(\gamma^* f)\text{-channel} \qquad \gamma_{H_{\gamma f}} + \gamma_{S_{\gamma f}} + \gamma_{F_f} + \gamma_{J_f} + \gamma_{J_g} + \gamma_{\mathcal{C}_f} + \gamma_{\mathcal{C}_g} + \gamma_\alpha = 0. \tag{3.59}$$

We write the perturbative expansion of these anomalous dimensions as

$$\gamma = \sum_{n=1} a_s^n \gamma^{[n]}, \tag{3.60}$$

with $a_s = \alpha_s/(4\pi)$. For the two channels in the dijet process, the relevant anomalous dimensions up to one-loop are,

$$\begin{aligned}
\gamma^{[1]}_{H_{\gamma g}} &= 4\Big\{C_F\Big[\ln\Big(\frac{\hat{s}^2}{\mu^4}\Big) - 2\gamma_q\Big] + C_A \ln\Big(\frac{\hat{t}\,\hat{u}}{\hat{s}\mu^2}\Big)\Big\}\,,\\
\gamma^{[1]}_{H_{\gamma f}} &= 4\Big\{C_F\Big[\ln\Big(\frac{\hat{u}^2}{\mu^4}\Big) - 2\gamma_q\Big] + C_A \ln\Big(\frac{\hat{s}\,\hat{t}}{\hat{u}\,\mu^2}\Big)\Big\}\,,\\
\gamma^{[1]}_{S_{\gamma g}} &= 4\Big\{-C_A \ln\zeta_2 + 2C_F\Big[\ln\big(B\mu^2\, e^{2\gamma_E}\big) - \ln\hat{s} + \ln p_T^2 + \ln\big(4c_{\boldsymbol{b}}^2\big)\Big]\Big\}\,,\\
\gamma^{[1]}_{S_{\gamma f}} &= 4\Big\{(C_F + C_A)\Big[\ln\big(B\mu^2 e^{2\gamma_E}\big) - \ln\hat{s} + \ln p_T^2 + \ln\big(4c_{\boldsymbol{b}}^2\big)\Big]\\
&\qquad + (C_F - C_A)\Big[\ln\Big(\frac{\hat{t}}{\hat{u}}\Big) - \kappa(v_f)\Big] - C_F\ln\zeta_2\Big\}\\
\gamma^{[1]}_{F_i} &= 4C_i\Big[-\ln\Big(\frac{\zeta_1}{\mu^2}\Big) + \gamma_i\Big]\,,\\
\gamma^{[1]}_{J_i} &= 4C_i\Big[-\ln\Big(\frac{p_T^2}{\mu^2}\Big) - \ln R^2 + \gamma_i\Big]\,,\\
\gamma^{[1]}_{\mathcal{C}_g} &= 4C_A\Big[-\ln\Big(B\mu^2\, e^{2\gamma_E}\Big) + \ln R^2 - \ln\big(4c_{\boldsymbol{b}}^2\big) + \kappa(v_g)\Big]\,,\\
\gamma^{[1]}_{\mathcal{C}_i} &= 4C_F\Big[-\ln\Big(B\mu^2\, e^{2\gamma_E}\Big) + \ln R^2 - \ln\big(4c_{\boldsymbol{b}}^2\big) + \kappa(v_i)\Big]\,,\\
\gamma^{[1]}_{\alpha} &= -4C_A\gamma_g\,,
\end{aligned} \tag{3.61}$$

The imaginary component in the soft and collinear-soft anomalous dimension is denoted by $\kappa(v_i)$ where

$$\kappa(v_f) = -\kappa(v_{\bar{f}}) = -\kappa(v_g) = i\pi\,\mathrm{sign}(c_{\boldsymbol{b}}). \tag{3.62}$$

These anomalous dimensions, except the soft function which we calculated here, can be found in [89, 90, 91, 83, 75, 77]. We also used 3.35 to expand $A_{\boldsymbol{b}}$ in the soft function anomalous dimension in terms of $\hat{s}$, p_T, and $c_{\boldsymbol{b}}$. It is now easy to confirm the cancelation of the anomalous dimensions at $\mathcal{O}(\alpha_s)$ which also serves as confirmation of the factorization theorem at the same order.

3.2 Heavy hadron pair imbalance

In this section, we consider the process of heavy-meson pair production, $\ell + p \to \ell + H + \bar{H} + X$, in the back-to-back limit for which the transverse momentum imbalance $\boldsymbol{r}_T$ is measured,

$$\boldsymbol{r}_T = \boldsymbol{p}_T^H + \boldsymbol{p}_T^{\bar{H}} \,, \tag{3.63}$$

where we use the notation H for generic heavy meson and $\bar{H}$ for the corresponding anti-particle. The imbalance is measured in the Breit frame and in the region sensitive to TMDs, i.e., $|\boldsymbol{r}_T| \ll p_T^{H,\bar{H}}$, the two heavy mesons are fragmented near the kinematic end-point and carry most of the energy of the heavy quark coming from the hard process.

In contrast to the dijet process, for the heavy-meson pair production, we only need to consider the photon-gluon fusion channel. From this perspective, the formalism is simpler, but on the other hand, the mass of the heavy meson, m_H, introduces a new scale that we need to consider. In the case when the heavy mesons are highly boosted, i.e., $p_T^H \gg m_H$, the factorization is similar to the dijet production discussed above. The cross-section is then expressed in terms of the same hard, soft, and beam functions, but the production of the final state heavy mesons is described by a heavy-quark jet function, $J_{Q\to H}$ [95, 73].

$$\begin{aligned}\frac{d\sigma(\gamma^* g)}{dx d\eta_H d\eta_{\bar{H}} dp_T d\boldsymbol{r}_T} = H^{\mu\nu}_{\gamma^* g\to Q\bar{Q}}(\hat{s},\hat{t},\hat{u},\mu) \int \frac{d\boldsymbol{b}}{(2\pi)^2} \exp(i\boldsymbol{b}\cdot\boldsymbol{r}_T)\, F_{g,\mu\nu}(\xi,\boldsymbol{b},\mu,\zeta_1) \\ \times S_{\gamma g}(\boldsymbol{b},\mu,\zeta_2)\, J_{Q\to H}(\boldsymbol{b},p_T,m_Q,\mu)\, J_{\bar{Q}\to\bar{H}}(\boldsymbol{b},p_T,m_Q,\mu) \,.\end{aligned} \tag{3.64}$$

with η_H and $\eta_{\bar{H}}$ referring to the pseudo-rapidities of the heavy mesons. Similarly to the dijet factorization, in the hard function we do not consider corrections due to the quark mass and we define,

$$p_T = \frac{|\boldsymbol{p}_T^H| + |\boldsymbol{p}_T^{\bar{H}}|}{2} \,, \tag{3.65}$$

The decomposition into the unpolarized and linearly polarized gluon contributions follows the same steps as in section 3.1 and thus we do not repeat here.

3.2.1 Refactorization of heavy-quark fragmentation function

The fragmentation of a heavy quark into a heavy meson is governed by the heavy-quark fragmentation function, a topic extensively explored in various processes (e.g., see [63, 64, 65]). The relatively large scale introduced by the heavy quark's mass permits the use of perturbation theory to compute the fragmentation function, accounting for minor and universally applicable non-perturbative corrections.

In our specific case, we examine the heavy-quark jet function, denoted as $J_{Q\to H}$, which characterizes the fragmentation of heavy mesons originating from heavy quarks. This function is differential in the two-dimensional transverse momentum of the fragments concerning the beam axis. In the regime where $r_T \ll p_T$, there exist two distinct scales integral to the fragmentation process.

$$\mu_+ = m_Q, \qquad \text{and} \qquad \mu_{\mathcal{J}} = m_Q \frac{r_T}{p_T} \,. \tag{3.66}$$

The perturbative calculation of the jet function involves logarithms of the ratios of scales, which, if left unaddressed, may spoil the convergence of the perturbative expansion. Hence, it is imperative to resum these logarithms to ensure the expansion's convergence. Notably, these logarithms are akin to those resummed by the TMD evolution. The resummation of the logarithms generated by the scales defined in 3.66 is feasible through factorization. To achieve this, we utilize the boosted-heavy-quark effective field theory (bHQET) [96], which facilitates the separation of the jet function into a hard matching coefficient and a matrix element dependent on transverse momentum. We provide here a description of the pertinent modes.

We start by examining the momentum of the heavy quark in the rest frame of the heavy meson, denoted as p_Q^μ. This momentum can be decomposed into a mass term and a residual soft component:

$$p_Q^\mu\Big|_{\text{rest frame}} = m_Q\beta^\mu + k_s^\mu\,, \qquad\qquad k_s^\mu \sim \Lambda_{\text{QCD}}(1,1,1)_v, \tag{3.67}$$

where k_s^μ is the typical size of soft (light) degrees of freedom in the heavy meson and $\beta^\mu = (1,1,0_\perp)_v$. Note that here we decomposed four-vectors into the light-cone coordinates along the direction of the boosted heavy meson, v. The momenta k_s^μ, in the boosted frame sets the size of energy loss of the heavy quark during fragmentation to a heavy meson. To obtain the boosted momenta we simply apply the following transformations,

$$v\cdot k \to \Lambda v\cdot k, \qquad\qquad \bar v\cdot k \to \frac{\bar v\cdot k}{\Lambda}, \qquad\qquad k_\perp \to k_\perp. \tag{3.68}$$

We can obtain Λ by comparing the momentum of the heavy quark at the rest frame of the heavy meson in 3.67 to the momentum of the boosted heavy quark (up to power-corrections $\sim m_H/p_T^H$),

$$p_Q^\mu\Big|_{\text{boosted frame}} \simeq \Big(2E_H, \frac{m_H^2}{2E_H}, \Lambda_{\text{QCD}}\Big)_v, \tag{3.69}$$

and thus $\Lambda = 2E_H/m_H$. The transformations in 3.68 give the momentum scaling of the so-called "ultra-collinear" modes which are simply the soft modes of HQET boosted to the frame where we perform the measurement,

$$k_{uc}^\mu \sim \Lambda_{\text{QCD}}\Big(\frac{2E_H}{m_H}, \frac{m_H}{2E_H}, 1\Big). \tag{3.70}$$

The contribution to the transverse momentum spectrum w.r.t. the beam axis, comes from the large component $\bar v\cdot k_{uc}$. Therefore, we can estimate the typical size of the transverse momentum imbalance, $r_T \sim \Lambda_{\text{QCD}}(2p_T^H/m_H)$. Since $p_T^H \gg m_H$, the typical soft scale, r_T, is perturbative and that justifies the approach of perturbative matching to the TMD matrix elements to which non-perturbative effects are incorporated as corrections.

To proceed with the factorization we match from the massive-SCET [96, 97], which includes collinear degrees of freedom, onto the boosted HQET where the degrees of freedom are the ultra-collinear modes. We are interested in the matching of the massive, collinear gauge invariant, quark building block, $\chi_v = W_v^\dagger\xi_v$ with

$$W_v^\dagger(x) = \text{P}\exp\left(ig\int_0^\infty ds\;\bar n\cdot A_n(\bar n s + x)\right), \tag{3.71}$$

onto the HQET heavy quark fields, $h_{v\beta_+}$,[5]

$$W_v^\dagger \, \xi_v \to C_+(m_Q,\mu) W_v^\dagger h_{v\beta_+}, \tag{3.72}$$

where $C_+(m_Q,\mu)$ is the short distance matching coefficient and β_+ denotes the heavy quark velocity in the boosted frame. With this matching we can now factorize the jet function into a short distance matching coefficient and a bHQET matrix element that depends on the transverse momentum of the ultra-collinear fragments,

$$J_{Q\to H}(\boldsymbol{b}, p_T, m_Q, \mu) = H_+(m_Q,\mu)\mathcal{J}_{Q\to H}\Big(\boldsymbol{b}, \frac{m_Q}{p_T}, \mu\Big), \tag{3.73}$$

where

$$H_+(m_Q,\mu) = |C_+(m_Q,\mu)|^2 \, . \tag{3.74}$$

The operator definition of the two-dimensional shape function is

$$\mathcal{J}_{Q\to H}(\boldsymbol{r}) = \frac{1}{2\,p_H^-\,N_C}\sum_X \langle 0|\delta^{(2)}\Big(\boldsymbol{r} - i\boldsymbol{v}\,(\bar v\cdot\partial\Big))W_v^\dagger h_{v\beta_+}|XH\rangle\langle XH|\bar h_{v,\beta_+} W_v\,\bar{\not{p}}|0\rangle, \tag{3.75}$$

where $\boldsymbol{v}$ is a Euclidean, two-dimensional, transverse component of light-like four-vector v^μ pointing along the direction of the boosted heavy meson. The impact parameter space expression is obtained by simply taking the Fourier transform,

$$\mathcal{J}_{Q\to H}\Big(\boldsymbol{b}, \frac{m_Q}{p_T}, \mu\Big) = \int d\boldsymbol{r}\exp(i\boldsymbol{b}\cdot\boldsymbol{r})\mathcal{J}_{Q\to H}(\boldsymbol{r}) \, . \tag{3.76}$$

The hard matching coefficient is known up to two loops but the jet function $\mathcal{J}_{Q\to H}(\boldsymbol{r})$, as defined above, appears here for the first time. However, as we discuss later in this section, this jet function is related at the operator level to the fragmentation shape function from [95, 73] in the near-end-point limit, ($z_H \to 1$). The one-loop hard function, H_+ is,

$$H_+(m_Q,\mu) = 1 + \frac{\alpha_s}{4\pi}C_F\Big\{\ln\Big(\frac{\mu^2}{m_Q^2}\Big) + \ln^2\Big(\frac{\mu^2}{m_Q^2}\Big) + 8 + \frac{\pi^2}{6}\Big\}, \tag{3.77}$$

and the corresponding anomalous dimension is

$$\gamma_+ = \frac{\alpha_s C_F}{\pi}\Big\{\frac{1}{2} - \ln\Big(\frac{m_Q^2}{\mu^2}\Big)\Big\} \, . \tag{3.78}$$

In the following section, we show the calculation of the bHQET matrix element, $\mathcal{J}_{Q\to H}$ at NLO and we use this result to derive the one-loop anomalous dimension. We demonstrate the consistency of anomalous dimensions for this process at NLO and we give an all-order statement that connects the matrix element $\mathcal{J}_{Q\to H}$ to the near-end-point fragmentation shape function for heavy mesons.

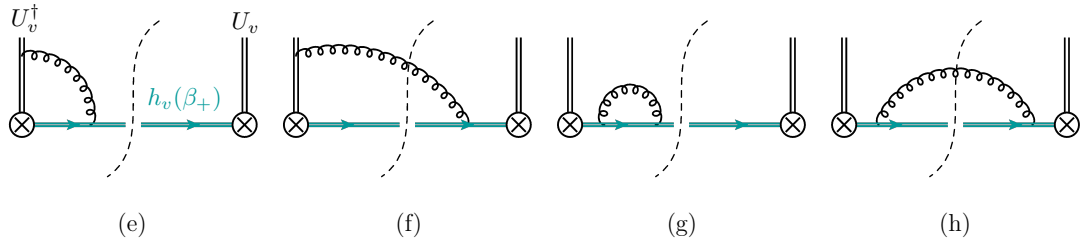

Figure 3.5: bHQET jet function at NLO diagrams.

3.2.2 bHQET matrix element at NLO

The one-loop contributions to $\mathcal{J}_{Q\to H}(\boldsymbol{b})$ in 3.76 are shown in fig. 3.5. We have non zero contributions only from diagrams (f) and (h) where a real gluon is exchanged. Virtual diagrams (e) and (g) are scaleless and vanish in our scheme,

$$\mathcal{J}_{Q\to Q}^{(\mathrm{f})+(\mathrm{h})} = \frac{\alpha_s C_F}{\pi}(1-\epsilon)\, e^{-\gamma_E \epsilon}\Gamma(\epsilon)\Gamma(-2\epsilon)\,\mathcal{R}^{2\epsilon} \tag{3.79}$$

where

$$\mathcal{R} = -\frac{i\, p_T \mu\, e^{\gamma_E}(\boldsymbol{v}\cdot\boldsymbol{b})}{m_Q|\boldsymbol{v}|} \tag{3.80}$$

where we have made the standard $\overline{\mathrm{MS}}$ scale replacement $\mu^2 \to \mu^2 \exp(\gamma_E)/(4\pi)$. Expanding 3.79 in the limit $\epsilon \to 0$ and keeping all ϵ poles and finite non-vanishing terms we have

$$\mathcal{J}_{Q\to Q}^{\mathrm{bare}}\Big(\boldsymbol{b}, \frac{m_Q}{p_T}\Big) = 1 + \frac{\alpha_s C_F}{\pi}\Big\{ -\frac{1}{2\epsilon^2} + \frac{1}{2\epsilon}\Big[1 - 2\ln\mathcal{R}\Big] + \ln\mathcal{R} - \ln^2\mathcal{R} - \frac{5\pi^2}{24}\Big\} \tag{3.81}$$

The renormalized jet function which in the $\overline{\mathrm{MS}}$-scheme is simply given by the finite terms in 3.81 is defined by the following equation,

$$\mathcal{J}_{Q\to Q}^{\mathrm{bare}}\Big(\boldsymbol{b}, \frac{m_Q}{p_T}\Big) = Z_{\mathcal{J}}\Big(\boldsymbol{b}, \frac{m_Q}{p_T}\mu\Big)\mathcal{J}_{Q\to Q}\Big(\boldsymbol{b}, \frac{m_Q}{p_T}, \mu\Big). \tag{3.82}$$

The corresponding anomalous dimension is

$$\gamma_{\mathcal{J}} = -Z_{\mathcal{J}}^{-1}\frac{d}{d\ln\mu}Z_{\mathcal{J}} = \frac{\alpha_s C_F}{\pi}\Big\{1 - 2\ln\mathcal{R}\Big\} \tag{3.83}$$

It is now trivial to show the consistency of the anomalous dimensions and therefore of factorization at NLO, since it is sufficient to show,

$$\gamma_{\mathcal{J}} + \gamma_+ = \gamma_J + \gamma_{\mathcal{C}_f}. \tag{3.84}$$

[5] In our notation β^μ is the collinear velocity of the heavy hadron and v^μ is the lightlike vector along the direction of the boosted quark. Thus we write $h_{v\beta_+}$ to indicate the typical velocity of the heavy quark expansion. The Wilson lines appearing on l.h.s. and r.h.s. of 3.72 are formally the same although the fields have a different scaling in the two cases.

The result presented in 3.81 contains logarithms related to the scale $m_Q/(p_T b_0)$, where $b_0 = b\exp(\gamma_E)/2$. On the other hand, the hard function H_+ as defined in 3.77 exclusively encompasses logarithms associated with m_Q. This separation indicates that we have effectively isolated these two distinct scales, allowing us to resum the ratios of these scales (i.e., logarithms of $p_T b_0$) by evaluating each function at its respective characteristic scale. Subsequently, we can evolve each of these functions to a common scale by solving their corresponding renormalization group equations.

3.2.3 Connection to the fragmentation shape function

In this section we show that the two dimensional bHQET jet function in 3.75 is related to the fragmentation shape function. We consider the operator definition of the shape function

$$S_{Q\to H}(\omega) = \frac{1}{2N_c}\sum_X \langle 0|\delta(\omega - i\sqrt{2}\,\bar v\cdot\partial) W_v^\dagger h_{v\beta_+}|H_\beta X\rangle\langle H_\beta X|\bar h_{v,\beta_+} W_v \frac{\bar n\!\!\!/}{\sqrt{2}}|0\rangle, \tag{3.85}$$

as in eq. 4.23 of [73]. The same shape function was written with a different notation in [95]. Taking the one-dimensional Fourier transform of this expression with respect to ω we have[6]

$$\begin{aligned}\tilde S_{Q\to H}(\tau) &= \int d\omega \exp(i\omega\tau) S_{Q\to H}(\omega)\\ &= \frac{1}{2\,m_H N_C}\sum_X \langle 0|\exp\Big(-\sqrt{2}\,\tau\,\bar v\cdot\partial\Big)\, W_v^\dagger h_{v\beta_+}|XH\rangle\langle XH|\bar h_{Qv} W_v \frac{\bar n\!\!\!/}{\sqrt{2}}|0\rangle.\end{aligned} \tag{3.86}$$

Comparing this result with the two-dimensional Fourier transform of 3.75 as prescribed in 3.76 we have

$$\mathcal{J}_{Q\to H}(\boldsymbol{b}) = \frac{m_H}{\sqrt{2}\,p_H^-}\tilde S_{Q\to H}\Big(\tau\to\frac{\boldsymbol{v}\cdot\boldsymbol{b}}{\sqrt{2}}\Big). \tag{3.87}$$

Using this equation we can confirm our perturbative calculation at NLO in 3.81 by comparing the finite terms of this equation against eq. 4.24 of [73]. To do that one needs the Fourier transformations of the regular plus-distributions which can be found in the literature but we also give here for completeness,

$$\mathcal{FT}\Big[\delta(\omega)\Big] = 1, \tag{3.88}$$

$$\mathcal{FT}\Big[\Big(\frac{\Theta(\omega)}{\omega}\Big)_+\Big] = -\ln(-i\tau e^{\gamma_E}), \tag{3.89}$$

$$\mathcal{FT}\Big[\Big(\frac{\Theta(\omega)\ln\omega}{\omega}\Big)_+\Big] = \frac{1}{2}\ln^2(-i\tau e^{\gamma_E}) + \frac{\pi^2}{12}. \tag{3.90}$$

Using these equations we can easily check that indeed 3.87 is satisfied up to NLO, although the perturbative validity of 3.87 is inferred beyond NLO. Therefore, since the anomalous dimension of the fragmentation shape function and the hard function H_+ is already known

[6] Note the normalization of the Hilbert states $|H\rangle = \sqrt{m_H}|H_\beta\rangle$

up to two loops, we can use the consistency of factorization to solve for the anomalous dimension of the global soft function $S_{\gamma g}$ up to two-loops,

$$\gamma_{S_{\gamma g}} = -\left(\gamma_{H_{\gamma g}} + \gamma_{F_g} + \gamma_\alpha + \gamma_{\mathcal{J}}(\boldsymbol{v}_1) + \gamma_{\mathcal{J}}(\boldsymbol{v}_2) + 2\gamma_+\right). \tag{3.91}$$

The anomalous dimensions at two and three loops are given in appendix A.2. We give the result for the soft function by organizing it into a term proportional to the cusp anomalous dimension, γ_{cusp} and a "non-cusp" term,

$$\gamma_{S_{\gamma g}} = \gamma_{\text{cusp}}\left[2C_F \ln\left(\frac{B\mu^2 e^{2\gamma_E}}{-A_{\boldsymbol{b}}}\right) - C_A \ln\zeta_2\right] + \delta\gamma_{S_{\gamma g}}, \tag{3.92}$$

where

$$\begin{aligned}
\delta\gamma^{[1]}_{S_{\gamma g}} &= 0 \\
\delta\gamma^{[2]}_{S_{\gamma g}} &= C_F\Big[C_A\Big(\frac{1616}{27} - \frac{22}{9}\pi^2 - 56\,\zeta_3\Big) + n_f T_F\Big(-\frac{448}{27} + \frac{8}{9}\pi^2\Big)\Big],
\end{aligned} \tag{3.93}$$

and we have used the same notation for the perturbative expansion of the cusp anomalous dimension as in 3.60. The lengthy and not so intuitive three-loop non-cusp component, $\delta\gamma^{[3]}_{S_{\gamma g}}$, is given in the appendix (see A.21).

With this result, we can push the calculation of the heavy-meson pair production up to NNLL with no additional perturbative calculations. Furthermore with the knowledge of the soft anomalous dimension and using 3.58 we can also solve for the collinear-soft anomalous dimension to the same order. This can now give us the NNLL cross-section of the dijet photon-gluon-fusion ($\gamma^* g$) process. For the full NNLL dijet cross-section, we are still missing the global-soft or collinear-soft anomalous dimensions from the photon-quark-initiated ($\gamma^* f$) process.

3.3 Cross-section used in phenomenology

The cross-sections presented previously are usually partially integrated in phenomenological observables. We discuss here these integrations, which also allow us to relate the normalization of our cross-section with the ones obtained in the literature.

3.3.1 Extracting the Born-level cross-sections

The tree-level cross-sections for the dijet and hadron pair production were considered at tree level in ref. [92]. We start considering the gluon case, from which one can easily deduce also the quark case. The gluon hard contribution to the cross-section is described by

$$\frac{d\sigma(\gamma^* g)}{dx\,d\eta_1 d\eta_2 d\boldsymbol{p}_T d\boldsymbol{r}_T} = \frac{\mathcal{N}}{xs}\Big[A_0 + A_1\cos 2\phi'_p + \cdots + B_0\cos 2\phi'_r + \cdots\Big], \tag{3.94}$$

and the azimuthal angles (ϕ'_r, ϕ'_p) of vectors $\boldsymbol{p}_T, \boldsymbol{r}_T$ are measured with respect to the lepton plane. However, our preferred frame is the one where the ϕ_ℓ angle is measured in

the plane defined by $\boldsymbol{p}_T$ and $\boldsymbol{q}_T$, the sum of the lepton momenta, and ϕ_r is the azimuthal angle between $\boldsymbol{r}_T$ and $\boldsymbol{p}_T$. In this frame and integrating over the angle ϕ_ℓ we are left with:

$$\frac{d\sigma(\gamma^* g)}{dx d\eta_1 d\eta_2 dp_T d\boldsymbol{r}_T} = 2\pi p_T \frac{\mathcal{N}}{xs}\Big[A_0 + B_2\cos(2\phi_r)\Big], \tag{3.95}$$

with the factor 2π coming from ϕ_ℓ integration. The LO expressions are obtained by separating the unpolarized and linearly polarized gluon contributions and Fourier transforming. The unpolarized partonic part has a similar form also for quarks, so that we find

$$\frac{d\sigma^U(\gamma^* g)}{dx d\eta_1 d\eta_2 dp_T d\boldsymbol{r}_T}\Big|_{\rm LO} = \sigma_0^{gU}\int \frac{d^2\boldsymbol{b}}{(2\pi)^2}\exp(i\boldsymbol{b}\cdot\boldsymbol{r}_T)\, f_1^g(\xi,\boldsymbol{b}) = \sigma_0^{gU} f_1^g(\xi,\boldsymbol{r}_T)\,, \tag{3.96}$$

$$\frac{d\sigma^U(\gamma^* f)}{dx d\eta_1 d\eta_2 dp_T d\boldsymbol{r}_T}\Big|_{\rm LO} = \sigma_0^{fU}\int \frac{d^2\boldsymbol{b}}{(2\pi)^2}\exp(i\boldsymbol{b}\cdot\boldsymbol{r}_T)\, f_1^f(\xi,\boldsymbol{b}) = \sigma_0^{fU} f_1^f(\xi,\boldsymbol{r}_T)\,, \tag{3.97}$$

The same for the linearly polarized gluons gives

$$\begin{aligned}
\frac{d\sigma^L(\gamma^* g)}{dx d\eta_1 d\eta_2 dp_T d\boldsymbol{r}_T}\Big|_{\rm LO} &= \sigma_0^{gL}\int \frac{d^2\boldsymbol{b}}{(2\pi)^2}\exp(i\boldsymbol{r}_T\cdot\boldsymbol{b})\,\frac{\sin^2\phi_b - \cos^2\phi_b}{2}\, h_1^\perp(\xi,\boldsymbol{b})\,. \\
&= -\sigma_0^{gL}\int \frac{b\,db\,d\phi_b}{8\pi^2}\exp\Big(ir_T b\cos(\phi_b-\phi_r)\Big)\,\cos(2\phi_b)\, h_1^\perp(\xi,\boldsymbol{b}) \\
&= \cos(2\phi_r)\,\sigma_0^{gL}\int \frac{b\,db}{4\pi} J_2(r_T b)\, h_1^\perp(\xi,\boldsymbol{b}) \\
&= -\frac{\cos(2\phi_r)}{2}\,\sigma_0^{gL}\, h_1^\perp(\xi,\boldsymbol{r}_T),
\end{aligned} \tag{3.98}$$

where notice that $h_1^\perp(\xi, r_T)$ is not the direct Fourier transform of $h_1^\perp(\xi, b)$ and both functions can be related through eq. 2.20 in [37]. We obtain the $\sigma_0^{(g,f)(U,L)}$ prefactors from the structure functions given in eq. 3.3 and eq. 3.5 in [92] and we list them in the appendix.

3.3.2 Angle integrated and azimuthally modulated cross-section

The scalar cross-section that we finally consider in the phenomenological studies is obtained by integrating over the ϕ_r angle

$$\frac{d\sigma}{d\Pi dr_T} = r_T\int_{-\pi}^{+\pi} d\phi_r \frac{d\sigma}{d\Pi d\boldsymbol{r}_T}, \tag{3.99}$$

where we use $d\Pi = dx d\eta_1 d\eta_2 dp_T$ for brevity. Because the factorized cross-section is always expressed in position space one can write (here $J_{0,2}$ are Bessel functions)

$$\begin{aligned}
\frac{d\sigma}{d\Pi dr_T} &= r_T\int_{-\pi}^{+\pi} d\phi_r \int \frac{d\boldsymbol{b}}{(2\pi)^2}\exp\Big[ir_T b\cos(\phi_b-\phi_r)\Big]\,\frac{d\tilde{\sigma}(\boldsymbol{b})}{d\Pi d\boldsymbol{b}} \\
&= r_T\int_0^\infty \frac{b\,db}{2\pi} J_0(r_T b)\int_{-\pi}^{+\pi} d\phi_b\,\frac{d\tilde{\sigma}(\boldsymbol{b})}{d\Pi d\boldsymbol{b}}
\end{aligned}$$

$$= r_T \int_0^\infty \frac{b\,db}{2\pi} J_0(r_T b) \int_{-\pi}^{+\pi} d\phi_b \left[\frac{d\tilde{\sigma}^U(\boldsymbol{b})}{d\Pi d\boldsymbol{b}} - \frac{\cos 2\phi_b}{2} \frac{d\tilde{\sigma}^L(\boldsymbol{b})}{d\Pi d\boldsymbol{b}} \right], \tag{3.100}$$

where $d\sigma^U = d\sigma^U(\gamma^* f) + d\sigma^U(\gamma^* g)$, $d\sigma^L = d\sigma^L(\gamma^* g)$ for the dijet case and $d\sigma^{U,L} = d\sigma^{U,L}(\gamma^* g)$ for the heavy hadron pair case.

In our phenomenological analysis we consider also the azimuthal angle average

$$\langle \cos 2\phi_r \rangle \equiv \left[\int_{-\pi}^{+\pi} d\phi_r \cos 2\phi_r \frac{d\sigma}{d\Pi d\boldsymbol{r}_T} \right] \Bigg/ \frac{d\sigma}{d\Pi dr_T}. \tag{3.101}$$

The denominator is what we have discussed in the previous section, so now we will only focus on the numerator,

$$\begin{aligned} \int_{-\pi}^{+\pi} d\phi_r \cos 2\phi_r \frac{d\sigma}{d\Pi d\boldsymbol{r}_T} &= r_T \int_{-\pi}^{+\pi} d\phi_r \cos 2\phi_r \int \frac{d\boldsymbol{b}}{(2\pi)^2} \exp\left[i r_T b \cos(\phi_b - \phi_r) \right] \frac{d\tilde{\sigma}(\boldsymbol{b})}{d\Pi d\boldsymbol{b}} \\ &= r_T \int_0^\infty \frac{b\,db}{2\pi} J_2(r_T b) \int_{-\pi}^{+\pi} d\phi_b \cos 2\phi_b \frac{d\tilde{\sigma}(\boldsymbol{b})}{d\Pi d\boldsymbol{b}} \\ &= r_T \int_0^\infty \frac{b\,db}{2\pi} J_2(r_T b) \int_{-\pi}^{+\pi} d\phi_b \left[\cos 2\phi_b \frac{d\tilde{\sigma}^U(\boldsymbol{b})}{d\Pi d\boldsymbol{b}} - \frac{\cos^2 2\phi_b}{2} \frac{d\tilde{\sigma}^L(\boldsymbol{b})}{d\Pi d\boldsymbol{b}} \right]. \end{aligned} \tag{3.102}$$

Eqs. 3.100-3.102 show the relation between the final cross-section in momentum space and the factorized cross-sections in position space, where we have distinguished between the unpolarized cross-sections generated by gluons and quarks, $d\tilde{\sigma}^U = d\tilde{\sigma}^U_g + d\tilde{\sigma}^U_f$ and the contribution from linearly polarized gluons $d\tilde{\sigma}^L$.

3.4 Angular dependence and evolution

The anomalous dimensions of soft, collinear-soft and heavy-jets matrix elements are angular dependent and complex-valued, and both these features are not common in the literature. The angular dependence is parameterized here by the angle ϕ_b. In order to discuss the issue we show in sec. 3.4.1 the dijet soft function as obtained in [98] and then we extend the conclusions to the other functions that have a similar angular dependent structure. The angular dependence of the anomalous dimension is strictly correlated with the imaginary parts of the cross-section in position space. The treatment of the angular dependence in the evolution has been discussed also in [99, 100, 101] which proposes an approximate treatment. In sec. 3.4.2 we perform an original analysis discussing in detail how passing from position space to momentum space in the cross-section allows us to obtain a real-valued cross-section, including resummation. The proof of this statement is here provided at one-loop, and the same mechanism can be conjectured to work at all orders in perturbation theory.

3.4.1 Dijet soft function and angle dependent anomalous dimensions

The dijet soft function presents several properties that result particularly interesting. The renormalized soft function is obtained from its bare expression

$$S_{\gamma i}^{\rm bare}(\boldsymbol{b},\zeta_2) = Z_{\gamma i}^{S}(\boldsymbol{b},\mu,\zeta_2) S_{\gamma i}(\boldsymbol{b},\mu,\zeta_2), \tag{3.103}$$

where the factor $Z_{\gamma i}^{S}$ was calculated in [98]. For our purposes it is sufficient to report the expression of the soft function in the $\overline{\rm MS}$ scheme for the $(\gamma^* g)$-channel

$$\begin{aligned} S_{\gamma g}(\boldsymbol{b},\mu,\zeta_2) = 1 + a_s\Big\{ C_F\Big[\frac{\pi^2}{3} + 2\ln^2\Big(\frac{B\mu^2 e^{2\gamma_E}}{-A_{\boldsymbol{b}}}\Big) + 4{\rm Li}_2(1+A_{\boldsymbol{b}})\Big] \\ + C_A\Big[-2\ln\big(B\mu^2 e^{2\gamma_E}\big)\ln\zeta_2 - \ln^2(-A_{\boldsymbol{b}}) - \frac{\pi^2}{3} - 2{\rm Li}_2(1+A_{\boldsymbol{b}})\Big]\Big\} + \mathcal{O}(a_s^2), \end{aligned} \tag{3.104}$$

and for the $(\gamma^* f)$-channel

$$\begin{aligned} S_{\gamma f}(\boldsymbol{b},\mu,\zeta_2) = 1 + a_s\Big\{ C_A\Big[\frac{\pi^2}{6} + \ln^2\Big(\frac{B\mu^2 e^{2\gamma_E}}{-A_{\boldsymbol{b}}}\Big) + 2{\rm Li}_2(1+A_{\boldsymbol{b}}) \\ + 2\ln\big(B\mu^2 e^{2\gamma_E}\big)\ln\frac{(n\cdot v_1)(\boldsymbol{v}_2\cdot\boldsymbol{b})}{(n\cdot v_2)(\boldsymbol{v}_1\cdot\boldsymbol{b})}\Big] + C_F\ln\big(B\mu^2 e^{2\gamma_E}\big)\Big[\ln\big(B\mu^2 e^{2\gamma_E}\big) \\ - 2\ln\zeta_2 + 2\ln\Big(\frac{2(n\cdot v_2)}{(v_1\cdot v_2)(n\cdot v_2)}\Big) + 4\ln(-i\,\boldsymbol{v}_1\cdot\hat{\boldsymbol{b}})\Big] - C_F\frac{\pi^2}{6}\Big\} + \mathcal{O}(a_s^2), \end{aligned} \tag{3.105}$$

respectively, where we have $A_{\boldsymbol{b}} = \frac{(v_1\cdot v_2)}{2\,(v_1\cdot\hat{b})\,(v_2\cdot\hat{b})}$. The expressions above depend explicitly on the angle ϕ_b and we have used $\hat{\boldsymbol{b}} = \boldsymbol{b}/|\boldsymbol{b}|$. The rapidity scale ζ_2 is responsible for the rapidity evolution of this factor and it is related to the TMD rapidity scale ζ_1 by the consistency constraint

$$\zeta_1\,\zeta_2 = \frac{(k^-)^2}{A_n} = \frac{\hat{u}\,\hat{t}}{\hat{s}}. \tag{3.106}$$

The values of ζ_1 and ζ_2 that minimize hard logs are

$$\zeta_1 = p_T^2, \qquad \zeta_2 = 1. \tag{3.107}$$

Despite the fact that the scale ζ_2 is dimensionless there are some formal similarities in the evolution of this soft function and the TMD. The dijet soft function double-scale evolution is dictated by

$$\frac{d}{d\ln\mu} S_{\gamma i}(\boldsymbol{b},\zeta,\mu) = \gamma_{S_{\gamma i}}(\boldsymbol{b},\mu,\zeta) S_{\gamma i}(\boldsymbol{b},\zeta,\mu), \tag{3.108}$$

$$\frac{d}{d\ln\zeta} S_{\gamma i}(\boldsymbol{b},\zeta,\mu) = -\mathcal{D}_i(\mu,b) S_{\gamma i}(\boldsymbol{b},\zeta,\mu), \tag{3.109}$$

where i is gluon or quark. The rapidity evolution kernel $\mathcal{D}_i$ is the same as in the TMD case, while for the rest we need special treatment.

3.4.2 Treatment of angular dependent anomalous dimensions and resummation

The dijet soft function, the collinear-soft function in dijets and the heavy meson jet function in hadron pair production have, as a common feature, an anomalous dimension that is ϕ_b-dependent and that can include some imaginary parts. The general structure of the anomalous dimension for these cases is

$$\gamma_i(\boldsymbol{b},\mu) = \gamma_{\rm cusp}[\alpha_s]\left(c_i\, 2\ln|\cos\phi_b| - c_i'\, i\pi\Theta(\phi_b)\right) + \text{other } \phi_b \text{ independent terms} \quad (3.110)$$

where

$$\Theta(\phi_b) = \begin{cases} +1 & : -\pi/2 < \phi_b < \pi/2 \\ -1 & : \text{otherwise} \end{cases} \quad (3.111)$$

and the consistency of anomalous dimensions requires

$$\sum_i c_i = \sum_i c_i' = 0, \quad (3.112)$$

where c_i and c_i' are the color coefficients that multiply the corresponding part of the cusp anomalous dimension. The construction of the evolution kernel involves an integration over the angle ϕ_b and after integration all imaginary parts cancel consistently. Note that this does not mean that one can ignore the imaginary components of the anomalous dimensions or fixed order functions as contributions of imaginary terms yield real contributions to the final result.

In order to show the cancellation of the imaginary part we separate the angular dependent part of the evolution kernel from the rest. For instance, for the soft function, we have

$$\begin{aligned} S_{\gamma i}(\boldsymbol{b},\mu_f,\zeta_{2,f}) &= \\ &= \exp\left[\int_P \left(\gamma_{S_{\gamma i}}(\boldsymbol{b},\mu,\zeta_2)d\ln\mu - \mathcal{D}_i(\mu,b)d\ln\zeta_2\right)\right] S(\boldsymbol{b};\mu_0,\zeta_{2,0}) \\ &= \exp\left[\int_P \left(\gamma^\phi_{S_{\gamma i}}(\phi)d\ln\mu + \bar\gamma_{S_{\gamma i}}(b,\mu,\zeta_2)d\ln\mu - \mathcal{D}_i(\mu,b)d\ln\zeta_2\right)\right] S_{\gamma i}(\boldsymbol{b},\mu_0,\zeta_{2,0}) \\ &= \exp\left[\int_{\mu_0}^{\mu_f}\left(\gamma^\phi_{S_{\gamma i}}(\phi)d\ln\mu\right)\right] \exp\left[\int_P \left(\bar\gamma_{S_{\gamma i}}(b,\mu,\zeta_2)d\ln\mu - \mathcal{D}_i(\mu,b)d\ln\zeta_2\right)\right] S_{\gamma i}(\boldsymbol{b},\mu_0,\zeta_{2,0}) \\ &= \mathcal{R}^\phi_{S_{\gamma i}}\ \mathcal{R}_{S_{\gamma i}}\ S_{\gamma i}(\boldsymbol{b},\mu_0,\zeta_{2,0})\,. \end{aligned} \quad (3.113)$$

The evolution factor is then split into an angular-dependent part and the rest. The splitting is clearly not unique, however this should not affect the final result once the angular integration is performed. We have

$$\frac{d}{d\ln\mu}\mathcal{R}^\phi_{S_{\gamma i}} = \gamma^\phi_S(\phi)\mathcal{R}^\phi_{S_{\gamma i}}, \quad \frac{d}{d\ln\zeta}\mathcal{R}^\phi_{S_{\gamma i}} = 0 \quad (3.114)$$

$$\frac{d}{d\ln\mu}\mathcal{R}_{S_{\gamma i}} = \bar\gamma_S\mathcal{R}_{S_{\gamma i}}, \quad \frac{d}{d\ln\zeta}\mathcal{R}_{S_{\gamma i}} = -\mathcal{D}_i\mathcal{R}_{S_{\gamma i}}, \quad (3.115)$$

A similar splitting is done for all other angular dependent evolution kernels, for which we have used

$$\gamma^{\phi}_{S_{\gamma g}} = \gamma_{\rm cusp}\Big[4C_F \ln|\cos\phi_b|\Big], \tag{3.116}$$

$$\gamma^{\phi}_{S_{\gamma f}} = \gamma_{\rm cusp}\Big[2(C_F+C_A)\ln|\cos\phi_b| - (C_F-C_A)i\pi\Theta(\phi_b)\Big], \tag{3.117}$$

$$\gamma^{\phi}_{\mathcal{C}_g} = \gamma_{\rm cusp}C_A\Big[-2\ln|\cos\phi_b| - i\pi\Theta(\phi_b)\Big], \tag{3.118}$$

$$\gamma^{\phi}_{\mathcal{C}_f} = \gamma_{\rm cusp}C_F\Big[-2\ln|\cos\phi_b| \pm i\pi\Theta(\phi_b)\Big], \tag{3.119}$$

$$\gamma^{\phi}_{J} = \gamma_{\rm cusp}C_F\Big[-2\ln|\cos\phi_b| \pm i\pi\Theta(\phi_b)\Big], \tag{3.120}$$

where the $\pm$ sign refers to quark and anti-quark jet respectively. The angular independent part of the anomalous dimension is simply obtained from the complete expression of the anomalous dimension

$$\gamma_i = \gamma^{\phi}_i + \bar{\gamma}_i \tag{3.121}$$

with $i = S_{\gamma g}, S_{\gamma f}, \mathcal{C}_g, \mathcal{C}_f, J$ for each channel.

In order to describe the implications of the angle integration we consider here the dijet production case, being the HHP one very similar. The separation of the evolution kernels of all functions in an angular dependent part and the rest allows to write the resummed cross-section in position space as

$$\begin{aligned} d\tilde{\sigma}(\boldsymbol{b}) &\sim \exp\Big[\mathcal{A}(\{\mu_i\})\,2\ln|\cos\phi_b| - \mathcal{B}(\{\mu_i\})\,i\pi\Theta(\phi_b)\Big]\mathcal{R}(\{\mu_k\}\to\mu) \\ &\qquad\times\Big[1+\sum_{k\in\{H,F,J,S,\mathcal{C}\}} a_s(\mu_k) f_k^{[1]}(b,\cos\phi_b)\Big] \\ &= |\cos\phi_b|^{2\mathcal{A}}\Big(\cos(\mathcal{B}\pi) - i\Theta(\phi_b)\sin(\mathcal{B}\pi)\Big)\mathcal{R}(\{\mu_k\}\to\mu)\Big[1+\sum_{k\in\{H,F,J,S,\mathcal{C}\}} a_s(\mu_k) f_k^{[1]}(b,\cos\phi_b)\Big] \end{aligned} \tag{3.122}$$

where we have omitted global scale independent hard factors and non-perturbative contributions that we assume independent of the angle ϕ_b. In this equation, we have combined the evolution kernel of the functions that appear in the cross-section in

$$\mathcal{A}(\{\mu_i\}) = \sum_{i\in\{S,\mathcal{C}\}} c_i \int_{\mu_i}^{\mu} \gamma_{\rm cusp}[\alpha_s] d\ln\mu', \quad \mathcal{B}(\{\mu_i\}) = \sum_{i\in\{S,\mathcal{C}\}} c'_i \int_{\mu_i}^{\mu} \gamma_{\rm cusp}[\alpha_s] d\ln\mu' \tag{3.123}$$

which are independent of the factorization scale μ because of eq. 3.112, and an angle independent part $\mathcal{R}(\{\mu_k\}\to\mu)$. The perturbative parts of all functions that appear in the cross-sections at one loop are collected in the factor $\Big[1+\sum_{k\in\{H,F,J,S,\mathcal{C}\}} a_s(\mu_k) f_k^{[1]}\Big]$. In eq. 3.122 the imaginary part of the cross-section is proportional to the odd function $\Theta(\phi_b)$. We expect so that this part cancel at all orders in perturbation theory when the ϕ_b the Fourier transform is performed like in eq. 3.100-3.102. In the next subsection, we show that this is explicitly the case at one loop.

In order to organize the discussion we first consider the case of $d\tilde{\sigma}^U$ and then deduce the necessary modifications to get the Fourier transform of $d\tilde{\sigma}^L$. The angular integration of the cross-section at one loop can always be expressed in terms of the following basic integrals:

$$I_n(\mathcal{A}) \equiv \int_{-\pi}^{+\pi} d\phi_b \, |\cos\phi_b|^{2\mathcal{A}} \, \ln^n |\cos\phi_b| \tag{3.124}$$

where

$$\begin{aligned}
I_0(\mathcal{A}) &= \frac{2\sqrt{\pi}\,\Gamma(1/2+\mathcal{A})}{\Gamma(1+\mathcal{A})}, \\
I_1(\mathcal{A}) &= \frac{\sqrt{\pi}\,\Gamma(1/2+\mathcal{A})}{\Gamma(1+\mathcal{A})}\,(H_{\mathcal{A}-1/2} - H_{\mathcal{A}}) \\
I_2(\mathcal{A}) &= \frac{\sqrt{\pi}\,\Gamma(1/2+\mathcal{A})}{2\Gamma(1+\mathcal{A})}\,\Big[(H_{\mathcal{A}-1/2} - H_{\mathcal{A}})^2 + \psi^{(1)}\Big(\frac{1}{2}+\mathcal{A}\Big) - \psi^{(1)}(1+\mathcal{A})\Big].
\end{aligned} \tag{3.125}$$

The results on the r.h.s. of eq. 3.125 are defined only for $\mathcal{A} > -1/2$. In order to satisfy this condition for every value of b the scales μ_S and $\mu_{\mathcal{C}}$ must be chosen appropriately, which at the current level of precision can be done. Next we show the contribution of each term of $f_k^{[1]}$ to the cross-section:

- *Constant terms:* In this case we consider the leading order term in eq. 3.122 together with all terms in the functions $f_k^{[1]}$ that are $\cos\phi_b$ independent. The integral we need to perform is,

$$I_{\text{const.}}(\mathcal{A},\mathcal{B}) \equiv \int_{-\pi}^{+\pi} d\phi_b \, |\cos\phi_b|^{2\mathcal{A}} \Big(\cos(\mathcal{B}\pi) - i\Theta(\phi_b)\sin(\mathcal{B}\pi)\Big) = I_0(\mathcal{A})\cos(\mathcal{B}\pi) \tag{3.126}$$

  and the imaginary part cancels because of parity.

- *Single logarithmic terms:* In this case we consider terms proportional to $\ln(-i\cos\phi_b)$ that appear in the soft and collinear-soft terms $f_S^{[1]}$ and $f_{\mathcal{C}}^{[1]}$ respectively. The relevant integral that we need to perform is

$$I_{\log}(\mathcal{A},\mathcal{B}) \equiv \int_{-\pi}^{+\pi} d\phi_b \, |\cos\phi_b|^{2\mathcal{A}} \Big(\cos(\mathcal{B}\pi) - i\Theta(\phi_b)\sin(\mathcal{B}\pi)\Big) \, \ln(-i\cos\phi_b). \tag{3.127}$$

  Expanding the logarithm as follows

$$\ln(-i\cos\phi_b) = \ln|\cos\phi_b| - \frac{i\pi}{2}\Theta(\phi_b) \tag{3.128}$$

  we can split the main integral into one part proportional to $\cos(\mathcal{B}\pi)$ and a second part proportional to $\sin(\mathcal{B}\pi)$. In terms of the integrals in eq. 3.125 we obtain the real-valued result

$$I_{\log}(\mathcal{A},\mathcal{B}) = I_1(\mathcal{A})\cos(\mathcal{B}\pi) - \frac{\pi}{2} I_0(\mathcal{A})\sin(\mathcal{B}\pi). \tag{3.129}$$

- *Logarithmic $A_{\boldsymbol{b}}$ terms:* In the soft function we observe the presence of terms that involve the following combination,

$$A_{\boldsymbol{b}} = \frac{(v_1 \cdot v_2)}{2(v_1 \cdot \hat{b})(v_1 \cdot \hat{b})} = -\frac{\hat{s}}{4p_T^2(\cos\phi_b)^2} \tag{3.130}$$

Particularly this term appears in logarithms and di-logarithms. Here we address the double logarithmic terms, i.e.,

$$\ln^2(-A_{\boldsymbol{b}}) = \ln^2\Big(\frac{\hat{s}}{4p_T^2}\Big) - 4\ln\Big(\frac{\hat{s}}{4p_T^2}\Big)\ln|\cos\phi_b| + 4\ln^2|\cos\phi_b| \tag{3.131}$$

Integrating over ϕ_b the above we obtain three contributions: a constant term, a single-log and a double-log. Thus we can immediately write,

$$\begin{aligned} I_{\rm logA}(\mathcal{A},\mathcal{B}) &\equiv \int_{-\pi}^{+\pi} d\phi_b\,|\cos\phi_b|^{2\mathcal{A}}\Big(\cos(\mathcal{B}\pi) - i\Theta(\phi_b)\sin(\mathcal{B}\pi)\Big)\ \ln^2(-A_{\boldsymbol{b}}) \\ &= \Big[\ln^2\Big(\frac{\hat{s}}{4p_T^2}\Big)I_0(\mathcal{A}) - 4\ln\Big(\frac{\hat{s}}{4p_T^2}\Big)I_1(\mathcal{A}) + 4I_2(\mathcal{A})\Big]\cos(\mathcal{B}\pi). \end{aligned} \tag{3.132}$$

- *Double logarithmic terms:* In this case we consider terms proportional to $\ln^2(-i\cos\phi_b)$ that appear in the soft and collinear-soft functions. The relevant integral that we need to perform is

$$I_{\rm log2}(\mathcal{A},\mathcal{B}) \equiv \int_{-\pi}^{+\pi} d\phi_b\,|\cos\phi_b|^{2\mathcal{A}}\Big(\cos(\mathcal{B}\pi) - i\Theta(\phi_b)\sin(\mathcal{B}\pi)\Big)\ \ln^2(-i\cos\phi_b) \tag{3.133}$$

we can then expand the logarithm as follows

$$\ln^2(-i\cos\phi_b) = \ln^2|\cos\phi_b| - \frac{\pi^2}{4} - i\pi\Theta(\phi_b)\ln|\cos\phi_b| \tag{3.134}$$

then we can expand as before in terms proportional to $\sin(\mathcal{B}\pi)$ and terms proportional to $\cos(\mathcal{B}\pi)$

$$I_{\rm log2}(\mathcal{A},\mathcal{B}) = \Big[-\frac{\pi^2}{4}I_0(\mathcal{A}) + I_2(\mathcal{A})\Big]\cos(\mathcal{B}\pi) - \pi I_1(\mathcal{A})\sin(\mathcal{B}\pi). \tag{3.135}$$

In addition we have poly-logarithmic terms which are proportional to $\mathrm{Li}_2(1 - A_{\boldsymbol{b}})$,

$$I_{\rm Li}(\mathcal{A},\mathcal{B},\bar{c}) \equiv \cos(\mathcal{B}\pi)\int_{-\pi}^{+\pi} d\phi_b\,|\cos\phi_b|^{2\mathcal{A}}\ \mathrm{Li}_2\Big(1 - \frac{1}{\bar{c}\ \cos^2\phi_b}\Big), \tag{3.136}$$

where

$$\bar{c} \equiv \frac{4p_T^2}{\hat{s}}\ , \qquad\qquad 0 < \bar{c} \leq 1, \tag{3.137}$$

and where we have dropped the terms proportional to $\sin(\mathcal{B}\pi)$ since they vanish after integration from parity. We can then use properties of the poly-logarithm in order to express this integral in the following form,

$$I_{\rm Li}(\mathcal{A},\mathcal{B},\bar{c}) = \cos(\mathcal{B}\pi)\Big\{ -\frac{1}{2}\Big[\Big(\ln^2\bar{c}+\frac{\pi^2}{3}\Big)I_0(\mathcal{A}) + 4\ln\bar{c}I_1(\mathcal{A}) + 4I_2(\mathcal{A})\Big] \\ + \int_{-\pi}^{+\pi} d\phi_b\,|\cos\phi_b|^{2\mathcal{A}}\,\Big[\mathrm{Li}_2(\bar{c}\,\cos^2\phi_b) + \ln\big(\bar{c}\,\cos^2\phi_b\big)\ln\big(1-\bar{c}\,\cos^2\phi_b\big)\Big]\Big\} \quad (3.138)$$

We can then expand the poly-logarithms and the $\ln\big(1-\bar{c}\,\cos^2\phi_b\big)$ in the region $0<c\leq 1$. This allows us to perform the integral over ϕ_b and obtain the following,

$$I_{\rm Li}(\mathcal{A},\mathcal{B},\bar{c}) = \cos(\mathcal{B}\pi)\Big\{ -\frac{1}{2}\Big[\Big(\ln^2\bar{c}+\frac{\pi^2}{3}\Big)I_0(\mathcal{A}) + 4I_1(\mathcal{A})\,\ln\bar{c} + 4I_2(\mathcal{A})\Big] \\ -\sum_{n=1}^{\infty}\frac{\bar{c}^n}{n}\Big[\Big(\ln\bar{c}-\frac{1}{n}\Big)I_0(\mathcal{A}+n) + 2I_1(\mathcal{A}+n)\Big]\Big\} \quad (3.139)$$

Although this expression is exact it includes a sum extending to infinity. In numerical applications, one can truncate this sum at the desired value to achieve a certain numerical precision. This concludes the discussion of all possible cases that appear in the Fourier transform of the unpolarized cross-section.

The part of the cross-section relative to linearly polarized gluons can be treated similarly. In this case, we need to incorporate an additional $\cos 2\phi_b$ term in the integrals but this is the only change since the soft and collinear-soft functions that appear in the two contributions are the same as for the dijet case. Using the trigonometric identity $\cos 2\phi_b = 2\cos^2\phi_b - 1$ the integrals for this case can be deduced from the discussion of the unpolarized cross-section by the replacement

$$I_n(\mathcal{A}) \quad\longrightarrow\quad -I_n(\mathcal{A}+1) + \frac{1}{2}I_n(\mathcal{A})\,. \quad (3.140)$$

Equivalently for the case of angular modulation in eq. 3.101 the following transformations have to be performed,

$$\begin{aligned} d\tilde{\sigma}^U(\boldsymbol{b}):&\qquad I_n(\mathcal{A}) \quad\longrightarrow\quad -I_n(\mathcal{A}) + 2I_n(\mathcal{A}+1) \\ d\tilde{\sigma}^L(\boldsymbol{b}):&\qquad I_n(\mathcal{A}) \quad\longrightarrow\quad -I_n(\mathcal{A}) + 2I_n(\mathcal{A}+1) - 2I_n(\mathcal{A}+2)\,. \end{aligned} \quad (3.141)$$

Additionally, for Sivers asymmetry, we check the $\sin(\phi_S-\phi_r)$ modulated cross-section which leads to the sustitution

$$I_n(\mathcal{A}) \quad\longrightarrow\quad I_n(\mathcal{A}+1) + \cos^2\phi_S[I_n(\mathcal{A}) - 2I_n(\mathcal{A}+1)]. \quad (3.142)$$

Notice that for the Sivers case, the result depends on the angle ϕ_S (the spin angle w.r.t. the plane defined by $\boldsymbol{p}_T$ and $\boldsymbol{q}_T$). We leave the implications of this fact as well as phenomenology for this case for future works. In all these cases one obtains a cancellation of the imaginary part of the cross-section. Other polarized contributions are possible and

have yet to be further explored. A more complete list of contributions can be found in [92].

Treating perturbatively the angular integration as discussed in this section leads to write eq. 3.100 for the dijet case as

$$\frac{d\sigma}{d\Pi dr_T} = \frac{d\sigma^U(\gamma^* g)}{d\Pi dr_T} + \frac{d\sigma^U(\gamma^* f)}{d\Pi dr_T} + \frac{d\sigma^L(\gamma^* g)}{d\Pi dr_T}, \tag{3.143}$$

where

$$\begin{aligned}\frac{d\sigma^U(\gamma^* g)}{d\Pi\, dr_T} &= \sum_f \sigma_0^{gU} H^U_{\gamma^* g\to f\bar f}(\hat s,\hat t,\hat u,\mu=p_T) J_f(p_T,R,\mu_J) J_{\bar f}(p_T,R,\mu_J) \\ &\times \int_0^{+\infty} b db\, J_0(br_T) f_1^g(\xi,\boldsymbol{b}) \mathcal{R}_g\Big((\{\mu_k\},\zeta_{1,0},\zeta_{2,0})\to(p_T,p_T^2,1)\Big)\hat\sigma_g^U(b,R,\{\mu_i\}),\end{aligned} \tag{3.144}$$

$$\begin{aligned}\frac{d\sigma^U(\gamma^* f)}{d\Pi\, dr_T} &= \sum_{f,\bar f} \sigma_0^{fU} H^U_{\gamma^* f\to g f}(\hat s,\hat t,\hat u,\mu=p_T) J_f(p_T,R,\mu_J) J_g(p_T,R,\mu_J) \\ &\times \int_0^{+\infty} b db\, J_0(br_T) f_1^f(\xi,\boldsymbol{b}) \mathcal{R}_q\Big((\{\mu_k\},\zeta_{1,0},\zeta_{2,0})\to(p_T,p_T^2,1)\Big)\hat\sigma_f^U(b,R,\{\mu_i\}),\end{aligned} \tag{3.145}$$

$$\begin{aligned}\frac{d\sigma^L(\gamma^* g)}{d\Pi\, dr_T} &= \sum_f \sigma_0^{gL} H^L_{\gamma^* g\to f\bar f}(\hat s,\hat t,\hat u,\mu=p_T) J_f(p_T,R,\mu_J) J_{\bar f}(p_T,R,\mu_J) \\ &\times \int_0^{+\infty} b db\, J_0(br_T) h_1^\perp(\xi,\boldsymbol{b}) \mathcal{R}_g\Big((\{\mu_k\},\zeta_{1,0},\zeta_{2,0})\to(p_T,p_T^2,1)\Big)\hat\sigma_g^L(b,R,\{\mu_i\}),\end{aligned} \tag{3.146}$$

where $\mathcal{R}_{f,g}$ are products of evolution kernels to be described in the next section, and $\hat\sigma^{U,L}_{f,g}$ are the result of ϕ_b angular integration and can be written as

$$\hat\sigma_g^U = I^{gU}_{\text{const.}} + a_s(\mu_{\mathcal{C}})\mathcal{C}_f^U(b,R,\mu_{\mathcal{C}}) + a_s(\mu_{\mathcal{C}})\mathcal{C}_{\bar f}^U(b,R,\mu_{\mathcal{C}}) + a_s(\mu_0) S^U_{\gamma g}(b,\zeta_2,\mu_0), \tag{3.147}$$

$$\hat\sigma_f^U = I^{fU}_{\text{const.}} + a_s(\mu_{\mathcal{C}})\mathcal{C}_f^U(b,R,\mu_{\mathcal{C}}) + a_s(\mu_{\mathcal{C}})\mathcal{C}_g^U(b,R,\mu_{\mathcal{C}}) + a_s(\mu_0) S^U_{\gamma f}(b,\zeta_2,\mu_0), \tag{3.148}$$

$$\hat\sigma_g^L = I^{gL}_{\text{const.}} + a_s(\mu_{\mathcal{C}})\mathcal{C}_f^L(b,R,\mu_{\mathcal{C}}) + a_s(\mu_{\mathcal{C}})\mathcal{C}_{\bar f}^L(b,R,\mu_{\mathcal{C}}) + a_s(\mu_0) S^L_{\gamma g}(b,\zeta_2,\mu_0). \tag{3.149}$$

The functions $\mathcal{C}$ and S in eq. 3.147-3.149 are the result of the ϕ_b integration in collinear-soft and dijet soft functions. For the heavy meson case we have just contributions from gluon scattering,

$$\frac{d\sigma}{d\Pi dr_T} = \frac{d\sigma^U(\gamma^* g)}{d\Pi dr_T} + \frac{d\sigma^L(\gamma^* g)}{d\Pi dr_T}, \tag{3.150}$$

and we have to change $J_{f,\bar f} \to H_+$ and $\mathcal{C}_f \to \mathcal{J}_{Q\to H}$ in eq. 3.144-3.146. In the case of angular modulation the cross-sections can also be written as in eq. 3.143-3.150, with the correct values of the functions $I_{\text{const.}}$, $\mathcal{C}$ and S. The non-perturbative effects are in all cases encoded in the evolution kernels, TMD and jet functions. In the next section we describe how the evolution kernels are defined.

3.5 Evolution kernels and scale choices

The evolution kernels appearing in eq. 3.143-3.150 are

$$\mathcal{R}_g\Big((\{\mu_k\},\zeta_{1,0},\zeta_{2,0})\to(p_T,p_T^2,1)\Big)=\mathcal{R}_{J_f}(\mu_J\to p_T)^2\mathcal{R}_{\mathcal{C}_f}(\mu_{\mathcal{C}}\to p_T)^2 \times\mathcal{R}_F^g\Big((\mu_0,\zeta_{1,0})\to(p_T,p_T^2)\Big)\mathcal{R}_S^q\Big((\mu_0,\zeta_{2,0})\to(p_T,1)\Big), \tag{3.151}$$

$$\mathcal{R}_q\Big((\{\mu_k\},\zeta_{1,0},\zeta_{2,0})\to(p_T,p_T^2,1)\Big)=\mathcal{R}_{J_f}(\mu_J\to p_T)\mathcal{R}_{J_g}(\mu_J\to p_T)\mathcal{R}_{\mathcal{C}_f}(\mu_{\mathcal{C}}\to p_T) \times\mathcal{R}_{\mathcal{C}_g}(\mu_{\mathcal{C}}\to p_T)\mathcal{R}_F^q\Big((\mu_0,\zeta_{1,0})\to(p_T,p_T^2)\Big)\mathcal{R}_S^g\Big((\mu_0,\zeta_{2,0})\to(p_T,1)\Big), \tag{3.152}$$

where $\mathcal{R}_{J_{f,g}}$ is a jet function kernel, $\mathcal{R}_{\mathcal{C}_{f,g}}$ is the one of collinear-soft functions, $\mathcal{R}_F^{q,g}$ the one of TMD and finally $\mathcal{R}_S^{qg}$ is the one of the dijet soft function. In the heavy quark case, the evolution kernels are parameterized like in eq. 3.151 with the usual changes $J_f\to H_+$ and $\mathcal{C}_f\to\mathcal{J}_{Q\to H}$. The kernels for single-scale evolution have a standard form and a review up to NLL is given in [102],

$$\mathcal{R}_i(\mu_i\to p_T)=e^{K_i(\mu_i\to p_T)}\Big(\frac{\mu_i}{m_i}\Big)^{\omega_i(\mu_i\to p_T)},\qquad i=\{\mathcal{C}_f,\mathcal{C}_g,J_f,J_g,\mathcal{J}_{Q\to H},H_+\} \tag{3.153}$$

where

$$\omega_i(\mu_i\to p_T)\Big|_{\rm NLL}=-\frac{\Gamma_i^0}{\beta_0}\left[\ln r+\left(\frac{\Gamma_1}{\Gamma_0}-\frac{\beta_1}{\beta_0}\right)\frac{\alpha_s(\mu_i)}{4\pi}(r-1)\right], \tag{3.154}$$

$$K_i(\mu_i\to p_T)\Big|_{\rm NLL}=-\frac{\gamma_i^0}{2\beta_0}\ln r-\frac{2\pi\Gamma_i^0}{(\beta_0)^2}\left[\frac{r-1-r\ln r}{\alpha_s(p_T)} +\left(\frac{\Gamma_1}{\Gamma_0}-\frac{\beta_1}{\beta_0}\right)\frac{1-r+\ln r}{4\pi}+\frac{\beta_1}{8\pi\beta_0}\ln^2 r\right], \tag{3.155}$$

with $r=\alpha_s(p_T)/\alpha_s(\mu_i)$ and

$$\begin{aligned}
&\Gamma^0_{\mathcal{C}_f}=-4C_F,\quad \Gamma^0_{\mathcal{C}_g}=-4C_A,\quad \gamma^0_{\mathcal{C}_{f/g}}=0,\quad m_{\mathcal{C}_{f/g}}=\frac{Re^{-\gamma_E}}{b},\\
&\Gamma^0_{J_f}=4C_F,\quad \Gamma^0_{J_g}=4C_A,\quad \gamma^0_{J_f}=6C_F,\quad \gamma^0_{J_g}=2\beta_0,\quad m_{J_{f/g}}=p_TR,\\
&\Gamma^0_{\mathcal{J}}=-4C_F,\quad \gamma^0_{\mathcal{J}}=4C_F,\quad m_{\mathcal{J}}=\frac{m_Q/p_Te^{-\gamma_E}}{b},\\
&\Gamma^0_{+}=4C_F,\quad \gamma^0_{+}=2C_F,\quad m_{+}=m_Q,
\end{aligned} \tag{3.156}$$

Initial scales μ_i choice is given in sec. 3.6. The TMD kernel is considered here in the ζ-prescription described in [33] and implemented in the code Artemide [81] that we use,

$$\mathcal{R}_F^{q,g}(\{\mu_0,\zeta_0\}\to\{\mu_f,\zeta_f\})=\Big(\frac{\zeta_f}{\zeta_\mu(b,\mu_f)}\Big)^{-\mathcal{D}_{q,g}(b,\mu_f)}. \tag{3.157}$$

In the next paragraph we define a ζ-prescription also for the dijet evolution kernel $\mathcal{R}_S^g\Big((\mu_0,\zeta_{2,0})\to(p_T,1)$, which is the only missing part.

3.5.1 ζ-prescription for dijet evolution kernel

The angular independent kernel of the dijet soft function is obtained as a solution of a coupled system of differential equations, reported in eq. 3.115, that are formally very similar to the TMD ones [94, 93]. The anomalous dimensions are given by

$$\bar{\gamma}_{S_{\gamma g}}(\mu,\zeta) = \gamma_{\rm cusp}\left[2C_F \ln\left(\frac{\mu^2}{\mu_0^2}\right) - C_A \ln\left(\frac{\zeta}{\zeta_{2,0}^{\gamma g}}\right)\right] + \delta\gamma_S^{\gamma g}, \tag{3.158}$$

$$\bar{\gamma}_{S_{\gamma f}}(\mu,\zeta) = \gamma_{\rm cusp}\left[(C_F+C_A) \ln\left(\frac{\mu^2}{\mu_0^2}\right) - C_F \ln\left(\frac{\zeta}{\zeta_{2,0}^{\gamma f}}\right)\right] + \delta\gamma_S^{\gamma f}, \tag{3.159}$$

where

$$\mu_0 = \frac{2}{be^{\gamma_E}}, \qquad \zeta_{2,0}^{\gamma g} = \left(\frac{4p_T^2}{\hat{s}}\right)^{\frac{2C_F}{C_A}}, \qquad \zeta_{2,0}^{\gamma f} = \left(\frac{4p_T^2}{\hat{s}}\right)^{\frac{C_F+C_A}{C_F}} \left(\frac{\hat{t}}{\hat{u}}\right)^{\frac{C_F-C_A}{C_F}}, \tag{3.160}$$

and $\delta\gamma_S$ are the non-cusp SF anomalous dimension, which is known up to three-loops for the gluon-channel and up to one-loop for the quark-channel and are reported in appendix. The anomalous dimension and the rapidity anomalous dimension (RAD) in eq. 3.108 and eq. 3.109 satisfy also

$$-\frac{d}{d\ln\zeta}\bar{\gamma}_{S_{\gamma i}}(\mu,\zeta) = \frac{d}{d\ln\mu}\mathcal{D}_i(\mu,b) = \Gamma_{\rm cusp}(\mu) \tag{3.161}$$

The evolution for the SF takes the general form

$$\mathcal{R}_S^i(\{\mu_i,\zeta_i\}\to\{\mu_f,\zeta_f\}) = \exp\left[\int_P \left(\bar{\gamma}_{S_\gamma i}(\mu,\zeta)d\ln\mu - \mathcal{D}_i(\mu,b)d\ln\zeta\right)\right] \tag{3.162}$$

with $i = q, g$ and $\{\mu_i,\zeta_i\}$ and $\{\mu_f,\zeta_f\}$ being the initial and final points of factorization and rapidity scales. The integration path P is an arbitrary path in the $\{\mu,\zeta\}$-plane. Eq. 3.161 ensures that the evolution kernel is only path-independent when one knows the complete perturbative expansion of the anomalous dimensions. Since this is not the case the path independence is broken. In order to partially restore the path independence we proceed as in [33] defining a ζ-prescription also for the dijet soft function evolution kernel. The ζ-prescription provides a way to choose the initial scale ζ_i of the evolution kernel as a function of μ and b so that the SF does not depend on the initial scale μ_i. This is done by taking the integration path through a null-evolution line in the $\{\mu,\zeta\}$-plane and then taking a fixed-μ evolution.

To find the null-evolution line we interpret the pair of differential equations 3.161 as a two-dimensional gradient equation $\boldsymbol{\nabla}F = \boldsymbol{E}F$, where $\boldsymbol{E} = (\gamma_S(\mu,\zeta), -\mathcal{D}_S(\mu,b))$. The null-evolution line is then an equipotential line of the field $\boldsymbol{E}$. In particular, there is a special null-evolution line that passes through the saddle-point $\{\mu_{\rm saddle},\zeta_{\rm saddle}\}$ of the evolution field. We find that the saddle point is exactly $\mu_{\rm saddle} = \mu_0$ and $\zeta_{\rm saddle}^{\gamma i} = \zeta_0^{\gamma i}$. If we parameterize the null-evolution line as $\{\mu,\zeta_\mu(b)\}$, the value of ζ_μ is given by

$$\gamma_{S_{\gamma i}}(\mu,\zeta_\mu(b)) = 2\mathcal{D}_{S_{\gamma i}}(\mu,b)\frac{d\ln\zeta_\mu(b)}{d\ln\mu^2}, \tag{3.163}$$

which is solved perturbatively order by order in α_s. The perturbative solution takes the form

$$\zeta^{\gamma g}_{\mu,\,\text{pert}}(b) = \left(\frac{\mu}{\mu_0}\right)^{\frac{2C_F}{C_A}} \zeta_0^{\gamma g} e^{v^{\gamma g}(\mu,b)}, \tag{3.164}$$

$$\zeta^{\gamma f}_{\mu,\,\text{pert}}(b) = \left(\frac{\mu}{\mu_0}\right)^{\frac{C_F+C_A}{C_F}} \zeta_0^{\gamma f} e^{v^{\gamma f}(\mu,b)}, \tag{3.165}$$

where

$$v^{\gamma i}(\mu,b) = \sum_{n=0}^{\infty} a_s^n(\mu) v_n^{\gamma i}(\mathbf{L}_\mu), \qquad \mathbf{L}_\mu = \ln\!\left(B\mu^2 e^{2\gamma_E}\right), \tag{3.166}$$

$$v_0^{\gamma g}\left(\mathbf{L}_\mu\right) = 0, \tag{3.167}$$

$$v_1^{\gamma g}\left(\mathbf{L}_\mu\right) = \frac{2C_F}{C_A}\Big[-\frac{\beta_0}{12}\mathbf{L}_\mu^2 + \frac{\frac{\gamma_2}{2C_F} - d^{(2,0)}}{\Gamma_0}\Big], \tag{3.168}$$

$$\begin{aligned} v_2^{\gamma g}\left(\mathbf{L}_\mu\right) = \frac{2C_F}{C_A}\Big[&-\frac{\beta_0^2}{24}\mathbf{L}_\mu^3 - \left(\frac{\beta_1}{12} + \frac{\beta_0\Gamma_1}{12\Gamma_0}\right)\mathbf{L}_\mu^2 + \left(\frac{\beta_0\frac{\gamma_2}{2C_F}}{2\Gamma_0} - \frac{4\beta_0 d^{(2,0)}}{3\Gamma_0}\right)\mathbf{L}_\mu \\ &- \frac{\frac{\gamma_2}{2C_F}\Gamma_1 - d^{(2,0)}\Gamma_1}{\Gamma_0^2} + \frac{\frac{\gamma_3}{2C_F} - d^{(3,0)}}{\Gamma_0}\Big], \end{aligned} \tag{3.169}$$

$$v_0^{\gamma f}\left(\mathbf{L}_\mu\right) = 0, \tag{3.170}$$

and we are using the following notation

$$\mathcal{D}_i(\mu,b) = C_i \sum_{n=1}^{\infty} a_s^n(\mu) \sum_{k=0}^{n} \mathbf{L}_\mu^k d^{(n,k)}, \quad \delta\gamma_S(\mu) = \sum_{n=1}^{\infty} a_s^n(\mu)\gamma_n, \tag{3.171}$$

$$\beta(a_s) = -\sum_{n=0}^{\infty} a_s^{n+2}\beta_n, \quad \Gamma_{\text{cusp}}(\mu) = C_i\gamma_{\text{cusp}}(\mu) = C_i\sum_{n=0}^{\infty} a_s^{n+1}(\mu)\Gamma_n, \tag{3.172}$$

with $C_i = C_F, C_A$ for quark and gluon channel respectively. Notice that v_0 vanishes as it is proportional to the LO non-cusp AD, which is zero for the SF. The non-cusp AD is not known beyond LO for the quark channel.

The RAD is a function of b and therefore has important non-perturbative corrections in the large-b region. These corrections can be implemented as a model. The way to proceed is to solve 3.163 for a generic non-perturbative RAD. The equation is solvable but it is difficult to obtain the cancellation of perturbative logarithms in the small-b region. Following [33] we use the perturbative solution for the small-b region and move to the exact (generic RAD) solution for large-b:

$$\zeta_\mu(b) = \zeta_\mu^{\text{pert}}(b)e^{-b^2/B_{\text{NP}}^2} + \zeta_\mu^{\text{exact}}(b)\left(1 - e^{-b^2/B_{\text{NP}}^2}\right), \tag{3.173}$$

with B_{NP} being the b value where non-perturbative (NP) effects become important (~ 2.5 GeV^{-1}). We have already discussed the perturbative solution to eq. 3.163. For the exact solution we find

$$\zeta^{\gamma g}_{\mu,\,\text{exact}}(b) = \left(\frac{\mu^2}{\mu_0^2}\right)^{\frac{2C_F}{C_A}} \zeta_0^{\gamma g} e^{-g^{\gamma g}(a_s,\mathcal{D}_S)/\mathcal{D}_S}, \tag{3.174}$$

$$\zeta^{\gamma f}_{\mu,\,\text{exact}}(b) = \Big(\frac{\mu^2}{\mu_0^2}\Big)^{\frac{C_F+C_A}{C_F}} \zeta_0^{\gamma f} e^{-g^{\gamma f}(a_s,\mathcal{D}_S)/\mathcal{D}_S}, \tag{3.175}$$

where

$$g^{\gamma i}(a_s,\mathcal{D}_S) = \frac{1}{a_s}\frac{\Gamma_0}{2\beta_0^2}\sum_{n=0}^{\infty} a_s^n g_n^{\gamma i}(\mathcal{D}_S), \tag{3.176}$$

$$g_0^{\gamma g} = \frac{2C_F}{C_A}\Big[e^{-p} - 1 + p\Big], \tag{3.177}$$

$$g_1^{\gamma g} = \frac{2C_F}{C_A}\Big[\frac{\beta_1}{\beta_0}\left(e^{-p} - 1 + p - \frac{p^2}{2}\right) - \frac{\Gamma_1}{\Gamma_0}\left(e^{-p} - 1 + p\right)\Big], \tag{3.178}$$

$$g_0^{\gamma f} = \frac{C_F + C_A}{C_F}\Big[e^{-p} - 1 + p\Big], \tag{3.179}$$

$$g_1^{\gamma f} = \frac{C_F + C_A}{C_F}\Big[\frac{\beta_1}{\beta_0}\left(e^{-p} - 1 + p - \frac{p^2}{2}\right) - \frac{\Gamma_1}{\Gamma_0}\left(e^{-p} - 1 + p\right)\Big], \tag{3.180}$$

and $p = 2\beta_0\mathcal{D}_S/\Gamma_0$.

Finally, the evolution kernel that provides the evolution from the null-evolution line and that passes through the saddle-point to the final ζ point is given by

$$\mathcal{R}_S^{q,g}(\{\mu_0,\zeta_0\}\to\{\mu_f,\zeta_f\}) = \Big(\frac{\zeta_f}{\zeta_\mu(b,\mu_f)}\Big)^{-\mathcal{D}_{q,g}(b,\mu_f)}, \tag{3.181}$$

and if we consider the evolution from an arbitrary initial scale we take

$$\mathcal{R}_S^{i}(\{\mu_i,\zeta_i\}\to\{\mu_f,\zeta_f\}) = \frac{\mathcal{R}_S^{i}(\{\mu_0,\zeta_0\}\to\{\mu_f,\zeta_f\})}{\mathcal{R}_S^{i}(\{\mu_0,\zeta_0\}\to\{\mu_i,\zeta_i\})}. \tag{3.182}$$

with $i = q, g$. This discussion concludes the analysis of all terms that appear in the factorization theorem and the scale prescription. We are now ready for the implementation in the code Artemide [81].

3.6 Phenomenology

In order to test the phenomenology developed in the previous sections we consider the case of the EIC. In [98] we already studied the coverage of the EIC and we concluded that the most favorable case is given for a value of mass energy for dijet production around $\sqrt{s} = 140\,\text{GeV}$ and central rapidity, $\eta_1 = \eta_2 = 0$. Typical values for jet radii and momenta at EIC are respectively $R \sim 0.7$ and $p_T \sim Q/2 \sim 20$ GeV. To simplify the discussion we show plots integrated over Bjorken variable x (the longitudinal fraction of momentum ξ that enters in the TMDPDFs is $\xi \sim 2x$) in the allowed kinematic intervals. For the case of central rapidity we have $x \in (0.0859, 0.5)$. The cross-sections that we plot are

$$\int_{x_{\min}}^{x_{\max}} dx \frac{d\sigma}{dx d\eta_1 d\eta_2 dp_T dr_T}\Big|_{\eta_1,\,\eta_2,\,p_T} \tag{3.183}$$

and its value is presented as a function of the small transverse momentum r_T. The cross-sections and the error bands are obtained by using and preparing specific moduli for the code Artemide [81]. In particular, we use the TMD and the TMD evolution kernels already coded in Artemide, which come from the fit [32], while the new functions studied in this work are included in this code for the first time. We use the PDF set NNPDF31. The gluon TMD is not fitted yet, however in Artemide there is a parameterization for it. The code takes into account that the contribution of linearly polarized gluons is highly suppressed because in the small-b regime the matching of the linearly polarized gluon TMD onto the gluon PDF starts at order α_s^1 and not at order α_s^0 like other distributions. In ref. [39] the cross section obtained in this way agrees with Pythya 8 and current experimental results for the Higgs transverse momentum spectrum, which are however not very precise. The non-perturbative effects are expected to be important in the high-b region and they should not alter the small-b behavior of this distribution. Notice also that the non-perturbative effects play a role in controlling the behavior of the distribution around the Landau pole at large-b, which means a further suppression effect at large-b (as we also observe in the case of unpolarized distributions). Summing up, given the current perturbative and non-perturbative knowledge of TMDs, at this stage we prefer not to push for a hypothetical non-perturbative enhancement of the contribution of linearly polarized gluon TMD.

	$\mathcal{C}$	$\mathcal{J}$	S		$\mathcal{C}$	$\mathcal{J}$
$B^i_{\rm NP}$ (GeV^{-1})	2.5	2.5	2.5	$b_{\rm max}$ (GeV^{-1})	0.5	0.3

Table 3.1: Values of non-perturbative parameter $B_{\rm NP}$ and $b_{\rm max}$ prescription chosen for collinear-soft function, heavy meson jet function and dijet soft function. Impact of the varition of $B_{\rm NP}$ is shown in fig. 3.6.

The factorization that we propose in general needs information of the non-perturbative effects in several functions. For the dijet case we have

$$\mathcal{C}(b,R;p_T) = \mathcal{R}_{\mathcal{C}}(b,R;p_T,\mu_{\mathcal{C}})\mathcal{C}^{pert}(b,R;\mu_{\mathcal{C}})f^{\rm NP}_{\mathcal{C}}(b,R), \tag{3.184}$$

$$S_{\gamma i}(b;p_T,1) = \mathcal{R}_S(\{\mu_0,\zeta_0\}\to\{p_T,1\})S^{pert}_{\gamma i}(b;\mu_0,\zeta_0)f^{\rm NP}_{\mathcal{S}}(b), \tag{3.185}$$

where the functions with suffix *pert* refer to their perturbative part in the $\overline{\rm MS}$ scheme which is currently known at one loop. Similarly for the HHP case we need

$$\mathcal{J}(b,m_Q/p_T;p_T) = \mathcal{R}_{\mathcal{J}}(b,m_Q/p_T;p_T,\mu_{\mathcal{J}})\mathcal{J}^{pert}(b,m_Q/p_T;\mu_{\mathcal{J}})f^{\rm NP}_{\mathcal{J}}(b;m_Q). \tag{3.186}$$

The non-perturbative effects are parameterized as

$$f^{\rm NP}_i(b) = \exp\Big(-\frac{b^2}{(B^i_{\rm NP})^2}\Big), \qquad i=\mathcal{C},\mathcal{J},S. \tag{3.187}$$

The values of $B^i_{\rm NP}$ define the non-perturbative model and we have tested several combinations as shown in fig. 3.6. Higher values of $B^i_{\rm NP}$ are more sensitive to the perturbative series in the low transverse momentum spectrum, and in general, provide higher values of the observables. In unpolarized TMD cases, we have usually that typical values of $B^i_{\rm NP}$ are around 1-3 GeV^{-1} so we find it reasonable to fix their values as in tab. 3.1.

The factorization scales $\mu_{\mathcal{C}}$ for dijet and $\mu_{\mathcal{J}}$ for HHP are chosen to minimize perturbative logarithms and to not hit the Landau pole of the strong coupling constant,

$$\mu_{\mathcal{C}} = 2e^{-\gamma_E}\Big(\frac{1}{b} + \frac{1}{b_{\max}}\Big), \tag{3.188}$$

$$\mu_{\mathcal{J}} = \frac{1}{2}e^{-\gamma_E}\Big(\frac{1}{b} + \frac{1}{b_{\max}}\Big). \tag{3.189}$$

This scale choice deserves some comments. In the dijet case, the scale choice does not include the dependence on the jet radius R. Similarly, the mass of the ratio m_Q/p_T does not enter the collinear-soft function and heavy meson jet. In all cases, this means that there is not a complete cancellation of the logarithms of these functions. The reason is that the ϕ_b integration imposes some constraints on the choice of scales. In fact, the function $\mathcal{A}(\{\mu_i\})$ defined in eq. 3.123, which depends on the initial scale choice for the soft function, collinear-soft function and heavy meson jet, needs to be $\mathcal{A} > -1/2$ in order to have a well defined angular integration. Because of this constraint, some scale choices could be considered, for instance

$$\mu_{\mathcal{C}} = \frac{Re^{-\gamma_E}}{b}, \qquad \mu_{\mathcal{J}} = \frac{m_Q/p_T e^{-\gamma_E}}{b}, \tag{3.190}$$

can not be used. As a result in our approach we only partially resum the logs in the collinear-soft function and the heavy meson jet in order to maintain the structure of ζ-prescription and double scale evolution in the soft function that is described in sec. 3.5. This leads to the initial scales in eq. 3.188, 3.189.

Finally, for the dijet soft function, we use the b^*-prescription in the same way as for the TMDPDF:

$$\mu_S = \frac{2e^{-\gamma_E}}{b^*}, \quad b^* = \frac{b}{\sqrt{1 + b^2/b_{\max}^2}}. \tag{3.191}$$

Concerning the theoretical errors, the scale variations in collinear-soft and heavy meson jet function are the main source. This is due to the non-cancellation of logs in the functions by the choice of the initial scales. The choice of the values $b_{\max}$ for collinear-soft function and heavy meson jet account for the convergence of our perturbative result. A more consistent way to treat the resummation of these scales is left for future work, involving the refactorization of these functions.

For functions that do not depend on b the initial scale choice does not require a prescription or NP-model and it is dictated by the cancellation of the logarithms. For the jet function and the H_+ matching coefficient, we have

$$\mu_J = p_T R, \qquad \mu_+ = m_Q. \tag{3.192}$$

We use a NP-model for the rapidity anomalous dimension that enters the exact solution for the null-evolution ζ_μ line as it is explained in sec. 3.5. In particular, we use the same model that has been used for TMDPDF in [32]

$$\mathcal{D}^{\rm NP}_{F,S} = c_0 b b^*, \qquad c_0 = 2.5 \cdot 10^{-2}. \tag{3.193}$$

This model dictates how the rapidity anomalous dimension behaves in the large-b region and is used for both dijet soft function and TMDPDF when performing double-scale

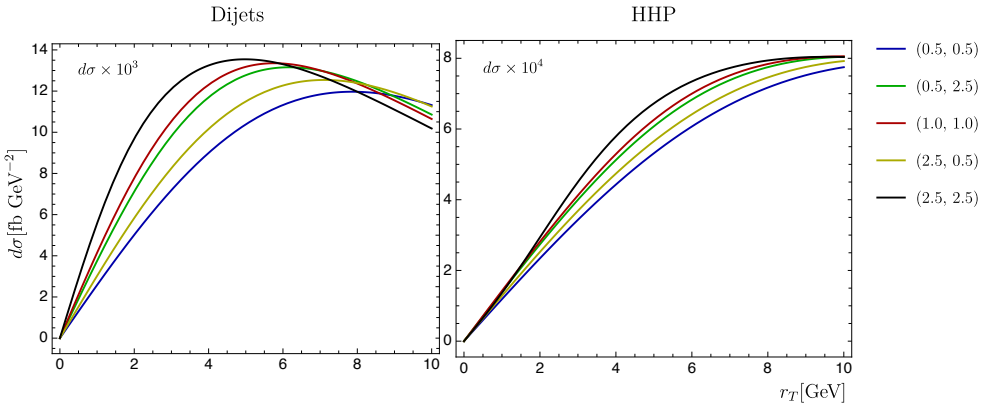

Figure 3.6: Impact of $B_{\rm NP}$ variation over dijets and heavy meson total cross-section. Legend correspond to $(B^S_{\rm NP}, B^{\mathcal{C}}_{\rm NP})$ and $(B^S_{\rm NP}, B^{\mathcal{J}}_{\rm NP})$ for dijet and HHP production respectively

evolution. While a color re-scaling of the non-perturbative models for gluon TMDPDF and gluon channel soft function with respect to their quark analogs is possible, we observe that this change does not have a significant impact on the cross-section and, therefore, we choose to keep the same model for both quarks and gluons.

3.6.1 Phenomenological results

In this section, we show our results for the differential cross-section for both dijet and heavy hadron pair production processes. Differential cross-sections are shown with error bands coming from scale variation of the different final and initial scales of the functions appearing in our factorization formulas. Scale variation bands are obtained by changing the considered scale by a factor of 2 up and down relative to its central value.

Results for dijet production

In fig. 3.7 we show the impact of the change of jet radius, jet transverse momentum (hard scale) and jet pseudorapidity over the total dijet cross-section. We show that for the variation of the jet radius, we see a change of around 20% on the cross-section from the central value when taking the jet radius to be ± 0.2 from $R = 0.7$. For p_T there is a variation of an order of magnitude in the total cross-section when taking ± 5 GeV from 20 GeV. This corresponds to $Q = 30, 40, 50$ GeV respectively. Finally, for pseudorapidity variation, we obtain an order of magnitude difference above and below when compared to the central rapidity case. Positive rapidities ($\eta_i = 0.5$) correspond to $Q \simeq 53$ GeV while negative rapidities ($\eta_i = -0.5$) correspond to $Q \simeq 32$ GeV, so both p_T and η plots are consistent. Notice that the total dijet cross-section is not symmetrical for both jet rapidities as for the quark channel we have both a quark and gluon jet in the final state. Every other plot is obtained taking $R = 0.7$, $p_T = 20$ GeV and $\eta_i = 0$.

In fig. 3.8 the result for the cross-section including quark and gluon channels is shown. We consider the contribution of linearly polarized gluons in a separate panel to show that

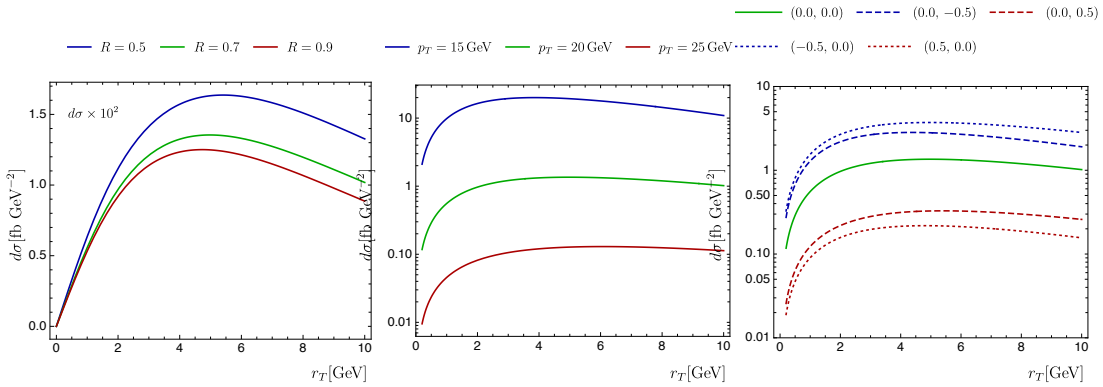

(a) R variation (b) p_T variation (c) η variation (η_1, η_2)

Figure 3.7: Impact of the variation of the jet radius (R), hard scale jet transverse momentum (p_T) and jet pseudorapidity (η_i) for dijet production. For pseudorapidity variation legend is shown referring to (η_1, η_2) pair, dashed and dotted lines correspond to negative and positive rapidity respectively.

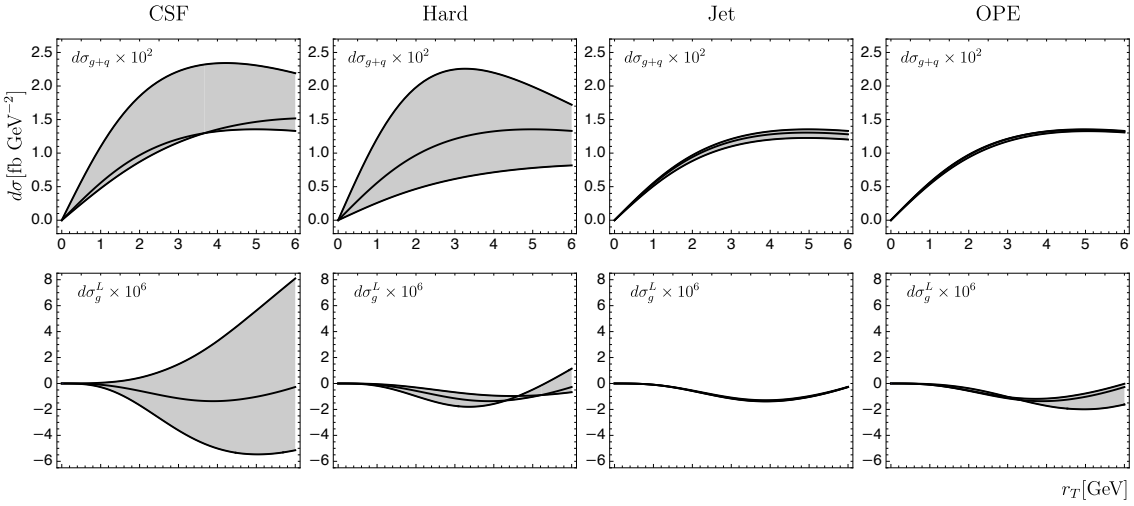

Figure 3.8: Cross-sections for dijet production at EIC with error-bands coming from scale dependence in collinear-soft factor (CSF), hard factor (Hard), jet distributions (Jet) and Wilson coefficients (OPE). Rows correspond to contributions from linearly polarized gluons (top) and total cross-section (bottom). Notice that the contribution from linearly polarized gluons is much smaller than the total cross-section. $\sqrt{s} = 140$ GeV, $R = 0.7$, $p_T = 20$ GeV, $\eta_1 = \eta_2 = 0$.

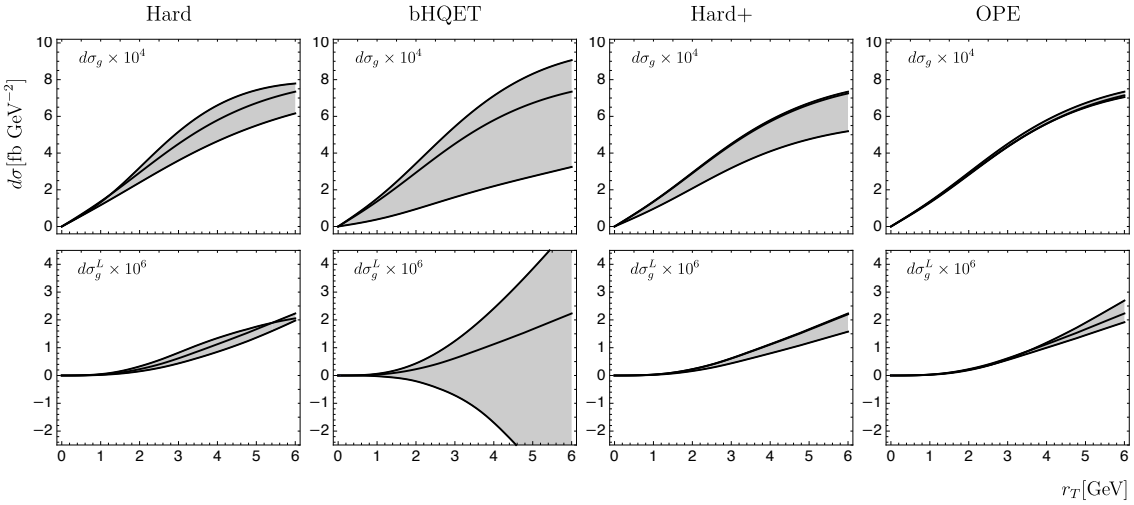

Figure 3.9: Cross-sections for HHP production at EIC with error-bands coming from scale dependence in hard factor (Hard), heavy meson jet function (bHQET), heavy meson jet function matching coefficient (Hard+) and Wilson coefficients (OPE). The rows correspond to contributions from total cross-section (top) and linearly polarized gluons (bottom). Notice that the contribution from linearly polarized gluons is much smaller than the total cross-section. $\sqrt{s} = 140$ GeV, $p_T = 20$ GeV, $\eta_1 = \eta_2 = 0$.

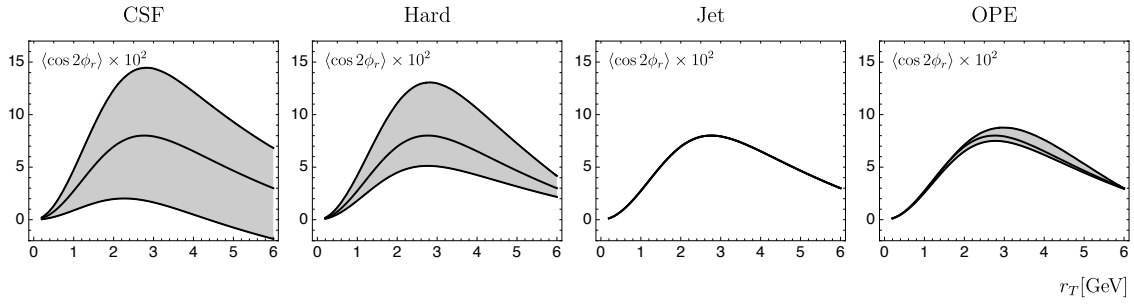

Figure 3.10: Angular modulation contribution for dijet production at EIC with error-bands coming from scale dependence in collinear-soft factor (CSF), hard factor (Hard), jet distributions (Jet) and Wilson coefficients (OPE). $\sqrt{s} = 140$ GeV, $R = 0.7$, $p_T = 20$ GeV, $\eta_1 = \eta_2 = 0$.

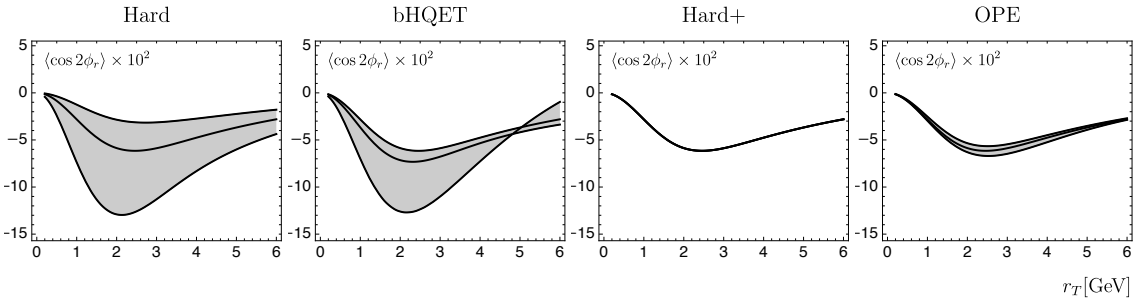

Figure 3.11: Angular modulation contribution for HHP production at EIC with error-bands coming from scale dependence in hard factor (Hard), heavy meson jet function (bHQET), heavy meson jet function matching coefficient (Hard+) and Wilson coefficients (OPE). $\sqrt{s} = 140$ GeV, $p_T = 20$ GeV, $\eta_1 = \eta_2 = 0$.

their contribution is completely negligible, being a factor 10^3-10^4 smaller. This leads to the conclusion that the contribution from the linearly polarized gluons can be neglected when considering the unpolarized cross-section.

The angular modulation asymmetry is shown in fig. 3.10, being around 5%.

Results for heavy hadron production

The analysis for HHP has followed similar steps of the dijet case when possible. The differential cross-section including all channels is plotted in fig. 3.9. A separate analysis of the contribution of linearly polarized gluons shows also in this case that they are completely negligible being suppressed by a factor 10^2-10^3. The angular modulation asymmetry is shown in fig. 3.11, being around 5%.

Chapter 4

Background field method

In chapters 1 and 2, we introduced SCET and outlined the methodology for achieving TMD factorization within its framework. In this chapter, an alternative approach for the development of factorization is presented, particularly suited to address higher power corrections, the background field method. This chapter is a review of the work presented in refs. [103, 104], which serves as the foundation for the novel work presented in chapter 5. In particular, this chapter is an introduction to factorization through the background field method and the systematic inclusion of power corrections, which we develop for the case of dijet production in SIA in chapter 5. For further details, we encourage readers to check the findings presented in ref. [103].

The history of TMD cross-section factorization dates back to the seminal works of refs. [13, 35, 14]. Recent advancements in achieving TMD factorization involve the utilization of specialized regulators for rapidity divergences and effective field theory [94, 17, 25], as well as the background field method [103]. In these studies, TMD factorization emerges through the expansion of the cross-section in powers of λ, representing the ratio of a small transverse momentum q_T and the scale Q of the hard scattering process.

Confining our focus to the leading power in this expansion and conducting perturbative calculations for the renormalization group energy evolution, researchers have successfully extracted unpolarized TMDs up to the next-to-next-to-next-to-next-to-leading logarithmic ($\mathrm{N^4LL}$) order [105, 106]. This currently stands as the highest logarithmic order employed to determine a nonperturbative distribution. Additionally, the TMD formalism has been applied to theoretically predict the Z-boson transverse momentum distribution at the same order [107].

In principle, comparable accuracy can be attained for other spin-dependent distributions described by TMD factorization. This is attributed to the spin-independence of the TMD evolution kernel [88, 87, 108, 109, 110], cusp anomalous dimension [111, 112], and hard factors [113, 114, 115, 116], all of which do not vary with spin.

With the cross-section exhibiting high theoretical precision at the leading power, recent progress has been made in delving into the exploration of hadron structure at higher orders of λ. These power corrections are anticipated to provide valuable insights into our comprehension of hadrons and their intrinsic properties [117, 103, 118, 104, 119, 120, 121]. The necessity for power corrections becomes evident, especially given the per-mille-level accuracy achieved in recent DY measurements at the LHC.

Furthermore, SIDIS and e^+e^- experiments, such as EIC [122], EIcC [123], and Belle, are typically conducted at low energy, where power corrections tend to be more substantial [124]. In summary, incorporating power corrections holds the potential to enhance precision in various experimental scenarios. The process under consideration here plays a crucial role in discerning the impact of non-leading power effects.

Recent advancements have paved the way for investigating power corrections within the TMD formalism. Currently, a comprehensive set of operators up to NLP is available, as detailed in [103, 118]. The evolution properties of these operators have been thoroughly examined in previous studies [103, 120], affirming the validity of factorization for the Drell-Yan and Semi-Inclusive Deep Inelastic Scattering processes up to NLP precision.

Nevertheless, the inclusion of additional non-perturbative operator matrix elements in the cross-section suggests the presence of new non-perturbative physics. Additionally, the factorized formula for the cross-section introduces extra divergences characteristic of sub-leading-power factorization, demanding careful treatment.

In this chapter, we provide a brief overview of the process involved in obtaining factorization beyond the leading power using the background field method.

Essentially, the background field method consists of the separation of QCD fields into dynamical and background components and the subsequent integration of the dynamical ones. The background field method proves particularly advantageous in calculating power corrections since it directly computes the operator expansion from the functional integral, eliminating the need for a matching procedure common in many other approaches. This allows a systematic analysis of the operators involved at each step.

In the same way as we did in chapter 2, we consider the Drell-Yan case as an instructive example and we comment on the generalization needed to apply factorization to SIDIS and SIA. Thus, let us consider here the hadronic tensors for DY:

$$W^{\mu\nu} = \int \frac{d^4y}{(2\pi)^4} e^{-i(yq)} \sum_X \langle p_1, p_2 | J^{\mu\dagger}(y) | X \rangle \langle X | J^{\nu}(0) | p_1, p_2 \rangle, \tag{4.1}$$

where $J_\mu(y) = \bar{q}\gamma^\mu q(y)$ is the elecromagnetic current and $q(y)$ is a quark field. Substituting the electromagnetic current with the electro-weak current merely alters the tensorial structure without impacting the factorization process. Similarly, it is easy to generalize the factorization procedure for SIDIS or SIA as it remains mostly identical, with the only distinction lying in the boundary conditions for the fields.

For completitude, we summarize here some of the notation and kinematics used before and during this chapter. The kinematics of the process is defined by the photon momentum q^μ, and the hadrons momenta p_1^μ and p_2^μ. Once again, we use light-cone coordinates and assume that hadrons are massless,

$$p_1^2 = p_2^2 = 0. \tag{4.2}$$

Hadrons momenta define two light-cone directions, which we traditionally denote as n^μ and $\bar{n}^\mu$ with $(n\bar{n}) = 1$,

$$p_1^\mu = \bar{n}^\mu p_1^+, \qquad p_2^\mu = n^\mu p_2^-. \tag{4.3}$$

The invariant mass of the virtual photon is

$$Q^2 = q^2 = 2q^+q^- - q_T^2, \tag{4.4}$$

where $q_T^2 = -q_T^\mu q_{T\mu} > 0$. The TMD factorization is derived in the limit

$$Q^2 \gg \Lambda^2, \qquad Q^2 \gg q_T^2, \tag{4.5}$$

where Λ is a typical low-energy QCD scale. It implies that the light-cone components of q^μ are large $q^+ \sim q^- \sim Q$. Additionally, we suppose that q^+/p_1^+ and q^-/p_2^- are fixed, which corresponds to a non-small-x regime.

4.1 Field modes and effective operators

The considered hadronic tensors exhibit two causally independent sectors engaged in the exchange of real emissions. In such cases, the functional integral can be expressed using Keldysh's method [125]. We introduce two sets of QCD fields, denoted as causal and anti-causal fields (notated with superscripts $(+)$ and $(-)$, respectively). These fields follow standard quantization rules, featuring time-ordered and anti-time-ordered evolution operators for causal and anti-causal fields respectively. At the future boundary, the values of the fields coincide: $\lim_{t\to\infty} q^{(+)}(t,x) = \lim_{t\to\infty} q^{(-)}(t,x)$ and $\lim_{t\to\infty} A_\mu^{(+)}(t,x) = \lim_{t\to\infty} A_\mu^{(-)}(t,x)$. On the perturbative level, this results in a real-particle propagator connecting $(+)$ and $(-)$ fields, equivalent to the conventional Feynman rules for cut diagrams.

Following this method we can express non-time-ordered operators as a functional integral. The hadronic tensor is rewritten as

$$\begin{aligned} W^{\mu\nu} \;=\; & \int \frac{d^4y}{(2\pi)^4} e^{-i(yq)} \int [D\bar{q}^{(+)} Dq^{(+)} DA^{(+)}] \int [D\bar{q}^{(-)} Dq^{(-)} DA^{(-)}] \\ & \times \Psi_{p_1}^{*(-)}\, \Psi_{p_2}^{*(-)}\, e^{iS_{\rm QCD}^{(+)} - iS_{\rm QCD}^{(-)}}\, J_\mu^{\dagger(-)}(y) J_\nu^{(+)}(0)\, \Psi_{p_1}^{(+)}\, \Psi_{p_2}^{(+)}, \end{aligned} \tag{4.6}$$

Ψ_p represents the wave function of the hadron (constructed in the distant past), and $S_{\rm QCD}$ denotes the QCD action. The superscript $(\pm)$ specifies that the element is exclusively composed of causal or anti-causal fields.

Now we need to identify the relevant field modes. Let us consider the scaling of the fields, in particular, for a hadron with the momentum along the n or $\bar{n}$ direction we have

$$\{\partial_+, \partial_-, \partial_T\}\, q_{\bar{n}} \;\lesssim\; Q\{1, \lambda^2, \lambda\}\, q_{\bar{n}}, \tag{4.7}$$

$$\{\partial_+, \partial_-, \partial_T\}\, q_n \;\lesssim\; Q\{\lambda^2, 1, \lambda\}\, q_n, \tag{4.8}$$

$$\{\partial_+, \partial_-, \partial_T\}\, A_{\bar{n}}^\mu \;\lesssim\; Q\{1, \lambda^2, \lambda\}\, A_{\bar{n}}^\mu, \tag{4.9}$$

$$\{\partial_+, \partial_-, \partial_T\}\, A_n^\mu \;\lesssim\; Q\{\lambda^2, 1, \lambda\}\, A_n^\mu. \tag{4.10}$$

In its particular kinematic sector, the background fields consist of regular QCD fields, therefore obeying the equations of motion of QCD.

The use of the $\lesssim$ symbol in these equations signifies that the fields incorporate all momenta within the corresponding boundaries. This stands as a fundamental distinction

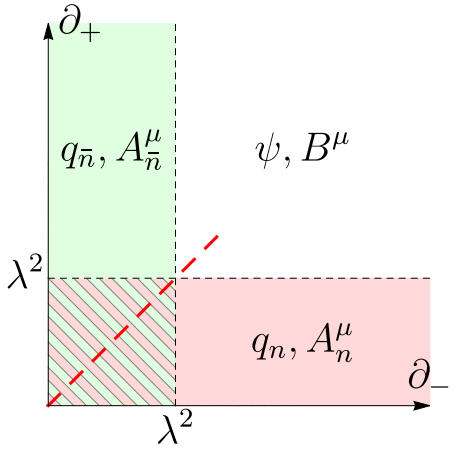

Figure 4.1: Regions of field domains in the plane of light-cone momentum components. Figure credited to V. Moos, I. Scimemi and A. Vladimirov, ref. [103]

in the background approach compared to SCET. In SCET, field modes are defined within boxes of momentum around a specific scale that labels the fields. Another distinction lies in the absence of modes scaling as $\{\partial_+, \partial_-, \partial_T\}q \sim Q\{\lambda, \lambda, \lambda\}q$, the so-called soft modes in SCET nomenclature.

As usual, we distinguish "good" and "bad" spinor components of the quark field, this is

$$q_{\bar{n}/n}(x) = \xi_{\bar{n}/n}(x) + \eta_{\bar{n}/n}(x), \tag{4.11}$$

where

$$\xi_{\bar{n}}(x) = \frac{\not{\bar{n}}\not{n}}{2} q_{\bar{n}}(x), \qquad \eta_{\bar{n}}(x) = \frac{\not{n}\not{\bar{n}}}{2} q_{\bar{n}}(x), \tag{4.12}$$

$$\xi_{n}(x) = \frac{\not{n}\not{\bar{n}}}{2} q_{n}(x), \qquad \eta_{n}(x) = \frac{\not{\bar{n}}\not{n}}{2} q_{n}(x). \tag{4.13}$$

We recall the scaling of the fields with the parameter λ. For quark fields we have

$$\xi_{\bar{n}/n} \sim \lambda, \qquad \eta_{\bar{n}/n} \sim \lambda^2. \tag{4.14}$$

For gluon fields we have

$$\begin{aligned} &A^+_{\bar{n}} \sim 1, \qquad A^\mu_{\bar{n},T} \sim \lambda, \qquad A^-_{\bar{n}} \sim \lambda^2, \\ &A^+_{n} \sim \lambda^2, \qquad A^\mu_{n,T} \sim \lambda, \qquad A^-_{n} \sim 1. \end{aligned} \tag{4.15}$$

The background-field method involves a separation of QCD fields into dynamical and background components, followed by the integration of the dynamical ones. TMD factorization is characterized by the background field having two distinct components: collinear and anticollinear. Quark and gluon fields separate as follows:

$$q^{(\pm)}(x) = \chi^{(\pm)}(x) + q^{(\pm)}_n(x) + q^{(\pm)}_{\bar{n}}(x),$$

$$A_\mu^{(\pm)}(x) \quad = \quad B_\mu^{(\pm)}(x) + A_{n\,\mu}^{(\pm)}(x) + A_{\bar{n}\,\mu}^{(\pm)}(x), \tag{4.16}$$

where χ and B are the dynamical components that cover the remaining part of the Hilbert space, as shown in fig. 4.1. The integration measure is split as

$$[D\bar{q}DqDA] = [D\bar{\chi}D\chi DB][D\bar{q}_{\bar{n}}Dq_{\bar{n}}DA_{\bar{n}}][D\bar{q}_nDq_nDA_n], \tag{4.17}$$

for $\pm$ fields respectively. The separation of field modes is executed while maintaining gauge invariance. The Lagrangian exhibits invariance solely under the gauge transformation of all fields by the same transformation parameter, irrespective of any power counting considerations. However, the gauge transformation for the background field and the dynamical field can be disentangled by employing the background gauge technique [126, 127]. In this way, the gauge fixation condition for the dynamical field is expressed as:

$$[\partial_\mu\delta^{AC} + gf^{ABC}(A_{\bar{n}\,\mu}^{(\pm)B} + A_{n\,\mu}^{(\pm)B})]B^{(\pm)\mu\,C} = D_\mu[A_{\bar{n}}^{(\pm)} + A_n^{(\pm)}]B^{(\pm)\mu} = 0, \tag{4.18}$$

where D_μ is the covariant derivative. Opting for this choice offers the advantage of allowing independent transformations for the background fields. Additionally, in the region where the momenta of the collinear and anticollinear fields do not overlap, we treat them as totally independent fields, and thus their gauge transformations are also independent.

Taking into account the definitions and considerations, the hadronic tensor is written as

$$\begin{aligned} W_{\text{unsub.}}^{\mu\nu} = & \int \frac{d^4y}{(2\pi)^4} e^{-i(yq)} \\ & \times \int [D\bar{q}_{\bar{n}}^{(+)} Dq_{\bar{n}}^{(+)} DA_{\bar{n}}^{(+)}][D\bar{q}_{\bar{n}}^{(-)} Dq_{\bar{n}}^{(-)} DA_{\bar{n}}^{(-)}] e^{iS_{\text{QCD}}^{(+)}[\bar{q}_{\bar{n}},q_{\bar{n}},A_{\bar{n}}] - iS_{\text{QCD}}^{(-)}[\bar{q}_{\bar{n}},q_{\bar{n}},A_{\bar{n}}]} \\ & \times \int [D\bar{q}_n^{(+)} Dq_n^{(+)} DA_n^{(+)}][D\bar{q}_n^{(-)} Dq_n^{(-)} DA_n^{(-)}] e^{iS_{\text{QCD}}^{(+)}[\bar{q}_n,q_n,A_n] - iS_{\text{QCD}}^{(-)}[\bar{q}_n,q_n,A_n]} \\ & \times \int [D\bar{\chi}^{(+)} D\chi^{(+)} DB^{(+)}][D\bar{\chi}^{(-)} D\chi^{(-)} DB^{(-)}] e^{iS_{\text{QCD}}^{(+)}[\bar{\chi},\chi,B] - iS_{\text{QCD}}^{(-)}[\bar{\chi},\chi,B]} \\ & \times \Psi_{p_1}^{*(-)} \Psi_{p_2}^{*(-)}\, J_\mu^{\dagger(-)}[\bar{\chi} + \bar{q}_{\bar{n}} + \bar{q}_n, ...](y)\, J_\nu^{(+)}[\bar{\chi} + \bar{q}_{\bar{n}} + \bar{q}_n, ...](0) \Psi_{p_1}^{(+)} \Psi_{p_2}^{(+)} e^{iS_{int}^{(+)} - iS_{int}^{(-)}}, \end{aligned} \tag{4.19}$$

where in the square brackets we denote the field content of each term. The "unsub". label indicates that this expression includes the unsubtracted overlapped region shown in fig. 4.1, which we will address later. The term accounting for cross-mode interactions is

$$S_{int} = S_{\text{QCD}}[\bar{\psi} + \bar{q}_{\bar{n}} + \bar{q}_n, ...] - S_{\text{QCD}}[\bar{q}_{\bar{n}}, q_{\bar{n}}, A_{\bar{n}}] - S_{\text{QCD}}[\bar{q}_n, q_n, A_n] - S_{\text{QCD}}[\bar{\psi}, \psi, B]. \tag{4.20}$$

The cross-mode interaction term can be divided into four different terms: S_{nh}, which characterizes the interaction between collinear fields and hard fields; $S_{n\bar{n}}$, representing the direct interaction between collinear and anticollinear fields; and $S_{n\bar{n}h}$, capturing the interaction among all fields simultaneously. Each action S_{nh} and $S_{\bar{n}h}$ corresponds to the standard QCD action with background field [127], while $S_{n\bar{n}h}$ and $S_{n\bar{n}}$ are specific to the composite background scenario. It is worth noting that $S_{n\bar{n}} = O(\lambda^3)$, reflecting the power-counting of the fields.

Following the parton model we can assume $\Psi_{p_1} = \Psi_{p_1}[\bar{q}_{\bar{n}}, q_{\bar{n}}, A_{\bar{n}}]$ and $\Psi_{p_2} = \Psi_{p_2}[\bar{q}_n, q_n, A_n]$ and then integrate over the hard mode, yielding

$$
\begin{aligned}
W^{\mu\nu}_{\text{unsub.}} = & \int \frac{d^4y}{(2\pi)^4} e^{-i(yq)} \\
& \times \int [D\bar{q}^{(+)}_{\bar{n}} Dq^{(+)}_{\bar{n}} DA^{(+)}_{\bar{n}}][D\bar{q}^{(-)}_{\bar{n}} Dq^{(-)}_{\bar{n}} DA^{(-)}_{\bar{n}}] e^{iS^{(+)}_{\text{QCD}}[\bar{q}_{\bar{n}}, q_{\bar{n}}, A_{\bar{n}}] - iS^{(-)}_{\text{QCD}}[\bar{q}_{\bar{n}}, q_{\bar{n}}, A_{\bar{n}}]} \\
& \times \int [D\bar{q}^{(+)}_{n} Dq^{(+)}_{n} DA^{(+)}_{n}][D\bar{q}^{(-)}_{n} Dq^{(-)}_{n} DA^{(-)}_{n}] e^{iS^{(+)}_{\text{QCD}}[\bar{q}_{n}, q_{n}, A_{n}] - iS^{(-)}_{\text{QCD}}[\bar{q}_{n}, q_{n}, A_{n}]} \\
& \times \Psi^{*(-)}_{p_1}[\bar{q}_{\bar{n}}, q_{\bar{n}}, A_{\bar{n}}] \Psi^{*(-)}_{p_2}[\bar{q}_n, q_n, A_n]\, \mathcal{J}^{\mu\nu}_{eff}[\bar{q}_{\bar{n}}, \bar{q}_n, ...](y)\, \Psi^{(+)}_{p_1}[\bar{q}_{\bar{n}}, q_{\bar{n}}, A_{\bar{n}}] \Psi^{(+)}_{p_2}[\bar{q}_n, q_n, A_n],
\end{aligned}
\tag{4.21}
$$

where $\mathcal{J}^{\mu\nu}_{eff}[\bar{q}_{\bar{n}}, \bar{q}_n, \bar{q}_s, ...]$ depends on all collinear and anticollinear background modes and is defined as

$$
\begin{aligned}
\mathcal{J}^{\mu\nu}_{eff}[\bar{q}_{\bar{n}}, \bar{q}_n, ...](y) = & \int [D\bar{\chi}^{(+)} D\chi^{(+)} DB^{(+)}][D\bar{\chi}^{(-)} D\chi^{(-)} DB^{(-)}] \\
& \times J^{\dagger(-)}_{\mu}[\bar{\chi} + \bar{q}_{\bar{n}} + \bar{q}_n, ...](y) J^{(+)}_{\nu}[\bar{\chi} + \bar{q}_{\bar{n}} + \bar{q}_n, ...](0) e^{iS^{(+)}_{\text{QCD}}[\bar{\chi}, \chi, B] - iS^{(-)}_{\text{QCD}}[\bar{\chi}, \chi, B]} e^{iS^{(+)}_{int} - iS^{(-)}_{int}}.
\end{aligned}
\tag{4.22}
$$

The effective operator satisfies

$$
\mathcal{J}^{\mu\nu}(y) = \mathcal{J}^{\dagger\nu\mu}(-y), \tag{4.23}
$$

$$
\frac{\partial}{\partial y^{\mu}} \mathcal{J}^{\mu\nu}(y) = 0, \tag{4.24}
$$

which are consequences of symmetry and transversality of the hadronic tensor.

4.2 Process dependence and gauge fixation

The effective operator in eq. 4.22 is gauge-invariant and maintains gauge invariance term by terms in the power expansion. By choosing an appropriate gauge fixing for collinear and anticollinear fields, we can largely simplify calculations in intermediate steps. In particular, we adopt light-cone gauges for background fields.

$$
n^{\mu} A^{(\pm)}_{\bar{n},\mu}(z) = 0, \qquad \bar{n}^{\mu} A^{(\pm)}_{n,\mu}(z) = 0. \tag{4.25}
$$

This choide eliminates $\mathcal{O}(1)$ gluon components in eq. 4.15. Consequently, the power counting for operators increases with the number of fields in the operator, significantly simplifying the computation process.

The light-cone gauge conditions outlined in equation (4.25) alone do not eliminate all gauge freedom, allowing for possible $z^{\mp}$-independent transformations (in the $A^{\pm} = 0$ gauge). To address the remaining gauge freedom, specific boundary conditions are imposed on the components of the gluon field. In particular, we impose the following set of boundary conditions:

$$
\lim_{z^- \to L} A^{\mu}_{\bar{n}}(z) = 0, \qquad \lim_{z^+ \to \bar{L}} A^{\mu}_{n}(z) = 0, \tag{4.26}
$$

with

$$(L,\bar{L}) = \begin{cases} (-\infty,-\infty), & \text{for DY,} \\ (+\infty,-\infty), & \text{for SIDIS,} \\ (+\infty,+\infty), & \text{for SIA.} \end{cases} \tag{4.27}$$

The value of $(L,\bar{L})$ is the only difference between processes at the operator level. The gauge-fixing condition in eq. 4.25 can then be inverted, yielding

$$A^{\mu}_{\bar{n}}(z) = -g\int_{L}^{0} d\sigma F^{\mu+}_{\bar{n}}(z+n\sigma), \qquad A^{\mu}_{n}(z) = -g\int_{\bar{L}}^{0} d\sigma F^{\mu-}_{n}(z+\bar{n}\sigma), \tag{4.28}$$

where $F^{\mu\nu}$ is the gluon field-strength tensor.

Once the computation is finished and the result is expressed in terms of $F_{\mu\nu}$, the explicit form of the gauge-invariant operator can be recovered by incorporating gauge links to the fields following the rules

$$\begin{aligned} q_{\bar{n}}(z) &\to [Ln+\infty_T, Ln+z][Ln+z,z]q_{\bar{n}}(z), \\ \bar{q}_{\bar{n}}(z) &\to \bar{q}_{\bar{n}}(z)[z,Ln+z][Ln+z,Ln+\infty_T], \\ F^{\mu\nu}_{\bar{n}}(z) &\to [Ln+\infty_T, Ln+z][Ln+z,z]F^{\mu\nu}_{\bar{n}}(z)[z,Ln+z][Ln+z,Ln+\infty_T], \end{aligned} \tag{4.29}$$

where ∞_T in an infinitely distant point in the transverse plane, and $[a,b]$ is a straight Wilson line

$$[a,b] = P\exp\left[-ig\int_a^b dz_\mu A^{\mu}_{\bar{n}}(z)\right], \tag{4.30}$$

and analogously for anticollinear fields.

4.3 Effective operators

In this section, we show the computation of the effective operator, accounting for next-to-leading power and leading order in perturbation theory. First, we show the tree order operator for LP as an example and then we move to the tree order for the NLP operator. We establish the tree order of the NLP effective operator and provide the essential definitions.

Throughout the evaluation process, it is important to remember that ultimately, the operators are inserted into matrix elements, where certain ones may vanish (for example, due to non-zero fermion number or non-singlet color representation). Such operators can be disregarded without exhaustive consideration. At each stage, we encounter a series of terms with increasing power and, therefore, only terms adhering to the desired power counting are retained in the final analysis.

4.3.1 Tree order for LP

We start with the decomposition of the electromagnetic current into collinear, anticollinear and dynamical fields:

$$J^{\mu}[\bar{\chi}+\bar{q}_{\bar{n}}+\bar{q}_n,...] = \bar{q}_{\bar{n}}\gamma^{\mu}q_n + \bar{q}_n\gamma^{\mu}q_{\bar{n}} \tag{4.31}$$

$$+\bar{\chi}\gamma^\mu\chi + \bar{q}_{\bar{n}}\gamma^\mu\chi + \bar{q}_n\gamma^\mu\chi + \bar{\chi}\gamma^\mu q_{\bar{n}} + \bar{\chi}\gamma^\mu q_n$$
$$+\bar{q}_{\bar{n}}\gamma^\mu q_{\bar{n}} + \bar{q}_n\gamma^\mu q_n$$

In the equation presented here, we observe distinct contributions:

1. The first line represents the leading tree-order contribution.
2. The second line involves fields χ to be paired with those from $S_{\rm QCD/int}$, contributing to NLP and NLO, addressed in the subsequent section.
3. Terms in the third line feature two fields from the same collinear sector, yielding disconnected contributions to matrix elements unless additional fields are extracted from $S_{\rm int}$. Non-vanishing contributions from these terms occur earliest at N^{4}LP.

Thus, we keep only the first line and perform the multipole expansion

$$\begin{aligned}&\bar{q}_{\bar{n}}\gamma^\mu q_n(y) + \bar{q}_n\gamma^\mu q_{\bar{n}}(y) \\ &\quad= \bar{q}_{\bar{n}}(y^- n + y_T)\gamma^\mu q_n(y^+\bar{n} + y_T) + \bar{q}_n(y^+\bar{n} + y_T)\gamma^\mu q_{\bar{n}}(y^- n + y_T) + \mathcal{O}(\lambda^4).\end{aligned} \tag{4.32}$$

where the terms in $\mathcal{O}(\lambda^4)$ contains derivatives, such as $y^+\bar{q}_{\bar{n}}\overleftarrow{\partial}_-\gamma^\mu q_n$. We now decompose the field q into "good" and "bad" components as in eq. 4.11:

$$\begin{aligned}\bar{q}_{\bar{n}}\gamma^\mu q_n + \bar{q}_n\gamma^\mu q_{\bar{n}} \;=\;& \bar{\xi}_{\bar{n}}\gamma_T^\mu\xi_n + \bar{\xi}_n\gamma_T^\mu\xi_{\bar{n}} \\ &+\bar{n}^\mu\bar{\xi}_{\bar{n}}\gamma^+\eta_n + n^\mu\bar{\xi}_n\gamma^-\eta_{\bar{n}} + n^\mu\bar{\eta}_{\bar{n}}\gamma^-\xi_n + \bar{n}^\mu\bar{\eta}_n\gamma^+\xi_{\bar{n}} \\ &+\bar{\eta}_{\bar{n}}\gamma_T^\mu\eta_n + \bar{\eta}_n\gamma_T^\mu\eta_{\bar{n}},\end{aligned} \tag{4.33}$$

The first, second, and third lines in eq. 4.33 are $\mathcal{O}(\lambda^2)$, $\mathcal{O}(\lambda^3)$, and $\mathcal{O}(\lambda^4)$ respectively. This term represents the LP term of EM current. Thus, the LP term is

$$J^\mu_{\rm LP}(y) = \bar{\xi}_{\bar{n}}(y^- n + y_T)\gamma_T^\mu\xi_n(y^+\bar{n} + y_T) + \bar{\xi}_n(y^+\bar{n} + y_T)\gamma_T^\mu\xi_{\bar{n}}(y^- n + y_T). \tag{4.34}$$

The final effective operator, including causal and anticausal fields, is given by

$$\begin{aligned}\mathcal{J}^{\mu\nu}_{\rm LP}(y) = &[\bar{\xi}^{(-)}_{\bar{n}}(y^- n + y_T)\gamma_T^\mu\xi^{(-)}_n(y^+\bar{n} + y_T) + \bar{\xi}^{(-)}_n(y^+\bar{n} + y_T)\gamma_T^\mu\xi^{(-)}_{\bar{n}}(y^- n + y_T)] \\ &\times[\bar{\xi}^{(+)}_{\bar{n}}(0)\gamma_T^\nu\xi^{(+)}_n(0) + \bar{\xi}^{(+)}_n(0)\gamma_T^\nu\xi^{(+)}_{\bar{n}}(0)].\end{aligned} \tag{4.35}$$

The quark fields ξ are operators of twist-1. Therefore, $\mathcal{J}^{\mu\nu}_{\rm LP}(y)$ adheres to a $(1+1)\times(1+1)$-twist classification, as per the nomenclature employed in background field derivations.

Let us delve into the concept of definite twist: the geometrical twist is characterized as the "dimension-minus-spin" of a specific operator. An operator possessing a definite geometrical twist belongs to an irreducible Lorentz group, ensuring it remains distinct from operators with different geometrical twists. This crucial attribute is preserved by perturbation theory, thereby allowing operators with definite geometrical twists to evolve independently, with their matrix elements representing distinct physical observables. The twist-decomposition involves an algebraic procedure, involving symmetrization and anti-symmetrization of indices, initially formulated for local operators but adaptable to non-local ones as well. In our context, the twist-1 operator consists of a single "good"

component of either quark ξ or gluon field $F_{\mu+}$ (where μ represents a transverse index) accompanied by a semi-infinite Wilson line. Given a TMD operator denoted $\mathcal{O}_{N,M}$ (where N and M denote the geometrical twist of each component), its TMD twist is defined as twist-$(N+M)$. TMD operators, and consequently TMD distributions, bearing distinct (N,M) labels do not mix, with their matrix elements representing unique combinations of independent nonperturbative functions.

Thus, we can rewrite this expression so that it includes TMD operators:

$$\mathcal{J}^{\mu\nu}_{\rm LP}(y) \;=\; \frac{\gamma^{\mu}_{T,ij}\gamma^{\nu}_{T,kl}}{N_c}\Big(\mathcal{O}^{li}_{11,\bar{n}}\,\overline{\mathcal{O}}^{jk}_{11,n}+\overline{\mathcal{O}}^{jk}_{11,\bar{n}}\,\mathcal{O}^{li}_{11,n}\Big) \tag{4.36}$$

where (i,j,k,l) are spinor indices, and O are TMD twist-(1+1) operators have the argument $(\{y^-,0\},y_T)$ defined as

$$\mathcal{O}^{ji}_{11,\bar{n}}(\{y^-,0\},y_T) \;=\; \bar{\xi}^{(-)}_{\bar{n},i}(y^-n+y_T)\,\xi^{(+)}_{\bar{n},j}(0), \tag{4.37}$$

$$\overline{\mathcal{O}}^{ji}_{11,\bar{n}}(\{y^-,0\},y_T) \;=\; \xi^{(-)}_{\bar{n},j}(y^-n+y_T)\,\bar{\xi}^{(+)}_{\bar{n},i}(0), \tag{4.38}$$

and respectively for anticollinear operators. This expression is widely recognized and forms the foundation for the LP TMD factorization, as discussed in, for example, [21, 128, 18]. The matrix elements of operators $\mathcal{O}_{11,\bar{n}}$ and $\overline{\mathcal{O}}_{11,\bar{n}}$ correspond to the quark and anti-quark TMD distributions, respectively. At this point, we have arrived at the same equations obtained for LP using SCET, with the remaining task being the application of Fierzing transformations to derive unpolarized and polarized TMD distributions.

4.3.2 Tree order for NLP

The NLP part of the effective operator emerges solely through the combination of an LP current with the NLP segment of another EM current. The NLP contribution can be constructed in two different ways:

- Pairing a "good" and a "bad" component of the quark fields from the second line of equation (4.33). This corresponds to diagrams A and B in fig. 4.2.
- Having three "good" field components, such as $\bar{\xi}A_T\xi$. Acquiring such a term requires extracting an interaction term from $e^{iS_{int}}$. This corresponds to diagrams C, D, E and F in fig. 4.2.

We do not go into the detailed computation of each diagram and further discussion can be found in ref. [103]. Evaluating each diagram we obtain the NLP EM current and the result can be split into the following parts

$$J^{\mu}_{\rm NLP} = J^{\mu}_{1'1}+J^{\mu}_{11'}+J^{\mu}_{21}+J^{\mu}_{12}+J^{\mu}_{21;\mathbf{8}}+J^{\mu}_{12;\mathbf{8}}. \tag{4.39}$$

We have two distinct types of terms in this expression. On one hand, we have derivatives of twist-1 operators

$$J^{\mu}_{1'1}(0) \;=\; -n^{\mu}\int_L^0 dz^-\Big[\bar{\xi}_{\bar{n}}(z^-n)\overleftarrow{\partial_T}\xi_n(0)+\bar{\xi}_n(0)\overrightarrow{\partial_T}\xi_{\bar{n}}(z^-n)\Big]. \tag{4.40}$$

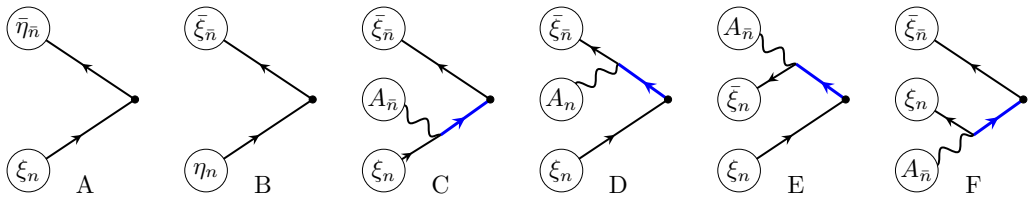

Figure 4.2: Diagrams contributing to the tree order of vector current at NLP. The blobs indicate the type of background field. The blue lines are the dynamical fields. Credit to V. Moos, I. Scimemi and A. Vladimirov, ref. [103].

On the other hand, we have terms containing operators of twist-2 and twist-1

$$J^\mu_{21}(0) = ig\bar{n}^\mu \int_{\bar{L}}^0 dz^+ \Big[\bar{\xi}_{\bar{n}}(0)A_{\bar{n},T}(0)\xi_n(z^+\bar{n}) - \bar{\xi}_n(z^+\bar{n})A_{\bar{n},T}(0)\xi_{\bar{n}}(0)\Big] \tag{4.41}$$
$$- ign^\mu \int_L^0 dz^- \Big[\bar{\xi}_{\bar{n}}(z^-n)A_{\bar{n},T}(z^-n)\xi_n(0) - \bar{\xi}_n(0)A_{\bar{n},T}(z^-n)\xi_{\bar{n}}(z^-n)\Big],$$
$$J^\mu_{21,\mathbf{8}}(0) = \frac{ig}{2}\int_L^0 dz^- \Big[\bar{\xi}_{\bar{n}}(z^-n)\gamma^+\gamma^\nu_T\gamma^\mu_T t^A\xi_{\bar{n}}(0) - \bar{\xi}_{\bar{n}}(0)\gamma^+\gamma^\mu_T\gamma^\nu_T t^A\xi_{\bar{n}}(z^-n)\Big]A^A_{n,\nu}(0), \tag{4.42}$$

where A is the color index in the adjoint representation and t^A is the generator of SU(N_c). The expression for $J^\mu_{11'}$, J^μ_{12} and $J^\mu_{12,\mathbf{8}}$ are obtained from $J^\mu_{1'1}$, J^μ_{21} and $J^\mu_{21,\mathbf{8}}$ by exchanging $n \leftrightarrow \bar{n}$. The terms $J^\mu_{21,\mathbf{8}}$ and $J^\mu_{12,\mathbf{8}}$ originate from diagrams E and F. However, they do not contribute at the NLP level because the formation of a color-neutral TMD operator necessitates another operator in the adjoint representation. In order to rewrite the NLP in a simpler form, we can define an inverse derivative operator:

$$\frac{1}{\partial_+}f(x) = \int_L^0 dz^- f(x+z^-n), \qquad \frac{1}{\partial_-}f(x) = \int_{\bar{L}}^0 dz^+ f(x+z^+\bar{n}). \tag{4.43}$$

The terms in the NLP current can then be rewritten as

$$J^\mu_{1'1} = -n^\mu\bar{\xi}_{\bar{n}}\frac{\overleftarrow{\partial_T}}{\overleftarrow{\partial_+}}\xi_n - n^\mu\bar{\xi}_n\frac{\overrightarrow{\partial_T}}{\overrightarrow{\partial_+}}\xi_{\bar{n}}, \tag{4.44}$$
$$J^\mu_{21} = ig\bar{\xi}_{\bar{n}}A_{\bar{n},T}\left(\frac{\bar{n}^\mu}{\overrightarrow{\partial_-}} - \frac{n^\mu}{\overleftarrow{\partial_+}}\right)\xi_n - ig\bar{\xi}_n\left(\frac{\bar{n}^\mu}{\overleftarrow{\partial_-}} - \frac{n^\mu}{\overrightarrow{\partial_+}}\right)A_{\bar{n},T}\xi_{\bar{n}}, \tag{4.45}$$

the operators $J^\mu_{1'1}$ and $J^\mu_{11'}$ can be combined with the LP current eq. 4.34 in the following way

$$J^\mu_{11} = J_{\rm LP} + J^\mu_{1'1} + J^\mu_{11'} \tag{4.46}$$
$$= \bar{\xi}_{\bar{n}}\gamma^\mu_T\xi_n + \bar{\xi}_n\gamma^\mu_T\xi_{\bar{n}} - n^\mu\bar{\xi}_{\bar{n}}\frac{\overleftarrow{\partial_T}}{\overleftarrow{\partial_+}}\xi_n - n^\mu\bar{\xi}_n\frac{\overrightarrow{\partial_T}}{\overrightarrow{\partial_+}}\xi_{\bar{n}} - \bar{n}^\mu\bar{\xi}_n\frac{\overleftarrow{\partial_T}}{\overleftarrow{\partial_-}}\xi_{\bar{n}} - \bar{n}^\mu\bar{\xi}_{\bar{n}}\frac{\overrightarrow{\partial_T}}{\overrightarrow{\partial_-}}\xi_n.$$

The effective operator at the NLP level is obtained by combining LP and NLP terms of electromagnetic currents. We obtain

$$\begin{aligned}
\mathcal{J}^{\mu\nu}_{\rm NLP} &= -\frac{n^\mu\gamma^\rho_{T,ij}\gamma^\nu_{T,kl}+n^\nu\gamma^\mu_{T,ij}\gamma^\rho_{T,kl}}{N_c}\Big(\frac{\partial_\rho}{\partial_+}\mathcal{O}^{li}_{11,\bar n}\overline{\mathcal{O}}^{jk}_{11,n}+\frac{\partial_\rho}{\partial_+}\overline{\mathcal{O}}^{jk}_{11,\bar n}\mathcal{O}^{li}_{11,n}\Big) \\
&\quad -\frac{\bar n^\mu\gamma^\rho_{T,ij}\gamma^\nu_{T,kl}+\bar n^\nu\gamma^\mu_{T,ij}\gamma^\rho_{T,kl}}{N_c}\Big(\mathcal{O}^{li}_{11,\bar n}\frac{\partial_\rho}{\partial_-}\overline{\mathcal{O}}^{jk}_{11,n}+\overline{\mathcal{O}}^{jk}_{11,\bar n}\frac{\partial_\rho}{\partial_-}\mathcal{O}^{li}_{11,n}\Big) \\
&\quad +ig\frac{\delta_{ij}\gamma^\nu_{T,kl}}{N_c}\Big\{\mathbb{O}^{li}_{21,\bar n}\left(\frac{\bar n^\mu}{\overrightarrow{\partial}_-}-\frac{n^\mu}{\overleftarrow{\partial}_+}\right)\overline{\mathcal{O}}^{jk}_{11,n}-\overline{\mathbb{O}}^{jk}_{21,\bar n}\left(\frac{\bar n^\mu}{\overrightarrow{\partial}_-}-\frac{n^\mu}{\overleftarrow{\partial}_+}\right)\mathcal{O}^{li}_{11,n} \\
&\qquad +\mathcal{O}^{li}_{11,\bar n}\left(\frac{\bar n^\mu}{\overrightarrow{\partial}_-}-\frac{n^\mu}{\overleftarrow{\partial}_+}\right)\overline{\mathbb{O}}^{jk}_{21,n}-\overline{\mathcal{O}}^{jk}_{11,\bar n}\left(\frac{\bar n^\mu}{\overrightarrow{\partial}_-}-\frac{n^\mu}{\overleftarrow{\partial}_+}\right)\mathbb{O}^{li}_{21,n}\Big\} \\
&\quad +ig\frac{\gamma^\mu_{T,ij}\delta_{kl}}{N_c}\Big\{\mathbb{O}^{li}_{12,\bar n}\left(\frac{\bar n^\nu}{\overrightarrow{\partial}_-}-\frac{n^\nu}{\overleftarrow{\partial}_+}\right)\overline{\mathcal{O}}^{jk}_{11,n}-\overline{\mathbb{O}}^{jk}_{12,\bar n}\left(\frac{\bar n^\nu}{\overrightarrow{\partial}_-}-\frac{n^\nu}{\overleftarrow{\partial}_+}\right)\mathcal{O}^{li}_{11,n} \\
&\qquad +\mathcal{O}^{li}_{11,\bar n}\left(\frac{\bar n^\nu}{\overrightarrow{\partial}_-}-\frac{n^\nu}{\overleftarrow{\partial}_+}\right)\overline{\mathbb{O}}^{jk}_{12,n}-\overline{\mathcal{O}}^{jk}_{11,\bar n}\left(\frac{\bar n^\nu}{\overrightarrow{\partial}_-}-\frac{n^\nu}{\overleftarrow{\partial}_+}\right)\mathbb{O}^{li}_{12,n}\Big\},
\end{aligned} \tag{4.47}$$

where δ_{ij} is the Kronecker delta for spinor indices. All derivatives are with respect to the coordinate y and act only on the subsequent operator. To derive this expression we have used the identity

$$\bar\xi_{\bar n,j}(y^-n+y_T)\frac{\overleftarrow{\partial_\rho}}{\overleftarrow{\partial}_+}\xi_{\bar n,i}(0)=\bar\xi_{\bar n,j}(y^-n+y_T)\frac{\overrightarrow{\partial_\rho}}{\overrightarrow{\partial}_+}\xi_{\bar n,i}(0)=\frac{\partial_\rho}{\partial_+}O^{ij}_{11,\bar n}(\{y^-,0\},y_T), \tag{4.48}$$

Here, we assume that the total derivatives of TMD operators can be eliminated since they do not contribute to the forward matrix elements. TMD operators of twist-(1+1) have the arguments $(\{y^-,0\},y_T)$. All TMD operators of twist-(1+2) and (2+1) have argument $(\{y^-,y^-,0\},y_T)$ and $(\{y^-,0,0\},y_T)$ respectively. Finally, the TMD operators of twist-(1+2) and twist-(2+1) are defined as

$$\mathbb{O}^{ji}_{21,\bar n}(\{y^-,y^-,0\},y_T)=[\bar\xi^{(-)}_{\bar n}A^{(-)}_{\bar n,T}(y^-n+y_T)]_i\xi^{(+)}_{\bar n,j}(0), \tag{4.49}$$

$$\mathbb{O}^{ji}_{12,\bar n}(\{y^-,0\ \ ,0\},y_T)=\bar\xi^{(-)}_{\bar n,i}(y^-n+y_T)[A^{(+)}_{\bar n,T}\xi^{(+)}_{\bar n}(0)]_j, \tag{4.50}$$

$$\overline{\mathbb{O}}^{ji}_{21,\bar n}(\{y^-,y^-,0\},y_T)=[A^{(-)}_{\bar n,T}\xi^{(-)}_{\bar n}(y^-n+y_T)]_j\bar\xi^{(+)}_{\bar n,i}(0), \tag{4.51}$$

$$\overline{\mathbb{O}}^{ji}_{12,\bar n}(\{y^-,0\ \ ,0\},y_T)=\xi^{(-)}_{\bar n,j}(y^-n+y_T)[\bar\xi^{(+)}_{\bar n}A^{(+)}_{\bar n,T}(0)]_i. \tag{4.52}$$

4.3.3 Gauge invariant expressions for TMD operators

The definitions in eq. 4.49-4.52 are given in light-cone gauge. They can be written in gauge invariant form using the relations in eq. 4.28. The elementary building blocks are the semi-compact operators of twist-1 and twist-2 can be generalized as

$$U_{1,\bar n}(z,b) = [Ln+b,zn+b]\xi_{\bar n}(zn+b), \tag{4.53}$$

$$U^\mu_{2,\bar n}(\{z_1,z_2\},b) = g[Ln+b,z_1n+b]F^{\mu+}_{\bar n}[z_1n+b,z_2n+b]\xi_{\bar n}(z_2n+b), \tag{4.54}$$

where index μ is transverse, with the transverse link omitted. The operator $U^{\mu}_{2,\bar{n}}$ has open spinor and vector indices and is more general than the operator appearing at NLP, which is contracted in the following way

$$U_{2,\bar{n}}(\{z_1,z_2\},b) = \gamma_{T\mu} U^{\mu}_{2,\bar{n}}(\{z_1,z_2\},b), \tag{4.55}$$

Additionally, we define the barred operators

$$\begin{aligned} \overline{U}_{1,\bar{n}}(z,b) &= \bar{\xi}_{\bar{n}}(zn+b)[zn+b,Ln+b], & (4.56)\\ \overline{U}^{\mu}_{2,\bar{n}}(\{z_1,z_2\},b) &= g\,\bar{\xi}_{\bar{n}}(z_1 n+b)[z_1 n+b,z_2 n+b]F^{\mu+}_{\bar{n}}[z_2 n+b,Ln+b]. & (4.57)\end{aligned}$$

The TMD operators can then be rewritten as products of semi-compact operators. The twist-(1+1) operators are

$$\begin{aligned} \mathcal{O}_{11,\bar{n}}(\{z_1,z_2\},b) &= \overline{U}^{(-)}_{1,\bar{n}}(z_1,b)U^{(+)}_{1,\bar{n}}(z_2,0), & (4.58)\\ \overline{\mathcal{O}}_{11,\bar{n}}(\{z_1,z_2\},b) &= U^{(-)}_{1,\bar{n}}(z_1,b)\overline{U}^{(+)}_{1,\bar{n}}(z_2,0). & (4.59)\end{aligned}$$

The twist-(2+1) and twist-(1+2) operators are

$$\begin{aligned} \mathcal{O}_{21,\bar{n}}(\{z_1,z_2,z_3\},b) &= \overline{U}^{(-)}_{2,\bar{n}}(\{z_1,z_2\},b)U^{(+)}_{1,\bar{n}}(z_3,0), & (4.60)\\ \mathcal{O}_{12,\bar{n}}(\{z_1,z_2,z_3\},b) &= \overline{U}^{(-)}_{1,\bar{n}}(z_1,b)U^{(+)}_{1,\bar{n}}(\{z_2,z_3\},0), & (4.61)\\ \overline{\mathcal{O}}_{21,\bar{n}}(\{z_1,z_2,z_3\},b) &= U^{(-)}_{2,\bar{n}}(\{z_2,z_1\},b)\overline{U}^{(+)}_{1,\bar{n}}(z_3,0), & (4.62)\\ \overline{\mathcal{O}}_{12,\bar{n}}(\{z_1,z_2,z_3\},b) &= U^{(-)}_{1,\bar{n}}(z_1,b)\overline{U}^{(+)}_{2,\bar{n}}(\{z_3,z_2\},0). & (4.63)\end{aligned}$$

Note the positional enumeration within the operators $\overline{\mathcal{O}}_{21,\bar{n}}$ and $\overline{\mathcal{O}}_{12,\bar{n}}$. This enumeration is arranged such that the gluon field consistently occupies coordinate z_2. All these operators act as matrices in spinor space while acting as singlets in color space. The operators $\overline{\mathcal{O}}$ are linked to $\mathcal{O}$ through charge conjugation. The matrix elements of these pairs define quark and antiquark TMD distributions, as illustrated in reference [128].

The definitions outlined in eqs. 4.53 through 4.57 are provided within the conventional QCD basis. However, in the context of SCET literature, one typically employs

$$\begin{aligned} \mathbb{U}^{\mu}_{2,\bar{n}}(\{z_1,z_2\},b) &= -i[Ln+b,z_1 n+b]\overleftarrow{D}^{\mu}_{\bar{n}}[z_1 n+b,z_2 n+b]\xi_{\bar{n}}(z_2 n+b), & (4.64)\\ \overline{\mathbb{U}}^{\mu}_{2,\bar{n}}(\{z_1,z_2\},b) &= i\,\bar{\xi}_{\bar{n}}(z_1 n+b)[z_2 n+b,z_2 n+b]\overrightarrow{D}^{\mu}_{\bar{n}}[z_2 n+b,Ln+b], & (4.65)\end{aligned}$$

where D is the covariant derivative. The operators $\mathbb{O}$ in eq. 4.49–4.52 are defined with replacement of $U \to \mathbb{U}$:

$$\mathbb{O}_{21,\bar{n}}(\{z_1,z_2,z_3\},b) = \overline{\mathbb{U}}^{(-)}_{2,\bar{n}}(\{z_1,z_2\},b)U^{(+)}_{1,\bar{n}}(z_3,0). \tag{4.66}$$

Both operators $\mathbb{O}$ and $\mathcal{O}$ are related as

$$\mathcal{O}_{NM,\bar{n}}(\{z_1,z_2,z_3\},b) = -\frac{\partial}{\partial z_2}\mathbb{O}_{NM,\bar{n}}(\{z_1,z_2,z_3\},b), \tag{4.67}$$

where N and M are 1 or 2. The relation (4.67) can be inverted

$$\mathbb{O}_{NM,\bar{n}}(\{z_1,z_2,z_3\},b) = -\int_L^{z_2}\mathcal{O}_{NM,\bar{n}}(\{z_1,\sigma,z_3\},b). \tag{4.68}$$

4.3.4 Effective operator in momentum space

Typically, TMD distributions are defined within the mixed momentum-coordinate representation. Specifically, they undergo a Fourier transformation solely in light-cone coordinates. This approach resembles parton densities, which are defined in terms of momentum fractions, and it maintains a straightforward structure of TMD evolution, which remains diagonal in transverse-position space. Here we also define

$$U_{1,\bar{n}}(z,b) = p_+ \int dx e^{ixzp_+} U_{1,\bar{n}}(x,b), \tag{4.69}$$

$$U_{2,\bar{n}}(\{z_1,z_2\},b) = p_+^2 \int dx_1 dx_2 e^{i(x_1 z_1 + x_2 z_2)p_+} U_{2,\bar{n}}(x_{1,2},b), \tag{4.70}$$

where $x_{1,2}$ is a shorthand notation for (x_1,x_2), which can be interpreted as the fraction parton's momentum, and p_+ is the momentum of the hadron. For TMD operators we define

$$\mathcal{O}_{11,\bar{n}}(\{z,0\},b) = p_+ \int dx\, e^{izxp_+} \mathcal{O}_{11,\bar{n}}(x,b), \tag{4.71}$$

$$\overline{\mathcal{O}}_{11,\bar{n}}(\{z,0\},b) = p_+ \int dx\, e^{izxp_+} \overline{\mathcal{O}}_{11,\bar{n}}(x,b), \tag{4.72}$$

$$\mathcal{O}_{MN,\bar{n}}(\{z_1,z_2,z_3\},b) = p_+^2 \int [dx]\, e^{i(z_1x_1+z_2x_2+z_3x_3)p_+} \mathcal{O}_{MN,\bar{n}}(x_{1,2,3},b), \tag{4.73}$$

$$\overline{\mathcal{O}}_{MN,\bar{n}}(\{z_1,z_2,z_3\},b) = p_+^2 \int [dx]\, e^{i(z_1x_1+z_2x_2+z_3x_3)p_+} \overline{\mathcal{O}}_{MN,\bar{n}}(x_{1,2,3},b), \tag{4.74}$$

where (M,N) are $(2,1)$ or $(1,2)$ and

$$\int [dx] = \int dx_1 dx_2 dx_3\, \delta(x_1+x_2+x_3). \tag{4.75}$$

Once the matrix elements are taken, the values of x are restricted $x \in [-1,1]$ for parton distributions. The relation between the operators $\mathbb{O}$ and $\mathcal{O}$ is simplified in momentum space:

$$\mathbb{O}_{MN,\bar{n}}(\{z_1,z_2,z_3\},b) = p_+^2 \int [dx]\, e^{i(z_1x_1+z_2x_2+z_3x_3)p_+} \frac{i}{x_2 p_+} \mathcal{O}_{MN,\bar{n}}(x_{1,2,3},b). \tag{4.76}$$

The terms contributing to the NLP EM current can then be rewritten as

$$\begin{aligned} J^\mu_{11}(x,\tilde{x}) = {} & \overline{U}_{1,\bar{n}}(x)\gamma_T^\mu U_{1,n}(\tilde{x}) + \overline{U}_{1,n}(\tilde{x})\gamma_T^\mu U_{1,\bar{n}}(x) \\ & + \frac{in^\mu}{x p_1^+}\Big(\overline{U}_{1,\bar{n}}(x)\overleftarrow{\partial_T} U_{1,n}(\tilde{x}) + \overline{U}_{1,n}(\tilde{x})\partial_T U_{1,\bar{n}}(x)\Big) \\ & + \frac{i\bar{n}^\mu}{\tilde{x} p_2^-}\Big(\overline{U}_{1,n}(\tilde{x})\overleftarrow{\partial_T} U_{1,\bar{n}}(x) + \overline{U}_{1,\bar{n}}(x)\partial_T U_{1,n}(\tilde{x})\Big), \end{aligned} \tag{4.77}$$

$$J^\mu_{21}(x_{1,2},\tilde{x}) = \frac{i}{x_2 p_1^+}\left(\frac{\bar{n}^\mu}{\tilde{x} p_2^-} - \frac{n^\mu}{(x_1+x_2)p_1^+}\right)\left(\overline{U}_{2,\bar{n}}(x_{1,2})U_{1,n}(\tilde{x}) - \overline{U}_{1,n}(\tilde{x})U_{2,\bar{n}}(x_{2,1})\right), \tag{4.78}$$

$$J^{\mu}_{12}(x,\tilde{x}_{1,2}) = \frac{i}{\tilde{x}_2 p_2^-}\left(\frac{n^\mu}{x p_1^+} - \frac{\bar{n}^\mu}{(\tilde{x}_1+\tilde{x}_2)p_2^-}\right)\left(\overline{U}_{2,n}(\tilde{x}_{1,2})U_{1,\bar{n}}(x) - \overline{U}_{1,\bar{n}}(x)U_{2,n}(\tilde{x}_{2,1})\right). \tag{4.79}$$

Here, $x_{2,1} = (x_2, x_1)$, and the repeating argument y_T is omitted for conciseness. It's noteworthy that the arguments x_1 and x_2 are arranged such that x_1 represents the momentum fraction of the quark or antiquark, while x_2 represents the momentum fraction of the gluon. Finally, we take the Fourier transform of the effective current

$$\mathcal{J}^{\mu\nu}_{\text{eff}}(q) = \int \frac{d^4y}{(2\pi)^4} e^{-i(qy)} \mathcal{J}^{\mu\nu}_{\text{eff}}(y), \tag{4.80}$$

yielding

$$\begin{aligned}\mathcal{J}^{\mu\nu}_{\text{eff}}(q) = \int \frac{d^2b}{(2\pi)^2} e^{-i(qb)} \Bigg\{ & \int dx d\tilde{x} \delta\left(x - \frac{q^+}{p_1^+}\right)\delta\left(\tilde{x} - \frac{q^-}{p_2^-}\right)\mathcal{J}^{\mu\nu}_{1111}(x,\tilde{x},b) \\ & + \int [dx] d\tilde{x} \delta\left(\tilde{x} - \frac{q^-}{p_2^-}\right)\left(\delta\left(x_1 - \frac{q_1^+}{p_1^+}\right)\mathcal{J}^{\mu\nu}_{1211}(x,\tilde{x},b) + \delta\left(x_3 + \frac{q_1^+}{p_1^+}\right)\mathcal{J}^{\mu\nu}_{2111}(x,\tilde{x},b)\right) \\ & + \int dx [d\tilde{x}] \delta\left(x - \frac{q^+}{p_1^+}\right)\left(\delta\left(\tilde{x}_1 - \frac{q^-}{p_2^-}\right)\mathcal{J}^{\mu\nu}_{1112}(x,\tilde{x},b) + \delta\left(\tilde{x}_3 + \frac{q^-}{p_2^-}\right)\mathcal{J}^{\mu\nu}_{1121}(x,\tilde{x},b)\right) \\ & + \ldots \Bigg\},\end{aligned} \tag{4.81}$$

where

$$\begin{aligned}\mathcal{J}^{\mu\nu}_{1111}(x,\tilde{x},b) = & \frac{\gamma^\mu_{T,ij}\gamma^\nu_{T,kl}}{N_c}\Big(\mathcal{O}^{li}_{11,\bar{n}}(x,b)\overline{\mathcal{O}}^{jk}_{11,n}(\tilde{x},b) + \overline{\mathcal{O}}^{jk}_{11,\bar{n}}(x,b)\mathcal{O}^{li}_{11,n}(\tilde{x},b)\Big) \\ & + i\frac{n^\mu\gamma^\rho_{T,ij}\gamma^\nu_{T,kl} + n^\nu\gamma^\mu_{T,ij}\gamma^\rho_{T,kl}}{q^+ N_c}\Big(\partial_\rho\mathcal{O}^{li}_{11,\bar{n}}(x,b)\overline{\mathcal{O}}^{jk}_{11,n}(\tilde{x},b) + \partial_\rho\overline{\mathcal{O}}^{jk}_{11,\bar{n}}(x,b)\mathcal{O}^{li}_{11,n}(\tilde{x},b)\Big) \\ & + i\frac{\bar{n}^\mu\gamma^\rho_{T,ij}\gamma^\nu_{T,kl} + \bar{n}^\nu\gamma^\mu_{T,ij}\gamma^\rho_{T,kl}}{q^- N_c}\Big(\mathcal{O}^{li}_{11,\bar{n}}(x,b)\partial_\rho\overline{\mathcal{O}}^{jk}_{11,n}(\tilde{x},b) + \overline{\mathcal{O}}^{jk}_{11,\bar{n}}(x,b)\partial_\rho\mathcal{O}^{li}_{11,n}(\tilde{x},b)\Big),\end{aligned} \tag{4.82}$$

$$\begin{aligned}\mathcal{J}^{\mu\nu}_{1211}(x,\tilde{x},b) = & \\ & \frac{ig}{x_2}\left(\frac{\bar{n}^\nu}{q^-} - \frac{n^\nu}{q^+}\right)\frac{\gamma^\mu_{T,ij}\delta_{kl}}{N_c}\Big(\mathcal{O}^{li}_{12,\bar{n}}(x,b)\overline{\mathcal{O}}^{jk}_{11,n}(\tilde{x},b) - \overline{\mathcal{O}}^{jk}_{12,\bar{n}}(x,b)\mathcal{O}^{li}_{11,n}(\tilde{x},b)\Big),\end{aligned} \tag{4.83}$$

$$\begin{aligned}\mathcal{J}^{\mu\nu}_{2111}(x,\tilde{x},b) = & \\ & \frac{ig}{x_2}\left(\frac{\bar{n}^\mu}{q^-} - \frac{n^\mu}{q^+}\right)\frac{\delta_{ij}\gamma^\nu_{T,kl}}{N_c}\Big(\mathcal{O}^{li}_{21,\bar{n}}(x,b)\overline{\mathcal{O}}^{jk}_{11,n}(\tilde{x},b) - \overline{\mathcal{O}}^{jk}_{21,\bar{n}}(x,b)\mathcal{O}^{li}_{11,n}(\tilde{x},b)\Big),\end{aligned} \tag{4.84}$$

$$\begin{aligned}\mathcal{J}^{\mu\nu}_{1112}(x,\tilde{x},b) = & \\ & \frac{ig}{\tilde{x}_2}\left(\frac{\bar{n}^\nu}{q^-} - \frac{n^\nu}{q^+}\right)\frac{\gamma^\mu_{T,ij}\delta_{kl}}{N_c}\Big(\mathcal{O}^{li}_{11,\bar{n}}(x,b)\overline{\mathcal{O}}^{jk}_{12,n}(\tilde{x},b) - \overline{\mathcal{O}}^{jk}_{11,\bar{n}}(x,b)\mathcal{O}^{li}_{12,n}(\tilde{x},b)\Big),\end{aligned} \tag{4.85}$$

$$\mathcal{J}^{\mu\nu}_{1121}(x,\tilde{x},b) = \tag{4.86}$$

$$\frac{ig}{\tilde{x}_2}\left(\frac{\bar{n}^\mu}{q^-}-\frac{n^\mu}{q^+}\right)\frac{\delta_{ij}\gamma^\nu_{T,kl}}{N_c}\Big(\mathcal{O}^{li}_{11,\bar{n}}(x,b)\overline{\mathcal{O}}^{jk}_{21,n}(\tilde{x},b)-\overline{\mathcal{O}}^{jk}_{11,\bar{n}}(x,b)\mathcal{O}^{li}_{21,n}(\tilde{x},b)\Big).$$

In twist-(1+2) and twist-(2+1) operators, the argument is denoted as $x=(x_1,x_2,x_3)$. It is worth noting that the operators $\mathcal{J}^{\mu\nu}_{1211}$ and $\mathcal{J}^{\mu\nu}_{2111}$ correspond to $\mathcal{J}^{\mu\nu}_{1112}$ and $\mathcal{J}^{\mu\nu}_{1121}$ with the interchange of n and $\bar{n}$.

For twist-(1+2) TMD operators, the values of $x_{1,2,3}$ lack definite signs. The momentum conservation delta function determines the value (and sign) of only one of them, while the other two variables undergo integration and can assume positive or negative values.

These expressions were derived considering the insignificance of the global positioning of the currents for DY, SIDIS and SIA processes.

4.4 Soft overlap

Up to this point, our analysis has presumed complete independence between collinear and anticollinear fields. This assumption enables the imposition of individual gauge-fixing conditions and the separation of fields into distinct gauge-invariant TMD operators. However, it is crucial to acknowledge the existence of a segment within the functional integration phase space where collinear and anticollinear fields merge into a single background field. In fig. 4.1, this particular area is depicted with diagonal shading, representing the so-called soft region (or glauber region in the SCET terminology). Fields within this region (denoted by s) satisfy the following counting scheme:

$$\{\partial_+,\partial_-,\partial_T\}q_s\lesssim Q\{\lambda^2,\lambda^2,\lambda\}q_s, \tag{4.87}$$
$$\{\partial_+,\partial_-,\partial_T\}A^\mu_s\lesssim Q\{\lambda^2,\lambda^2,\lambda\}A^\mu_s. \tag{4.88}$$

The soft region is double-counted in the functional integral. It is important to emphasize that the double-counting issue within the soft region does not impact the TMD factorization process described. Rather, each TMD operator exhibits an unresolved rapidity divergence. While these rapidity divergences are anticipated to cancel between collinear and anticollinear TMD operators, they persist due to the overlapping of the soft region. Several approaches have been proposed to address this challenge, but we take the following approach:

The product structure of the functional integral allows to deal with the double-counting by dividing it with the functional integral over soft modes. The resultant factor is commonly referred to as the soft factor [94, 17] or zero-bin subtraction [7], which has already been described in chapter 2. However, there exists no universal method to determine the soft factor operators at higher powers. It is plausible that such a straightforward multiplicative structure does not hold for higher power operators.

In order to determine the soft contribution we split the soft parts of collinear and anticollinear fields

$$q_{\bar{n}}(x)\to q_{\bar{n}}(x)+q_s(x),\qquad q_n(x)\to q_n(x)+q_s(x),\qquad A^\mu_{\bar{n}}(x)\to A^\mu_{\bar{n}}(x)+A^\mu_s(x), \tag{4.89}$$

and similar for other components. Next, we isolate the soft fields into a single factor, disregarding power-suppressed contributions. For instance, in the case of the first term of

the LP effective operator in eq. 4.36

$$\begin{aligned}
&\bar{\xi}^{(-)}_{\bar{n}}\gamma^{\mu}_{T}\xi^{(-)}_{n}\bar{\xi}^{(+)}_{n}\gamma^{\nu}_{T}\xi^{(+)}_{\bar{n}} \to \\
&(\bar{\xi}^{(-)}_{\bar{n}}+q^{(-)}_{s})[y^{-}n+y_{T},Ln+y_{T}]^{(-)}_{s}\gamma^{\mu}_{T}[\bar{L}\bar{n}+y_{T},-y^{+}\bar{n}+y_{T}]^{(-)}_{s}(\xi^{(-)}_{n}+q^{(-)}_{s}) \\
&\times(\bar{\xi}^{(+)}_{n}+q^{(+)}_{s})[0,\bar{L}\bar{n}]^{(+)}_{s}\gamma^{\nu}_{T}[Ln,0]^{(+)}_{s}(\xi^{(+)}_{\bar{n}}+q^{(+)}_{s}) \\
&=\bar{\xi}^{(-)}_{\bar{n}}\gamma^{\mu}_{T}\xi^{(-)}_{n}\bar{\xi}^{(+)}_{n}\gamma^{\nu}_{T}\xi^{(+)}_{\bar{n}}\times\widetilde{\mathcal{S}}_{\rm LP}(y_{T})+\mathcal{O}(\lambda^{4}),
\end{aligned} \tag{4.90}$$

where $[a,b]_s$ is the Wilson line with the soft gluon field. The operator for the LP soft factor is

$$\widetilde{\mathcal{S}}_{\rm LP}(y_{T}) \;=\; \frac{{\rm tr_c}}{N_c}[\bar{L}\bar{n}+y_{T},y_{T}]^{(-)}[y_{T},Ln+y_{T}]^{(-)}[Ln,0]^{(+)}[0,\bar{L}\bar{n}]^{(+)}. \tag{4.91}$$

The trace is performed with respect to color indices.

The operator $\widetilde{\mathcal{S}}$ is the soft part of the LP effective operator. Therefore, the soft component corresponding to the functional integral at the LP level is determined by the vacuum matrix element of eq. 4.91, under the assumption that the hadrons do not carry soft partons.

$$\mathcal{S}_{\rm LP}(y_{T}) \;=\; \frac{{\rm tr_c}}{N_c}\sum_{X}\langle 0|[\bar{L}\bar{n}+y_{T},y_{T}][y_{T},Ln+y_{T}]|X\rangle\langle X|[Ln,0][0,\bar{L}\bar{n}]|0\rangle, \tag{4.92}$$

which is called the soft factor. This is the same soft factor obtained in chapter 2. To remove the double counting from the LP term, eq. 4.34, we divide TMD operators by the soft factor

$$\mathcal{O}^{li}_{11,\bar{n}}\overline{\mathcal{O}}^{jk}_{11,n}\to\frac{\mathcal{O}^{li}_{11,\bar{n}}\overline{\mathcal{O}}^{jk}_{11,n}}{\mathcal{S}_{\rm LP}(y_{T})}. \tag{4.93}$$

It is important to note that the issue of overlapping modes does not affect TMD factorization. Therefore, the substitution in eq. 4.93 remains valid to all orders in perturbation theory.

A similar analysis can be done for operators contributing to $\mathcal{J}^{\mu\nu}_{\rm NLP}$. We encounter two main scenarios: operators featuring derivatives (the first and second lines in eq. 4.47), and operators with an additional field A^{μ}_{T} (other lines in eq. 4.47). In both cases, we find that the contribution from the soft overlap equals the LP soft factor given in eq. 4.92, as the presence of a derivative of a soft Wilson line or an additional factor A^{μ}_{s} inevitably elevates the power counting. Consequently, the subtraction of the soft region for NLP operators follows the same format as for LP operators, as shown in eq. 4.93. Namely,

$$\partial_{\rho}\mathcal{O}^{li}_{11,\bar{n}}\overline{\mathcal{O}}^{jk}_{11,n}\to\frac{\partial_{\rho}\mathcal{O}^{li}_{11,\bar{n}}\overline{\mathcal{O}}^{jk}_{11,n}}{\mathcal{S}_{\rm LP}(y_{T})},\qquad \mathcal{O}^{li}_{12,\bar{n}}\overline{\mathcal{O}}^{jk}_{11,n}\to\frac{\mathcal{O}^{li}_{11,\bar{n}}\overline{\mathcal{O}}^{jk}_{12,n}}{\mathcal{S}_{\rm LP}(y_{T})}, \tag{4.94}$$

and similarly for other terms of effective operator eq. 4.47. The LP soft factor is independent of $y^{\pm}$ and thus does modify convolutions in $\mathcal{J}^{\mu\nu}_{\rm eff}$ at NLP.

The equivalence of soft factors between LP and NLP operators yields the following implications:

- LP and NLP operators should exhibit identical rapidity divergence, consequently yielding the same rapidity anomalous dimension.
- LP and NLP operators must share the collinear divergent part of UV renormalization.

Indeed, these divergences arise in the interaction of soft modes, and they are canceled by the soft factor. This can be seen in detail in ref. [103]. δ-regularization is used to regularize rapidity divergencies appearing in the soft factor in the same way already described in chapter 2.

As stated at the beginning of this section, this approach does not hold in principle when going to higher powers and a more systematic procedure should be developed.

Chapter 5

Dijet production in SIA at NLP

In this chapter, we build upon the background field method introduced in chapter 4. In particular, we use to describe in detail the NLP in a semi-inclusive annihilation process. We focus on TMDs in the final state and work with jets rather than hadrons because they can be described in perturbation theory. The results presented in this chapter constitute one of the main results of this thesis along with the results presented in Chapter 3.

It is advantageous to explore cross-sections with minimal non-perturbative QCD effects to facilitate direct tests of NLP operators and gain insights into the formalism. In pursuit of this goal, we investigate NLP effects using jets as the final states of hadronic interactions. Jets are particularly suitable for this purpose as they are infrared-safe quantities, and their properties can be predominantly determined perturbatively[1]. This is in contrast to T-odd jets in references [129, 130], which necessitate a nonperturbative hypothesis.

Specifically, our focus lies in examining the impact of NLP corrections on dijet production in e^+e^- collisions. This approach presents an opportunity to scrutinize NLP factorization at e^+e^- colliders like LEP and Belle. Furthermore, its extension to SIDIS will be particularly valuable at facilities such as the EIC [131].

The utilization of jets within TMD factorization has been explored in various studies, as evidenced by works such as [132, 133, 134, 78, 79, 135, 91, 136, 137, 138, 139, 140]. Notably, references [78, 79] have primarily focused on verifying the consistency of TMD factorization theorems with jet definitions and algorithms. These studies emphasize the critical role played by the definition of the jet axis and radius in establishing factorization.

The conventional jet definition faces challenges related to non-global logarithms, arising from its sensitivity to whether soft radiation becomes clustered into the jet or not, thereby limiting overall accuracy. In contrast, recoil-insensitive schemes, such as the Winner-Takes-All (WTA) jet axis [141], mitigate this issue by being insensitive to such effects, enabling high-precision calculations.

In this study, we address two key inquiries. Firstly, we aim to identify the novel jet functions arising from additional operators at NLP. Secondly, our objective is to derive the factorized expression for the cross-section in terms of jet functions and hard-matching coefficients. The insights gained from these answers enable us to investigate the impact of NLP corrections on transverse-momentum-dependent measurements, including angular

[1] Our jet functions may receive nonperturbative corrections suppressed by $\Lambda^2_{\rm QCD}/q_T^2$, which should not be confused with the q_T/Q power corrections we consider here.

asymmetries. In particular, we observe that to elicit a non-vanishing contribution from NLP operators, there must be a breaking of symmetry between the energetic radiation directed into two distinct directions. In the context of dijet production, achieving this asymmetry can be facilitated, for instance, by employing two different (recoil-free) recombination schemes.

Despite the intricacy of the subject matter, we endeavor to present the material in a didactic manner. The process selection and the chosen jet definitions serve to significantly reduce the number of independent distributions and simplify the evolution compared to the original papers [142, 103, 143, 121], as illustrated in eq. 5.72. In this regard, this work can also be regarded as an introductory overview of the exploration of next-to-leading power effects in transverse momentum dependent factorization.

5.1 Kinematics

The process that we consider in this paper is the annihilation of an electron and positron, with momenta ℓ and ℓ', into two jets with momenta P_1 and P_2,

$$e^-(\ell)\, e^+(\ell') \to j_1(P_1)\, j_2(P_2)\, X\,. \tag{5.1}$$

We assume a large jet radius, such that all collinear final-state particles are clustered in one of the two jets, and any radiation outside the jets X is soft[2]. At lowest order in the electromagnetic coupling, this process proceeds by the electron and positron annihilating into an intermediate photon with momentum $q = \ell + \ell'$, which subsequently creates a quark-antiquark pair that produces two jets. In the following, we assume that the jet algorithm yields massless jet momenta, $P_1^2 = P_2^2 = 0$ (as in the WTA recombination scheme), and we introduce light-like vectors n and $\bar{n}$ such that

$$P_1^\mu = P_1^- n^\mu, \quad P_2^\mu = P_2^+ \bar{n}^\mu, \quad \text{and} \quad n\cdot\bar{n} = 1. \tag{5.2}$$

In order to introduce our observables, we define two planes, which we will refer to as the transverse and perpendicular planes. The transverse plane is orthogonal to the two outgoing jets and the perpendicular plane is orthogonal to the intermediate photon momentum q and one of the outgoing jets. These planes can be described in terms of the metric tensors that project onto the corresponding sub-spaces,

$$g_T^{\mu\nu} = g^{\mu\nu} - \frac{1}{P_1\cdot P_2}\big(P_1^\mu P_2^\nu + P_2^\mu P_1^\nu\big), \tag{5.3}$$

$$g_\perp^{\mu\nu} = g^{\mu\nu} + \frac{Q^2}{(P_2\cdot q)^2} P_2^\mu P_2^\nu - \frac{1}{P_2\cdot q}\big(q^\mu P_2^\nu + P_2^\mu q^\nu\big), \tag{5.4}$$

and we define the transverse and perpendicular components of a vector v as

$$v_T^\mu = g_T^{\mu\nu} v_\nu\,, \qquad v_\perp^\mu = g_\perp^{\mu\nu} v_\nu\,. \tag{5.5}$$

[2]To be precise, we assume $QR \gg q_T$, such that the transverse momentum measurement restricts the collinear radiation to be inside the jets.

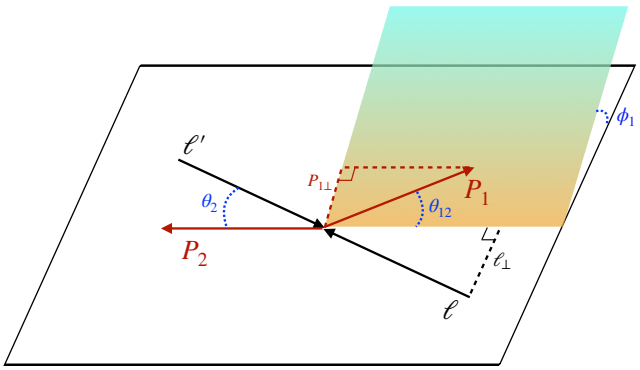

Figure 5.1: Kinematics of the dijet production in e^+e^-.

Note that, by construction,

$$P^\mu_{1,T} = P^\mu_{2,T} = 0\,, \qquad q^\mu_\perp = P^\mu_{2,\perp} = 0\,. \tag{5.6}$$

We sometimes write two-dimensional vectors in boldface notation, where it is implied that the two-dimensional metric has positive signature. As we mostly encounter transverse vectors, we suppress the subscript T, e.g. $\mathbf{b} = \mathbf{b}_T$.

We now list the variables that we use to describe the cross-section, which is the same as in ref. [144] for the massless case:

$$z_i = \frac{P_i \cdot q}{\ell \cdot q}\,, \qquad y = \frac{P_2 \cdot \ell}{P_2 \cdot q}\,, \qquad Q_T^2 = -q_T^2 = -g_T^{\mu\nu} q_\mu q_\nu\,, \qquad Q^2 = q^2\,, \tag{5.7}$$

as well as an azimuthal angle

$$\cos\phi_1 = \frac{\boldsymbol{\ell}_\perp \cdot \mathbf{P}_{1\perp}}{|\boldsymbol{\ell}_\perp||\mathbf{P}_{1\perp}|} \qquad \text{or} \qquad \cos\alpha = \frac{\boldsymbol{\ell}\cdot\mathbf{q}}{|\boldsymbol{\ell}||\mathbf{q}|}\,. \tag{5.8}$$

The angles ϕ_1 and α are not independent. It is natural to use the former in the center-of-mass frame and as depicted in fig. 5.1, while it is convenient to use the latter in the frame where the jets are exactly back-to-back. They are related by

$$\cos\phi_1 = \pm\cos\alpha\sqrt{1 - \frac{Q_T^2}{Q^2}\frac{y}{1-y}\sin^2\alpha} + \frac{Q_T}{Q}\sqrt{\frac{y}{1-y}}\sin^2\alpha = \cos\alpha + \mathcal{O}\Big(\frac{Q_T}{Q}\Big)\,. \tag{5.9}$$

All dot products of four-vectors can be expressed in terms of the observables listed above.

While the above expressions are Lorentz invariant, the interpretation we now give is valid for the (di-lepton) center-of-mass frame: First of all, the z_i ($i = 1,\ 2$) are the energy fractions of the two jets. The variable y corresponds to the angle θ_2 between the momentum of the jet and the lepton, $y = (1 - \cos\theta_2)/2$. Next, ϕ_1 is the azimuthal angle between the perpendicular component of jet 1 and the electron momentum ℓ. Finally,

$$Q_T^2 = -Q^2 + \frac{z_1 z_2 Q^4}{2P_1\cdot P_2} \approx \tfrac{1}{4}\theta_{12}^2 Q^2\,, \tag{5.10}$$

where θ_{12} is the angular decorrelation of the two jets. These angles are shown in fig. 5.1. Note that the invariant mass Q of the collision is not an observable, but it is determined by the initial state of the experiment.

In this chapter, we consider the large jet radius limit, where $z_1 = z_2 = 1$ up to power corrections, so we will not be differential in them. This leads us to consider the following cross-section

$$\frac{\mathrm{d}\sigma}{\mathrm{d}y\,\mathrm{d}^2\mathbf{q}} = \frac{\pi\alpha_{\mathrm{em}}^2 Q_q^2}{Q^4} L_{\mu\nu} W^{\mu\nu}\,, \tag{5.11}$$

where $L_{\mu\nu}$ and $W^{\mu\nu}$ are respectively the leptonic and hadronic tensor. The leptonic tensor reads

$$L_{\mu\nu} = 2\big(\ell_\mu \ell'_\nu + \ell'_\mu \ell_\nu\big) - Q^2 g_{\mu\nu} + 2\mathrm{i}\,\lambda_e\,\epsilon_{\mu\nu\rho\sigma}\ell^\rho \ell'^\sigma\,, \quad \epsilon_{0123} = 1, \tag{5.12}$$

and in this chapter, we neglect the lepton helicity contribution proportional to λ_e. Our main focus is thus on the hadronic tensor, which contains all QCD effects. For this, the recent work of ref. [103] opens the door to a more systematic study of the hadronic tensor up to NLP, and this is the subject of the next section.

The case of two hadrons (instead of jets) has been studied before, especially in relation to Belle experiment, see the reviews in refs. [124, 145, 146, 147]. The distributions in this case were classified in ref. [144], and mass corrections to kinematics have been included in ref. [148].

5.2 Factorization at NLP

The goal of this section is to obtain a factorized expression for the cross-section in terms of a set of jet functions and hard functions. The expression we obtain holds at the bare and unsubtracted level, and we postpone the discussion of renormalization and overlap subtraction for the next section.

To obtain a factorized expression for the cross section we first expand the hadronic tensor up to next-to-leading power using the TMD operator product expansion method. The complete and un-expanded hadronic tensor for the process under consideration is given by,

$$W^{\mu\nu}(q) = \int \frac{\mathrm{d}^4 y}{(2\pi)^4}\, e^{\mathrm{i}q\cdot y} \sum_X \langle 0|\, J^{\mu\,\dagger}(y)\,|J^n_{\mathrm{alg}} J^{\bar{n}}_{\mathrm{alg}} X\rangle\,\langle J^n_{\mathrm{alg}} J^{\bar{n}}_{\mathrm{alg}} X|\, J^\nu(0)\,|0\rangle\,, \tag{5.13}$$

where $J^\mu(y)$ is the electromagnetic current

$$J^\mu(y) = \bar{\psi}(y)\gamma^\mu\psi(y)\,. \tag{5.14}$$

Since we assume a large jet radius, all energetic final-state particles are clustered into one of the two jets and X only contains soft radiation. The explicit notation that we use for the power expansion of the hadronic tensor is

$$W^{\mu\nu}(q) = W^{\mu\nu}_{\mathrm{LP}}(q) + W^{\mu\nu}_{\mathrm{NLP}}(q) + \mathcal{O}\Big(\frac{1}{Q^2}\Big)\,. \tag{5.15}$$

In order to arrive at our final expressions for $W_{\text{LP,NLP}}$, we proceed in several steps, starting from the TMD operator expansion method and the basis of operators in sec. 5.2.1. In particular, we list a set of operator building blocks that have definite twist, which allow for a clean separation in terms of power counting. We use these definitions in sec. 5.2.2, to obtain the power expansion of the product of currents in eq. 5.13 in position space (indicated by the tilde)

$$\tilde{\mathcal{W}}^{\mu\nu}(y) = J^{\mu\dagger}(y)\, J^{\nu}(0) = \tilde{\mathcal{W}}^{\mu\nu}_{\text{LP}}(y) + \tilde{\mathcal{W}}^{\mu\nu}_{\text{NLP}}(y)\,. \tag{5.16}$$

Next, we include the external jet states and Fourier transform back to momentum space, to obtain an expression for the hadronic tensor in terms of a set of jet functions with open spinor indices. In sec. 5.2.3, we apply Fierz relations to obtain a set of jet functions with closed spinor indices, and use discrete symmetries and Lorentz decomposition to simplify and reduce the basis of jet functions, resulting in just one new jet function at NLP. Sec. 5.2.4 contains the final expression for the hadronic tensor in terms of jet functions, as well as its contraction with the leptonic tensor.

5.2.1 Operator basis

In this section, we include the necessary operators for our derivation. Most operators have already been included in the previous chapter, but we include them here for completitude. We make use of the TMD operator product expansion [103]. In this method, background fields are introduced for the two collinear directions

$$\psi(x) = \chi(x) + q_n(x) + q_{\bar{n}}(x)\,, \qquad A^{\mu}(x) = B^{\mu}(x) + A^{\mu}_n(x) + A^{\mu}_{\bar{n}}(x)\,. \tag{5.17}$$

The background fields $q_n, q_{\bar{n}}, A^{\mu}_n, A^{\mu}_{\bar{n}}$ are used to construct our operators, while the fields χ, B^{μ} are purely dynamical. As usual, we decompose the quark background fields into "good" and "bad" components,

$$q_{\bar{n}}(x) = \xi_{\bar{n}}(x) + \eta_{\bar{n}}(x)\,, \qquad q_n(x) = \xi_n(x) + \eta_n(x)\,, \tag{5.18}$$

where

$$\begin{aligned} \xi_{\bar{n}}(x) &= \frac{\bar{\not{n}}\not{n}}{2} q_{\bar{n}}(x), & \eta_{\bar{n}}(x) &= \frac{\not{n}\bar{\not{n}}}{2} q_{\bar{n}}(x), \\ \xi_n(x) &= \frac{\not{n}\bar{\not{n}}}{2} q_n(x), & \eta_n(x) &= \frac{\bar{\not{n}}\not{n}}{2} q_n(x)\,, \end{aligned} \tag{5.19}$$

such that each field has a definite power counting ($\xi \sim \lambda$, $\eta \sim \lambda^2$). The collinear and anti-collinear regions overlap in the soft region. To avoid the double counting of this region its contribution must be carefully subtracted. We discuss the subtraction of the overlap region in sec. 5.3.1.

Using the background fields one can construct a set of building-block operators of definite twist (dimension minus spin),

$$\begin{aligned} U_{1,\bar{n}}(y^-, b) &= [Ln + b, y^- n + b]\, \xi_{\bar{n}}(y^- n + b)\,, \\ U_{1,n}(y^+, b) &= [\bar{L}\bar{n} + b, y^+ \bar{n} + b]\, \xi_n(y^+ \bar{n} + b)\,, \end{aligned} \tag{5.20}$$

$$U_{2,\bar{n}}(\{y_1^-, y_2^-\}, b) = g\,[Ln + b, y_2^- n + b]\,\gamma_{T,\rho} F_{\bar{n}}^{\rho+}(y_2^- n + b)[y_2^- n + b, y_1^- n + b]\,\xi_{\bar{n}}(y_1^- n + b)\,,$$
$$U_{2,n}(\{y_1^+, y_2^+\}, b) = g\,[\bar{L}\bar{n} + b, y_2^+ \bar{n} + b]\,\gamma_{T,\rho} F_{n}^{\rho-}(y_2^+ \bar{n} + b)[y_2^+ \bar{n} + b, y_1^+ \bar{n} + b]\,\xi_{n}(y_1^+ \bar{n} + b)\,. \tag{5.21}$$

Here, the first subscript on the operator denotes the twist of the operator and the second subscript denotes the collinear sector to which the operator belongs. These operators contain Wilson lines, which we denote by

$$[a, b] = P \exp\left[-ig \int_a^b \mathrm{d}z_\mu\, A^\mu(z)\right]. \tag{5.22}$$

The gauge field appearing in the Wilson line matches the collinear direction under consideration, e.g. A_n ($A_{\bar{n}}$) for the Wilson line in $U_{2,n}$ ($U_{2,\bar{n}}$). The operators in eqs. 5.20 and 5.21 will enter the matrix-element definition of the jet functions. Note that these operators are process-dependent via their dependence on L and $\bar{L}$, with $L = -\infty$ for incoming partons and $L = +\infty$ for outgoing partons. Since we consider jet production, we set $L = \bar{L} = +\infty$ from now on. In the Wilson lines, we introduce the δ-regulator whenever necessary (see refs. [103, 30] for more details).

Operator basis at LP

At the lowest order in the power expansion of the product of currents in eq. 5.16, for which the result is shown in sec. 5.2.2, the following combinations of operators appear

$$\mathcal{O}_{11,\bar{n}}^{ij}(\{y^-, 0\}, y_T) = \bar{\xi}_{\bar{n},j}^{(-)}(y^- n + y_T)\,\xi_{\bar{n},i}^{(+)}(0)\,,$$
$$\mathcal{O}_{11,n}^{ij}(\{y^+, 0\}, y_T) = \bar{\xi}_{n,j}^{(-)}(y^+ \bar{n} + y_T)\,\xi_{n,i}^{(+)}(0)\,,$$

$$\overline{\mathcal{O}}_{11,\bar{n}}^{ij}(\{y^-, 0\}, y_T) = \mathrm{tr}_c\big[\xi_{\bar{n},i}^{(-)}(y^- n + y_T)\,\bar{\xi}_{\bar{n},j}^{(+)}(0)\big]\,,$$
$$\overline{\mathcal{O}}_{11,n}^{ij}(\{y^+, 0\}, y_T) = \mathrm{tr}_c\big[\xi_{n,i}^{(-)}(y^+ \bar{n} + y_T)\,\bar{\xi}_{n,j}^{(+)}(0)\big]\,. \tag{5.23}$$

The $(\pm)$ superscript denote causal and anti-causal fields from the Keldysh formalism [125]. The color indices of the fields are contracted, which is made explicit for $\overline{\mathcal{O}}_{11}$ by the color trace tr_c, and i, j are spin indices. The gauge invariance in the expressions above is restored using the building-block operators in eqs. 5.20 and 5.21, by

$$\mathcal{O}_{11,\bar{n}}^{ij} = \big[\overline{U}_{1,\bar{n}}(y^-, y_T)\big]_j^{(-)}\big[U_{1,\bar{n}}(0,0)\big]_i^{(+)}\,,$$
$$\mathcal{O}_{11,n}^{ij} = \big[\overline{U}_{1,n}(y^+, y_T)\big]_j^{(-)}\big[U_{1,n}(0,0)\big]_i^{(+)}\,,$$

$$\overline{\mathcal{O}}_{11,\bar{n}}^{ij} = \mathrm{tr}_c\big\{\big[U_{1,\bar{n}}(y^-, y_T)\big]_i^{(-)}\big[\overline{U}_{1,\bar{n}}(0,0)\big]_j^{(+)}\big\}\,,$$
$$\overline{\mathcal{O}}_{11,n}^{ij} = \mathrm{tr}_c\big\{\big[U_{1,n}(y^+, y_T)\big]_i^{(-)}\big[\overline{U}_{1,n}(0,0)\big]_j^{(+)}\big\}\,. \tag{5.24}$$

Operator basis at NLP

At next-to-leading power in the expansion of eq. 5.16, one finds contributions from the following operators

$$\mathbb{O}_{21,\bar{n}}^{ij}(\{y^-, y^-, 0\}, y_T) = \big[\bar{\xi}_{\bar{n}}^{(-)} \not{A}_{\bar{n},T}^{(-)}(y^- n + y_T)\big]_j \xi_{\bar{n},i}^{(+)}(0)\,,$$

$$\mathbb{O}^{ij}_{21,n}(\{y^+,y^+,0\},y_T) = \big[\bar\xi^{(-)}_n \not{A}^{(-)}_{n,T}(y^+\bar n + y_T)\big]_j\, \xi^{(+)}_{n,i}(0)\,,$$

$$\overline{\mathbb{O}}^{ij}_{21,\bar n}(\{y^-,y^-,0\},y_T) = \mathrm{tr}_c\big\{\big[\not{A}^{(-)}_{\bar n,T}\xi^{(-)}_{\bar n}(y^- n + y_T)\big]_i\, \bar\xi^{(+)}_{\bar n,j}(0)\big\}\,,$$
$$\overline{\mathbb{O}}^{ij}_{21,n}(\{y^+,y^+,0\},y_T) = \mathrm{tr}_c\big\{\big[\not{A}^{(-)}_{n,T}\xi^{(-)}_{n}(y^+\bar n + y_T)\big]_i\, \bar\xi^{(+)}_{n,j}(0)\big\}\,,$$

$$\mathbb{O}^{ij}_{12,\bar n}(\{y^-,0,0\},y_T) = \bar\xi^{(-)}_{\bar n,j}(y^- n + y_T)\,\big[\not{A}^{(+)}_{\bar n,T}\xi^{(+)}_{\bar n}(0)\big]_i\,,$$
$$\mathbb{O}^{ij}_{12,n}(\{y^+,0,0\},y_T) = \bar\xi^{(-)}_{n,j}(y^+\bar n + y_T)\,\big[\not{A}^{(+)}_{n,T}\xi^{(+)}_{n}(0)\big]_i\,,$$

$$\overline{\mathbb{O}}^{ij}_{12,\bar n}(\{y^-,0,0\},y_T) = \mathrm{tr}_c\big\{\xi^{(-)}_{\bar n,i}(y^- n + y_T)\,\big[\bar\xi^{(+)}_{\bar n}\not{A}^{(+)}_{\bar n,T}(0)\big]_j\big\}\,,$$
$$\overline{\mathbb{O}}^{ij}_{12,n}(\{y^+,0,0\},y_T) = \mathrm{tr}_c\big\{\xi^{(-)}_{n,i}(y^+\bar n + y_T)\big[\bar\xi^{(+)}_{n}\not{A}^{(+)}_{n,T}(0)\big]_j\big\}\,. \tag{5.25}$$

To write these in terms of the building-block operators we need to do a few manipulations. First we replace the transverse gauge fields that appear here by a field strength via the following relations,

$$A^\mu_{\bar n}(y) = g\int_0^\infty \mathrm{d}z^-\, e^{-z^-\delta^+}\, F^{\mu+}_{\bar n}(y+z^- n)\,, \qquad A^\mu_n(y) = g\int_0^\infty \mathrm{d}z^+\, e^{-z^+\delta^-}\, F^{\mu-}_{n}(y+z^+ \bar n)\,, \tag{5.26}$$

which introduces a δ-regulator for rapidity divergences. Subsequently, we apply the following identity

$$\int_0^\infty \mathrm{d}z\, e^{-z\delta}\, f(z) = -i\int_{-\infty}^\infty \mathrm{d}\xi\, \frac{1}{\pm\xi - i\delta^\pm_E}\int\frac{\mathrm{d}z}{2\pi}\, e^{\pm i\xi q^\pm z}\, f(z)\,,$$

where a positive $\delta^\pm_E = \delta^\pm/q^\pm$ ensures that the integral is well defined and shows how δ regulates rapidity divergences. Note that in this identity the sign of ξ may be chosen freely as it is integrated over all values. It turns out that it is convenient to choose $+\xi$ for the $\mathbb{O}_{21}$ operators and $-\xi$ for the $\mathbb{O}_{12}$ operators, as the jet functions that will be built from these operators then have support for $\xi\in[0,1]$. This convention differs from earlier work, and allows for several simplifications in our case.

The above manipulations allow us to express the operators in eq. 5.25 in the NLP hadronic tensor in terms of the building-block operators in eqs. 5.20 and 5.21 as follows,

$$\mathbb{O}^{ij}_{21,\bar n} = -i\int\mathrm{d}\xi\,\frac{1}{\xi - i\delta^+_E}\int\frac{\mathrm{d}z^-}{2\pi}\, e^{i\xi(z^- - y^-)q^+}\,\big[\overline{U}_{2,\bar n}(\{y^-,z^-\},y_T)\big]^{(-)}_j\big[U_{1,\bar n}(0,0)\big]^{(+)}_i\,,$$
$$\mathbb{O}^{ij}_{21,n} = -i\int\mathrm{d}\xi\,\frac{1}{\xi - i\delta^-_E}\int\frac{\mathrm{d}z^+}{2\pi}\, e^{i\xi(z^+ - y^+)q^-}\,\big[\overline{U}_{2,n}(\{y^+,z^+\},y_T)\big]^{(-)}_j\big[U_{1,n}(0,0)\big]^{(+)}_i\,,$$

$$\overline{\mathbb{O}}^{ij}_{21,\bar n} = -i\int\mathrm{d}\xi\,\frac{1}{\xi - i\delta^+_E}\int\frac{\mathrm{d}z^-}{2\pi}\, e^{i\xi(z^- - y^-)q^+}\,\mathrm{tr}_c\big\{\big[U_{2,\bar n}(\{y^-,z^-\},y_T)\big]^{(-)}_i\big[\overline{U}_{1,\bar n}(0,0)\big]^{(+)}_j\big\}\,,$$
$$\overline{\mathbb{O}}^{ij}_{21,n} = -i\int\mathrm{d}\xi\,\frac{1}{\xi - i\delta^-_E}\int\frac{\mathrm{d}z^+}{2\pi}\, e^{i\xi(z^+ - y^+)q^-}\,\mathrm{tr}_c\big\{\big[U_{2,n}(\{y^+,z^+\},y_T)\big]^{(-)}_i\big[\overline{U}_{1,n}(0,0)\big]^{(+)}_j\big\}\,,$$

$$
\begin{aligned}
\mathbb{O}^{ij}_{12,\bar n} &= i\int \mathrm{d}\xi\,\frac{1}{\xi+i\delta_E^+}\int\frac{\mathrm{d}z^-}{2\pi}\,e^{-i\xi z^- q^+}\,\big[\overline{U}_{1,\bar n}(y^-,y_T)\big]^{(-)}_j\big[U_{2,\bar n}(\{0,z^-\},0)\big]^{(+)}_i\,,\\
\mathbb{O}^{ij}_{12,n} &= i\int \mathrm{d}\xi\,\frac{1}{\xi+i\delta_E^-}\int\frac{\mathrm{d}z^+}{2\pi}\,e^{-i\xi z^+ q^-}\,\big[\overline{U}_{1,n}(y^+,y_T)\big]^{(-)}_j\big[U_{2,n}(\{0,z^+\},0)\big]^{(+)}_i\,,\\
\overline{\mathbb{O}}^{ij}_{12,\bar n} &= i\int \mathrm{d}\xi\,\frac{1}{\xi+i\delta_E^+}\int\frac{\mathrm{d}z^-}{2\pi}\,e^{-i\xi z^- q^+}\,\mathrm{tr}_c\big\{\big[U_{1,\bar n}(y^-,y_T)\big]^{(+)}_i\big[\overline{U}_{2,\bar n}(\{0,z^-\},0)\big]^{(+)}_j\big\}\,,\\
\overline{\mathbb{O}}^{ij}_{12,n} &= i\int \mathrm{d}\xi\,\frac{1}{\xi+i\delta_E^-}\int\frac{\mathrm{d}z^+}{2\pi}\,e^{-i\xi z^+ q^-}\,\mathrm{tr}_c\big\{\big[U_{1,n}(y^+,y_T)\big]^{(+)}_i\big[\overline{U}_{2,n}(\{0,z^+\},0)\big]^{(+)}_j\big\}\,.
\end{aligned}
\tag{5.27}
$$

We have omitted the space-time arguments on the operators on the left-hand side as they are the same as in eq. 5.25. The sign in front of $i\delta$ differs between $\mathbb{O}_{12}$ and $\mathbb{O}_{21}$. As we will see, their matrix elements are related by complex conjugation.

5.2.2 Expansion of the hadronic tensor

The aim of this section is to write the hadronic tensor in terms of matrix elements of the building-block operators in sec. 5.2.1. For this, we first consider the power expansion of the product of currents in eq. 5.16 in position space. Following [103], the leading power contribution can be written at leading perturbative order as

$$
\tilde{\mathcal{W}}^{\mu\nu}_{\mathrm{LP}}(y) = \frac{1}{N_c}(\gamma_T^\mu)_{ij}(\gamma_T^\nu)_{kl}\Big(\mathcal{O}^{li}_{11,\bar n}\,\overline{\mathcal{O}}^{jk}_{11,n}+\overline{\mathcal{O}}^{jk}_{11,\bar n}\,\mathcal{O}^{li}_{11,n}\Big)\,. \tag{5.28}
$$

For brevity we suppressed the space-time arguments of the operators, but they are the same as in eq. 5.24. At next-to-leading power more operators appear and the expression for the hadronic tensor is a bit more involved,

$$
\begin{aligned}
\tilde{\mathcal{W}}^{\mu\nu}_{\mathrm{NLP}}(y) = &-\frac{1}{N_c}\big[n^\mu(\gamma_T^\rho)_{ij}(\gamma_T^\nu)_{kl}+n^\nu(\gamma_T^\mu)_{ij}(\gamma_T^\rho)_{kl}\big]\left[\left(\frac{\partial_\rho}{\partial_+}\mathcal{O}^{li}_{11,\bar n}\right)\overline{\mathcal{O}}^{jk}_{11,n}+\left(\frac{\partial_\rho}{\partial_+}\overline{\mathcal{O}}^{jk}_{11,\bar n}\right)\mathcal{O}^{li}_{11,n}\right]\\
&-\frac{1}{N_c}\big[\bar n^\mu(\gamma_T^\rho)_{ij}(\gamma_T^\nu)_{kl}+\bar n^\nu(\gamma_T^\mu)_{ij}(\gamma_T^\rho)_{kl}\big]\left[\mathcal{O}^{li}_{11,\bar n}\left(\frac{\partial_\rho}{\partial_-}\overline{\mathcal{O}}^{jk}_{11,n}\right)+\overline{\mathcal{O}}^{jk}_{11,\bar n}\left(\frac{\partial_\rho}{\partial_-}\mathcal{O}^{li}_{11,n}\right)\right]\\
&+\frac{ig}{N_c}\,\delta_{ij}(\gamma_T^\nu)_{kl}\left[\mathbb{O}^{li}_{21,\bar n}\left(\frac{\bar n^\mu}{\overrightarrow{\partial}_-}-\frac{n^\mu}{\overleftarrow{\partial}_+}\right)\overline{\mathcal{O}}^{jk}_{11,n}-\overline{\mathbb{O}}^{jk}_{21,\bar n}\left(\frac{\bar n^\mu}{\overrightarrow{\partial}_-}-\frac{n^\mu}{\overleftarrow{\partial}_+}\right)\mathcal{O}^{li}_{11,n}\right.\\
&\qquad\left.+\mathcal{O}^{li}_{11,\bar n}\left(\frac{\bar n^\mu}{\overrightarrow{\partial}_-}-\frac{n^\mu}{\overleftarrow{\partial}_+}\right)\overline{\mathbb{O}}^{jk}_{21,n}-\overline{\mathcal{O}}^{jk}_{11,\bar n}\left(\frac{\bar n^\mu}{\overrightarrow{\partial}_-}-\frac{n^\mu}{\overleftarrow{\partial}_+}\right)\mathbb{O}^{li}_{21,n}\right]\\
&+\frac{ig}{N_c}\,(\gamma_T^\mu)_{ij}\delta_{kl}\left[\mathbb{O}^{li}_{12,\bar n}\left(\frac{\bar n^\nu}{\overrightarrow{\partial}_-}-\frac{n^\nu}{\overleftarrow{\partial}_+}\right)\overline{\mathcal{O}}^{jk}_{11,n}-\overline{\mathbb{O}}^{jk}_{12,\bar n}\left(\frac{\bar n^\nu}{\overrightarrow{\partial}_-}-\frac{n^\nu}{\overleftarrow{\partial}_+}\right)\mathcal{O}^{li}_{11,n}\right.\\
&\qquad\left.+\mathcal{O}^{li}_{11,\bar n}\left(\frac{\bar n^\nu}{\overrightarrow{\partial}_-}-\frac{n^\nu}{\overleftarrow{\partial}_+}\right)\overline{\mathbb{O}}^{jk}_{12,n}-\overline{\mathcal{O}}^{jk}_{11,\bar n}\left(\frac{\bar n^\nu}{\overrightarrow{\partial}_-}-\frac{n^\nu}{\overleftarrow{\partial}_+}\right)\mathbb{O}^{li}_{12,n}\right],
\end{aligned}
\tag{5.29}
$$

where again we have considered the leading perturbative order and have suppressed the space-time arguments of the operators for brevity. The non-trivial Wilson coefficients

that enter beyond leading order in perturbation theory involve a convolution in the light-cone positions, so we prefer to include them only when switching to momentum space in eq. 5.31. As explained in more detail in ref. [103], two different types of power corrections can be distinguished in eq. 5.29, those involving derivatives of twist-2 operators (kinematic power corrections) and genuine twist-3 contributions.

At this point we are ready to write the hadronic tensor in momentum space, including the Wilson coefficients and external states, allowing us to pass from operators to jet functions. To switch to momentum-space, we note that the inverse derivatives that appear in eq. 5.29 can be treated using the following identity,

$$\int \frac{\mathrm{d}y^\pm}{2\pi}\, e^{iy^\pm q^\mp}\, \frac{1}{\partial_\mp} f(y^\pm) = \frac{i}{q^\mp} \int \frac{\mathrm{d}y^\pm}{2\pi}\, e^{iy^\pm q^\mp}\, f(y^\pm)\,. \tag{5.30}$$

Since the background fields of the different collinear sectors are not coupled at this order in the power counting, the matrix elements factorize and the result for the hadronic tensor can be written in terms of products of jet functions,

$$\begin{aligned}
W^{\mu\nu}_{\mathrm{LP}}(q) &= \frac{1}{N_c}(\gamma_T^\mu)_{ij}(\gamma_T^\nu)_{kl}\left|C_1(2q^+q^-)\right|^2 \\
&\quad\times \int \frac{\mathrm{d}^2b}{(2\pi)^2}\, e^{ib\cdot q}\Big\{\big[J^{\bar q}_{11,\bar n}(b)\big]^{li}\big[J^{q}_{11,n}(b)\big]^{jk} + \big[J^{q}_{11,\bar n}(b)\big]^{jk}\big[J^{\bar q}_{11,n}(b)\big]^{li}\Big\}\,. \qquad (5.31)\\
W^{\mu\nu}_{\mathrm{NLP}}(q) &= -\frac{i}{N_c}\frac{1}{q^+}\big[n^\mu(\gamma_T^\rho)_{ij}(\gamma_T^\nu)_{kl} + n^\nu(\gamma_T^\mu)_{ij}(\gamma_T^\rho)_{kl}\big]\left|C_1(2q^+q^-)\right|^2 \\
&\quad\times \int \frac{\mathrm{d}^2b}{(2\pi)^2}\, e^{ib\cdot q}\Big\{\partial_\rho\big[J^{\bar q}_{11,\bar n}(b)\big]^{li}\big[J^{q}_{11,n}(b)\big]^{jk} + \partial_\rho\big[J^{q}_{11,\bar n}(b)\big]^{jk}\big[J^{\bar q}_{11,n}(b)\big]^{li}\Big\} \\
&\quad - \frac{i}{N_c}\frac{1}{q^-}\big[\bar n^\mu(\gamma_T^\rho)_{ij}(\gamma_T^\nu)_{kl} + \bar n^\nu(\gamma_T^\mu)_{ij}(\gamma_T^\rho)_{kl}\big]\left|C_1(2q^+q^-)\right|^2 \\
&\quad\times \int \frac{\mathrm{d}^2b}{(2\pi)^2}\, e^{ib\cdot q}\Big\{\big[J^{\bar q}_{11,\bar n}(b)\big]^{li}\partial_\rho\big[J^{q}_{11,n}(b)\big]^{jk} + \big[J^{q}_{11,\bar n}(b)\big]^{jk}\partial_\rho\big[J^{\bar q}_{11,n}(b)\big]^{li}\Big\} \\
&\quad + \frac{i}{N_c}\left[\frac{\bar n^\mu}{q^-} - \frac{n^\mu}{q^+}\right]\delta_{ij}(\gamma_T^\nu)_{kl}\int_0^1 \mathrm{d}\xi\, C_2^*(\xi;2q^+q^-)C_1(2q^+q^-) \\
&\quad\times \int \frac{\mathrm{d}^2b}{(2\pi)^2}\, e^{ib\cdot q}\Big\{\big[J^{\bar q}_{21,\bar n}(\xi,b)\big]^{li}\big[J^{q}_{11,n}(b)\big]^{jk} - \big[J^{q}_{21,\bar n}(\xi,b)\big]^{jk}\big[J^{\bar q}_{11,n}(b)\big]^{li} \\
&\qquad + \big[J^{\bar q}_{11,\bar n}(b)\big]^{li}\big[J^{q}_{21,n}(\xi,b)\big]^{jk} - \big[J^{q}_{11,\bar n}(b)\big]^{jk}\big[J^{\bar q}_{21,n}(\xi,b)\big]^{li}\Big\} \\
&\quad + \frac{i}{N_c}\left[\frac{\bar n^\nu}{q^-} - \frac{n^\nu}{q^+}\right](\gamma_T^\mu)_{ij}\delta_{kl}\int_0^1 \mathrm{d}\xi\, C_1^*(q^+q^-)C_2(\xi;2q^+q^-) \\
&\quad\times \int \frac{\mathrm{d}^2b}{(2\pi)^2}\, e^{ib\cdot q}\Big\{\big[J^{\bar q}_{12,\bar n}(\xi,b)\big]^{li}\big[J^{q}_{11,n}(b)\big]^{jk} - \big[J^{q}_{12,\bar n}(\xi,b)\big]^{jk}\big[J^{\bar q}_{11,n}(b)\big]^{li} \\
&\qquad + \big[J^{\bar q}_{11,\bar n}(b)\big]^{li}\big[J^{q}_{12,n}(\xi,b)\big]^{jk} - \big[J^{q}_{11,\bar n}(b)\big]^{jk}\big[J^{\bar q}_{12,n}(\xi,b)\big]^{li}\Big\}\,. \qquad (5.32)
\end{aligned}$$

Here, C_1 and C_2 are matching coefficients that can be calculated in perturbation theory. These coefficients arise when the current operator is written in terms of the background fields, and we follow the definitions of [103], and the symbol J denotes jet functions

with open spinor indices. At leading order in perturbation theory $C_i = 1$, consistent with eqs. 5.28 and 5.29. The coefficient C_1 is known up to three-loops [115] (see also [149, 112]), while the coefficient C_2 is calculated up to NLO in [103], section 6. For definiteness, the C_2 in eq. 5.31 is related to the one in ref. [103] by $C_2(\xi, 2q^+q^-) = C_2^{\text{[103]}}(x_1 = \xi, x_2 = -\xi)$. The bounds of the ξ integral arise from the range over which the jet functions have support.

The jet functions that appear above are defined in terms of matrix elements of the building-block operators in eqs. 5.20 and 5.21. The twist-2 jet functions are given by

$$\begin{aligned}
\left[J^q_{11,\bar{n}}(b)\right]^{jk} &= \mathrm{tr}_c \int \frac{\mathrm{d}y^-}{2\pi}\, e^{iy^-q^+}\ \langle 0|\left[U_{1,\bar{n}}(y^-,b)\right]^{(-)}_j |J^{\bar{n}}_{\text{alg}}\rangle \langle J^{\bar{n}}_{\text{alg}}|\left[\overline{U}_{1,\bar{n}}(0,0)\right]^{(+)}_k |0\rangle\ , \\
\left[J^q_{11,n}(b)\right]^{jk} &= \mathrm{tr}_c \int \frac{\mathrm{d}y^+}{2\pi}\, e^{iy^+q^-}\ \langle 0|\left[U_{1,n}(y^+,b)\right]^{(-)}_j |J^{n}_{\text{alg}}\rangle \langle J^{n}_{\text{alg}}|\left[\overline{U}_{1,n}(0,0)\right]^{(+)}_k |0\rangle\ , \\
\left[J^{\bar{q}}_{11,\bar{n}}(b)\right]^{li} &= \int \frac{\mathrm{d}y^-}{2\pi}\, e^{iy^-q^+}\ \langle 0|\left[\overline{U}_{1,\bar{n}}(y^-,b)\right]^{(-)}_i |J^{\bar{n}}_{\text{alg}}\rangle \langle J^{\bar{n}}_{\text{alg}}|\left[U_{1,\bar{n}}(0,0)\right]^{(+)}_l |0\rangle\ , \\
\left[J^{\bar{q}}_{11,n}(b)\right]^{li} &= \int \frac{\mathrm{d}y^+}{2\pi}\, e^{iy^+q^-}\ \langle 0|\left[\overline{U}_{1,n}(y^+,b)\right]^{(-)}_i |J^{n}_{\text{alg}}\rangle \langle J^{n}_{\text{alg}}|\left[U_{1,n}(0,0)\right]^{(+)}_l |0\rangle\ ,
\end{aligned} \tag{5.33}$$

and the twist-3 jet functions are defined as

$$\begin{aligned}
\left[J^q_{21,\bar{n}}(\xi,b)\right]^{jk} &= \frac{1}{\xi - i\delta^+_E}\ \mathrm{tr}_c \int \frac{\mathrm{d}y_1^-}{2\pi}\frac{\mathrm{d}y_2^-}{2\pi}\, e^{i(\bar{\xi}y_1^- + \xi y_2^-)q^+} \\
&\quad \times \langle 0|\left[U_{2,\bar{n}}(\{y_1^-,y_2^-\},b)\right]^{(-)}_j |J^{\bar{n}}_{\text{alg}}\rangle \langle J^{\bar{n}}_{\text{alg}}|\left[\overline{U}_{1,\bar{n}}(0,0)\right]^{(+)}_k |0\rangle\ , \\
\left[J^q_{21,n}(\xi,b)\right]^{jk} &= \frac{1}{\xi - i\delta^-_E}\ \mathrm{tr}_c \int \frac{\mathrm{d}y_1^+}{2\pi}\frac{\mathrm{d}y_2^+}{2\pi}\, e^{i(\bar{\xi}y_1^+ + \xi y_2^+)q^-} \\
&\quad \times \langle 0|\left[U_{2,n}(\{y_1^+,y_2^+\},b)\right]^{(-)}_j |J^{n}_{\text{alg}}\rangle \langle J^{n}_{\text{alg}}|\left[\overline{U}_{1,n}(0,0)\right]^{(+)}_k |0\rangle\ , \\
\left[J^{\bar{q}}_{21,\bar{n}}(\xi,b)\right]^{li} &= \frac{1}{\xi - i\delta^+_E} \int \frac{\mathrm{d}y_1^-}{2\pi}\frac{\mathrm{d}y_2^-}{2\pi}\, e^{i(\bar{\xi}y_1^- + \xi y_2^-)q^+} \\
&\quad \times \langle 0|\left[\overline{U}_{2,\bar{n}}(\{y_1^-,y_2^-\},b)\right]^{(-)}_i |J^{\bar{n}}_{\text{alg}}\rangle \langle J^{\bar{n}}_{\text{alg}}|\left[U_{1,\bar{n}}(0,0)\right]^{(+)}_l |0\rangle\ , \\
\left[J^{\bar{q}}_{21,n}(\xi,b)\right]^{li} &= \frac{1}{\xi - i\delta^-_E} \int \frac{\mathrm{d}y_1^+}{2\pi}\frac{\mathrm{d}y_2^+}{2\pi}\, e^{i(\bar{\xi}y_1^+ + \xi y_2^+)q^-} \\
&\quad \times \langle 0|\left[\overline{U}_{2,n}(\{y_1^+,y_2^+\},b)\right]^{(-)}_i |J^{n}_{\text{alg}}\rangle \langle J^{n}_{\text{alg}}|\left[U_{1,n}(0,0)\right]^{(+)}_l |0\rangle\ , \\
\left[J^q_{12,\bar{n}}(\xi,b)\right]^{jk} &= -\frac{1}{\xi + i\delta^+_E}\ \mathrm{tr}_c \int \frac{\mathrm{d}y^-}{2\pi}\frac{\mathrm{d}z^-}{2\pi}\, e^{i(y^- - \xi z^-)q^+} \\
&\quad \times \langle 0|\left[U_{1,\bar{n}}(y^-,b)\right]^{(-)}_j |J^{\bar{n}}_{\text{alg}}\rangle \langle J^{\bar{n}}_{\text{alg}}|\left[\overline{U}_{2,\bar{n}}(\{0,z^-\},0)\right]^{(+)}_k |0\rangle\ , \\
\left[J^q_{12,n}(\xi,b)\right]^{jk} &= -\frac{1}{\xi + i\delta^-_E}\ \mathrm{tr}_c \int \frac{\mathrm{d}y^+}{2\pi}\frac{\mathrm{d}z^+}{2\pi}\, e^{i(y^+ - \xi z^+)q^-} \\
&\quad \times \langle 0|\left[U_{1,n}(y^+,b)\right]^{(-)}_j |J^{n}_{\text{alg}}\rangle \langle J^{n}_{\text{alg}}|\left[\overline{U}_{2,n}(\{0,z^+\},0)\right]^{(+)}_k |0\rangle\ ,
\end{aligned}$$

$$\begin{aligned}
\left[J^{\bar{q}}_{12,\bar{n}}(\xi,b)\right]^{li} &= -\frac{1}{\xi+i\delta_E^+}\int\frac{\mathrm{d}y^-}{2\pi}\frac{\mathrm{d}z^-}{2\pi}\,e^{i(y^--\xi z^-)q^+} \\
&\quad\times\langle 0|\left[\overline{U}_{1,\bar{n}}(y^-,b)\right]^{(-)}_i|J^{\bar{n}}_{\mathrm{alg}}\rangle\langle J^{\bar{n}}_{\mathrm{alg}}|\left[U_{2,\bar{n}}(\{0,z^-\},0)\right]^{(+)}_l|0\rangle\,, \\
\left[J^{\bar{q}}_{12,n}(\xi,b)\right]^{li} &= -\frac{1}{\xi+i\delta_E^-}\int\frac{\mathrm{d}y^+}{2\pi}\frac{\mathrm{d}z^+}{2\pi}\,e^{i(y^+-\xi z^+)q^-} \\
&\quad\times\langle 0|\left[\overline{U}_{1,n}(y^-,b)\right]^{(-)}_i|J^{n}_{\mathrm{alg}}\rangle\langle J^{n}_{\mathrm{alg}}|\left[U_{2,n}(\{0,z^+\},0)\right]^{(+)}_l|0\rangle\,,
\end{aligned}\tag{5.34}$$

and we have introduced for convenience

$$\bar{\xi}=1-\xi\,.\tag{5.35}$$

Note that whether the operator appears in the amplitude or conjugate amplitude is determined by whether the operator is causal or anti-causal. From now on we drop these superscripts on the operators.

5.2.3 Jet function definitions

The next step in the factorization is to define a minimal set of (bare) jet functions that have no open spinor or Lorentz indices, as the set of jet functions in sec. 5.2.2 contains redundancy.

First, to get rid of the open spinor indices, we apply the Fierz relations in app. B.1. This gives rise to four twist-2 jet functions with no Lorentz index

$$\begin{aligned}
(\gamma^+)_{kj}\left[J^{q}_{11,\bar{n}}(b)\right]^{jk} &= 2N_c\,J^{q}_{11,\bar{n}}(b)\,, & (\gamma^+)_{il}\left[J^{\bar{q}}_{11,\bar{n}}(b)\right]^{li} &= 2N_c\,J^{\bar{q}}_{11,\bar{n}}(b)\,, \\
(\gamma^-)_{kj}\left[J^{q}_{11,n}(b)\right]^{jk} &= 2N_c\,J^{q}_{11,n}(b)\,, & (\gamma^-)_{il}\left[J^{\bar{q}}_{11,n}(b)\right]^{li} &= 2N_c\,J^{\bar{q}}_{11,n}(b)\,,
\end{aligned}\tag{5.36}$$

and eight twist-3 jet functions with one open Lorentz index,

$$\begin{aligned}
+\epsilon_T^{\mu\alpha}(\sigma^{\alpha+}\gamma^5)_{kj}\left[J^{q}_{21,\bar{n}}(\xi,b)\right]^{jk} &= 2N_c\,J^{\mu,q}_{21,\bar{n}}(\xi,b)\,, & +\epsilon_T^{\mu\alpha}(\sigma^{\alpha+}\gamma^5)_{il}\left[J^{\bar{q}}_{21,\bar{n}}(\xi,b)\right]^{li} &= 2N_c\,J^{\mu,\bar{q}}_{21,\bar{n}}(\xi,b)\,, \\
-\epsilon_T^{\mu\alpha}(\sigma^{\alpha-}\gamma^5)_{kj}\left[J^{q}_{21,n}(\xi,b)\right]^{jk} &= 2N_c\,J^{\mu,q}_{21,n}(\xi,b)\,, & -\epsilon_T^{\mu\alpha}(\sigma^{\alpha-}\gamma^5)_{il}\left[J^{\bar{q}}_{21,n}(\xi,b)\right]^{li} &= 2N_c\,J^{\mu,\bar{q}}_{21,n}(\xi,b)\,, \\
-\epsilon_T^{\mu\alpha}(\sigma^{\alpha+}\gamma^5)_{kj}\left[J^{q}_{12,\bar{n}}(\xi,b)\right]^{jk} &= 2N_c\,J^{\mu,q}_{12,\bar{n}}(\xi,b)\,, & -\epsilon_T^{\mu\alpha}(\sigma^{\alpha+}\gamma^5)_{il}\left[J^{\bar{q}}_{12,\bar{n}}(\xi,b)\right]^{li} &= 2N_c\,J^{\mu,\bar{q}}_{12,\bar{n}}(\xi,b)\,, \\
+\epsilon_T^{\mu\alpha}(\sigma^{\alpha-}\gamma^5)_{kj}\left[J^{q}_{12,n}(\xi,b)\right]^{jk} &= 2N_c\,J^{\mu,q}_{12,n}(\xi,b)\,, & +\epsilon_T^{\mu\alpha}(\sigma^{\alpha-}\gamma^5)_{il}\left[J^{\bar{q}}_{12,n}(\xi,b)\right]^{li} &= 2N_c\,J^{\mu,\bar{q}}_{12,n}(\xi,b)\,.
\end{aligned}\tag{5.37}$$

The factor $2N_c$ accounts for averaging over the spin and color of the initial quark field. The different overall sign between $J_{21,n}$ and $J_{21,\bar{n}}$ is chosen because $\epsilon_T^{\mu\nu}=\epsilon^{\mu\nu\rho\sigma}n_\rho\bar{n}_\sigma$ changes sign when $n\leftrightarrow\bar{n}$.

Discrete symmetries provide an additional reduction of independent jet functions. Jet algorithms are spin-independent and respect the C,P and T symmetries of QCD. This allows us to derive that the LP jet functions satisfy,

$$J^{\bar{q}}_{11,\bar{n}}(b)=J^{q}_{11,\bar{n}}(b)\,,\qquad\qquad J^{\bar{q}}_{11,n}(b)=J^{q}_{11,n}(b)\,,\tag{5.38}$$

reducing the number of independent twist-2 jet functions down to two, one for n and one for the $\bar{n}$ direction. For the twist-3 jet functions we have

$$\begin{aligned} J^{\rho,q}_{12,\bar{n}}(\xi,b) &= -\big[J^{\rho,q}_{21,\bar{n}}(\xi,-b)\big]^*\,, & J^{\rho,\bar{q}}_{21,\bar{n}}(\xi,b) &= J^{\rho,q}_{21,\bar{n}}(\xi,b)\,, \\ J^{\rho,q}_{12,n}(\xi,b) &= -\big[J^{\rho,q}_{21,n}(\xi,-b)\big]^*\,, & J^{\rho,\bar{q}}_{21,n}(\xi,b) &= J^{\rho,q}_{21,n}(\xi,b)\,, \end{aligned} \tag{5.39}$$

and similarly for $J^{\bar{q}}_{12}$. This reduces the number of independent twist-3 jet functions from eight down to two. Since the quark and anti-quark distributions are identical we will drop the corresponding label from now on. The minus signs appearing in the complex conjugation cancel when performing the decomposition in eq. 5.40. Thus the signs in eq. 5.37 were chosen precisely such that these symmetry relations do not contain minus signs.

Both the NLP jet functions and the derivatives of the LP jet functions that appear in the hadronic tensor carry an open (transverse) Lorentz index. To achieve a fully factorized formula for the hadronic tensor we must decompose these objects into the available structures b^μ and $\epsilon_T^{\mu\nu} b_\nu$. Parity implies that only b^μ contributes, leading us to define

$$\begin{aligned} J^{\rho}_{21,\bar{n}}(\xi,b) &= \frac{b^\rho}{b^2} J_{21,\bar{n}}(\xi,\mathbf{b}^2)\,, & \partial_\rho J_{11,\bar{n}}(b) &= \frac{b_\rho}{b^2} J'_{11,\bar{n}}(\mathbf{b}^2)\,, \\ J^{\rho}_{21,n}(\xi,b) &= \frac{b^\rho}{b^2} J_{21,n}(\xi,\mathbf{b}^2)\,, & \partial_\rho J^q_{11,n}(b) &= \frac{b_\rho}{b^2} J'^{\,q}_{11,n}(\mathbf{b}^2)\,. \end{aligned} \tag{5.40}$$

This final step removes all open Lorentz indices from the jet definitions. Since all functions now only depend on the magnitude of b, we can perform the angular integration using the following identities,

$$\begin{aligned} \int \frac{\mathrm{d}^2 b}{(2\pi)^2}\, e^{ib\cdot q}\, f(\mathbf{b}^2) &= \frac{1}{2}\int_0^\infty \mathrm{d}|\mathbf{b}|^2\, \frac{J_0(|\mathbf{b}||\mathbf{q}|)}{2\pi}\, f(\mathbf{b}^2)\,, \\ \int \frac{\mathrm{d}^2 b}{(2\pi)^2}\, e^{ib\cdot q}\, \frac{ib^\rho}{b^2}\, f(\mathbf{b}^2) &= \frac{q_T^\rho}{2}\int_0^\infty \mathrm{d}|\mathbf{b}|^2\, \frac{J_1(|\mathbf{b}||\mathbf{q}|)}{2\pi|\mathbf{b}||\mathbf{q}|}\, f(\mathbf{b}^2)\,. \end{aligned} \tag{5.41}$$

Applying the above decomposition to the definitions presented in eqs. 5.33 and 5.34, the final expressions for the jet functions read,

$$J^{\mathrm{bare}}_{11,\bar{n}}(\mathbf{b}^2) = \frac{1}{2N_c}\int \frac{\mathrm{d}y^-}{2\pi}\, e^{iy^- q^+}\ \mathrm{tr}\big[\gamma^+ \langle 0|\, U_{1,\bar{n}}(y^-,b)\, |J^{\bar{n}}_{\mathrm{alg}}\rangle \langle J^{\bar{n}}_{\mathrm{alg}}|\, \overline{U}_{1,\bar{n}}(0,0)\, |0\rangle\big]\,, \tag{5.42}$$

$$J'^{\,\mathrm{bare}}_{11,\bar{n}}(\mathbf{b}^2) = b^\mu \frac{\partial}{\partial b^\mu} J^{\mathrm{bare}}_{11,\bar{n}}(\mathbf{b}^2)\,, \tag{5.43}$$

$$\begin{aligned} J^{\mathrm{bare}}_{21,\bar{n}}(\xi,\mathbf{b}^2) = n^\mu \bar{n}^\nu b^\rho \epsilon_{\mu\nu\rho\sigma}\, \frac{1}{\xi - i\delta_E^+}\, \frac{1}{2N_c} \int \frac{\mathrm{d}y_1^-}{2\pi}\frac{\mathrm{d}y_2^-}{2\pi}\, e^{i(\bar{\xi}y_1^- + \xi y_2^-)q^+} \\ \times \mathrm{tr}\Big[\sigma^{\sigma+}\gamma^5 \langle 0|\, U_{2,\bar{n}}(\{y_1^-,y_2^-\},b)\, |J^{\bar{n}}_{\mathrm{alg}}\rangle \langle J^{\bar{n}}_{\mathrm{alg}}|\, \overline{U}_{1,\bar{n}}(0,0)\, |0\rangle\Big]\,, \end{aligned} \tag{5.44}$$

where the trace is over both the color and Dirac indices. The jet functions for the n-collinear sector can be obtained by replacing $n \leftrightarrow \bar{n}$.

5.2.4 Factorization

Starting from eq. 5.31, we now apply the relations and definitions of the previous section to obtain a factorized expression for the hadronic tensor,

$$W^{\mu\nu}_{\text{LP}}(q) = N_c\,(-g_T^{\mu\nu})H_1(Q^2)\int \mathrm{d}|\mathbf{b}|^2\,\frac{J_0(|\mathbf{b}||\mathbf{q}|)}{2\pi}J_{11,\bar{n}}(\mathbf{b}^2)\,J_{11,n}(\mathbf{b}^2)\,, \tag{5.45}$$

$$\begin{aligned}
W^{\mu\nu}_{\text{NLP}}(q) = {} & N_c\left[\frac{n^\mu q_T^\nu}{q^+}+\frac{n^\nu q_T^\mu}{q^+}\right]H_1(Q^2)\int_0^\infty \mathrm{d}|\mathbf{b}|^2\,\frac{J_1(|\mathbf{b}||\mathbf{q}|)}{2\pi|\mathbf{b}||\mathbf{q}|}\,J'_{11,\bar{n}}(\mathbf{b}^2)\,J_{11,n}(\mathbf{b}^2)\\
& + N_c\left[\frac{\bar{n}^\mu q_T^\nu}{q^-}+\frac{\bar{n}^\nu q_T^\mu}{q^-}\right]H_1(Q^2)\int_0^\infty \mathrm{d}|\mathbf{b}|^2\,\frac{J_1(|\mathbf{b}||\mathbf{q}|)}{2\pi|\mathbf{b}||\mathbf{q}|}\,J_{11,\bar{n}}(\mathbf{b}^2)\,J'_{11,n}(\mathbf{b}^2)\\
& + N_c\left[\frac{\bar{n}^\mu q_T^\nu}{q^-}-\frac{n^\mu q_T^\nu}{q^+}\right]\int_0^1 \mathrm{d}\xi\,H_2(\xi,Q^2)\\
& \quad\times\int_0^\infty \mathrm{d}|\mathbf{b}|^2\,\frac{J_1(|\mathbf{b}||\mathbf{q}|)}{2\pi|\mathbf{b}||\mathbf{q}|}\left\{J_{21,\bar{n}}(\xi,\mathbf{b}^2)J_{11,n}(\mathbf{b}^2)-J_{11,\bar{n}}(\mathbf{b}^2)J_{21,n}(\xi,\mathbf{b}^2)\right\}\\
& + N_c\left[\frac{\bar{n}^\nu q_T^\mu}{q^-}-\frac{n^\nu q_T^\mu}{q^+}\right]\int_0^1 \mathrm{d}\xi\,H_2^*(\xi,Q^2)\\
& \quad\times\int_0^\infty \mathrm{d}|\mathbf{b}|^2\,\frac{J_1(|\mathbf{b}||\mathbf{q}|)}{2\pi|\mathbf{b}||\mathbf{q}|}\left\{J^*_{21,\bar{n}}(\xi,\mathbf{b}^2)J_{11,n}(\mathbf{b}^2)-J_{11,\bar{n}}(\mathbf{b}^2)J^*_{21,n}(\xi,\mathbf{b}^2)\right\}.
\end{aligned}$$

Here, H_1 and H_2 are defined in terms of the Wilson coefficients and are referred to as the hard functions

$$\begin{aligned}
H_1(Q^2) &= |C_1(Q^2)|^2\,,\\
H_2(\xi,Q^2) &= C_2^*(\xi,Q^2)\,C_1(Q^2)\,.
\end{aligned} \tag{5.46}$$

There are two things to note here. First, note that the hard function H_2 is complex-valued for the process we consider here. Second, we have replaced the arguments $2q^+q^-$ of the Wilson coefficients by Q^2, as this replacement can be made up to power corrections (these are kinematic power corrections, see ref. [150]). For this latter point, it has been shown that higher-power corrections in fact lead to the replacement $2q^+q^- \to Q^2$ in the Wilson coefficients, as expected by Lorentz invariance.

Next, we combine the hadronic tensor with the leptonic tensor to obtain the cross-section for $e^+e^- \to 2$ jets. In the above expression, the hadronic tensor is decomposed into several Lorentz structures. As an intermediate step, we record the following results for the contractions between these Lorentz structures and the leptonic tensor,

$$\begin{aligned}
(-g_T^{\mu\nu})L_{\mu\nu} &= 2Q^2\,(1-2y+2y^2)\;-\;4Q_TQ\,\cos(\phi_1)\,(1-2y)\sqrt{y(1-y)}+\mathcal{O}(Q_T^2)\,,\\
\frac{\bar{n}^\mu q_T^\nu}{q^-}L_{\mu\nu} &= -\frac{n^\mu q_T^\nu}{q^+}L_{\mu\nu} = 4Q_TQ\,\cos(\phi_1)\,(1-2y)\sqrt{y(1-y)}+\mathcal{O}(Q_T^2)\,.
\end{aligned} \tag{5.47}$$

Note that the power-suppressed contributions coming from the two Lorentz structures are identical, making it experimentally impossible to distinguish between the different

types of power corrections. Combining the full expression for the hadronic tensor of eq. 5.45 with the leptonic tensor in eq. 5.12, we find that the cross-section is given by

$$\begin{aligned}
\frac{\mathrm{d}\sigma}{\mathrm{d}y\,\mathrm{d}^2\mathbf{q}} &= \frac{\pi\alpha_{\mathrm{em}}^2 Q_q^2 N_c}{Q^2}\,(2-4y+4y^2)\int_0^\infty \mathrm{d}|\mathbf{b}|^2\,\frac{J_0(|\mathbf{b}||\mathbf{q}|)}{2\pi}\,H_1(Q^2)\,J_{11,\bar{n}}(\mathbf{b}^2)\,J_{11,n}(\mathbf{b}^2) \\
&\quad - \frac{\pi\alpha_{\mathrm{em}}^2 Q_q^2 N_c}{Q^2}\,\frac{Q_T}{Q}\,4\cos(\phi_1)\,(1-2y)\sqrt{y(1-y)} \\
&\quad\quad \times \Bigg\{ \int_0^\infty \mathrm{d}|\mathbf{b}|^2\,\frac{J_0(|\mathbf{b}||\mathbf{q}|)}{2\pi}\,H_1(Q^2)\,J_{11,\bar{n}}(\mathbf{b}^2)\,J_{11,n}(\mathbf{b}^2) \\
&\quad\quad\quad + 2\int_0^\infty \mathrm{d}|\mathbf{b}|^2\,\frac{J_1(|\mathbf{b}||\mathbf{q}|)}{2\pi|\mathbf{b}||\mathbf{q}|}\,H_1(Q^2)\left[J'_{11,\bar{n}}(\mathbf{b}^2)\,J_{11,n}(\mathbf{b}^2) - J_{11,\bar{n}}(\mathbf{b}^2)\,J'_{11,n}(\mathbf{b}^2)\right] \\
&\quad\quad\quad - 2\int_0^\infty \mathrm{d}|\mathbf{b}|^2\,\frac{J_1(|\mathbf{b}||\mathbf{q}|)}{2\pi|\mathbf{b}||\mathbf{q}|}\int_0^1 \mathrm{d}\xi\,H_2(\xi,Q^2) \\
&\quad\quad\quad\quad \times \left[J_{21,\bar{n}}(\xi,\mathbf{b}^2)\,J_{11,n}(\mathbf{b}^2) - J_{11,\bar{n}}(\mathbf{b}^2)\,J_{21,n}(\xi,\mathbf{b}^2)\right] + \text{c.c.} \Bigg\}\,. \qquad (5.48)
\end{aligned}$$

Note that in the above expression, the hard functions and jet functions are bare and unsubtracted quantities.

5.3 Subtraction and renormalization

In the previous section, we arrived at a factorized expression for the cross-section in terms of a set of jet functions and Wilson coefficients. We still need to treat the soft overlap between the collinear and anti-collinear regions and renormalize all ingredients. Furthermore, the above result for the cross-section contains some divergences, known in the literature as special rapidity divergences and endpoint divergences, that require treatment. In this section, we discuss the overlap subtraction and the resulting cancellation of these divergences, as well as the renormalization of the jet functions. For other cases, a scheme needs to be developed for treating endpoint divergences [151, 152, 153].

First, in sec. 5.3.1, we discuss the subtraction of the overlap region. In summary, the lack of a clear boundary between the collinear and anti-collinear regions gives rise to rapidity divergences, which cancel once the overlap region has been properly subtracted. In the method employed in this work, not all divergences cancel after the overlap region has been subtracted. These remaining special rapidity divergences already enter at lowest order in $a_s = \alpha_s/(4\pi)$, and are contained in the kinematic and higher-twist corrections. As a consequence, ill-defined convolutions between plus distributions and logarithms appear in finite terms at higher orders in perturbation theory, which are commonly referred to as endpoint divergences. We discuss the subtraction and cancellation of these divergences in sec. 5.3.2. The treatment of the overlap region is one of the main differences between the approach in SCET and the TMD operator expansion, which we compare in sec. 5.3.3. Finally, the renormalization of the jet functions and the corresponding evolution equations are discussed in sec. 5.3.4.

5.3.1 Overlap subtraction

As mentioned in sec. 5.2.1, the two collinear regions overlap in the soft region, which is doubly counted. The presence of this overlap has been extensively discussed in the literature about TMD factorization [94, 17, 25], and it has a similar treatment in the background field method [103].

In the TMD operator expansion method, the overlap between the collinear and anti-collinear regions can be subtracted for bare operators by making the following replacements

$$\mathcal{O}_{11,\bar{n}}\overline{\mathcal{O}}_{11,n} \to \frac{\mathcal{O}_{11,\bar{n}}\overline{\mathcal{O}}_{11,n}}{\mathcal{S}_{\rm LP}}\,, \quad \partial_\rho\mathcal{O}_{11,\bar{n}}\overline{\mathcal{O}}_{11,n} \to \frac{\partial_\rho\mathcal{O}_{11,\bar{n}}\overline{\mathcal{O}}_{11,n}}{\mathcal{S}_{\rm LP}}\,, \quad \mathcal{O}_{21,\bar{n}}\overline{\mathcal{O}}_{11,n} \to \frac{\mathcal{O}_{21,\bar{n}}\overline{\mathcal{O}}_{11,n}}{\mathcal{S}_{\rm LP}}\,, \tag{5.49}$$

with similar replacements for the other combinations of operators that appear in eq. 5.29. Using the δ-regulator, the overlap factor is identical for both the leading twist and sub-leading twist operators, and is given by the soft function

$$\mathcal{S}^{\rm bare}_{\rm LP}(\mathbf{b}^2,\epsilon,2\delta^+\delta^-) = \frac{1}{N_c}\,{\rm tr}_c\big\{\langle 0|\,[\infty\bar{n}+b,b][b,\infty n+b][\infty n,0][0,\infty\bar{n}]\,|0\rangle\big\}\,. \tag{5.50}$$

The overlap subtraction as presented in eq. 5.49 happens at the level of the product of two operators from the different collinear sectors, and the rapidity divergences cancel between the $\mathcal{O}_n$, $\mathcal{O}_{\bar{n}}$ and $\mathcal{S}$. However, it is desirable to express the cross-section in terms of ingredients that are each individually free of rapidity divergences. To define a rapidity-finite jet function, it is necessary to implement this subtraction by absorbing a square root of the soft function into each of the jet functions. To do this we use the fact that the soft function can be separated into two pieces,

$$\mathcal{S}^{\rm bare}_{\rm LP}(\mathbf{b}^2,\epsilon,2\delta^+\delta^-) = \sqrt{\mathcal{S}^{\rm bare}_{\rm LP}\big(\mathbf{b}^2,\epsilon,(\delta_E^+)^2\zeta\big)}\sqrt{\mathcal{S}^{\rm bare}_{\rm LP}\big(\mathbf{b}^2,\epsilon,(\delta_E^-)^2\zeta\big)}\,, \tag{5.51}$$

where

$$\delta_E^+ = \frac{\delta^+}{q^+}\,, \qquad \delta_E^- = \frac{\delta^-}{q^-}\,, \qquad \text{and} \qquad \zeta^2 = (2q^+q^-)^2\,, \tag{5.52}$$

and ζ is referred to as the rapidity scale. Using the above identity, the overlap subtraction procedure can be implemented by making the following replacements

$$J^{\rm bare}_{11,\bar{n}}(\mathbf{b}^2,\epsilon,\delta_E^+) \to \frac{J^{\rm bare}_{11,\bar{n}}(\mathbf{b}^2,\epsilon,\delta_E^+)}{\sqrt{\mathcal{S}_{\rm LP}(\mathbf{b}^2,\epsilon,(\delta_E^+)^2\zeta)}} = J^{\rm bare,sub}_{11,\bar{n}}(\mathbf{b}^2,\zeta,\epsilon)\,, \tag{5.53}$$

$$J'^{\rm bare}_{11,\bar{n}}(\mathbf{b}^2,\epsilon,\delta_E^+) \to \frac{J'^{\rm bare}_{11,\bar{n}}(\mathbf{b}^2,\epsilon,\delta_E^+)}{\sqrt{\mathcal{S}_{\rm LP}(\mathbf{b}^2,\epsilon,(\delta_E^+)^2\zeta)}}\,, \tag{5.54}$$

$$J^{\rm bare}_{21,\bar{n}}(\xi,\mathbf{b}^2,\epsilon,\delta_E^+) \to \frac{J^{\rm bare}_{21,\bar{n}}(\xi,\mathbf{b}^2,\epsilon,\delta_E^+)}{\sqrt{\mathcal{S}_{\rm LP}(\mathbf{b}^2,\epsilon,(\delta_E^+)^2\zeta)}}\,, \tag{5.55}$$

and similarly for the n-collinear direction. After the subtraction procedure, the leading-power jet function $J^{\rm bare,sub}_{11}$ is free of rapidity divergences but depends on the rapidity scale ζ. The dependence on ζ will be discussed in sec. 5.3.4.

5.3.2 Special rapidity and endpoint divergences

The subtraction procedure of the TMD operator expansion method does not cancel all rapidity divergences. Specifically, J'_{11} and J_{21}, which respectively correspond to the kinematical and higher-twist corrections, still contain divergences. These divergences can be subtracted and cancel in the cross section between the n and the $\bar{n}$ sectors. We now discuss the cancellation of these divergences separately for the kinematic and higher-twist corrections.

Higher-twist correction

For the twist-3 jet functions $J_{21}(\xi, \mathbf{b}^2)$ divergences appear in the convolution with H_2 in eq. 5.48 as $\xi \to 0$. In most of the literature this is referred to as the problem of endpoint divergences, while in the TMD operator expansion literature these divergences are considered part of the special rapidity divergences. In the case of TMD factorization, different methods for treating these divergences exist and we compare the two in sec. 5.3.3. In this work, we subtract the singular behavior of the jet functions as $\xi \to 0$ by means of a sub-leading-power soft function. This ensures that the integral of the hard function and the twist-3 jet function is well defined. This was first discussed in refs. [154, 155, 156], which focused on SIDIS.

The key insight is that in the limit $\xi \to 0$ the gluon field strength becomes soft. In the soft limit, the gluon decouples from the collinear sector and the field strength can be factored out of the collinear matrix element. As a result, the limit $\xi \to 0$ is captured by

$$\lim_{\xi\to 0} J^{\text{bare}}_{21,\bar{n}}(\xi, \mathbf{b}^2)\, \mathcal{S}^{\text{bare}}_{\text{LP}}(\mathbf{b}^2)\, J^{\text{bare}}_{11,n}(\mathbf{b}^2) = J^{\text{bare}}_{11,\bar{n}}(\mathbf{b}^2) S^{\text{bare}}_{21,\bar{n}}(\xi, \mathbf{b}^2) J^{\text{bare}}_{11,n}(\mathbf{b}^2) + \dots\,, \tag{5.56}$$

where $\dots$ denotes terms that are regular as $\xi \to 0$ and a similar expression holds for the opposite collinear sector. In this expression, the jet functions on the right-hand side are the familiar twist-2 jet functions and $S_{21,\bar{n}}$ is an NLP soft function. The NLP soft functions for the two collinear sectors are defined as

$$\begin{aligned} S^{\text{bare}}_{21,\bar{n}}(\xi, \mathbf{b}^2, \epsilon, \delta_E^+, 2\delta^+\delta^-) = +\frac{b_\rho}{\xi - i\delta_E^+} \int \frac{\mathrm{d}y_2^-}{2\pi}\, e^{i\xi y_2^- q^+}\, \frac{1}{N_c}\, \mathrm{tr}\Big[&\langle 0|\, [b + y_2^- n + \infty n, b + y_2^- n] \\ &\times [b + y_2^- n, b + y_2^- n + \infty \bar{n}] g F^{\rho+}(y_2^- n + b)\; |X\rangle \langle X|\, [\infty\bar{n}, 0][0, \infty n]\, |0\rangle \Big]\,, \end{aligned} \tag{5.57}$$

$$\begin{aligned} S^{\text{bare}}_{21,n}(\xi, \mathbf{b}^2, \epsilon, \delta_E^-, 2\delta^+\delta^-) = -\frac{b_\rho}{\xi - i\delta_E^-} \int \frac{\mathrm{d}y_2^+}{2\pi}\, e^{i\xi y_2^+ q^-}\, \frac{1}{N_c}\, \mathrm{tr}\Big[&\langle 0|\, g F^{\rho-}(y_2^+ \bar{n} + b) \\ &\times [b + y_2^- n + \infty n, b + y_2^- n][b + y_2^- n, b + y_2^- n + \infty \bar{n}] S_{\bar{n}}\, |X\rangle \\ &\times \langle X|\, [\infty\bar{n}, 0][0, \infty n]\, |0\rangle \Big]\,. \end{aligned} \tag{5.58}$$

This definition follows from replacing the collinear field strength operator in the $\mathbb{O}_{21}$ operators in eq. 5.29 by soft field strength and following the same steps as in sec. 5.2. Note that, strictly speaking, this derivation requires the introduction of a background

field for the soft modes, although the soft function drops out in the final result for the NLP case we consider here.

Using eq. 5.56, we can subtract the singular behavior from the jet functions in the $\xi \to 0$ limit

$$J^{\text{bare,sub}}_{21,\bar{n}}(\xi, \mathbf{b}^2, \zeta, \epsilon) = \frac{J^{\text{bare}}_{21,\bar{n}}(\xi, \mathbf{b}^2)}{\sqrt{\mathcal{S}_{\text{LP}}(\mathbf{b}^2, \epsilon, (\delta_E^+)^2\zeta)}} - S^{\text{bare}}_{21,\bar{n}}(\xi, \mathbf{b}^2, \epsilon, \delta_E^+, \zeta)\, J^{\text{bare,sub}}_{11,\bar{n}}(\mathbf{b}^2, \zeta, \epsilon)\,. \tag{5.59}$$

Note that the subtracted jet function is regular as $\xi \to 0$. As a result, its convolution with the hard function is well-defined and free of any endpoint divergences.

The divergent $\ln \delta_E^{\pm}$ and singular $1/\xi_+$ parts of the jet function are now contained in the subtraction terms, which cancel in the hadronic tensor between the two collinear sectors as the jet functions only appear in the combination

$$J_{21,\bar{n}}(\xi, \mathbf{b}^2)\, J_{11,n}(\mathbf{b}^2) - J_{11,\bar{n}}(\mathbf{b}^2)\, J_{21,n}(\xi, \mathbf{b}^2)\,.$$

For this cancellation to work, one needs the two soft functions in eq. 5.57 to be identical, which is only the case if

$$\delta_E^+ = \delta_E^-\,, \tag{5.60}$$

see ref. [118]. Note that this constraint arises beyond the leading order in a_s, where the hard function contains terms involving $\ln \xi$. Summarizing, the special rapidity and endpoint divergences in the higher-twist correction can be subtracted and canceled between the n and $\bar{n}$ sector on the condition that the rapidity regulators for the two sectors are related.

Kinematical correction

For the kinematical correction, only the following combination of jet functions appears after the subtraction procedure of sec. 5.3.1 has been performed,

$$\frac{J'^{\text{bare}}_{11,\bar{n}}(\mathbf{b}^2, \epsilon, \delta_E^+)}{\sqrt{\mathcal{S}_{\text{LP}}(\mathbf{b}^2, \epsilon, (\delta_E^+)^2\zeta)}}\, J^{\text{bare,sub}}_{11,n}(\mathbf{b}^2, \zeta, \epsilon) - J^{\text{bare,sub}}_{11,\bar{n}}(\mathbf{b}^2, \zeta, \epsilon)\, \frac{J'^{\text{bare}}_{11,n}(\mathbf{b}^2, \epsilon, \delta_E^-)}{\sqrt{\mathcal{S}_{\text{LP}}(\mathbf{b}^2, \epsilon, (\delta_E^-)^2\zeta)}}\,. \tag{5.61}$$

Special rapidity divergences also appear in this expression because the derivative that defines J'_{11} is taken before the soft function is divided out.

As for the higher-twist correction, the divergences in the above expression can be cancelled between the two collinear sectors. To see this we first define a subtracted jet function J'_{11},

$$J'^{\text{bare,sub}}_{11,\bar{n}}(\mathbf{b}^2, \zeta, \epsilon) = b^\rho \partial_\rho J^{\text{bare,sub}}_{11,\bar{n}}(\mathbf{b}^2, \zeta, \epsilon)\,. \tag{5.62}$$

that is free of any rapidity divergences, because we take the derivative after subtracting. Using this definition, one can write

$$\frac{J'^{\text{bare}}_{11,\bar{n}}(\mathbf{b}^2, \epsilon, \delta_E^+)}{\sqrt{\mathcal{S}_{\text{LP}}(\mathbf{b}^2, \epsilon, (\delta_E^+)^2\zeta)}} = J'^{\text{bare,sub}}_{11,\bar{n}}(\mathbf{b}^2, \zeta, \epsilon) + \frac{1}{2} J^{\text{bare,sub}}_{11,\bar{n}}(\mathbf{b}^2, \zeta, \epsilon)\, \frac{b^\rho \partial_\rho \mathcal{S}_{\text{LP}}(\mathbf{b}^2, \epsilon, (\delta_E^+)^2\zeta)}{\mathcal{S}_{\text{LP}}(\mathbf{b}^2, \epsilon, (\delta_E^+)^2\zeta)}\,, \tag{5.63}$$

where the special rapidity divergences are contained in the second term. Inserting this in eq. 5.61, we see that the rapidity divergent terms combine as follows,

$$\frac{b^\rho \partial_\rho \mathcal{S}_{\rm LP}(\mathbf{b}^2, \epsilon, (\delta_E^+)^2\zeta)}{\mathcal{S}_{\rm LP}(\mathbf{b}^2, \epsilon, (\delta_E^+)^2\zeta)} - \frac{b^\rho \partial_\rho \mathcal{S}_{\rm LP}(\mathbf{b}^2, \epsilon, (\delta_E^-)^2\zeta)}{\mathcal{S}_{\rm LP}(\mathbf{b}^2, \epsilon, (\delta_E^-)^2\zeta)} = 2b^\rho \partial_\rho \mathcal{D}(b) \ln\left(\frac{\delta_E^+}{\delta_E^-}\right), \tag{5.64}$$

where the expression on the right-hand side can be obtained using the exponentiation of the soft factor with $\mathcal{D}(b)$ the Collins-Soper kernel. We thus see that the special rapidity divergences for the kinematical corrections cancel. In fact, if one takes $\delta_E^+ = \delta_E^-$, as required by the cancellation of divergences for the higher-twist corrections, the subtraction terms cancel altogether.

5.3.3 Discussion of special rapidity and endpoint divergences

The subtraction of the overlap region and the cancellation of special rapidity and endpoint divergences is treated differently in SCET [118, 154, 155, 156] and the TMD operator expansion literature [103, 143, 104]. Here we compare the two approaches.

In SCET, a soft mode is included explicitly, and its contribution to next-to-leading power leads to a family of soft functions [118]. At the level of bare matrix elements, however, the contributions of these soft functions cancel in the cross-section and as a result, no NLP soft factor needs to be introduced. Nevertheless, these soft functions can be used to subtract the overlap regions and define subtracted TMD distributions at NLP [154, 155, 156]. On the other hand, in the TMD operator expansion method, no soft mode is included and the overlap between the regions is subtracted by the same soft function that appears at leading power. The main consequence is that in this method, at NLP, not all rapidity divergences are canceled by the subtraction procedure. The divergences that remain after the subtraction procedure are referred to as special rapidity divergences. This includes the singular behavior in the higher-twist corrections that appear as $\xi \to 0$, which in the literature are commonly referred to as endpoint divergences.

For both approaches, the remaining divergences cancel in the cross-section between the n and $\bar{n}$ sectors. However, the subtraction and cancellation of the divergences are formulated differently between the two methods. In this work and in the SCET literature, it is formulated at all orders in perturbation theory by means of a soft matrix element. After the singular behavior of the jet functions has been subtracted, the divergent subtraction terms cancel in the combination

$$\int_0^1 \mathrm{d}\xi\, H_2(\xi)\, J_{11,\bar{n}}(\mathbf{b}^2, \zeta)\, \frac{S_{21,\bar{n}}(\xi, \mathbf{b}^2, \delta_E^+, 2\delta^+\delta^-) - S_{21,n}(\xi, \mathbf{b}^2, \delta_E^-, 2\delta^+\delta^-)}{\mathcal{S}_{\rm LP}(\mathbf{b}^2, 2\delta^+\delta^-)}\, J_{11,n}(\mathbf{b}^2, \zeta)\,. \tag{5.65}$$

Since the hard function contains logarithms of ξ at higher orders in perturbation theory, the only way for the divergences to cancel in the above expression is to have $\delta_E^+ = \delta_E^-$. The above cancellation holds at the bare and renormalized level, however, for the latter, the distributions for the n and $\bar{n}$ sectors have to be evolved together from the same initial to the same final scale.

In refs. [143, 104, 105], on the other hand, the cancellation of special rapidity divergences is formulated order-by-order in perturbation theory. In ref. [104] a subtracted

distribution is defined by

$$\boldsymbol{J}_{21}(\xi, \mathbf{b}^2) = J_{21}(\xi, \mathbf{b}^2) - \big[\mathcal{R}_{21} \otimes J_{11}\big](\xi, \mathbf{b}^2)\,, \tag{5.66}$$

where $\mathcal{R}$ is to be constructed order-by-order in α_s such that the convolution between $\boldsymbol{J}_{21}$ and H_2 is finite. Note that we have converted their expression to our notation. At leading order in perturbation theory, the hard function contains no terms involving $\ln \xi$, and so no constraint on the rapidity regulators arises. However, at higher orders in perturbation theory one would run into additional divergences coming from the integral of $\ln \xi$ in the hard function with the $1/(\xi - i\delta_E^{\pm})$ in the jet functions, leading to $\ln^2 \delta_E^{\pm}$. It is the cancellation of these additional divergences that constrains $\delta_E^+ = \delta_E^-$. We, therefore, conjecture that if the approach of ref. [104] is extended to higher orders, one would find such a constraint.

5.3.4 Renormalization and evolution

The subtracted jet functions defined above are at the bare level and require renormalization. Since renormalization and evolution takes place at the operator level, it is independent of the recoil-free jet algorithm that is employed.

For the twist-2 jet functions the renormalization is multiplicative, and we define the renormalized jet function as

$$J_{11,\bar{n}}(\mathbf{b}^2, \mu, \zeta) = Z_{J_{11}}(\zeta, \mu, \epsilon)\, J_{11,\bar{n}}^{\text{bare,sub}}(\mathbf{b}^2, \zeta, \epsilon)\,. \tag{5.67}$$

The renormalized jet functions depend on a renormalization scale μ and their evolution is given by

$$\frac{\mathrm{d}}{\mathrm{d}\ln\mu^2} J_{11}(\mathbf{b}^2, \mu, \zeta) = \frac{1}{2}\left[\Gamma_{\text{cusp}} \ln\left(\frac{\mu^2}{\zeta}\right) - \gamma_V\right] J_{11}(\mathbf{b}^2, \mu, \zeta)\,. \tag{5.68}$$

Here, Γ_{cusp} is the cusp anomalous dimension and γ_V is the anomalous dimension of the quark vector form factor, which to one-loop are given by,

$$\Gamma_{\text{cusp}} = 4a_s C_F + \mathcal{O}(a_s^2)\,, \qquad \gamma_V = -6a_s C_F + \mathcal{O}(a_s^2)\,. \tag{5.69}$$

The same equations apply to J'_{11} as the renormalization and evolution kernels do not depend on b.

The renormalization and evolution of the twist-3 operators is well known [142, 157, 158, 159, 104] and involves a convolution in the momentum fraction ξ. A few simplifications allow us to recast the evolution presented in refs. [142, 104] in a more elegant form. Since we consider large radii jets, our twist-3 jet functions depend on a single momentum fraction ξ. In our case, ξ is restricted to the interval $[0, 1]$, which can be shown by inserting a complete set of states in between each field that enters the matrix-element definition of the jet function. Because of this constraint, the mixing between different regions of momentum fraction space and mixing between T-even and T-odd contributions, as discussed in ref. [104], is absent in our case. Following this, the renormalized twist-3 jet functions can be expressed as

$$J_{21,\bar{n}}(\xi, \mathbf{b}^2, \mu, \zeta) = \int_0^1 \mathrm{d}\xi'\, Z_{J_{21}}(\xi, \xi', \mu, \zeta, \epsilon)\, J_{21,\bar{n}}^{\text{bare,sub}}(\xi', \mathbf{b}^2, \zeta, \epsilon)\,, \tag{5.70}$$

and the evolution reads

$$\frac{\mathrm{d}}{\mathrm{d}\ln\mu^2} J_{21,\bar{n}}(\xi,\mathbf{b}^2,\mu,\zeta,\delta_E^+) = \int_0^1 \mathrm{d}\xi'\,\gamma_{J_{21}}(\xi,\xi',\mu,\zeta)\,J_{21,\bar{n}}(\xi',\mathbf{b}^2,\mu,\zeta,\delta_E^+)\,. \tag{5.71}$$

The anomalous dimension for the twist-3 jet functions has been calculated to one-loop order [142] and is given by

$$\begin{aligned}\gamma_{J_{21}}(\xi,\xi',\mu,\zeta) = a_s\Bigg\{&\delta(\xi-\xi')\left[2C_F\ln\left(\frac{\mu^2}{\zeta}\right)+3C_F-2C_A\ln\xi-2C_F\ln\bar{\xi}\right]\\ &+C_A\left(\left[\frac{\Theta(\xi'-\xi)}{\xi'-\xi}\right]_+-\left[\frac{\Theta(\xi-\xi')}{\xi'-\xi}\right]_+ +\Theta(\xi'-\xi)\frac{\xi\xi'-\bar{\xi}}{\xi'}-\Theta(\xi-\xi')\frac{\bar{\xi}(\bar{\xi}'-\xi\xi')+\xi}{\xi\bar{\xi}'}\right)\\ &-(2C_F-C_A)\left(\Theta(\xi-\bar{\xi}')\frac{\bar{\xi}[2\xi-(1+\xi)\bar{\xi}']}{\xi\xi'}+\Theta(\bar{\xi}'-\xi)\frac{\xi\xi'}{\bar{\xi}'}\right)\Bigg\}\,.\end{aligned} \tag{5.72}$$

The subtracted and renormalized jet functions also depend on the rapidity scale ζ, in addition to their renormalization scale dependence. For all jet functions the rapidity scale dependence is described by the Collins-Soper kernel, but for J'_{11} there is an extra additive term as the Collins-Soper kernel depends also on b. The rapidity evolution is given by

$$\frac{\mathrm{d}}{\mathrm{d}\ln\zeta} J_{11}(\mathbf{b}^2,\mu,\zeta) = -\mathcal{D}(\mathbf{b}^2,\mu)\,J_{11}(\mathbf{b}^2,\mu,\zeta)\,, \tag{5.73}$$

$$\frac{\mathrm{d}}{\mathrm{d}\ln\zeta} J'_{11}(\mathbf{b}^2,\mu,\zeta) = -\mathcal{D}(\mathbf{b}^2,\mu)\,J'_{11}(\mathbf{b}^2,\mu,\zeta) - 2\frac{\mathrm{d}\mathcal{D}(\mathbf{b}^2,\mu)}{\mathrm{d}\ln\mathbf{b}^2}\,J_{11}(\mathbf{b}^2,\mu,\zeta)\,, \tag{5.74}$$

$$\frac{\mathrm{d}}{\mathrm{d}\ln\zeta} J_{21}(\xi,\mathbf{b}^2,\mu,\zeta) = -\mathcal{D}(\mathbf{b}^2,\mu)\,J_{21}(\xi,\mathbf{b}^2,\mu,\zeta)\,, \tag{5.75}$$

where $\mathcal{D}(\mathbf{b}^2,\mu)$ is the Collins-Soper kernel.

In principle, one could worry about the role of the subtraction term in the evolution. Specifically, one could argue that the introduction of subtraction terms alters the anomalous dimension. However, the contribution of the subtraction term cancels between the two jet functions in the cross-section. Therefore, as long as one evolves the jet functions from the two collinear sectors together, the presence of the subtraction term will not have an effect on phenomenology.

5.4 Ingredients at order a_s

In the previous sections, we obtained a factorization formula for the hadronic tensor in terms of a set of jet functions. While the factorization relies on a recoil-free jet axis, the form of the factorization and the above definitions are independent of the precise choice. In order to make a theoretical prediction for the cross-section, however, the jet functions must be calculated for a specific jet axis. We discuss the jet axes we consider in sec. 5.4.1, and we will present the calculation of the corresponding jet functions in sec. 5.4.2.

5.4.1 Jet algorithms

In this work, we consider the jet axes defined through the E^n-recombination schemes, with the special case of the winner-take-all (WTA) axis corresponding to the $n \to \infty$ limit. This is a direct generalization of the p_T^n-scheme [160, 161] to e^+e^- collisions. In principle, these axes also depend on the clustering, e.g. anti-k_T vs. Cambridge/Aachen, but this distinction is not relevant at the order we are working, where the final state in the fixed-order jet function contains at most two partons[3]. The resummed jet function will of course contain the dominant effect of multiple emissions.

For all axes, we consider the large radius limit, such that all final-state particles will be clustered into the jet. For this reason, we write the final state of the jet function as $|J_{\rm alg}\rangle$. The jet axis enters our calculation as follows

$$|J_{\rm alg}\rangle \langle J_{\rm alg}| = (2\pi)^{d-1} \sum_X \delta^{(d-2)}\big(\mathbf{P}_J^{\rm alg}\big) |X\rangle \langle X| \,. \tag{5.76}$$

Here X is the collinear final state produced by the fields, and the prefactor cancels that of the phase-space integral over the total jet momentum. Our transverse momentum measurement is encoded in the transverse position of the fields, by fixing our coordinate system such that the jet transverse momentum $\mathbf{P}_J^{\rm alg}$ vanishes. This allowed us to use the same operators as in other transverse momentum measurements.

We now present the specific formulae to determine the transverse momentum of the jet for the E^n scheme, which depends on the number of particles in the final state. In the case where the final state consists of a single parton with momentum k, we simply have $\mathbf{P}_J = \mathbf{k}$. When the final state contains two partons with on-shell momenta k_1 and k_2, respectively, the 3-momentum of the jet in the E^n-scheme is given by

$$\vec{P}_J^{E^n} = \frac{k_1^0 + k_2^0}{\sqrt{(k_1^0)^{2n} + 2(k_1^0)^{n-1}(k_2^0)^{n-1}\vec{k}_1\cdot\vec{k}_2 + (k_2^0)^{2n}}} \left[(k_1^0)^{n-1}\vec{k}_1 + (k_2^0)^{n-1}\vec{k}_2\right], \tag{5.77}$$

where the complicated prefactor arises from the condition that the resulting 4-momentum is massless. However, up to NLP, we can approximate $\vec{k}_1\cdot\vec{k}_2 \approx k_1^0 k_2^0$, since their angle is small due to being in the same collinear direction. This leads to

$$\mathbf{P}_J^{E^n} = \frac{k_1^0 + k_2^0}{(k_1^0)^n + (k_2^0)^n} \left[(k_1^0)^{n-1}\mathbf{k}_1 + (k_2^0)^{n-1}\mathbf{k}_2\right] + \mathcal{O}\Big(\frac{Q_T^3}{Q^2}\Big) \,. \tag{5.78}$$

We will restrict ourselves to $n > 1$ for which the resulting jet axis is recoil-free and our factorization analysis is justified. For $n = 1$, $\mathbf{P}_J^{E^n}$ is simply the total transverse momentum of particles in the jet, and thus not recoil-free. The WTA recombination scheme corresponds to the $n \to \infty$ limit, in which case eq. 5.78 simplifies to

$$\mathbf{P}_J^{\rm WTA} = \Theta(k_1^0 - k_2^0)\,\frac{k_1^0 + k_2^0}{k_1^0}\,\mathbf{k}_1 + \Theta(k_2^0 - k_1^0)\,\frac{k_1^0 + k_2^0}{k_2^0}\,\mathbf{k}_2 \,. \tag{5.79}$$

[3] This dependence has been studied in ref. [79] at order a_s^2 using EVENT2 [162].

5.4.2 Calculation

We now calculate all jet functions to first order in a_s. For convenience, we summarize their definitions here. The bare and unsubtracted jet functions are defined as

$$
\begin{aligned}
J^{\text{bare}}_{11,\bar{n}}(\mathbf{b}^2) &= \frac{1}{2N_c}\int\frac{\mathrm{d}y^-}{2\pi}\,e^{iy^-q^+}\;\mathrm{tr}\Big[\gamma^+\,\langle 0|\,U_{1,\bar{n}}(y^-,b)\,|J^{\bar{n}}_{\text{alg}}\rangle\,\langle J^{\bar{n}}_{\text{alg}}|\,\overline{U}_{1,\bar{n}}(0,0)\,|0\rangle\Big]\,,\\
J'^{\text{bare}}_{11,\bar{n}}(\mathbf{b}^2) &= b^\mu\frac{\partial}{\partial b^\mu}J^{\text{bare}}_{11,\bar{n}}(b)\,,\\
J^{\text{bare}}_{21,\bar{n}}(\xi,\mathbf{b}^2) &= n^\mu\bar{n}^\nu b^\rho\epsilon_{\mu\nu\rho\sigma}\,\frac{1}{\xi-i\delta_E^+}\,\frac{1}{2N_c}\int\frac{\mathrm{d}y_1^-}{2\pi}\frac{\mathrm{d}y_2^-}{2\pi}\,e^{i(\bar{\xi}y_1^-+\xi y_2^-)q^+}\\
&\quad\times\mathrm{tr}\Big[\sigma^{\sigma+}\gamma^5\,\langle 0|\,U_{2,\bar{n}}(\{y_1^-,y_2^-\},b)\,|J^{\bar{n}}_{\text{alg}}\rangle\,\langle J^{\bar{n}}_{\text{alg}}|\,\overline{U}_{1,\bar{n}}(0,0)\,|0\rangle\Big]\,,
\end{aligned}
\tag{5.80}
$$

with U_1 and U_2 defined in eqs. 5.20 and 5.21 and similar definitions hold for the jet functions in the n direction. The subtracted jet functions are given by

$$
\begin{aligned}
J^{\text{bare,sub}}_{11,\bar{n}}(\mathbf{b}^2,\zeta,\epsilon) &= \frac{J^{\text{bare}}_{11,\bar{n}}(\mathbf{b}^2,\epsilon,\delta_E^+)}{\sqrt{\mathcal{S}_{\text{LP}}(\mathbf{b}^2,\epsilon,(\delta_E^+)^2\zeta)}}\,,\\
J'^{\text{bare,sub}}_{11,\bar{n}}(\mathbf{b}^2,\zeta,\epsilon) &= b^\mu\frac{\partial}{\partial b^\mu}J^{\text{bare,sub}}_{11,\bar{n}}(\mathbf{b}^2,\zeta,\epsilon)\,,\\
J^{\text{bare,sub}}_{21,\bar{n}}(\xi,\mathbf{b}^2,\zeta,\epsilon) &= \frac{J^{\text{bare}}_{21,\bar{n}}(\xi,\mathbf{b}^2)}{\sqrt{\mathcal{S}_{\text{LP}}(\mathbf{b}^2,\epsilon,(\delta_E^+)^2\zeta)}} - S^{\text{bare}}_{21,\bar{n}}(\xi,\mathbf{b}^2,\epsilon,\delta_E^+,(\delta_E^+)^2\zeta)\,J^{\text{bare,sub}}_{11,\bar{n}}(\mathbf{b}^2,\zeta,\epsilon)\,,
\end{aligned}
\tag{5.81}
$$

with

$$
\mathcal{S}^{\text{bare}}_{\text{LP}}(\mathbf{b}^2,\epsilon,2\delta^+\delta^-) = \frac{1}{N_c}\,\mathrm{tr}_c\big\{\langle 0|\,[\infty\bar{n}+b,b][b,\infty n+b][\infty n,0][0,\infty\bar{n}]\,|0\rangle\big\}\,,
\tag{5.82}
$$

$$
\begin{aligned}
S^{\text{bare}}_{21,\bar{n}}(\xi,\mathbf{b}^2,\epsilon,\delta_E^+,2\delta^+\delta^-) &= +\frac{b_\rho}{\xi-i\delta_E^+}\int\frac{\mathrm{d}y_2^-}{2\pi}\,e^{i\xi y_2^-q^+}\,\frac{1}{N_c}\,\mathrm{tr}\Big[\langle 0|\,[b+y_2^-n+\infty n,b+y_2^-n]\\
&\quad\times[b+y_2^-n,b+y_2^-n+\infty\bar{n}]gF^{\rho+}(y_2^-n+b)\;|X\rangle\,\langle X|\,[\infty\bar{n},0][0,\infty n]\,|0\rangle\Big]\,.
\end{aligned}
$$

Finally, the renormalized jet functions are given by

$$
\begin{aligned}
J_{11,\bar{n}}(\mathbf{b}^2,\mu,\zeta) &= Z_{J_{11}}(\zeta,\mu,\epsilon)\,J^{\text{bare,sub}}_{11,\bar{n}}(\mathbf{b}^2,\zeta,\epsilon)\,,\\
J_{21,\bar{n}}(\xi,\mathbf{b}^2,\mu,\zeta) &= \int_0^1\mathrm{d}\xi'\,Z_{J_{21}}(\xi,\xi',\mu,\zeta,\epsilon)\,J^{\text{bare,sub}}_{21,\bar{n}}(\xi',\mathbf{b}^2,\zeta,\epsilon)\,.
\end{aligned}
\tag{5.83}
$$

Bare jet functions

The (leading-order) matrix elements that are required in this calculation are given by

$$
\langle 0|\,U_{1,\bar{n}}(y^-,b)\,|q(p)\rangle^{(0)} = e^{i\mathbf{b}\cdot\mathbf{p}}e^{-iy^-p^+}\,u(p)\,,
\tag{5.84}
$$

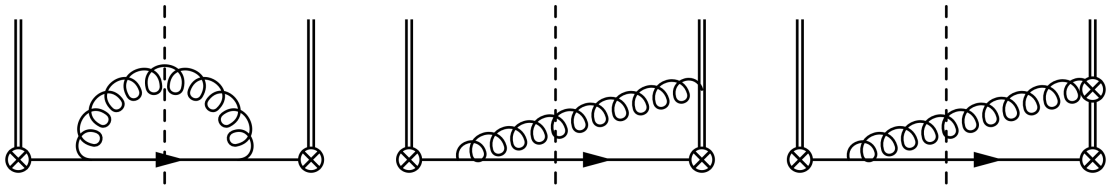

Figure 5.2: Diagrams for the matrix elements that enter the calculation of the twist-2 jet function at NLO (left and middle) and the twist-3 jet function at LO (right). The double line represents the Wilson line, and the $\otimes$ denote insertions of the quark field (at the corners) and gluon field strength (on the double line). The diagrams that give a vanishing result are not shown.

$$\langle 0|\, U_{1,\bar{n}}(y^-,b)\,|q(p-k)g(k)\rangle^{(0)} = e^{i\mathbf{b}\cdot\mathbf{p}}e^{-iy^-p^+}\,(-g)\left[\frac{\not{p}\gamma^\nu}{p^2}-\frac{n^\nu}{k^+-i\delta^+}\right]t^a\,u(p-k)\epsilon^a_\nu(k)\,,$$

$$\langle 0|\, U_{2,\bar{n}}(\{y_1^-,y_2^-\},b)\,|q(p-k)g(k)\rangle^{(0)} = e^{i\mathbf{b}\cdot\mathbf{p}}e^{-iy_1^-(p-k)^+}e^{-iy_2^-k^+}\,(-ig)\left[\not{k}_T n^\mu - k^+\gamma_T^\mu\right]t^a\,u(p-k)\epsilon^a_\mu(k)\,,$$

with the relevant diagrams shown in fig. 5.2. The index a on the polarization vector indicates the color of the gluon (though technically is not part of the polarization). We have omitted the virtual corrections, as the virtual correction to J_{11} vanishes in dimensional regularization, and the virtual correction to J_{21} is exactly zero. Inserting the expressions in eq. 5.84 in eq. 5.80, we find to order a_s

$$\begin{aligned} J^{\rm bare}_{11,\bar{n}} = 1 + \; & 4g^2C_F\int\frac{\mathrm{d}^dp}{(2\pi)^d}\frac{\mathrm{d}^dk}{(2\pi)^d}\,(2\pi)\delta_+(k^2)\,(2\pi)\delta_+[(p-k)^2]\,(2\pi)^{d-1}\delta^{(d-2)}(\mathbf{P}_J^{\rm alg}) \\ & \times e^{i\mathbf{b}\cdot\mathbf{p}}\,\delta(p^+-q^+)\,\frac{k^+}{p^2}\left[\frac{(p^+)^2+(p^+-k^+)^2}{(k^+)^2+(\delta^+)^2}-\epsilon\right], \end{aligned} \tag{5.85}$$

$$\begin{aligned} J^{\rm bare}_{21,\bar{n}} = & -4ig^2C_F\,\frac{1}{\xi-i\delta_E^+}\int\frac{\mathrm{d}^dp}{(2\pi)^d}\frac{\mathrm{d}^dk}{(2\pi)^d}\,(2\pi)\delta_+(k^2)\,(2\pi)\delta_+[(p-k)^2]\,(2\pi)^{d-1}\delta^{(d-2)}(\mathbf{P}_J^{\rm alg}) \\ & \times e^{i\mathbf{b}\cdot\mathbf{p}}\,\delta(q^+-p^+)\delta(\xi q^+-k^+)\,\frac{(q^+)^2}{p^2}\,(\bar{\xi}+\epsilon\xi)\left[\bar{\xi}k^\mu-\xi(p-k)^\mu\right]b_\mu\,. \end{aligned} \tag{5.86}$$

These expressions only depend on the details of the jet algorithm through $\mathbf{P}_J^{\rm alg}$.

From here, one performs the integral over $\mathbf{k}$ using $\delta^{(d-2)}(\mathbf{P}_J^{\rm alg})$, and the lightcone components of p and k. For the E^n scheme,

$$p^2 = \frac{\xi\bar{\xi}(\bar{\xi}^n+\xi^n)^2}{(\xi^n\bar{\xi}-\xi\bar{\xi}^n)^2}\mathbf{p}^2\,, \tag{5.87}$$

leading to

$$J^{\rm bare}_{11,\bar{n}} = 1+\frac{g^2C_F}{(2\pi)^{d-1}}\left(\int\mathrm{d}^{d-2}\mathbf{p}\,\frac{e^{i\mathbf{b}\cdot\mathbf{p}}}{\mathbf{p}^2}\right)\int_0^1\mathrm{d}\xi\left|\frac{\bar{\xi}^n+\xi^n}{\xi^{n-1}-\bar{\xi}^{n-1}}\right|^{d-4}\left[\frac{\xi(1+\bar{\xi}^2)}{\xi^2+(\delta_E^+)^2}-\epsilon\xi\right], \tag{5.88}$$

$$J_{21,\bar{n}}^{\text{bare}} = -\frac{ig^2 C_F}{(2\pi)^{d-1}} \left(\int \mathrm{d}^2\mathbf{p}\, \frac{e^{i\mathbf{b}\cdot\mathbf{p}}}{\mathbf{p}^2}\, \mathbf{p}\cdot\mathbf{b} \right) \Theta(\xi)\Theta(\bar{\xi}) \frac{\bar{\xi}}{\xi - i\delta_E^+} \frac{\xi^n + \bar{\xi}^n}{\xi^{n-1} - \bar{\xi}^{n-1}} \,. \tag{5.89}$$

The remaining integral over $\mathbf{p}$ in J_{11} can then be performed by using

$$\int \mathrm{d}^{d-2}\mathbf{p}\, \frac{e^{i\mathbf{b}\cdot\mathbf{p}}}{\mathbf{p}^2} = 4^{-\epsilon}\pi^{1-\epsilon}\Gamma(-\epsilon)\,(\mathbf{b}^2)^{\epsilon} \,, \tag{5.90}$$

and the integral that appears for J_{21} can be obtained by differentiating with respect to $\mathbf{b}$. Finally, we perform the integral over ξ for $J_{11,\bar{n}}$ and expand the result in ϵ

$$J_{11,\bar{n}}^{\text{bare}} = 1 + a_s C_F \left\{ \left[\frac{1}{\epsilon} + \ln\!\left(\frac{\mu_0^2 \mathbf{b}^2}{4e^{-2\gamma_E}} \right) \right] (3 + 4\ln\delta_E^+) + J_{C_F} \right\} , \tag{5.91}$$

$$J_{21,\bar{n}}^{\text{bare}} = -4a_s C_F\, \Theta(\xi)\Theta(\bar{\xi}) \frac{\bar{\xi}}{\xi - i\delta_E^+} \frac{\xi^n + \bar{\xi}^n}{\bar{\xi}^{n-1} - \xi^{n-1}} \,, \tag{5.92}$$

with

$$J_{C_F} = 1 + 4\int_0^1 \mathrm{d}\xi\, \frac{1 + (1-\xi)^2}{\xi}\, \ln\left| \frac{(1-\xi)^n + \xi^n}{(1-\xi)^{n-1} - \xi^{n-1}} \right| . \tag{5.93}$$

Subtraction and renormalization

To obtain the subtracted and renormalized jet functions at first order in a_s, we need the LP and NLP soft functions and the renormalization factor $Z_{J_{11}}$ to order a_s. We do not need the one-loop expression for $Z_{J_{21}}$ at this order. The LP soft function with δ regulator has been calculated to one-loop order in ref. [17], and the result reads

$$\begin{aligned} \mathcal{S}_{\text{LP}}(\mathbf{b}^2, \epsilon, 2\delta^+\delta^-) = 1 - 4a_s C_F \left\{ \frac{1}{\epsilon^2} - \left[\frac{1}{\epsilon} + \ln\left(\frac{\mu^2\mathbf{b}^2}{4e^{-2\gamma_E}} \right) \right] \ln\left(\frac{2\delta^+\delta^-}{\mu^2} \right) - \frac{1}{2}\ln^2\left(\frac{\mu^2\mathbf{b}^2}{4e^{-2\gamma_E}} \right) - \frac{\pi^2}{12} \right\} \\ + \mathcal{O}(a_s^2) \,. \end{aligned} \tag{5.94}$$

The renormalization factor for J_{11} is given by

$$Z_{J_{11}}(\zeta, \mu, \epsilon) = 1 + 2a_s C_F \left\{ -\frac{1}{\epsilon^2} - \frac{1}{\epsilon}\left[\ln\left(\frac{\mu^2}{\zeta} \right) + \frac{3}{2} \right] \right\} . \tag{5.95}$$

The NLP soft function can be calculated from its matrix element definition. At leading order only one diagram contributes, depicted in fig. 5.3. The diagrams that do not contribute are two virtual diagrams which vanish in dimensional regularization and a real-emission diagram that vanishes because $n^2 = \bar{n}^2 = 0$. The remaining diagram results in

$$S_{21,\bar{n}}^{\text{bare}}(\xi, \mathbf{b}^2, \epsilon, \delta_E^+, 2\delta^+\delta^-) = \frac{g^2 C_F}{(2\pi)^{d-1}} \frac{b_\rho \partial^\rho}{\xi - i\delta_E^+} \int \mathrm{d}^d k\, \delta_+(k^2)\delta(\xi q^+ - k^+)\, \frac{e^{-ib\cdot k}}{k^- - i\delta^-} + \mathcal{O}(a_s^2) \,. \tag{5.96}$$

The integrals over k^+ and k^- can be performed using the delta functions and the remaining integral over $\mathbf{k}$ can be performed using eq. 5.90. The final result for the NLP soft function reads

$$S_{21,\bar{n}}^{\text{bare}}(\xi, \mathbf{b}^2, \epsilon, \delta_E^+, 2\delta^+\delta^-) = -4a_s C_F\, \Theta(\xi) \frac{1}{\xi - i\delta_E^+} + \mathcal{O}(a_s^2) \,. \tag{5.97}$$

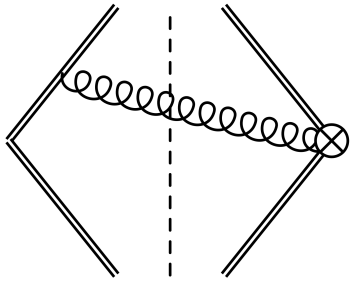

Figure 5.3: The only diagram contributing to the NLP soft function at leading order. The $\otimes$ denotes the field strength operator and the double lines represent the Wilson lines.

Final results

We now present the final results for all the ingredients of the cross section to first order in a_s. The subtracted and renormalized jet functions read

$$\begin{aligned}
J_{11,\bar{n}}^{E^n}(\mathbf{b}^2) &= 1 + a_s C_F \left\{ -\ln^2\left(\frac{\mu^2\mathbf{b}^2}{4e^{-2\gamma_E}}\right) + \ln\left(\frac{\mu^2\mathbf{b}^2}{4e^{-2\gamma_E}}\right)\left[3 + 2\ln\left(\frac{\mu^2}{\zeta}\right)\right] + J_{C_F} - \frac{\pi^2}{6} \right\}, \\
J'^{E^n}_{11,\bar{n}}(\mathbf{b}^2) &= 2a_s C_F \left\{ -2\ln\left(\frac{\zeta\mathbf{b}^2}{4e^{-2\gamma_E}}\right) + 3 \right\}, \\
J_{21,\bar{n}}^{E^n}(\xi, \mathbf{b}^2) &= -4a_s C_F\, \Theta(\xi)\Theta(\bar{\xi})\, \frac{[1+\xi-\xi^2]\xi^{n-2} - [2-\xi](1-\xi)^{n-1}}{(1-\xi)^{n-1} - \xi^{n-1}}\,.
\end{aligned} \tag{5.98}$$

Note that since J_{21} and J'_{11} only start at order a_s, the renormalization does not effect them at this order in perturbation theory. The WTA axis corresponds to the $n \to \infty$ limit. In this case,

$$\begin{aligned}
\lim_{n\to\infty} J_{C_F} &= 7 - \frac{2\pi^2}{3} - 6\log(2)\,, \\
\lim_{n\to\infty} \frac{[1+\xi-\xi^2]\xi^{n-2} - [2-\xi](1-\xi)^{n-1}}{(1-\xi)^{n-1} - \xi^{n-1}} &= -(2-\xi)\Theta(\tfrac{1}{2}-\xi) - \frac{1+\xi-\xi^2}{\xi}\Theta(\xi-\tfrac{1}{2})\,.
\end{aligned} \tag{5.99}$$

The twist-3 jet function J_{21} is shown in fig. 5.4 for $n = 2, 3$ and ∞ (which corresponds to WTA). By dividing J_{21} by a_s, we removed dependence on the renormalization scale. Note that these jet functions have a singularity at $\xi = \frac{1}{2}$ arising from the E^n scheme. However, since the hard function is smooth at this point, there is a cancellation between $\xi = \frac{1}{2} + \delta\xi$ and $\xi = \frac{1}{2} - \delta\xi$ to yield a finite result (principle value). For completeness, we also present the one-loop results for the hard functions,

$$\begin{aligned}
H_1(Q^2, \mu) &= 1 + 2a_s C_F \left(-\ln^2\left(\frac{Q^2}{\mu^2}\right) + 3\ln\left(\frac{Q^2}{\mu^2}\right) - 8 + \frac{7\pi^2}{6} \right), \\
H_2(\xi, Q^2, \mu) &= 1 + 2a_s \left[C_F \left(-\ln^2\left(\frac{Q^2}{\mu^2}\right) + 2\ln\left(\frac{Q^2}{\mu^2}\right) - \frac{11}{2} + \frac{7\pi^2}{6} - i\pi \right) - \tfrac{1}{2} C_A \frac{\ln\xi}{1-\xi} \right.
\end{aligned}$$

$$- \left(C_F - \tfrac{1}{2}C_A\right)\left(\ln\left(\frac{Q^2}{\mu^2}\right) + i\pi + \tfrac{1}{2}\ln(1-\xi) - 2\right)\frac{\ln(1-\xi)}{\xi}\Bigg]. \tag{5.100}$$

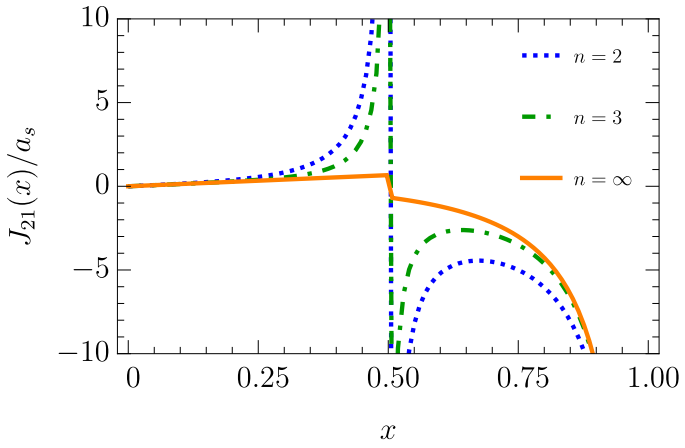

Figure 5.4: The twist-3 jet function J_{21} in eq. 5.98, divided by a_s, as function of x for $n = 2, 3, \infty$.

Conclusions

This thesis represents a significant contribution to the understanding of transverse momentum dependent distributions (TMDs) and their pivotal role in unraveling the intricate structure of hadrons and the distribution of quarks and gluons within them. We have underscored the fundamental importance of TMDs across a spectrum of theoretical frameworks and experimental contexts.

Our exploration has not only explored the theoretical intricacies of TMDs but has also provided concrete methodologies for their study within the framework of factorization theorems. By delving into processes such as Drell-Yan, semi-inclusive deep inelastic scattering (SIDIS), and semi-inclusive annihilation (SIA), we have demonstrated the universality and versatility of TMDs in describing a diverse array of phenomena in high-energy particle physics.

Moreover, the intricacies of factorization have been enriched by a dual approach, navigating through the realms of soft-collinear effective theory (SCET) and the background field method. By extending our analysis to next-to-leading power in the small transverse momentum expansion, we have advanced the frontier of theoretical understanding within this field, laying the groundwork for future developments.

The original contributions of this thesis have been multifaceted. Firstly, our detailed investigation into dijet production in SIDIS has not only shed light on the sensitivity of this process to gluon TMDs but has also highlighted its potential as a target for future experimental endeavors, particularly at facilities like the Electron-Ion Collider (EIC). Secondly, our work in establishing factorization theorems for dijet production in SIA at next-to-leading power represents a significant milestone in the theoretical toolkit available for studying jet production processes and NLP contributions.

In particular, we have established a new factorization theorem for dijet and heavy-meson pair production in DIS which can be valuable in the quest of processes with a clear sensitivity to gluon TMDs. The factorization involves a new soft function, which we have calculated at one-loop, and whose anomalous dimension has been deduced at two and three loops from consistency relations. All the calculations have been performed with the δ-regulator, combined with standard dimensional regularization. The cross-section is sensitive to both unpolarized and linearly polarized gluon TMDs and a new TMD soft function is presented in the factorization theorem.

The influence of this new soft function is certainly an element that should be studied in the future. In particular one should understand how large is its non-perturbative contribution to the cross-section and whether it appears in multiple processes, i.e. whether it is a universal quantity.

The evolution of the functions that appear in the factorization theorem is non-trivial and we propose an original solution, which is generic and independent of the resummation framework. We also note that it is consistent with the ζ-prescription of TMD [33] which we implement in this work. The used prescription allows us to separate the evolution kernels from other scale-independent factors in the cross-section so that in our final computations we can use some results already coded in the literature. This is the case for the TMD and their respective evolution kernels extracted from DY and SIDIS data and presented in the code Artemide [81].

The phenomenological analysis that we have performed has revealed several issues that need further study in the future. Estimating the errors due to scale dependence, we have found that several functions need a higher loop calculation to achieve sufficient precision for the low-energy jets that will be available at EIC. This is the case for instance of the collinear-soft function that appears in the dijet process and more urgently on the heavy hadron jet function. The fact that the perturbative convergence of these functions is limited to small values of the b may lead to consider also a re-factorization of these functions, such that the small-b effects are separately resummed. This possibility can eventually be considered in future works.

In all cross-sections, we have found a contribution of unpolarized and linearly polarized gluon TMD. For both of these distributions, we have used their re-factorization in coefficient functions and collinear PDF studied at higher loops in the literature [30, 39, 84, 163]. In accordance with this well-tested procedure, the linearly polarized gluon contribution results to be particularly suppressed in all considered cases, because its matching to collinear PDF starts at order α_s^1, instead of α_s^0 like the unpolarized distributions. The effect of this suppression is particularly evident in the estimate of the angular modulation of $\cos 2\phi_r$ asymmetry that is here estimated to be around 5%. The study of next-to-leading power effects is beyond the purpose of the present work, therefore further study is necessary to confirm the magnitude of this asymmetry.

A source of uncertainty in our prediction comes from the usage of models for many functions that have not been yet compared against data. In this case, we have studied several possibilities with simple Gaussian models, assigning values to the non-perturbative parameters according to an educated guess. The models do not alter the overall conclusions about scale choices or precision but can have some effect on the shape of the curves that we have computed. Only a strict comparison with data or eventual lattice calculations can finally resolve this issue.

As a result of this study, we can see that the extraction of gluon TMDs from dijet processes at the EIC is conditioned yet by the possible theoretical and experimental precision. In particular, the linearly polarized gluon TMD appears generally too suppressed and hardly accessible if one uses the usual matching of TMDs onto their collinear counterpart distributions. Nevertheless, the discussed theoretical issues can potentially be solved or improved in future studies.

On the other hand, our study on the next-to-leading power contributions to dijet production in dilepton annihilation marks an advancement in the theoretical arsenal for investigating jet production phenomena and NLP contributions.

With the exceptional precision of the Large Hadron Collider and the forthcoming Electron-Ion Colliders, there has been a surge in interest surrounding TMDs, offering a

unique opportunity to explore these distributions with unprecedented accuracy. A deeper exploration needs a heightened precision in their theoretical depiction, demanding a deeper understanding of the factorization theorem for cross-sections differentially dependent on transverse momenta.

In the work presented, we examine specific facets of the recently developed operator basis contributing to the differential cross sections at the next-to-leading power (NLP). Our focus has been on jets, which provide an infrared and collinear safe observable computable within perturbation theory. To simplify the description, we have limited ourselves to large radii ensuring that all energetic radiation remains confined within the jets. Utilizing a recoil-free jet recombination scheme, we can avoid non-global logarithms.

We have also explored how higher twist operators emerging at NLP contribute to the characterization of jets, introducing novel measurable effects. These aspects have been described through the prism of a $e^+e^- \to 2$ jets process, notable for its theoretical simplicity and experimental relevance. The culmination of our analysis has yielded the final factorized hadronic tensor, obtained by beginning with its power expansion, decomposing it into spin structures, and applying discrete symmetries. Notably, this has marked the first determination of the contribution of a twist-3 operator to a jet.

We have observed that NLP effects manifest in $e^+e^- \to 2$ jets solely when the two jets exhibit dissimilarity, such as when employing distinct recoil-free jet algorithms or replacing a jet with a hadron. Furthermore, we have computed the twist-3 jet functions utilizing the WTA axis and E^n recombination schemes at leading order in perturbation theory. We have discussed their overlap subtraction and renormalization, noting the role of the soft factor in describing the overlap, and the subsequent cancellation of special rapidity divergences.

Moreover, we have simplified the evolution equation initially derived at the operator level in ref. [103], making it much simpler in our specific scenario. Several aspects of this study hold relevance for future applications. Particularly, the measurement we consider allows for a significant simplification of the NLP formalism, rendering it more accessible. Although the process described can be measured in the Belle experiment, a detailed phenomenological analysis has been left to future studies. Additionally, exploring the impact of the nonperturbative effects studied on QCD research at the Future Circular Collider (FCC) presents an intriguing avenue. Importantly, our NLP jet analysis stands to enhance measurements of hadron structure at the EIC. Furthermore, our framework can be naturally extended to describe polarized targets at the EIC.

In conclusion, this thesis stands as a testament to the profound impact of TMDs on our understanding of particle physics. By elucidating factorization theorems and exploring novel processes, we have not only expanded the boundaries of theoretical knowledge but have also paved the way for future experimental investigations.

Appendix A

Dijet production in SIDIS

A.1 Elements of factorization

In this section, we some useful functions involved in the factorization for the dijet production in SIDIS case

A.1.1 Hard function

The hard kernel can be found in [89, 90, 91]. The μ-dependent part for both channels is given by

$$H^U_{\gamma^* g} = 1 + a_s \left[-(2C_F + C_A)\ln^2\frac{\mu^2}{\hat{s}} + \left(2C_A \ln\frac{\hat{t}\hat{u}}{\hat{s}^2} - 6C_F\right)\ln\frac{\mu^2}{\hat{s}} + \ldots \right] + \mathcal{O}(a_s^2),$$

$$H^U_{\gamma^* f} = 1 + a_s \left[-(2C_F + C_A)\ln^2\frac{\mu^2}{\hat{s}} + \left(2C_A \ln\frac{\hat{t}}{\hat{u}} + 4C_F \ln\frac{-\hat{u}}{\hat{s}} - 6C_F\right)\ln\frac{\mu^2}{\hat{s}} + \ldots \right] + \mathcal{O}(a_s^2),$$

$$H^L_{\gamma^* g} = 1 + \mathcal{O}(a_s). \tag{A.1}$$

A.1.2 Jet function

The definition of the jet function is as in [164],

$$J_{f,v}(v\cdot p, R) = \frac{1}{2\sqrt{2}N_c}\mathrm{Tr}\int d^4x e^{ipx}\langle 0|\bar{\chi}_v(p)\bar{\not{v}}\delta_{\mathrm{alg}}(R)\chi_v(0)|0\rangle \tag{A.2}$$

$$\eta_\perp^{\rho\nu} J_{g,v}(v\cdot p, R) = -\frac{1}{(N_c^2-1)}\sum_A \int d^4x(\sqrt{2}\bar{v}\cdot p)e^{ipx}\langle 0|B_v^{\perp\rho A}(x)\delta_{\mathrm{alg}}(R)gB_v^{\perp\nu A}(0)|0\rangle \tag{A.3}$$

where the symbol $\perp$ refers to the plane orthogonal to v and whose trasverse components are obtained with the tensor $\eta^\perp_{\alpha\beta} = g_{\alpha\beta} - (v_\alpha\bar{v}_\beta + \bar{v}_\alpha v_\beta)$. The perturbative calculation of the jet function can be found in [83] and is given by

$$J_i^{\mathrm{exc.}}(p_T, R, \mu) = 1 + 2a_s\left[C_i\left(\frac{1}{\epsilon^2} + \frac{\gamma_i}{\epsilon}\right)\left(\frac{\mu}{p_T R}\right)^{2\epsilon} + d_J^{i,\mathrm{alg}}\right] + \mathcal{O}(a_s^2), \tag{A.4}$$

The finite corrections $d_J^{i,\text{alg}}$ are given by

$$\begin{aligned} d_J^{i,\text{ cone}} &= C_i\Big(2\gamma_i \ln 2 - \frac{5\pi^2}{12}\Big) + \begin{cases} C_F\frac{7}{2} & \text{if } i = q \\ C_A\frac{137}{36} - T_R N_f \frac{23}{18} & \text{if } i = g \end{cases} \\ d_J^{i,k_T} &= -C_i\frac{3\pi^2}{4} + \begin{cases} C_F\frac{13}{2} & \text{if } i = q \\ C_A\frac{67}{9} - T_R N_f \frac{23}{9} & \text{if } i = g \end{cases} \end{aligned} \tag{A.5}$$

where d_J^{i,k_T} is the same constant for all k_T-type algorithms (k_T, anti-k_T, and C/A).

A.1.3 Collinear-soft function

The collinear-soft function can be found in [75] and is given by the following matrix element,

$$\mathcal{C}_i(\boldsymbol{b}, R, \mu) = \int d\boldsymbol{b}\exp(\boldsymbol{b}\cdot\boldsymbol{v}\,\bar{v}\cdot\partial)\frac{1}{N_R}\text{Tr}\langle 0|T\Big[U_n^\dagger W_t(0)\Big]\,\Theta_{\text{alg.}}\,\bar{T}\Big[W_t^\dagger U_n(0)\Big]|0\rangle\,, \tag{A.6}$$

where $\boldsymbol{v}$ is a Euclidean, two dimensional, transverse component of light-like four-vector v^μ pointing along the direction of the jet. The normalization constant N_R is simply the size of the representation for SU(N_c) of the W_t and U_n Wilson lines. For quark jets (fundamental representation) we have $N_R = N_c$ and for gluon jets (adjoint representation) we have $N_R = N_c^2 - 1$. The function $\Theta_{\text{alg.}}$ ensures that only contribution from outside the jet will contribute to the jet-imbalance. At NLO the bare collinear-soft function is given by

$$\mathcal{C}_i^{\text{bare}}(\boldsymbol{b}, R) = 1 + 4a_s C_i\frac{\exp(-\gamma_E\epsilon)\Gamma(-2\epsilon)}{\epsilon\,\Gamma(1-\epsilon)}\Big(-\frac{i\mu e^{\gamma_E}(\boldsymbol{v}\cdot\boldsymbol{b})}{|\boldsymbol{v}|\,R}\Big)^{2\epsilon} + \mathcal{O}(a_s^2). \tag{A.7}$$

A.1.4 Beam function

The quark, anti-quark and gluon beam functions are given in [30] by

$$\begin{aligned} \hat{B}_q\,(x,\boldsymbol{b}) &= \frac{1}{2}\sum_X\int\frac{d\xi^+}{2\pi}e^{-ixp^-\xi^+}\left\{T\left[\bar{q}_i\tilde{W}_n^T\right]_a\left(\frac{\xi}{2}\right)|X\rangle\gamma_{ij}^-\langle X|\bar{T}\left[\tilde{W}_n^{T\dagger}q_j\right]_a\left(-\frac{\xi}{2}\right)\right\}, \\ \hat{B}_{\bar{q}}\,(x,\boldsymbol{b}) &= \frac{1}{2}\sum_X\int\frac{d\xi^+}{2\pi}e^{-ixp^-\xi^+}\left\{T\left[\tilde{W}_n^{T\dagger}q_j\right]_a\left(\frac{\xi}{2}\right)|X\rangle\gamma_{ij}^-\langle X|\bar{T}\left[\bar{q}_i\tilde{W}_n^T\right]_a\left(-\frac{\xi}{2}\right)\right\}, \\ \hat{B}_{g\mu\nu}\,(x,\boldsymbol{b}) &= \frac{1}{xp^-}\sum_X\int\frac{d\xi^+}{2\pi}e^{-ixp^-\xi^+}\left\{T\left[F_{-\mu}\tilde{W}_n^T\right]_a\left(\frac{\xi}{2}\right)|X\rangle\langle X|\bar{T}\left[\tilde{W}_n^{T\dagger}F_{-\nu}\right]_a\left(-\frac{\xi}{2}\right)\right\}, \end{aligned} \tag{A.8}$$

where $\xi = (\xi^+, 0^-, \boldsymbol{b})_n$. The repeated color indices a ($a = 1,\ldots,N_c$ for quarks and $a = 1,\ldots,N_c^2-1$ for gluons) are summed up. The representations of the color SU(3) generators inside the Wilson lines are the same as the representation of the corresponding partons. The Wilson lines $\tilde{W}_n^T(x)$ are rooted at the coordinate x and continue to the light-cone infinity along the vector n, where it is connected by a transverse link to the transverse infinity (that is indicated by the superscript T). The TMDs are obtained from the beam functions $\hat{B}_i$ as explained in sec. 3.1.4.

A.2 Anomalous dimensions

In this appendix, we collect from the literature the anomalous dimensions of the elements of the cross-section needed to obtain the dijet soft function anomalous dimension at two and three loops for the $\gamma^* g$-channel, as explained in 3.91. We follow the standard procedure of separating all anomalous dimensions into a term proportional to the cusp anomalous dimension and a non-cusp term. We first give the three-loop cusp which applies to all functions and then proceed to give the non-cusp term for each function separately. The anomalous dimensions we give here are the ones that correspond to the renormalization group equation in 3.57.

A.2.1 The cusp anomalous dimension and β function

$$\Gamma^i_{\text{cusp}}(a_s) = 4C_i \sum_n \Gamma^{[n]} a_s^n, \qquad \gamma_{\text{cusp}}(\alpha_s) = \frac{1}{C_i}\Gamma^i_{\text{cusp}}(a_s) = 4\sum_n \Gamma^{[n]} a_s^n, \tag{A.9}$$

where

$$\begin{aligned}
\Gamma^{[1]} &= 1,\\
\Gamma^{[2]} &= \left(\frac{67}{9} - \frac{\pi^2}{3}\right) C_A - \frac{20}{9} T_F n_f,\\
\Gamma^{[3]} &= C_A^2 \left(\frac{245}{6} - \frac{134\pi^2}{27} + \frac{11\pi^4}{45} + \frac{22}{3}\zeta_3\right) + C_A T_F n_f \left(-\frac{418}{27} + \frac{40\pi^2}{27} - \frac{56}{3}\zeta_3\right)\\
&\quad + C_F T_F n_f \left(-\frac{55}{3} + 16\zeta_3\right) - \frac{16}{27} T_F^2 n_f^2,
\end{aligned} \tag{A.10}$$

and for $i = f, g$ we have $C_f = C_F$ and $C_g = C_A$. The β-function is given by

$$\beta(a_s) = -2\alpha_s \sum_{n=1} \beta^{[n-1]} a_s^n, \tag{A.11}$$

where

$$\begin{aligned}
\beta^{[0]} &\equiv \beta_0 = \frac{11}{3} C_A - \frac{4}{3} T_F n_f,\\
\beta^{[1]} &= \frac{34}{3} C_A^2 - \frac{20}{3} C_A T_F n_f - 4 C_F T_F n_f,\\
\beta^{[2]} &= \frac{2857}{54} C_A^2 + \left(2C_F^2 - \frac{205}{9} C_F C_A - \frac{1415}{27} C_A^2\right) T_F n_f + \left(\frac{44}{9} C_F + \frac{158}{27} C_A\right) T_F^2 n_f^2,\\
\beta^{[3]} &= \frac{149753}{6} + 3564\zeta_3 - \left(\frac{1078361}{162} + \frac{6508}{27}\zeta_3\right) n_f + \left(\frac{50065}{162} + \frac{6472}{81}\zeta_3\right) n_f^2 + \frac{1093}{729} n_f^3.
\end{aligned} \tag{A.12}$$

A.2.2 bHQET heavy-quark jet function

As explained in 3.73, the heavy-quark jet function factorizes into a bHQET hard function H_+ and a bHQET jet function $\mathcal{J}_{Q\to Q}$. Their anomalous dimension are given by

$$\begin{aligned}\gamma_{\mathcal{J}} &= -2\Gamma^q_{\text{cusp}} \ln\left(-i\frac{p_T\mu e^{\gamma_E}(\boldsymbol{v}\cdot\boldsymbol{b})}{m_Q|\boldsymbol{v}|}\right) + 2\delta\gamma_{\mathcal{J}}.\\ \gamma_+ &= \Gamma^q_{\text{cusp}} \ln\frac{\mu^2}{m_Q^2} + 2\delta\gamma_+\end{aligned} \tag{A.13}$$

The non-cusp anomalous dimensions for the hard function and the jet function are known up to two-loops [73] and are given by

$$\begin{aligned}\delta\gamma^{[1]}_{\mathcal{J}} &= 2C_F,\\ \delta\gamma^{[2]}_{\mathcal{J}} &= -C_F\left[C_A\left(\frac{110}{27}+\frac{\pi^2}{18}-18\zeta_3\right)+T_F n_f\left(\frac{8}{27}+\frac{2\pi^2}{9}\right)\right],\\ \delta\gamma^{[1]}_{+} &= C_F,\\ \delta\gamma^{[2]}_{+} &= C_F\left[C_F\left(\frac{3}{2}-2\pi^2+24\zeta_3\right)+C_A\left(\frac{373}{54}+\frac{5}{2}\pi^2-30\zeta_3\right)-T_F n_f\left(\frac{10}{27}+\frac{2}{3}\pi^2\right)\right].\end{aligned} \tag{A.14}$$

Their sum is known up to three loops and is given by

$$\begin{aligned}\delta\gamma^{[3]}_{+}+\delta\gamma^{[3]}_{\mathcal{J}} =& C_F^3\left(\frac{29}{2}+3\pi^2+\frac{8\pi^4}{5}+68\zeta_3-\frac{16\pi^2\zeta_3}{3}-240\zeta_5\right)\\ &+C_A^2C_F\left(-\frac{1657}{36}+\frac{2248\pi^2}{81}-\frac{\pi^4}{18}-\frac{1552\zeta_3}{9}+40\zeta_5\right)\\ &+C_AC_F^2\left(\frac{151}{4}-\frac{205\pi^2}{9}-\frac{247\pi^4}{135}+\frac{844\zeta_3}{3}+\frac{8\pi^2\zeta_3}{3}+120\zeta_5\right)\\ &+C_AC_FT_Fn_f\left(40-\frac{1336\pi^2}{81}+\frac{2\pi^4}{45}+\frac{400\zeta_3}{9}\right)\\ &+C_F^2T_Fn_f\left(-46+\frac{20\pi^2}{9}+\frac{116\pi^4}{135}-\frac{272\zeta_3}{3}\right)\\ &+C_FT_F^2n_f^2\left(-\frac{68}{9}+\frac{160\pi^2}{81}-\frac{64\zeta_3}{9}\right).\end{aligned} \tag{A.15}$$

A.2.3 TMDPDF

The universal TMDPDF anomalous dimension is given in [30] by

$$\gamma_F = \Gamma^i_{\text{cusp}}\ln\frac{\mu^2}{\zeta_1}-\gamma^i_V. \tag{A.16}$$

The non-cusp anomalous dimension for the TMDPDF is known up to three loops and is given by

$$\begin{aligned}
\gamma_V^{q[1]} &= -6C_F \\
\gamma_V^{q[2]} &= C_F^2\left(-3+4\pi^2-48\zeta_3\right)+C_FC_A\left(-\frac{961}{27}-\frac{11\pi^2}{3}+52\zeta_3\right)+C_FT_Fn_f\left(\frac{260}{27}+\frac{4\pi^2}{3}\right) \\
\gamma_V^{q[3]} &= C_F^3\left(-29-6\pi^2-\frac{16\pi^4}{5}-136\zeta_3+\frac{32\pi^2}{3}\zeta_3+480\zeta_5\right) \\
&\quad + C_F^2C_A\left(-\frac{151}{2}+\frac{410\pi^2}{9}+\frac{494\pi^4}{135}-\frac{1688}{3}\zeta_3-\frac{16\pi^2}{3}\zeta_3-240\zeta_5\right) \\
&\quad + C_FC_A^2\left(-\frac{139345}{1458}-\frac{7163\pi^2}{243}-\frac{83\pi^4}{45}+\frac{7052}{9}\zeta_3-\frac{88\pi^2}{9}\zeta_3-272\zeta_5\right) \\
&\quad + C_F^2T_Fn_f\left(\frac{5906}{27}-\frac{52\pi^2}{9}-\frac{56\pi^4}{27}+\frac{1024}{9}\zeta_3\right) \\
&\quad + C_FC_AT_Fn_f\left(-\frac{34636}{729}+\frac{5188\pi^2}{243}+\frac{44\pi^4}{45}-\frac{3856}{27}\zeta_3\right)+C_FT_F^2n_f^2\left(\frac{19336}{729}-\frac{80\pi^2}{27}-\frac{64}{27}\zeta_3\right)
\end{aligned} \tag{A.17}$$

$$\begin{aligned}
\gamma_V^{g[1]} &= -\frac{22}{3}C_A+\frac{8}{3}T_Fn_f, \\
\gamma_V^{g[2]} &= C_A^2\left(-\frac{1384}{27}+\frac{11\pi^2}{9}+4\zeta_3\right)+C_AT_Fn_f\left(\frac{512}{27}-\frac{4\pi^2}{9}\right)+8C_FT_Fn_f, \\
\gamma_V^{g[3]} &= 2C_A^3\left(\frac{-97186}{729}+\frac{6109}{486}\pi^2-\frac{319}{270}\pi^4+\frac{122}{3}\zeta_3-\frac{20}{9}\pi^2\zeta_3-16\zeta_5\right) \\
&\quad + 2C_A^2T_Fn_f\left(\frac{30715}{729}-\frac{1198}{243}\pi^2+\frac{82}{135}\pi^4+\frac{712}{27}\zeta_3\right) \\
&\quad + 2C_AC_FT_Fn_f\left(\frac{2434}{27}-\frac{2}{3}\pi^2-\frac{8}{45}\pi^4-\frac{304}{9}\zeta_3\right)-4C_F^2T_Fn_f \\
&\quad + 2C_AT_F^2n_f^2\left(-\frac{538}{729}+\frac{40}{81}\pi^2-\frac{224}{27}\zeta_3\right)-\frac{88}{9}C_FT_F^2n_f^2.
\end{aligned} \tag{A.18}$$

A.2.4 Hard Function

The hard function $H_{\gamma^* g}$ anomalous dimension is given in [89] by

$$\gamma_H = (2C_F+C_A)\gamma_{\text{cusp}}\ln\frac{p_T^2}{\mu^2}-2C_F\gamma_{\text{cusp}}\ln\frac{\hat{t}\hat{u}}{\hat{s}^2}+\delta\gamma_H-\frac{\beta(\alpha_s)}{\alpha_s} \tag{A.19}$$

The non-cusp anomalous dimensions is given by

$$\delta\gamma_H^{[1]} = -2\beta_0-12C_F,$$

$$\delta\gamma_H^{[2]} = \left(\frac{256}{27} - \frac{2\pi^2}{9}\right) 2C_A T_F n_f + \left(\frac{368}{27} + \frac{4\pi^2}{3}\right) 2C_F T_F n_f + \left(-3 + 4\pi^2 - 48\zeta_3\right) 2C_F^2 + \left(-\frac{692}{27} + \frac{11\pi^2}{18} + 2\zeta_3\right) 2C_A^2 + \left(-\frac{961}{27} - \frac{11\pi^2}{3} + 52\zeta_3\right) 2C_A C_F,$$

$$\delta\gamma_H^{[3]} = \gamma_V^{q[3]} + \frac{1}{2}\gamma_V^{g[3]}. \tag{A.20}$$

A.2.5 Dijet soft function

The dijet anomalous dimension for the $\gamma^* g$-channel is given by eq. 3.92. The non-cusp three-loop anomalous dimension is given by

$$\begin{aligned}\delta\gamma_{S_{\gamma g}}^{[3]} = \frac{1}{7290}\Big\{ & 8C_F n_f T_F \Big[27\left(2280\zeta_3 + 12\pi^4 + 45\pi^2 - 4480\right) C_F - 5\left(-3024\zeta_3 + 180\pi^2 + 4753\right) n_f T_F\Big] \\ & + 4C_A n_f T_F \Big[5\left(-3024\zeta_3 + 180\pi^2 - 4535\right) n_f T_F + \left(36720\zeta_3 - 2268\pi^4 + 19995\pi^2 + 188110\right) C_F\Big] \\ & - C_A^3 \Big[15\pi^2\left(1080\zeta_3 - 6109\right) + 20\left(-14823\zeta_3 + 5832\zeta_5 + 48593\right) + 8613\pi^4\Big] \\ & + 2C_A^2 \Big[- 385695 + \left(96120\zeta_3 + 2214\pi^4 - 17970\pi^2 + 535625\right) n_f T_F \\ & - \left(-1598940\zeta_3 + 33\pi^2\left(1080\zeta_3 + 216\pi^2 - 2875\right) + 699840\zeta_5 + 683905\right) C_F\Big]\Big\}.\end{aligned} \tag{A.21}$$

A.3 Soft function integrals and δ-regulator

In this section, we give a pedagogical review of the integrals needed to obtain the dijet soft function result at NLO. The integrals are introduced in 3.32. The real diagrams are shown in fig. 3.4 and are the only ones contributing to the soft function. The virtual diagrams vanish, as we show in this section, and are not shown in this work. In the following, we use $d = 4 - 2\epsilon$.

Real diagram n - v_J

The integral we need to compute is given by the expression

$$I_{JB} = \int \frac{d^d k}{(2\pi)^d} \frac{e^{i\boldsymbol{k}\cdot\boldsymbol{b}}\delta(k^2)\theta(k_+)}{(n\cdot k + i\delta^+)(v_J\cdot k)}. \tag{A.22}$$

Using the delta to integrate over k_- we get

$$I_{JB} = \frac{1}{2\pi}\int\frac{dk_+}{2\pi}\int\frac{d^{d-2}\boldsymbol{k}}{(2\pi)^{d-2}}\frac{e^{i\boldsymbol{k}\cdot\boldsymbol{b}}\theta(k_+)}{(k_+ + i\delta^+)(2v_J^- k_+^2 + v_J^+\boldsymbol{k}^2 - 2k_+\boldsymbol{v}_J\cdot\boldsymbol{k})}. \tag{A.23}$$

Completing the square, the denominator can be written as

$$2v_J^- k_+^2 + v_J^+\boldsymbol{k}^2 - 2k_+\boldsymbol{v}_J\cdot\boldsymbol{k} = v_J^+(\boldsymbol{k} - \frac{k_+}{v_J^+}\boldsymbol{v}_J)^2. \tag{A.24}$$

We change variables $\boldsymbol{k}' \to \boldsymbol{k} - \frac{k_+}{v_J^+}\boldsymbol{v}_J$. In this way, the integral simplifies to the following expression,

$$I_{JB} = \frac{1}{2\pi v_J^+}\int \frac{dk_+}{2\pi}\frac{\theta(k_+)e^{i\frac{\boldsymbol{v}_J\cdot\boldsymbol{b}}{v_J^+}k_+}}{k_+ + i\delta^+}\int \frac{d^{d-2}\boldsymbol{k}}{(2\pi)^{d-2}}\frac{e^{i\boldsymbol{k}\cdot\boldsymbol{b}}}{\boldsymbol{k}^2}. \tag{A.25}$$

This allows us to perform each integral separately, which leads us to the final result of the integral,

$$I_{JB} = -\frac{4B^\epsilon\Gamma(-\epsilon)}{(4\pi)^{3-\epsilon}v_J^+}\Big[\ln\Big(\frac{(\boldsymbol{v}_J\cdot\boldsymbol{b})\delta^+}{v_J^+}\Big) + \gamma_E\Big]. \tag{A.26}$$

Real diagram $\boldsymbol{v_1}$ - $\boldsymbol{v_2}$

The integral we need to compute is given by

$$I_{12} = \int \frac{d^dk}{(2\pi)^d}\frac{e^{i\boldsymbol{k}\cdot\boldsymbol{b}}\delta(k^2)\theta(k_+)}{(v_1\cdot k)(v_2\cdot k)}. \tag{A.27}$$

Using the delta to integrate over k_- we get

$$I_{12} = \frac{1}{2\pi}\int\frac{dk_+}{2\pi}\int\frac{d^{d-2}\boldsymbol{k}}{(2\pi)^{d-2}}\frac{e^{i\boldsymbol{k}\cdot\boldsymbol{b}}\theta(k_+)2k_+}{(2v_1^-k_+^2 + v_1^+\boldsymbol{k}^2 - 2k_+\boldsymbol{v}_1\cdot\boldsymbol{k})(2v_2^-k_+^2 + v_2^+\boldsymbol{k}^2 - 2k_+\boldsymbol{v}_2\cdot\boldsymbol{k})}. \tag{A.28}$$

We use Feynman parametrization in order to rewrite the denominator,

$$\frac{1}{AB} = \int_0^1 dx\frac{1}{[Ax + (1-x)B]^2}. \tag{A.29}$$

In our case, we identify

$$A = \frac{2v_1^-k_+^2}{v_1^+} + \boldsymbol{k}^2 - \frac{2k_+\boldsymbol{v}_1\cdot\boldsymbol{k}}{v_1^+}, \qquad B = \frac{2v_2^-k_+^2}{v_2^+} + \boldsymbol{k}^2 - \frac{2k_+\boldsymbol{v}_2\cdot\boldsymbol{k}}{v_2^+}. \tag{A.30}$$

In this way, the denominator can be rewritten the following way:

$$xA + (1-x)B = [\boldsymbol{k} - k_+\boldsymbol{R}_1(x)]^2 + k_+^2R_2(x), \tag{A.31}$$

where

$$\boldsymbol{R}_1(x) = \frac{x\boldsymbol{v}_1}{v_1^+} + \frac{(1-x)\boldsymbol{v}_2}{v_2^+}, \qquad R_2(x) = 2x(1-x)\frac{v_1\cdot v_2}{v_1^+v_2^+}. \tag{A.32}$$

We can perform a change of variables $\boldsymbol{k}' = \boldsymbol{k} - k_+\boldsymbol{R}_1^\mu(x)$ and the integral simplifies as follows,

$$I_{12} = \frac{1}{2\pi v_1^+v_2^+}\int_0^1 dx\int\frac{dk_+}{2\pi}\int\frac{d^{d-2}\boldsymbol{k}}{(2\pi)^{d-2}}\frac{e^{i\boldsymbol{k}\cdot\boldsymbol{b}}e^{ik_+\boldsymbol{R}_1\cdot\boldsymbol{b}}\theta(k_+)2k_+}{[\boldsymbol{k}^2 + R_2(x)k_+^2]^2}. \tag{A.33}$$

We perform a Mellin-Barnes transformation in order to be able to integrate over $\boldsymbol{k}$ and k_+ separately,

$$\frac{1}{[\boldsymbol{k}^2 + R_2k_+^2]^2} = \int_{-i\infty}^{+i\infty}\frac{dz}{2\pi i}\Gamma(2+z)\Gamma(-z)\frac{(R_2k_+^2)^z}{(\boldsymbol{k}^2)^{2+z}}. \tag{A.34}$$

In this way, we integrate over $\boldsymbol{k}$ and get

$$I_{12} = \frac{4}{(4\pi)^{2-\epsilon} v_1^+ v_2^+} B^{\epsilon+1} \int_0^1 dx \int_{-i\infty}^{+i\infty} \frac{dz}{2\pi i} \Gamma(-z)\Gamma(-\epsilon-1-z) B^z R_2^z \int_0^{+\infty} \frac{dk_+}{2\pi} k_+^{2z+1} e^{ik_+ \boldsymbol{R}_1 \cdot \boldsymbol{b}}. \tag{A.35}$$

Next, we integrate over k_+,

$$I_{12} = \frac{8}{(4\pi)^{3-\epsilon} v_1^+ v_2^+} B^{\epsilon+1} \int_0^1 dx \int_{-i\infty}^{+i\infty} \frac{dz}{2\pi i} \Gamma(-z)\Gamma(-\epsilon-1-z)\Gamma(2+2z) B^z (-i\boldsymbol{R}_1 \cdot \boldsymbol{b})^{-2(1+z)} R_2^z. \tag{A.36}$$

We integrate in z using residues. We close the integration path to the right side of the imaginary axis and sum all the residues due to $\Gamma(-z)$ and $\Gamma(-\epsilon-1-z)$. The residues are given by the expressions

$$\text{Res}[\Gamma(-z), n] = \frac{(-1)^{n+1}}{\Gamma(n+1)} \qquad \text{and} \qquad \text{Res}[\Gamma(-1-\epsilon-z), n-1-\epsilon] = \frac{(-1)^{n+1}}{\Gamma(n+1)}, \tag{A.37}$$

for $n = 0, 1, 2, ...$ We then arrive at the sum

$$I_{12} = \frac{-8}{(4\pi)^{3-\epsilon} v_1^+ v_2^+} B^{\epsilon+1} \int_0^1 dx \sum_{n=0}^{\infty} \Big\{ \frac{\Gamma(-1-\epsilon-n)\Gamma(2+2n)}{\Gamma(n+1)} \frac{(BR_2)^n}{(\boldsymbol{R}_1^2)^{n+1}} - \frac{\Gamma(1+\epsilon-n)\Gamma(-2\epsilon+2n)}{\Gamma(n+1)} (-1)^{\epsilon} \frac{(BR_2)^{n-1-\epsilon}}{(\boldsymbol{R}_1^2)^{n-\epsilon}} \Big\},$$

Now, we perform the x integral, where remember that the x dependence is through the $\boldsymbol{R}_1(x)$ and $R_2(x)$ functions. Finally, we perform the sum over n and arrive at the final result:

$$I_{12} = \frac{4}{(4\pi)^{3-\epsilon}(v_1 \cdot v_2)} B^{\epsilon} A_{\boldsymbol{b}} \Big[-\Gamma(-1-\epsilon)\, {}_2F_1(1, 1, 2+\epsilon, -A_{\boldsymbol{b}}) + \Gamma^2(-\epsilon)\Gamma(1+\epsilon)(-1)^{\epsilon} A_{\boldsymbol{b}}^{-1-\epsilon} (1+A_{\boldsymbol{b}})^{\epsilon} \Big]. \tag{A.38}$$

where $A_{\boldsymbol{b}}$ is given in 3.35.

Virtual diagram n - v_J

The integral for this diagram is given by

$$I_{JB}^{\text{virtual}} = \int \frac{d^d k}{(2\pi)^d} \frac{1}{(n \cdot k + i\delta^+)(\boldsymbol{v}_J \cdot \boldsymbol{k})\boldsymbol{k}^2}. \tag{A.39}$$

We begin integrating over k_-. This integration restricts k_+ values to be negative ($k_+ < 0$), otherwise all poles would be located in the negative part of the imaginary axis (due to $v_J^+ > 0$), and the integral would vanish. In this way, we get

$$I_{JB}^{\text{virtual}} = i \int \frac{dk_+}{2\pi} \int \frac{d^{d-2}\boldsymbol{k}}{(2\pi)^{d-2}} \frac{\theta(-k_+)}{(k_+ + i\delta^+)(2v_J^- k_+^2 + v_J^+ \boldsymbol{k}^2 - 2k_+ \boldsymbol{v}_J \cdot \boldsymbol{k})}. \tag{A.40}$$

Completing the square and performing the same change of variable as in the real diagram $n - v_J$, we get

$$I_{JB}^{\text{virtual}} = \frac{i}{v_J^+}\int\frac{dk_+}{2\pi}\frac{\theta(-k_+)}{k_+ + i\delta^+}\int\frac{d^{d-2}\boldsymbol{k}}{(2\pi)^{d-2}}\frac{1}{\boldsymbol{k}^2} = 0. \tag{A.41}$$

This integral vanishes due to the integral over $\boldsymbol{k}$ being a scaleless integral, which is set to zero in dimensional regularization. This was expected as the result of real diagram $n - v_J$ has no IR divergent part.

Virtual diagram v_1 - v_2

The integral that has to be computed is given by

$$I_{12}^{\text{virtual}} = \int\frac{d^dk}{(2\pi)^d}\frac{1}{(v_1\cdot k + i0)(v_2\cdot k - i0)(k^2+i0)}. \tag{A.42}$$

First, we integrate over k_-. We get a different result depending on the sign of k_+, which leads to the addition of $\theta(k_+)$ and $\theta(-k_+)$,

$$\mathcal{I}_1 = \int\frac{dk_+}{2\pi}\int\frac{d^{d-2}\boldsymbol{k}}{(2\pi)^{d-2}}\frac{i\theta(-k_+)}{\left[\frac{2v_1^-}{v_1^+}k_+^2 + \boldsymbol{k}^2 - \frac{2k_+\boldsymbol{v_1}\cdot\boldsymbol{k}}{v_1^+}\right]\left[\boldsymbol{k}\cdot(\boldsymbol{v}_2v_1^+ - \boldsymbol{v}_1v_2^+) + k_+(v_2^+v_1^- - v_2^-v_1^+)\right]}, \tag{A.43}$$

$$\mathcal{I}_2 = \int\frac{dk_+}{2\pi}\int\frac{d^{d-2}\boldsymbol{k}}{(2\pi)^{d-2}}\frac{i\theta(k_+)}{\left[\frac{2v_2^-}{v_2^+}k_+^2 + \boldsymbol{k}^2 - \frac{2k_+\boldsymbol{v_2}\cdot\boldsymbol{k}}{v_2^+}\right]\left[\boldsymbol{k}\cdot(\boldsymbol{v}_2v_1^+ - \boldsymbol{v}_1v_2^+) + k_+(v_2^+v_1^- - v_2^-v_1^+)\right]}, \tag{A.44}$$

$$I_{12}^{\text{virtual}} = \mathcal{I}_1 + \mathcal{I}_2. \tag{A.45}$$

Both integrals are computed the same way, so we focus in one of them, $\mathcal{I}_1$ for example. Here, we use Feynman parametrization in order to rewrite the denominator,

$$\frac{1}{AB} = \int_0^1 dx\frac{1}{[Ax + (1-x)B]^2}. \tag{A.46}$$

In our case, we identify

$$A = \frac{2v_1^-}{v_1^+}k_+^2 + \boldsymbol{k}^2 - \frac{2k_+\boldsymbol{v}_1\cdot\boldsymbol{k}}{v_1^+}, \quad B = \boldsymbol{k}\cdot(\boldsymbol{v}_2v_1^+ - \boldsymbol{v}_1v_2^+) + k_+(v_2^+v_1^- - v_2^-v_1^+). \tag{A.47}$$

In this way, the denominator can be rewritten the following way:

$$xA + (1-x)B = R_1(x)[\boldsymbol{k} - k_+\boldsymbol{E}_1(x) - \boldsymbol{E}_2(x)]^2 + k_+F_1(x) + F_2(x), \tag{A.48}$$

where

$$\begin{gathered} R_1(x) = x, \\ \boldsymbol{E}_1(x) = \frac{\boldsymbol{v_1}}{v_1^+}, \quad \boldsymbol{E}_2(x) = \frac{1}{2}\left(\frac{v_2^+\boldsymbol{v}_1(1-x)}{x} - \frac{v_1^+\boldsymbol{v}_2(1-x)}{x}\right), \\ F_1(x) = -(v_1\cdot v_2)(1-x) \quad \text{and} \quad F_2(x) = -(v_1\cdot v_2)\frac{v_2^+v_1^+(1-x)^2}{2x}. \end{gathered} \tag{A.49}$$

We can perform a change of variables $\boldsymbol{k}' = \boldsymbol{k} - k_+\boldsymbol{E}_1(x) - \boldsymbol{E}_2(x)$ and the integral simplifies to

$$\mathcal{I}_1 = \int_0^1 dx \int \frac{dk_+}{2\pi} \int \frac{d^{d-2}\boldsymbol{k}}{(2\pi)^{d-2}} \frac{i\theta(-k_+)}{[R_1(x)\boldsymbol{k}^2 + k_+F_1(x) + F_2(x)]^2}. \tag{A.50}$$

We can integrate over $\boldsymbol{k}$ we get

$$\mathcal{I}_1 = \frac{i}{(4\pi)^{1-\epsilon}} \frac{\Gamma(\epsilon+1)}{\Gamma(2)} \int_0^1 dx \int \frac{dk_+}{2\pi} \theta(-k_+)[k_+F_1(x) + F_2(x)]^{-\epsilon-1} \frac{1}{(R_1(x))^{1-\epsilon}}. \tag{A.51}$$

Finally, integrating over k_+ we have

$$\mathcal{I}_1 = \frac{-2i}{(4\pi)^{2-\epsilon}} \frac{\Gamma(\epsilon+1)}{\Gamma(2)} \int_0^1 dx \frac{F_2^{-\epsilon}}{R_1^{1-\epsilon}F_1} = 0, \tag{A.52}$$

which evaluates to zero if we perform the integration over x. The term I_2 is zero for the same reason, we can compute it following the same steps. This means

$$I_{12}^{\text{virtual}} = 0. \tag{A.53}$$

A.4 Hard prefactors

The hard prefactors for each channel are given in ref. [92]. We include in this section the ones relevant to our cases

$$\sigma_0^{gU} = 2\pi p_T \frac{\mathcal{N}}{xs} \frac{A_0^{gU}}{f_1^g(\xi, \boldsymbol{r}_T)}, \qquad \sigma_0^{fU} = 2\pi p_T \frac{\mathcal{N}}{xs} \frac{A_0^{fU}}{f_1^f(\xi, \boldsymbol{r}_T)}, \qquad \sigma_0^{gL} = -4\pi p_T \frac{\mathcal{N}}{xs} \frac{B_2}{h_1^\perp(\xi, \boldsymbol{r}_T)}, \tag{A.54}$$

where

$$\mathcal{N} = \frac{\alpha^2\alpha_s}{\pi s p_T^2} \frac{1}{xy^2}, \tag{A.55}$$

$$A_0^{gU} = e_q^2 T_R \Big[\Big(1 + (1-y^2)\Big) A_{U+L}^{gU} - y^2 A_L^{gU} \Big] f_1^g(\xi, \boldsymbol{r}_T), \tag{A.56}$$

$$A_0^{fU} = e_q^2 C_F \Big[\Big(1 + (1-y^2)\Big) A_{U+L}^{fU} - y^2 A_L^{fU} \Big] f_1^q(\xi, \boldsymbol{r}_T), \tag{A.57}$$

$$B_2 = e_q^2 T_R \Big[\Big(1 + (1-y^2)\Big) B_{U+L} - y^2 B_L \Big] \frac{r_T^2}{M_p^2} h_1^{\perp g}(\xi, \boldsymbol{r}_T), \tag{A.58}$$

and A and B factors are given by

$$A_{U+L}^{fU} = \frac{1-z}{D^2} \left\{ 1 + z^2 + \left[2z(1-z) + 4z^2(1-z)^2\right] \frac{Q^2}{p_T^2} + \left[z^2(1-z)^2\right] \left[1 + (1-z)^2\right] \frac{Q^4}{p_T^4} \right\}, \tag{A.59}$$

$$A_{U+L}^{gU} = \frac{1}{D^3} - \frac{z(1-z)}{D^3} \left\{ 2 - 8z(1-z)\frac{Q^2}{p_T^2} - z(1-z)[1 - 2z(1-z)]\frac{Q^4}{p_T^4} \right\}, \tag{A.60}$$

$$B_{U+L} = \frac{z(1-z)}{D^3}\left\{[1-6z(1-z)]\frac{Q^2}{p_T^2}\right\}, \tag{A.61}$$

$$A_L^{fU} = 4\frac{z^2(1-z)^3}{D^2}\frac{Q^2}{p_T^2}, \tag{A.62}$$

$$A_L^{gU} = 8\frac{z^2(1-z)^2}{D^3}\frac{Q^2}{p_T^2}, \tag{A.63}$$

$$B_L = -4\frac{z^2(1-z)^2}{D^3}\frac{Q^2}{p_T^2}, \tag{A.64}$$

where D is defined as

$$D = 1 + z(1-z)\frac{Q^2}{p_T^2}. \tag{A.65}$$

Appendix B

Dijet production in SIA

B.1 Fierz relations

The jet functions defined in eqs. 5.33 and 5.34 have open spinor indices. These spinor indices are at first contracted between the jet functions for the two different collinear directions, see eq. 5.31. To remove contractions between different jet functions and obtain our factorized hadronic tensor, we apply the following Fierz relations

$$\begin{aligned}
4(\gamma^\mu)_{ij}(\gamma^\nu)_{kl} = g^{\mu\nu}\Big[&\delta_{il}\delta_{kj} + (i\gamma^5)_{il}(i\gamma^5)_{kj} - (\gamma^\alpha)_{il}(\gamma_\alpha)_{kj} \\
&- (\gamma^\alpha\gamma^5)_{il}(\gamma_\alpha\gamma^5)_{kj} + \frac{1}{2}(i\sigma^{\alpha\beta}\gamma^5)_{il}(i\sigma_{\alpha\beta}\gamma^5)_{kj}\Big] \\
&+ (\gamma^{\{\mu})_{il}(\gamma^{\nu\}})_{kj} + (\gamma^{\{\mu}\gamma^5)_{il}(\gamma^{\nu\}}\gamma^5)_{kj} - (i\sigma^{\alpha\{\mu}\gamma^5)_{il}(i\sigma^{\nu\}}{}_\alpha\gamma^5)_{kj} \\
&- \frac{i}{2}\epsilon^{\mu\nu\lambda\eta}\Big[(i\sigma^{\lambda\eta}\gamma^5)_{il}\delta_{kj} - \delta_{il}(i\sigma^{\lambda\eta}\gamma^5)_{kj}\Big] \\
&+ (i\sigma^{\mu\nu}\gamma^5)_{il}(\gamma^5)_{kj} + (\gamma^5)_{il}(i\sigma^{\mu\nu}\gamma^5)_{kj} \\
&+ i\epsilon^{\mu\nu\alpha\beta}\Big[(\gamma^\alpha\gamma^5)_{il}(\gamma^\beta)_{kj} + (\gamma^\alpha)_{il}(\gamma^\beta\gamma^5)_{kj}\Big]\,,
\end{aligned}$$

$$\begin{aligned}
4(\gamma^\mu)_{ij}\delta_{kl} = &(\gamma^\mu)_{il}\delta_{kj} + \delta_{il}(\gamma^\mu)_{kj} + (\gamma^5)_{il}(\gamma^\mu\gamma^5)_{kj} - (\gamma^\mu\gamma^5)_{il}(\gamma^5)_{kj} \\
&- \frac{i}{2}\epsilon^{\mu\nu\tau\eta}\Big[(i\sigma^{\nu\tau}\gamma^5)_{il}(\gamma^\eta)_{kj} - (\gamma^\eta)_{il}(i\sigma^{\nu\tau}\gamma^5)_{kj}\Big] \\
&+ (\gamma^\eta\gamma^5)_{il}(i\sigma^{\mu\eta}\gamma^5)_{kj} + (i\sigma^{\mu\eta}\gamma^5)_{il}(\gamma^\eta\gamma^5)_{kj}\,.
\end{aligned} \tag{B.1}$$

Inserting these expressions in eq. 5.31, many of the above Dirac structures lead to vanishing expressions. Due to the collinear nature of the jet functions, only structures that contain an explicit γ^+ or γ^- survive (see eq. 5.19). Moreover, because the jet algorithm/measurement is spin-independent and due to parity symmetry, we are left with

$$4(\gamma_T^\mu)_{ij}(\gamma_T^\nu)_{kl} = -g_T^{\mu\nu}\Big[(\gamma^+)_{il}(\gamma^-)_{kj} + (\gamma^-)_{il}(\gamma^+)_{kj}\Big] + \dots\,,$$

$$\begin{aligned}
4(\gamma_T^\mu)_{ij}\delta_{kl} = +i\epsilon_T^{\mu\alpha}\Big[&(\gamma^+)_{il}(i\sigma^{\alpha-}\gamma^5)_{kj} + (i\sigma^{\alpha+}\gamma^5)_{il}(\gamma^-)_{kj} \\
&- (\gamma^-)_{il}(i\sigma^{\alpha+}\gamma^5)_{kj} - (i\sigma^{\alpha-}\gamma^5)_{il}(\gamma^+)_{kj}\Big] + \dots\,,
\end{aligned} \tag{B.2}$$

where the "..." are terms in eq. B.1 which give a vanishing contribution when inserted into eq. 5.31.

Abstract

This thesis studies in detail two novel processes where transverse momentum dependent parton distribution functions (TMDPDFs or TMDs) play a crucial role. These two processes are dijet production in semi-inclusive deep inelastic scattering (SIDIS) and dijet production in semi-inclusive annihilation (SIA).

Parton distribution functions (PDFs) play a pivotal role in unraveling hadron structure and provide insights into the longitudinal momentum distribution of quarks and gluons inside hadrons. However, they lack crucial insights into their transverse momentum distribution. This limitation led to the development of TMDs, which can be understood as a generalization of PDFs and constitute a more comprehensive framework for characterizing the three-dimensional structure of hadrons. TMDs are indispensable for understanding phenomena involving the intrinsic transverse motion of partons, such as the spin structure of the nucleon and the orbital angular momentum.

We delve into TMDs through two complementary approaches: Soft Collinear Effective Theory (SCET) and the background field method. SCET constitutes the traditional way of tackling transverse momentum dependent physics. The development of the effective theory allows us to derive general properties of TMD distributions. On the other hand, the background field method has recently been used as an alternative approach to describe TMD processes and is particularly suitable for deriving higher-power corrections. We provide a review of both theoretical approaches and use them to describe distinct cases sensible to TMDs. We also provide a review of TMD factorization theorems. Factorization theorems allow us to write a particular cross-section in terms of a product of universal functions that describe each of the energy scales in a given process. For the case of TMDs, we describe how factorization leads to their proper definition and their evolution following renormalization group equations and double-scale evolution.

The novel work of this thesis consists on analyzing TMD distributions in two distinct processes: dijet production in SIDIS and dijet production in SIA.

For SIDIS, we develop a theoretical framework for factorization for the first time as well as providing phenomenological predictions. The SIDIS process is sensible to gluon TMDs, which are difficult to access from other similar processes. Additionally, the factorized cross-section depends on a soft function that appears in this process for the first time and we compute up to next-to-leading order (NLO). The soft function describes soft radiation emitted by the hadronic states. We also give a prescription on how to evolve this soft function following renormalization group equation and dealing with double-scale evolution, as the soft function depends on an extra rapidity scale in the same way the TMDs do. We perform a phenomenological study of the cross-section of the given process, describing

the contribution of each of the channels in the process and including a consideration of theoretical errors. Our findings exhibit promising potential for measurement at the forthcoming Electron Ion Collider (EIC).

In the case of SIA, we establish factorization at next-to-leading power (NLP) in the small transverse momentum expansion for the first time following the background field prescriptions. The SIA process is interesting as it depends on TMD jet states, which largely simplifies computations and expressions at NLP, letting us present the results in a didactic manner. We observe that to obtain a non-vanishing contribution from NLP operators, there must be a breaking of symmetry between the energetic radiation directed into the two distinct directions.

This thesis contributes novel insight through the study of these two new processes and shows the profound impact of TMDs on describing particle physics as well as pointing to future experimental research of the presented results.

Resumen

Esta tesis estudia en detalle dos procesos originales en los que las funciones de distribución de partones dependientes del momento transverso (TMDPDF o TMD, por sus siglas en inglés) juegan un papel fundamental. Estos dos procesos consisten en producción de dijets en semi-inclusive deep inelastic scattering (SIDIS) y producción de dijets en semi-inclusive annihilation (SIA).

Las funciones de distribución de partones (PDF, por sus siglas en inglés) tienen un papel fundamental en la descripción de la estructura hadrónica y de la distribución longitudinal de momento de los quarks y gluones dentro de los hadrones. Sin embargo, carecen de información sobre su distribución de momento transverso. Esta limitación da lugar al desarrollo de las TMD, que pueden ser entendidas como una generalización de las PDF y constituyen un marco más completo para describir la estructura tridimensional de los hadrones. Las TMD son indispensables para comprender fenómenos que implican el movimiento transverso intrínseco de los partones, tales como la estructura de espín del nucleón y su momento angular orbital.

Exploramos las TMD a través de dos enfoques complementarios: Soft Collinear Effective Theory (SCET) y el método del background field. SCET constituye el enfoque tradicional para lidiar con distribuciones dependientes del momento transverso. El desarrollo de la teoría efectiva nos permite obtener propiedades generales de las TMD. Por otro lado, el método del background field ha sido utilizado recientemente como enfoque alternativo para describir procesos dependientes del momento transverso y es particularmente útil para obtener contribuciones de ordenes superiores (NLP, por sus siglas en inglés). Presentamos una revisión de ambos acercamientos teóricos y los utilizamos para describir distintos casos sensibles a las TMD. A su vez, tambien presentamos una revisión de los teoremas de factorización de TMD. Los teoremas de factorización nos permiten escribir una determinada sección eficaz en términos del producto de funciones universales que describen cada una de las escalas de energía presentes en un determinado proceso. En el caso de las TMD, describimos como la factorización nos lleva a su definición adecuada y su evolución siguiendo las ecuaciones del grupo de renormalización y la evolución de doble escala.

El trabajo original de esta tesis consiste en el análisis de las distribuciones TMD en dos procesos: producción de dijets en SIDIS y producción de dijets en SIA.

Para el caso de SIDIS, desarrollamos un marco teórico para la factorización por primera vez a la vez que ofrecemos predicciones fenomenológicas. El proceso SIDIS es sensible a las TMD de gluones, el acceso a las cuales suele ser complicado en otros procesos similares. Además, la sección eficaz factorizada depende de una función soft que aparece en este

proceso por primera vez y que calculamos hasta primer orden (NLO, por sus siglas en inglés). La función soft describe la radiación soft emitida por los estados hadrónicos. A su vez, ofrecemos una prescripción sobre como evolucionar esta función soft siguiendo las ecuaciones del grupo de renormalización y la evolución de doble escala. Esto último se debe a que la función soft depende de una escala de rapidity adicional de la misma forma que lo hacen las TMD. Por último, llevamos a cabo un estudio fenomenológico de la sección eficaz del proceso, describiendo la contribución de cada uno de los canales e incluyendo una discusión de los errores teóricos. Nuestras conclusiones apuntan a potencial para su medición en el futuro Electron Ion Collider (EIC).

Para el caso de SIA, establecemos la factorización a NLP en la expansión para pequeños momentos transversos por primera vez siguiendo el método del background field. El proceso SIA es interesante ya que depende de jets TMD, los cuales simplifican los cálculos y expresiones a NLP. Esto nos permite presentar los resultados de una forma didactica. Podemos observar que para obtener una contribución distinta de cero por parte de los operadores a NLP, necesitamos una ruptura de la simetria entre la radiación emitida en las dos direcciones relevantes.

Esta tesis constituye una contribución original al estudio de estos dos nuevos procesos y muestra el profundo impacto de las TMD en la descripción de la fisica de particulas a la vez que señala hacía la posibilidad de futuras investigaciones experimentales de los resultados presentados.

spanish

Bibliography

[1] T. Becher, A. Broggio and A. Ferroglia, *Introduction to Soft-Collinear Effective Theory*, *Lect. Notes Phys.* **896** (2015) pp.1–206, [1410.1892].

[2] M. García Echevarría, *Definition and properties of transverse momentum distributions*. PhD thesis, UCM, Madrid, Dept. Phys., 2013.

[3] D. Gutiérrez Reyes, *Transverse momentum dependent distributions for the Electron-Ion Collider era*. PhD thesis, UCM, Madrid, Dept. Phys., Madrid U., 2020.

[4] M. Beneke and V. A. Smirnov, *Asymptotic expansion of Feynman integrals near threshold*, *Nucl. Phys. B* **522** (1998) 321–344, [hep-ph/9711391].

[5] V. A. Smirnov, *Applied asymptotic expansions in momenta and masses*, *Springer Tracts Mod. Phys.* **177** (2002) 1–262.

[6] V. A. Smirnov, *Problems of the strategy of regions*, *Phys. Lett. B* **465** (1999) 226–234, [hep-ph/9907471].

[7] A. V. Manohar and I. W. Stewart, *The Zero-Bin and Mode Factorization in Quantum Field Theory*, *Phys. Rev. D* **76** (2007) 074002, [hep-ph/0605001].

[8] M. Beneke, A. P. Chapovsky, M. Diehl and T. Feldmann, *Soft collinear effective theory and heavy to light currents beyond leading power*, *Nucl. Phys.* **B643** (2002) 431–476, [hep-ph/0206152].

[9] A. V. Manohar, T. Mehen, D. Pirjol and I. W. Stewart, *Reparameterization invariance for collinear operators*, *Phys. Lett. B* **539** (2002) 59–66, [hep-ph/0204229].

[10] A. von Manteuffel, E. Panzer and R. M. Schabinger, *Cusp and collinear anomalous dimensions in four-loop QCD from form factors*, *Phys. Rev. Lett.* **124** (2020) 162001, [2002.04617].

[11] P. A. Baikov, K. G. Chetyrkin, A. V. Smirnov, V. A. Smirnov and M. Steinhauser, *Quark and gluon form factors to three loops*, *Phys. Rev. Lett.* **102** (2009) 212002, [0902.3519].

[12] T. Gehrmann, E. W. N. Glover, T. Huber, N. Ikizlerli and C. Studerus, *The quark and gluon form factors to three loops in QCD through to $O(\epsilon^2)$*, *JHEP* **11** (2010) 102, [1010.4478].

[13] J. C. Collins and D. E. Soper, *Back-To-Back Jets in QCD*, *Nucl. Phys. B* **193** (1981) 381.

[14] J. C. Collins, D. E. Soper and G. F. Sterman, *Transverse Momentum Distribution in Drell-Yan Pair and W and Z Boson Production*, *Nucl. Phys. B* **250** (1985) 199–224.

[15] X.-d. Ji, J.-P. Ma and F. Yuan, *QCD factorization for spin-dependent cross sections in DIS and Drell-Yan processes at low transverse momentum*, *Phys. Lett. B* **597** (2004) 299–308, [hep-ph/0405085].

[16] P. Chen, A. Idilbi and X. Ji, *Qcd factorization for deep-inelastic scattering at large bjorken xb1o(qcd/q)*, *Nuclear Physics B* **763** (2007) 183–197.

[17] M. G. Echevarria, A. Idilbi and I. Scimemi, *Factorization Theorem For Drell-Yan At Low q_T And Transverse Momentum Distributions On-The-Light-Cone*, *JHEP* **07** (2012) 002, [1111.4996].

[18] M. G. Echevarría, A. Idilbi and I. Scimemi, *Soft and Collinear Factorization and Transverse Momentum Dependent Parton Distribution Functions*, *Phys. Lett. B* **726** (2013) 795–801, [1211.1947].

[19] A. V. Belitsky, X. Ji and F. Yuan, *Final state interactions and gauge invariant parton distributions*, *Nucl. Phys. B* **656** (2003) 165–198, [hep-ph/0208038].

[20] X.-d. Ji and F. Yuan, *Parton distributions in light cone gauge: Where are the final state interactions?*, *Phys. Lett. B* **543** (2002) 66–72, [hep-ph/0206057].

[21] D. Boer, P. J. Mulders and F. Pijlman, *Universality of T odd effects in single spin and azimuthal asymmetries*, *Nucl. Phys. B* **667** (2003) 201–241, [hep-ph/0303034].

[22] M. Garcia-Echevarria, A. Idilbi and I. Scimemi, *SCET, Light-Cone Gauge and the T-Wilson Lines*, *Phys. Rev. D* **84** (2011) 011502, [1104.0686].

[23] C. W. Bauer, S. Fleming, D. Pirjol and I. W. Stewart, *An Effective field theory for collinear and soft gluons: Heavy to light decays*, *Phys. Rev. D* **63** (2001) 114020, [hep-ph/0011336].

[24] C. Lee and G. F. Sterman, *Momentum Flow Correlations from Event Shapes: Factorized Soft Gluons and Soft-Collinear Effective Theory*, *Phys. Rev. D* **75** (2007) 014022, [hep-ph/0611061].

[25] J.-Y. Chiu, A. Jain, D. Neill and I. Z. Rothstein, *A Formalism for the Systematic Treatment of Rapidity Logarithms in Quantum Field Theory*, *JHEP* **05** (2012) 084, [1202.0814].

[26] T. Becher and G. Bell, *Analytic Regularization in Soft-Collinear Effective Theory*, *Phys. Lett. B* **713** (2012) 41–46, [1112.3907].

[27] J.-y. Chiu, A. Jain, D. Neill and I. Z. Rothstein, *The Rapidity Renormalization Group*, *Phys. Rev. Lett.* **108** (2012) 151601, [1104.0881].

[28] Y. Li, D. Neill and H. X. Zhu, *An exponential regulator for rapidity divergences*, *Nucl. Phys. B* **960** (2020) 115193, [1604.00392].

[29] M. G. Echevarria, I. Scimemi and A. Vladimirov, *Transverse momentum dependent fragmentation function at next-to–next-to–leading order*, *Phys. Rev. D* **93** (2016) 011502, [1509.06392].

[30] M. G. Echevarria, I. Scimemi and A. Vladimirov, *Unpolarized Transverse Momentum Dependent Parton Distribution and Fragmentation Functions at next-to-next-to-leading order*, *JHEP* **09** (2016) 004, [1604.07869].

[31] J. G. M. Gatheral, *Exponentiation of Eikonal Cross-sections in Nonabelian Gauge Theories*, *Phys. Lett. B* **133** (1983) 90–94.

[32] I. Scimemi and A. Vladimirov, *Non-perturbative structure of semi-inclusive deep-inelastic and Drell-Yan scattering at small transverse momentum*, *JHEP* **06** (2020) 137, [1912.06532].

[33] I. Scimemi and A. Vladimirov, *Systematic analysis of double-scale evolution*, *JHEP* **08** (2018) 003, [1803.11089].

[34] A. Vladimirov, *Pion-induced Drell-Yan processes within TMD factorization*, 1907.10356.

[35] J. C. Collins and D. E. Soper, *Back-To-Back Jets: Fourier Transform from B to K-Transverse*, *Nucl. Phys. B* **197** (1982) 446–476.

[36] Y. Gao, C. S. Li and J. J. Liu, *Transverse momentum resummation for Higgs production in soft-collinear effective theory*, *Phys. Rev. D* **72** (2005) 114020, [hep-ph/0501229].

[37] M. G. Echevarria, T. Kasemets, P. J. Mulders and C. Pisano, *QCD evolution of (un)polarized gluon TMDPDFs and the Higgs q_T-distribution*, *JHEP* **07** (2015) 158, [1502.05354].

[38] D. Neill, I. Z. Rothstein and V. Vaidya, *The Higgs Transverse Momentum Distribution at NNLL and its Theoretical Errors*, *JHEP* **12** (2015) 097, [1503.00005].

[39] D. Gutierrez-Reyes, S. Leal-Gomez, I. Scimemi and A. Vladimirov, *Linearly polarized gluons at next-to-next-to leading order and the Higgs transverse momentum distribution*, *JHEP* **11** (2019) 121, [1907.03780].

[40] P. F. Monni, L. Rottoli and P. Torrielli, *Higgs transverse momentum with a jet veto: a double-differential resummation*, *Phys. Rev. Lett.* **124** (2020) 252001, [1909.04704].

[41] X. Chen, T. Gehrmann, E. N. Glover, A. Huss, Y. Li, D. Neill et al., *Precise QCD Description of the Higgs Boson Transverse Momentum Spectrum*, *Phys. Lett. B* **788** (2019) 425–430, [1805.00736].

[42] P. Mulders and J. Rodrigues, *Transverse momentum dependence in gluon distribution and fragmentation functions*, *Phys. Rev. D* **63** (2001) 094021, [hep-ph/0009343].

[43] D. Boer and C. Pisano, *Polarized gluon studies with charmonium and bottomonium at LHCb and AFTER*, *Phys. Rev. D* **86** (2012) 094007, [1208.3642].

[44] J. Ma, J. Wang and S. Zhao, *Transverse momentum dependent factorization for quarkonium production at low transverse momentum*, *Phys. Rev. D* **88** (2013) 014027, [1211.7144].

[45] G.-P. Zhang, *Probing transverse momentum dependent gluon distribution functions from hadronic quarkonium pair production*, *Phys. Rev. D* **90** (2014) 094011, [1406.5476].

[46] J. Ma and C. Wang, *QCD factorization for quarkonium production in hadron collisions at low transverse momentum*, *Phys. Rev. D* **93** (2016) 014025, [1509.04421].

[47] D. Boer, *Linearly polarized gluon effects in unpolarized collisions*, *PoS* **QCDEV2015** (2015) 023, [1510.05915].

[48] R. Bain, Y. Makris and T. Mehen, *Transverse Momentum Dependent Fragmenting Jet Functions with Applications to Quarkonium Production*, *JHEP* **11** (2016) 144, [1610.06508].

[49] A. Mukherjee and S. Rajesh, *Probing Transverse Momentum Dependent Parton Distributions in Charmonium and Bottomonium Production*, *Phys. Rev. D* **93** (2016) 054018, [1511.04319].

[50] A. Mukherjee and S. Rajesh, *Linearly polarized gluons in charmonium and bottomonium production in color octet model*, *Phys. Rev. D* **95** (2017) 034039, [1611.05974].

[51] J.-P. Lansberg, C. Pisano and M. Schlegel, *Associated production of a dilepton and a $\Upsilon(J/\psi)$ at the LHC as a probe of gluon transverse momentum dependent distributions*, *Nucl. Phys. B* **920** (2017) 192–210, [1702.00305].

[52] J.-P. Lansberg, C. Pisano, F. Scarpa and M. Schlegel, *Pinning down the linearly-polarised gluons inside unpolarised protons using quarkonium-pair production at the LHC*, *Phys. Lett. B* **784** (2018) 217–222, [1710.01684].

[53] A. Bacchetta, D. Boer, C. Pisano and P. Taels, *Gluon TMDs and NRQCD matrix elements in J/ψ production at an EIC*, *Eur. Phys. J. C* **80** (2020) 72, [1809.02056].

[54] C. Hadjidakis et al., *A Fixed-Target Programme at the LHC: Physics Case and Projected Performances for Heavy-Ion, Hadron, Spin and Astroparticle Studies*, 1807.00603.

[55] U. D'Alesio, F. Murgia, C. Pisano and P. Taels, *Azimuthal asymmetries in semi-inclusive J/ψ + jet production at an EIC*, *Phys. Rev. D* **100** (2019) 094016, [1908.00446].

[56] M. G. Echevarria, *Proper TMD factorization for quarkonia production: $pp \to \eta_{c,b}$ as a study case*, *JHEP* **10** (2019) 144, [1907.06494].

[57] S. Fleming, Y. Makris and T. Mehen, *An effective field theory approach to quarkonium at small transverse momentum*, *JHEP* **04** (2020) 122, [1910.03586].

[58] F. Scarpa, D. Boer, M. G. Echevarria, J.-P. Lansberg, C. Pisano and M. Schlegel, *Studies of gluon TMDs and their evolution using quarkonium-pair production at the LHC*, *Eur. Phys. J. C* **80** (2020) 87, [1909.05769].

[59] M. Grewal, Z.-B. Kang, J.-W. Qiu and A. Signori, *Predictive power of transverse-momentum-dependent distributions*, *Phys. Rev. D* **101** (2020) 114023, [2003.07453].

[60] D. Boer, U. D'Alesio, F. Murgia, C. Pisano and P. Taels, *J/ψ meson production in SIDIS: matching high and low transverse momentum*, 2004.06740.

[61] M. G. Echevarria, Y. Makris and I. Scimemi, *Quarkonium TMD fragmentation functions in NRQCD*, 2007.05547.

[62] F. Dominguez, B.-W. Xiao and F. Yuan, *k_t-factorization for Hard Processes in Nuclei*, *Phys. Rev. Lett.* **106** (2011) 022301, [1009.2141].

[63] R. Zhu, P. Sun and F. Yuan, *Low Transverse Momentum Heavy Quark Pair Production to Probe Gluon Tomography*, *Phys. Lett. B* **727** (2013) 474–479, [1309.0780].

[64] G.-P. Zhang, *Back-to-back heavy quark pair production in Semi-inclusive DIS*, *JHEP* **11** (2017) 069, [1709.08970].

[65] D. Boer, S. J. Brodsky, P. J. Mulders and C. Pisano, *Direct Probes of Linearly Polarized Gluons inside Unpolarized Hadrons*, *Phys. Rev. Lett.* **106** (2011) 132001, [1011.4225].

[66] X. Chu, E.-C. Aschenauer, J.-H. Lee and L. Zheng, *Photon structure studied at an Electron Ion Collider*, *Phys. Rev. D* **96** (2017) 074035, [1705.08831].

[67] A. Dumitru, V. Skokov and T. Ullrich, *Measuring the Weizsäcker-Williams distribution of linearly polarized gluons at an electron-ion collider through dijet azimuthal asymmetries*, *Phys. Rev. C* **99** (2019) 015204, [1809.02615].

[68] L. Zheng, E. Aschenauer, J. Lee, B.-W. Xiao and Z.-B. Yin, *Accessing the gluon Sivers function at a future electron-ion collider*, *Phys. Rev. D* **98** (2018) 034011, [1805.05290].

[69] B. Page, X. Chu and E. Aschenauer, *Experimental Aspects of Jet Physics at a Future EIC*, *Phys. Rev. D* **101** (2020) 072003, [1911.00657].

[70] M. Arratia, Y. Furletova, T. J. Hobbs, F. Olness and S. J. Sekula, *Charm jets as a probe for strangeness at the future Electron-Ion Collider*, *Phys. Rev. D* **103** (2021) 074023, [2006.12520].

[71] E. Chudakov, D. Higinbotham, C. Hyde, S. Furletov, Y. Furletova, D. Nguyen et al., *Heavy quark production at an Electron-Ion Collider*, *J. Phys. Conf. Ser.* **770** (2016) 012042, [1610.08536].

[72] H. T. Li, Z. L. Liu and I. Vitev, *Heavy meson tomography of cold nuclear matter at the electron-ion collider*, *Phys. Lett. B* **816** (2021) 136261, [2007.10994].

[73] M. Fickinger, S. Fleming, C. Kim and E. Mereghetti, *Effective field theory approach to heavy quark fragmentation*, *JHEP* **11** (2016) 095, [1606.07737].

[74] D. P. Anderle, T. Kaufmann, M. Stratmann, F. Ringer and I. Vitev, *Using hadron-in-jet data in a global analysis of D^* fragmentation functions*, *Phys. Rev. D* **96** (2017) 034028, [1706.09857].

[75] M. G. A. Buffing, Z.-B. Kang, K. Lee and X. Liu, *A transverse momentum dependent framework for back-to-back photon+jet production*, 1812.07549.

[76] Y.-T. Chien, D. Y. Shao and B. Wu, *Resummation of Boson-Jet Correlation at Hadron Colliders*, *JHEP* **11** (2019) 025, [1905.01335].

[77] M. G. Echevarria, I. Scimemi and A. Vladimirov, *Universal transverse momentum dependent soft function at NNLO*, *Phys. Rev. D* **93** (2016) 054004, [1511.05590].

[78] D. Gutierrez-Reyes, I. Scimemi, W. J. Waalewijn and L. Zoppi, *Transverse momentum dependent distributions with jets*, *Phys. Rev. Lett.* **121** (2018) 162001, [1807.07573].

[79] D. Gutierrez-Reyes, I. Scimemi, W. J. Waalewijn and L. Zoppi, *Transverse momentum dependent distributions in e^+e^- and semi-inclusive deep-inelastic scattering using jets*, *JHEP* **10** (2019) 031, [1904.04259].

[80] D. Gutierrez-Reyes, Y. Makris, V. Vaidya, I. Scimemi and L. Zoppi, *Probing Transverse-Momentum Distributions With Groomed Jets*, *JHEP* **08** (2019) 161, [1907.05896].

[81] "`artemide` web-page, https://teorica.fis.ucm.es/artemide/
`artemide` repository, https://github.com/vladimirovalexey/artemide-public."

[82] M. Arratia, Y. Makris, D. Neill, F. Ringer and N. Sato, *Asymmetric jet clustering in deep-inelastic scattering*, 2006.10751.

[83] A. Hornig, Y. Makris and T. Mehen, *Jet Shapes in Dijet Events at the LHC in SCET*, *JHEP* **04** (2016) 097, [1601.01319].

[84] M.-X. Luo, T.-Z. Yang, H. X. Zhu and Y. J. Zhu, *Transverse Parton Distribution and Fragmentation Functions at NNLO: the Gluon Case*, *JHEP* **01** (2020) 040, [1909.13820].

[85] M. G. Echevarria, A. Idilbi, A. Schäfer and I. Scimemi, *Model-Independent Evolution of Transverse Momentum Dependent Distribution Functions (TMDs) at NNLL*, *Eur. Phys. J. C* **73** (2013) 2636, [1208.1281].

[86] M. G. Echevarria, A. Idilbi and I. Scimemi, *Unified treatment of the QCD evolution of all (un-)polarized transverse momentum dependent functions: Collins function as a study case*, *Phys. Rev.* **D90** (2014) 014003, [1402.0869].

[87] Y. Li and H. X. Zhu, *Bootstrapping Rapidity Anomalous Dimensions for Transverse-Momentum Resummation*, *Phys. Rev. Lett.* **118** (2017) 022004, [1604.01404].

[88] A. A. Vladimirov, *Correspondence between Soft and Rapidity Anomalous Dimensions*, *Phys. Rev. Lett.* **118** (2017) 062001, [1610.05791].

[89] T. Becher and M. D. Schwartz, *Direct photon production with effective field theory*, *JHEP* **02** (2010) 040, [0911.0681].

[90] T. Becher, C. Lorentzen and M. D. Schwartz, *Precision Direct Photon and W-Boson Spectra at High p_T and Comparison to LHC Data*, *Phys. Rev. D* **86** (2012) 054026, [1206.6115].

[91] Y.-T. Chien, R. Rahn, S. Schrijnder van Velzen, D. Y. Shao, W. J. Waalewijn and B. Wu, *Recoil-free azimuthal angle for precision boson-jet correlation*, *Phys. Lett. B* **815** (2021) 136124, [2005.12279].

[92] D. Boer, P. J. Mulders, C. Pisano and J. Zhou, *Asymmetries in Heavy Quark Pair and Dijet Production at an EIC*, *JHEP* **08** (2016) 001, [1605.07934].

[93] M. G. Echevarria, A. Idilbi and I. Scimemi, *Factorization Theorem For Drell-Yan At Low q_T And Transverse Momentum Distributions On-The-Light-Cone*, *JHEP* **07** (2012) 002, [1111.4996].

[94] J. Collins, *Foundations of perturbative QCD*, vol. 32. Cambridge University Press, 11, 2013.

[95] R. Jaffe and L. Randall, *Heavy quark fragmentation into heavy mesons*, *Nucl. Phys. B* **412** (1994) 79–105, [hep-ph/9306201].

[96] S. Fleming, A. H. Hoang, S. Mantry and I. W. Stewart, *Jets from massive unstable particles: Top-mass determination*, *Phys. Rev. D* **77** (2008) 074010, [hep-ph/0703207].

[97] S. Fleming, A. H. Hoang, S. Mantry and I. W. Stewart, *Top Jets in the Peak Region: Factorization Analysis with NLL Resummation*, *Phys. Rev. D* **77** (2008) 114003, [0711.2079].

[98] R. F. del Castillo, M. G. Echevarria, Y. Makris and I. Scimemi, *TMD factorization for dijet and heavy-meson pair in DIS*, *JHEP* **01** (2021) 088, [2008.07531].

[99] Z.-B. Kang, K. Lee, D. Y. Shao and J. Terry, *The Sivers Asymmetry in Hadronic Dijet Production*, 2008.05470.

[100] P. Sun, C. P. Yuan and F. Yuan, *Soft Gluon Resummations in Dijet Azimuthal Angular Correlations in Hadronic Collisions*, *Phys. Rev. Lett.* **113** (2014) 232001, [1405.1105].

[101] P. Sun, C. P. Yuan and F. Yuan, *Transverse Momentum Resummation for Dijet Correlation in Hadronic Collisions*, *Phys. Rev. D* **92** (2015) 094007, [1506.06170].

[102] A. Hornig, Y. Makris and T. Mehen, *Jet shapes in dijet events at the lhc in scet*, *Journal of High Energy Physics* **2016** (Apr, 2016) 1?41.

[103] A. Vladimirov, V. Moos and I. Scimemi, *Transverse momentum dependent operator expansion at next-to-leading power*, *JHEP* **01** (2022) 110, [2109.09771].

[104] S. Rodini and A. Vladimirov, *Definition and evolution of transverse momentum dependent distribution of twist-three*, *JHEP* **08** (2022) 031, [2204.03856].

[105] V. Moos, I. Scimemi, A. Vladimirov and P. Zurita, *Extraction of unpolarized transverse momentum distributions from fit of Drell-Yan data at N^4LL*, 2305.07473.

[106] T. Neumann and J. Campbell, *Fiducial Drell-Yan production at the LHC improved by transverse-momentum resummation at N4LLp+N3LO*, *Phys. Rev. D* **107** (2023) L011506, [2207.07056].

[107] S. Camarda, L. Cieri and G. Ferrera, *Drell-Yan lepton-pair production: q_T resummation at approximate N^4LL+N^4LO accuracy*, 2303.12781.

[108] A. Vladimirov, *Structure of rapidity divergences in multi-parton scattering soft factors*, *JHEP* **04** (2018) 045, [1707.07606].

[109] C. Duhr, B. Mistlberger and G. Vita, *Four-Loop Rapidity Anomalous Dimension and Event Shapes to Fourth Logarithmic Order*, *Phys. Rev. Lett.* **129** (2022) 162001, [2205.02242].

[110] I. Moult, H. X. Zhu and Y. J. Zhu, *The four loop QCD rapidity anomalous dimension*, *JHEP* **08** (2022) 280, [2205.02249].

[111] S. Moch, J. A. M. Vermaseren and A. Vogt, *The Three loop splitting functions in QCD: The Nonsinglet case*, *Nucl. Phys. B* **688** (2004) 101–134, [hep-ph/0403192].

[112] S. Moch, B. Ruijl, T. Ueda, J. A. M. Vermaseren and A. Vogt, *Low moments of the four-loop splitting functions in QCD*, *Phys. Lett. B* **825** (2022) 136853, [2111.15561].

[113] G. Kramer and B. Lampe, *Two Jet Cross-Section in e+ e- Annihilation*, *Z. Phys.* **C34** (1987) 497.

[114] T. Matsuura, S. C. van der Marck and W. L. van Neerven, *The Calculation of the Second Order Soft and Virtual Contributions to the Drell-Yan Cross-Section*, *Nucl. Phys. B* **319** (1989) 570–622.

[115] T. Gehrmann, E. W. N. Glover, T. Huber, N. Ikizlerli and C. Studerus, *Calculation of the quark and gluon form factors to three loops in QCD*, *JHEP* **06** (2010) 094, [1004.3653].

[116] R. N. Lee, A. von Manteuffel, R. M. Schabinger, A. V. Smirnov, V. A. Smirnov and M. Steinhauser, *Quark and Gluon Form Factors in Four-Loop QCD*, *Phys. Rev. Lett.* **128** (2022) 212002, [2202.04660].

[117] M. A. Ebert, I. Moult, I. W. Stewart, F. J. Tackmann, G. Vita and H. X. Zhu, *Subleading power rapidity divergences and power corrections for q_T*, *JHEP* **04** (2019) 123, [1812.08189].

[118] M. A. Ebert, A. Gao and I. W. Stewart, *Factorization for azimuthal asymmetries in SIDIS at next-to-leading power*, *JHEP* **06** (2022) 007, [2112.07680].

[119] L. Gamberg, Z.-B. Kang, D. Y. Shao, J. Terry and F. Zhao, *Transverse-momentum-dependent factorization at next-to-leading power*, 2211.13209.

[120] S. Rodini, A. C. Alvaro and B. Pasquini, *Collinear matching for next-to-leading power transverse-momentum distributions*, 2306.15052.

[121] S. Rodini and A. Vladimirov, *Transverse momentum dependent factorization for SIDIS at next-to-leading power*, 2306.09495.

[122] R. Abdul Khalek et al., *Science Requirements and Detector Concepts for the Electron-Ion Collider: EIC Yellow Report*, 2103.05419.

[123] D. P. Anderle et al., *Electron-ion collider in China*, *Front. Phys. (Beijing)* **16** (2021) 64701, [2102.09222].

[124] R. Boussarie et al., *TMD Handbook*, 2304.03302.

[125] L. V. Keldysh, *Diagram technique for nonequilibrium processes*, *Zh. Eksp. Teor. Fiz.* **47** (1964) 1515–1527.

[126] L. F. Abbott, *The Background Field Method Beyond One Loop*, *Nucl. Phys. B* **185** (1981) 189–203.

[127] L. F. Abbott, *Introduction to the Background Field Method*, *Acta Phys. Polon. B* **13** (1982) 33.

[128] A. Bacchetta, M. Diehl, K. Goeke, A. Metz, P. J. Mulders and M. Schlegel, *Semi-inclusive deep inelastic scattering at small transverse momentum*, *JHEP* **02** (2007) 093, [hep-ph/0611265].

[129] X. Liu and H. Xing, *The time-reversal odd side of a jet*, *Fund. Res.* **3** (2023) 346–350, [2104.03328].

[130] W. K. Lai, X. Liu, M. Wang and H. Xing, *Unveiling Nucleon 3D Chiral-Odd Structure with Jet Axes*, 2205.04570.

[131] R. Abir et al., *The case for an EIC Theory Alliance: Theoretical Challenges of the EIC*, 2305.14572.

[132] D. Neill, I. Scimemi and W. J. Waalewijn, *Jet axes and universal transverse-momentum-dependent fragmentation*, *JHEP* **04** (2017) 020, [1612.04817].

[133] Z.-B. Kang, X. Liu, F. Ringer and H. Xing, *The transverse momentum distribution of hadrons within jets*, *JHEP* **11** (2017) 068, [1705.08443].

[134] X. Liu, F. Ringer, W. Vogelsang and F. Yuan, *Lepton-jet Correlations in Deep Inelastic Scattering at the Electron-Ion Collider*, *Phys. Rev. Lett.* **122** (2019) 192003, [1812.08077].

[135] M. Arratia, Y. Song, F. Ringer and B. V. Jacak, *Jets as precision probes in electron-nucleus collisions at the future Electron-Ion Collider*, *Phys. Rev. C* **101** (2020) 065204, [1912.05931].

[136] M. Arratia, Z.-B. Kang, A. Prokudin and F. Ringer, *Jet-based measurements of Sivers and Collins asymmetries at the future electron-ion collider*, *Phys. Rev. D* **102** (2020) 074015, [2007.07281].

[137] X. Liu, F. Ringer, W. Vogelsang and F. Yuan, *Lepton-jet Correlation in Deep Inelastic Scattering*, *Phys. Rev. D* **102** (2020) 094022, [2007.12866].

[138] Z.-B. Kang, K. Lee, D. Y. Shao and F. Zhao, *Spin asymmetries in electron-jet production at the future electron ion collider*, *JHEP* **11** (2021) 005, [2106.15624].

[139] Y.-T. Chien, R. Rahn, D. Y. Shao, W. J. Waalewijn and B. Wu, *Precision boson-jet azimuthal decorrelation at hadron colliders*, *JHEP* **02** (2023) 256, [2205.05104].

[140] M. Arratia, Z.-B. Kang, S. J. Paul, A. Prokudin, F. Ringer and F. Zhao, *Neutrino-tagged jets at the Electron-Ion Collider*, *Phys. Rev. D* **107** (2023) 094036, [2212.02432].

[141] D. Bertolini, T. Chan and J. Thaler, *Jet Observables Without Jet Algorithms*, *JHEP* **04** (2014) 013, [1310.7584].

[142] V. M. Braun, A. N. Manashov and B. Pirnay, *Scale dependence of twist-three contributions to single spin asymmetries*, *Phys. Rev. D* **80** (2009) 114002, [0909.3410].

[143] S. Rodini and A. Vladimirov, *Factorization for quasi-TMD distributions of sub-leading power*, 2211.04494.

[144] D. Boer, R. Jakob and P. J. Mulders, *Asymmetries in polarized hadron production in e^+e^- annihilation up to order 1/Q*, *Nucl. Phys. B* **504** (1997) 345–380, [hep-ph/9702281].

[145] US Belle II Group, Belle II/SuperKEKB e- Polarization Upgrade Working Group collaboration, D. M. Asner et al., *Snowmass 2021 White Paper on Upgrading SuperKEKB with a Polarized Electron Beam: Discovery Potential and Proposed Implementation*, in *Snowmass 2021*, 5, 2022. 2205.12847.

[146] A. Accardi et al., *Opportunities for precision QCD physics in hadronization at Belle II – a snowmass whitepaper*, in *Snowmass 2021*, 4, 2022. 2204.02280.

[147] Belle collaboration, R. Seidl et al., *Measurement of Azimuthal Asymmetries in Inclusive Production of Hadron Pairs in e^+e^- Annihilation at $\sqrt{s} = 10.58$ GeV*, *Phys. Rev. D* **78** (2008) 032011, [0805.2975].

[148] P. J. Mulders and C. Van Hulse, *Noncollinearity in dijet fragmentation in electron-positron scattering*, *Phys. Rev. D* **100** (2019) 034011, [1903.11467].

[149] G. Das, S.-O. Moch and A. Vogt, *Soft corrections to inclusive deep-inelastic scattering at four loops and beyond*, *JHEP* **03** (2020) 116, [1912.12920].

[150] A. Vladimirov, *Kinematic power corrections in TMD factorization theorem*, *JHEP* **12** (2023) 008, [2307.13054].

[151] Z. L. Liu and M. Neubert, *Factorization at subleading power and endpoint-divergent convolutions in $h \to \gamma\gamma$ decay*, *JHEP* **04** (2020) 033, [1912.08818].

[152] Z. L. Liu, B. Mecaj, M. Neubert and X. Wang, *Factorization at subleading power, Sudakov resummation, and endpoint divergences in soft-collinear effective theory*, *Phys. Rev. D* **104** (2021) 014004, [2009.04456].

[153] M. Beneke, M. Garny, S. Jaskiewicz, J. Strohm, R. Szafron, L. Vernazza et al., *Next-to-leading power endpoint factorization and resummation for off-diagonal "gluon" thrust*, *JHEP* **07** (2022) 144, [2205.04479].

[154] A. Gao, *Transverse Momentum Distributions at Subleading Power and Quark-Gluon-Quark Correlators*, Presented at REF workshop 2022.

[155] A. Gao, *Renormalization for NLP TMD Quark-Gluon-Quark Correlators*, Presented at SCET workshop 2023.

[156] J. Michel, *Subleading-Power Soft Subtleties in SIDIS*, Presented at the ESI workshop "Quantum Field Theory at the Frontiers of the Strong Interaction" in 2023.

[157] S. M. Freedman and R. Goerke, *Renormalization of Subleading Dijet Operators in Soft-Collinear Effective Theory*, *Phys. Rev. D* **90** (2014) 114010, [1408.6240].

[158] R. Goerke and M. Inglis-Whalen, *Renormalization of dijet operators at order $1/Q^2$ in soft-collinear effective theory*, *JHEP* **05** (2018) 023, [1711.09147].

[159] M. Beneke, M. Garny, R. Szafron and J. Wang, *Anomalous dimension of subleading-power N-jet operators*, *JHEP* **03** 001, [1712.04416].

[160] J. M. Butterworth, J. P. Couchman, B. E. Cox and B. M. Waugh, *KtJet: A C++ implementation of the K-perpendicular clustering algorithm*, *Comput. Phys. Commun.* **153** (2003) 85–96, [hep-ph/0210022].

[161] M. Cacciari, G. P. Salam and G. Soyez, *FastJet User Manual*, *Eur. Phys. J. C* **72** (2012) 1896, [1111.6097].

[162] S. Catani and M. H. Seymour, *A General algorithm for calculating jet cross-sections in NLO QCD*, *Nucl. Phys. B* **485** (1997) 291–419, [hep-ph/9605323].

[163] M.-x. Luo, T.-Z. Yang, H. X. Zhu and Y. J. Zhu, *Unpolarized quark and gluon TMD PDFs and FFs at N^3LO*, *JHEP* **06** (2021) 115, [2012.03256].

[164] S. D. Ellis, C. K. Vermilion, J. R. Walsh, A. Hornig and C. Lee, *Jet Shapes and Jet Algorithms in SCET*, *JHEP* **11** (2010) 101, [1001.0014].